UNIVERSIDAD COMPLUTENSE DE MADRID
FACULTAD DE CIENCIAS FÍSICAS

TESIS DOCTORAL

Transverse momentum dependent distributions for the Electron-Ion Collider era

Distribuciones dependientes de momento transverso para la era del Electron-Ion Collider

MEMORIA PARA OPTAR AL GRADO DE DOCTOR

PRESENTADA POR

Daniel Gutiérrez Reyes

DIRECTOR

Ignazio Scimemi

Madrid

UNIVERSIDAD COMPLUTENSE DE MADRID
FACULTAD DE CIENCIAS FÍSICAS

TESIS DOCTORAL

Transverse momentum dependent distributions for the Electron-Ion Collider era

Distribuciones dependientes de momento transverso para la era del Electron-Ion Collider

MEMORIA PARA OPTAR AL GRADO DE DOCTOR

PRESENTADA POR
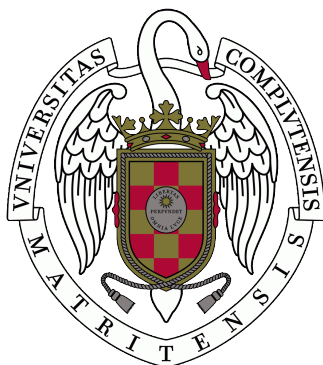
Daniel Gutiérrez Reyes

DIRECTOR

Ignazio Scimemi

Transverse momentum dependent distributions for the Electron-Ion Collider era

Author:
Daniel GUTIÉRREZ REYES

Supervisor:
Prof. Ignazio SCIMEMI

*A thesis submitted in partial fulfillment of the requirements
for the degree of Doctor of Philosophy in Physics*

"We are not going in circles, we are going upwards. The path is a spiral; we have already climbed many steps."

Hermann Hesse, *Siddhartha*

Acknowledgements

First of all, I would like to thank to my advisor, Ignazio Scimemi, for his guidance along this doctorate. I really enjoyed to work with you and I have no words to thank your labour from the very begining, when I was just finishing my degree. Your door has been always open to me and I have always felt supported and motivated. I was very lucky of having you as an advisor.

I want to thank all the people who I had the pleasure to work with along these years. Alexey Vladimirov, whose help along my doctorate studies has been essential and from whom I have learnt a lot of physics. Wouter Waalewijn, from whom I learnt a lot when I was introduced into the world of jets and one of the clearer minds I have known. Lorenzo Zoppi, it was a pleasure to work with you. I think we connected very well from the beginning and I felt very comfortable working with you. Sergio, whom I wish a lot of success along his doctorate that is now on course, I am sure you will do big things. Also, I want to thank to Yiannis Makris and Varun Vaidya who help me to have a better understanding about jet physics. It is great to work with friends. Also, I would like to thank the work done by Alessandro Bacchetta and Thomas Becher as external referees of this thesis, giving to me their feedback about the manuscript.

I want to thank all the people that have been by my side every day in the Universidad Complutense. This experience would not have the same without you and you made me feel at home in the department: Arkaitz, José Manuel, Héctor, Santiago, Santos, Juanmi, Miguel, Ted, Andrea, Clara, Laura, Roberto, José Carrasco, Adolfo, Miguel Echevarría, Merce, Carlos, Isi, José Cembranos, Prado, Juanjo, José Manuel Alarcón, Julio, Pipo, Luis, Fer, Adri, Rita, Mercè, Pablo, and many more people I am sure I am forgetting now.

Futhermore, I would like to thank my lifelong friends, Vieira and Corcho, for their unconditional support and friendship not only along this stage of my life, but as long I can remember. You are my second family, guys. Also, I do not want to forget to thank the friends I made along my physics studies: Alonso, Alfredo, Luis and Andrés. I am very happy to have found friends like you in this adventure.

I am deeply grateful to you, Cristina, because you are always by my side no matter the situation. We have shared all the good and bad moments along this stage and you have thought me to look ahead and to be strong enough. With you I always find the way to see the bright side of life. This thesis is yours because you are the motor of whatever I do in my life. With you I am better and I hope I make you feel so good as you make to me. I love you.

And last but no least, I would like to thank my parents and sister. You have always trusted in me giving me confidence to do everything I have done. You have always been by my side giving me the freedom to choose my way in life. Thank you for your generosity, support and love every day. I hope you feel proud of me.

List of publications and conferences

The content of this thesis is partially based in the following publications:

- **Probing Transverse-Momentum Distributions With Groomed Jets**
  Daniel Gutierrez-Reyes, Yiannis Makris, Varun Vaidya, Ignazio Scimemi, Lorenzo Zoppi
  Published in JHEP 08 (2019) 161. arXiv: 1907.05896

- **Linearly polarized gluons at next-to-next-to leading order and the Higgs transverse momentum distribution**
  Daniel Gutierrez-Reyes, Sergio Leal-Gomez, Ignazio Scimemi, Alexey Vladimirov
  Published in JHEP 11 (2019) 121. arXiv: 1907.03780

- **Transverse momentum dependent distributions in e^+e^- and semi-inclusive deep-inelastic scattering using jets**
  Daniel Gutierrez-Reyes, Ignazio Scimemi, Wouter J. Waalewijn, Lorenzo Zoppi
  Published in JHEP 10 (2019) 031. arXiv: 1904.04259

- **Transverse momentum dependent distributions with jets**
  Daniel Gutierrez-Reyes, Ignazio Scimemi, Wouter J. Waalewijn, Lorenzo Zoppi
  Published in Phys.Rev.Lett. 121 (2018) 16, 162001. arXiv: 1807.07573

- **Transverse momentum dependent transversely polarized distributions at next-to-next-to-leading-order**
  Daniel Gutierrez-Reyes, Ignazio Scimemi, Alexey Vladimirov
  Published in JHEP 07 (2018) 172. arXiv: 1805.07243

- **Twist-2 matching of transverse momentum dependent distributions**
  Daniel Gutierrez-Reyes, Ignazio Scimemi, Alexey Vladimirov
  Published in Phys.Lett.B 769 (2017) 84-89. arXiv: 1702.06558

The content of these publications has been presented in the following international conferences and workshops:

- **XIVth annual workshop on Soft-Collinear Effective Theory (SCET 2017)**
  Wayne State University, Detroit, MI, US
  March 2017
  Title of the talk: Features of spin dependent transverse momentum distributions: the helicity and transversity case

- **Electron-Ion Collider User Group Meeting 2017**
  University of Trieste, Trieste, Italy
  July 2017
  Title of the talk: Features of spin dependent TMDs

- **13th International Symposium on Radiative Corrections (RADCOR 2017)**
  Sankt Gilgen, Austria
  September 2017
  Title of the talk: Twist-2 transverse momentum dependent distributions at NNLO

- **Resummation, Evolution, Factorization 2017 (REF 2017)**
  Universidad Complutense de Madrid, Madrid, Spain
  November 2017
  Title of the talk: Twist-2 TMDs at NNLO in QCD

- **XVth annual workshop on Soft-Collinear Effective Theory (SCET 2018)**
  University of Amsterdam, Amsterdam, The Netherlands
  March 2018
  Title of the talk: Twist-2 TMDs at NNLO in QCD

- **QCD Evolution 2018**
  Santa Fe, NM, US
  May 2018
  Title of the talk: Twist-2 transverse momentum distributions at NNLO in QCD

- **Diffraction and Low-x 2018**
  Reggio Calabria, Italy
  August 2018
  Title of the talk: Twist-2 transverse momentum distributions at NNLO in QCD

- **23rd International Spin Symposium (SPIN 2018)**
  University of Ferrara, Ferrara, Italy
  September 2018
  Title of the talk: Twist-2 transverse momentum distributions at NNLO in QCD

- **X CPAN DAYS**
  Universidad de Salamanca, Salamanca, Spain
  October 2018
  Title of the talk: Measuring transverse momentum distributions with jets

- **XVIth annual workshop on Soft-Collinear Effective theory (SCET 2019)**
  UCSD, San Diego, CA, US
  March 2019
  Title of the invited talk: Investigating transverse momentum distributions with jets

- **Light-Cone 2019**
  École Polytechnique, Palaiseau, France
  September 2019
  Title of the talk: Investigating transverse momentum distributions with jets

As a result, the content of the published articles has contributed to the following conference proceedings:

- **Twist-2 Transverse Momentum Distributions at Next-to-next-to-leading Order in QCD**
  Daniel Gutierrez-Reyes, Ignazio Scimemi, Alexey Vladimirov
  Published in Acta Phys.Polon.Supp. 12 (2019) 4, 849-854

- **Studying transverse momentum distributions with jets at N^{3}LL**
  Daniel Gutierrez-Reyes, Ignazio Scimemi, Wouter J. Waalewijn, Lorenzo Zoppi
  Published in PoS DIS2019 (2019) 144

- **Linearly polarized gluons Transverse Momentum Dependent Parton Distribution Function at NNLO in QCD**
  Sergio Leal-Gomez, Daniel Gutierrez-Reyes, Ignazio Scimemi, Alexey Vladimirov
  Published in PoS DIS2019 (2019) 183

- **Twist-2 transverse momentum dependent distributions**
  Daniel Gutierrez-Reyes, Ignazio Scimemi, Alexey Vladimirov
  Published in PoS RADCOR2017 (2018) 040

Contents

Prelude and outline of the thesis

The physical theory which deals with the strong interactions between quarks and gluons in known as Quantum Chromodynamics (QCD). This theory, together with the ones that deal with electromagnetic and weak interactions (unified in electroweak theory) are combined into the Standard Model (SM). The gravitational interaction, the other known force in nature, is well described by General Relativity. The Standard Model is built in terms of a Lagrangian of quantized fields describing fundamental degrees of freedom, quarks and leptons, and bosons that act as carriers of the cited interactions.

One of the more fundamental open questions in QCD is to understand how the observed properties of hadrons are generated by the dynamics of their inner constituents. In order to shed some light on this question physicists use different theoretical approaches from different perspectives, like perturbative QCD, effective field theories, lattice QCD, etc. A very interesting research field to test and understand QCD is the exploration of the multi-dimensional structure of hadrons. The main goal of this field is to reconstruct multi-dimensional images of a hadron investigating the distribution of partons, namely quarks and gluons, inside it. In this way, issues such as the the role of quarks and gluons in generating the nucleon's spin or partonic angular momentum can be investigated. There is a high interest into hadron structure in the experimental community, with important facilities such JLab, DESY, BNL, CERN, KEK, running experiments to study the multi-dimensional structure of hadrons. Also, the LHC can help a lot in this field, especially to understand the role of gluons inside the protons. Recently, the US government has approved the construction of a new accelerator, the Electron-Ion Collider (EIC) at BNL. Part of the predictions given in this thesis are suitable to be tested in this new accelerator.

A very interesting type of observables that can give information about hadron structure are the ones with non-vanishing transverse momentum dependence. This interest was already there in the first years after the establishment of QCD as a fundamental theory of strong interactions [1–5]. These observables are very interesting for hadron colliders and have very relevant impact on, e.g., the study of Higgs boson production and the search for physics Beyond Standard Model. A crucial point to deal with these type of processes is obtaining well defined factorization theorems and resumming large logarithmic contributions to perform phenomenological analyses and predictions. A large amount of work has been done to establish factorization theorems with un-integrated transverse momentum for very relevant processes as Drell-Yan production (proton-proton collision leading to a pair of leptons in the final state) or semi-inclusive deep inelastic scattering (electron-proton collisions leading to a hadron in the final state) [6–17]. In general terms, a factorized cross section is written in terms of a hard factor that includes all the high-energy physics and two objects that include information about the distribution of partons inside the hadrons in the process. These elements are known as transverse momentum dependent parton distribution functions (TMDPDFs [1]). In the derivation of factorization theorems

---

[1]The TMD acronym stands for transverse momentum distributions or to indicate transverse momentum dependence of a particular object. Along the thesis we will use TMDPDF for transverse

we use the machinery of Soft Collinear Effective Theory (see chapter 1). A more dedicated study about factorization theorems is given in chapter 2.

The main body of this thesis is divided in two parts, studying factorization theorems and the hadronic information in two different contexts, but aiming at the same goal: improving the extraction of the three-dimensional information of hadrons.

Part I of this thesis is dedicated to the study of spin dependent TMDPDFs arising from factorization theorems established for processes involving hadrons with a particular polarization. In chapter 3 the definition of the unpolarized TMDPDF of [18] is extended in order to obtain definitions for spin dependent TMDPDFs. At leading dynamical twist we obtain different spin-dependent distributions for quarks and gluons. The results of the perturbative information derived from the large transverse momentum limit of these TMDPDFs (known as matching coefficients) up to second order in perturbation theory will be given in chapter 4. In this way we achieve the same level of precision for spin dependent TMDPDFs as for their unpolarized counterparts. This improvement of the perturbative order known for the different spin-dependent TMDs will help to decrease the theoretical errors in phenomenological predictions involving polarized hadrons and will allow a cleaner extraction of nonperturbative physics associated to the transverse momentum dependent distributions. As an application, in chapter 5 we use the new perturbative results obtained for linearly polarized gluon TMD to see their impact in the transverse momentum spectrum of the Higgs boson.

Part II of this thesis is dedicated to establishing factorization theorems including jets in final states of the considered processes. In principle, the use of jets in the final state decreases the nonperturbative contamination compared to using hadrons in a final state, because jet properties can be calculated to a large extent in perturbation theory. Thus, processes with jets in the final state (e.g. jet SIDIS) should offer a cleaner way to access information about the structure of hadrons in the initial state. Of course, some hadronization effects associated with the jets appear (e.g. due to the determination of the position of the axis). Thus, in this part of the thesis we study the establishment of different factorization theorems for some particularly interesting processes using different jet definitions. This allows one to study the advantages and disadvantages of different jet definitions in the extraction of information about hadrons in initial states. In chapter 6 a new definition for TMD jets is given through the establishment of different factorization theorems in different regimes related mainly to the size of the considered jet. This leads to a particular choice of the jet axis that allows the establishment of factorization theorems in any regime and will allow us to obtain numerical predictions that can be tested in future experiments as the EIC. Finally, in chapter 7 a different definition of the jet is used in order to obtain numerical predictions. In this case, we introduce the concept of grooming that removes the soft contamination to the jet. Thus only the collinear core of the jet remains and the hadronization effects should be mostly suppressed. So, this way to proceed represent another way to access to the nonperturbative information of hadrons in a cleaner manner of using processes with hadrons in the final state.

---

momentum parton distribution functions and TMDFF for transverse momentum fragmentation functions.

Chapter 1

Introduction to Soft-Collinear Effective Theory

The study of problems with at least two different energy scales, in quantum field theory is usually simplified with the use of Effective Field Theories (EFTs). These theories allow one to expand physical quantities in the small ratio of the scales and to separate the low energy contributions from the high energy part of the problem. The expansion in this ratio of scales usually simplifies this problem and it is often necessary in order to attack field-theory problems. In Quantum Chromodynamics (QCD) the low-energy part of the problem is usually nonperturbative, while the high-energy part can be computed perturbatively. EFTs are able to separate the two pieces and compute them individually with appropriate techniques. In particular, as this thesis is focused on hadron-collider observables, the leading nonperturbative contributions will be encoded in parton distribution functions.

Commonly EFTs are used in low energy QCD, in particular in flavor physics. However, in recent years several applications of EFTs to high energy physics were developed. This is not surprising, since processes at high energy colliders are perfect examples of problems with different energy scales. Processes in hadron colliders involve physics from large scales such as the center-of-mass-energy and very low scales such as the proton mass. Thus, in order to obtain some theoretical predictions for any process in a hadron collider we need to disentangle the physics associated with these scales. Traditionally this factorization is obtained using diagrammatic methods, establishing some properties at all orders in perturbation theory from the Feynman diagrams in the high-energy limit. Reviews of these traditional diagrammatic techniques can be found in [6, 10]. Soft-Collinear Effective Theory (SCET) [19–21] provides an alternative formalism which allows to derive these factorization theorems. This EFT provides an effective Lagrangian that simplifies the way we organize the computations. The existence of an EFT to do this kind of computations is extremely useful because for more complex problems, such as calculations of power corrections, a purely diagrammatic approach can be too difficult. Although the EFT approach has important advantages, there is a close connection between both approaches, because the diagrams of SCET are in one-to-one correspondence with the expanded QCD diagrams.

A typical example for the type of processes that can be studied with SCET and that lead to hadron collider observables is two jet production from electron-positron annihilation. This process involves sprays of energetic particles along two directions with momenta p_n and $p_{\bar{n}}$ which form the jet and additional soft radiation with momentum p_s. Also, if the hadronic sources are in the initial state, another important process is the Drell-Yan production in which a proton-proton collision leads to a dilepton pair in the final state. The factorization of this process will be studied in detail in chapter 2. Graphically this kind of process is sketched in fig. 1.1.
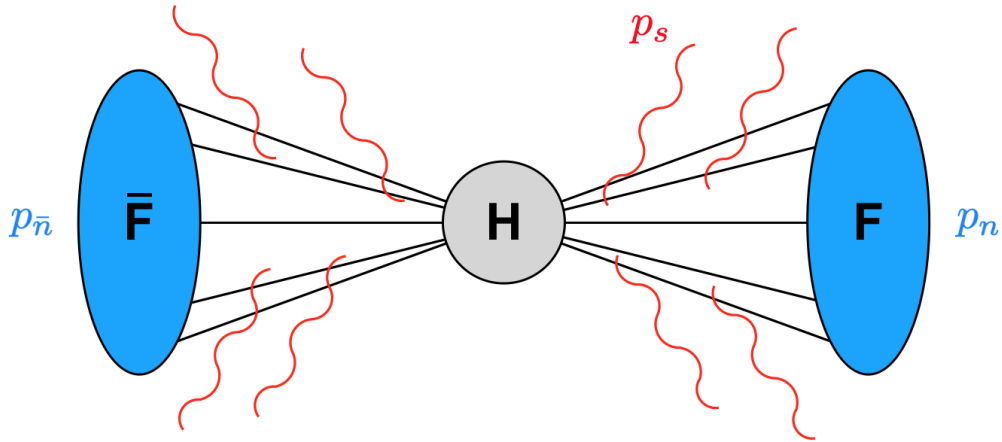
FIGURE 1.1: Typical two hadron/jet production.

The momenta involved in the process are related by a scale hierarchy

$$Q^2 \equiv (p_n + p_{\bar{n}})^2 \gg p_n^2 \sim p_{\bar{n}}^2 \gg p_s^2, \tag{1.1}$$

where Q^2 represents the hard scale of the process and its associated physics can be isolated and absorbed into Wilson coefficients of effective theory operators. This procedure is analogous to integrating out a heavy particle when one is constructing a low energy effective theory for light particles only. Then, SCET involves two different types of fields, collinear and soft. They describe the physics associated with the two low energy scales p_n^2 and p_s^2.

In this thesis, we will use SCET to analyze cross sections of processes such as the one presented in fig. 1.1 (see e.g. chapter 2). The result of these kind of analyses is often a factorization theorem of the cross section as

$$\sigma = H \cdot F \otimes \bar{F} \otimes S. \tag{1.2}$$

The hard function H encodes the integrated physics at the scale Q^2. The hadron or jet function F $(\bar{F})$ depends on the scale p_n^2 $(p_{\bar{n}}^2)$ and the soft function S describes the physics at the soft momentum scale, p_s^2. Depending on the observable considered these elements are multiplied or convolved as indicated by the symbol $\otimes$. The formula in eq. (1.2) is obtained expanding in the ratios of the scales in eq. (1.1). Its main virtue is that each piece is sensitive only to one scale and they fulfill independent renormalization group (RG) equations (see section 1.3.5). This fact allows us to solve one dimensional differential equations for each piece of the cross section and to evolve them from their natural scales to the matching scale in order to do reliable phenomenological predictions.

Two main extra complications arise when SCET is compared to other traditional EFTs. The first one is that quarks and gluons are present in all the regimes of energies. So, we cannot simply integrate out particles. Instead the quark and gluon fields are split into *modes* associated with the different energy scales. There is a hard mode which describes the contributions when the particles are purely off-shell. This term is integrated out in a path integral sense (this mode would not appear as an

external state) and the low-energy collinear and soft modes are the fields of the effective theory. Section 1.1 is dedicated to illustrate in a simple form the concept of modes and their factorization with a simple example based in QED, in which only hard and soft modes appear. Then, we introduce collinear modes in sections 1.2 and 1.3 to complete the picture.

A second complication is that the different momentum components of the fields scale differently. The components of the momentum that are transverse to the hadron or jet direction are always small, but the ones along the hadron or jet direction are large. To perform a derivative expansion of the effective Lagrangian one needs to split the momenta into different components. This is done by introducing two vectors in the directions of the two hadrons or jets, i.e. $n^\mu \sim p_n^\mu$ and $\bar{n}^\mu \sim p_{\bar{n}}^\mu$.

1.1 An example of factorization: electron scattering

To study all the main features of SCET in an understandable way, we begin studying an illustrative example of soft photon production in electron scattering. This is a simple study case because only hard and soft modes are present. This case will give us a clear picture of the definition of modes and how they are separated from each other. With this example we will obtain some results faster and then the study of the complete theory introducing collinear modes will be easier. Thus, we dedicate this section to study electron-electron scattering in QED as in [22].

We cannot avoid the presence of soft photons in QED processes, i.e. soft photons which cost little energy to produce are always included in final states. Indeed, trying to compute higher order cross sections without taking into account the contribution of soft photons leads to divergent results. These divergences tell us that completely exclusive QED cross sections are not physical. So, when we talk about electron-electron scattering we are referring to the inclusive process,

$$e^-(p_1) + e^-(p_2) \to e^-(p_3) + e^-(p_4) + X_s(q_s), \tag{1.3}$$

where X_s is any state with an arbitrary number of soft photons which carry the total momentum q_s. In this section we assume that the electron energies are of the order of the electron mass, m_e. Instead of SCET we will study Soft Effective Theory (SET) to study the factorization of these soft photon radiation in QED. In this case we will assume that the energy of these bunch of soft photons fulfills $E_s \ll m_e$ and we will analyze the cross section of this process up to leading powers of the expansion parameter $\lambda = E_\gamma / m_e$.

The first step is the study of the effective Lagrangian for soft photons with $E_\gamma \ll m_e$. So, we should organize the operators in the effective Lagrangian by their dimension

$$\mathcal{L}_{\text{eff}}^\gamma = \mathcal{L}_4^\gamma + \frac{1}{m_e^2}\mathcal{L}_6^\gamma + \frac{1}{m_e^4}\mathcal{L}_8^\gamma, \tag{1.4}$$

where the coefficients of the non-leading terms of the Lagrangian are suppressed by inverse powers of the hard scale of the process, in this case m_e. Thus, these operators are suppressed by powers of λ and will not be further considered in our analysis. A further dedicated study about power correction operators can be found in [23, 24]. The leading Lagrangian only involves the term

$$\mathcal{L}_4^\gamma = -\frac{1}{4}F_{\mu\nu}F^{\mu\nu}, \tag{1.5}$$
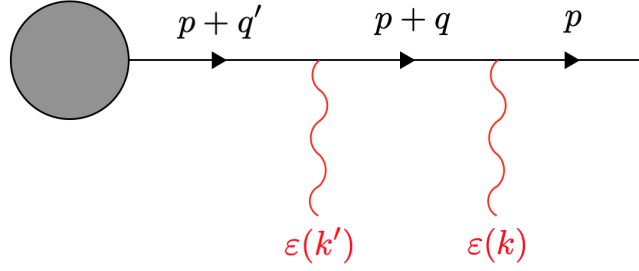
FIGURE 1.2: Outgoing electron with soft photon emissions. Note that
$q' = k + k'$ and $q = k$

where its coefficient can be adjusted to its canonical value by rescaling the photon field, $F_{\mu\nu}$. Thus, the leading power effective Lagrangian is simply the one for free photons. This makes sense, because the effective theory is made integrating out all the particles which are not photons.

However, $\mathcal{L}_{\text{eff}}^{\gamma}$ is not sufficient by itself. Even if the energy is too small to produce electron-positron pairs we do need to include the incoming and outgoing electrons in the effective theory. To obtain this contributions we consider an outgoing electron with momentum $p^{\mu} = m_e v^{\mu}$, as in fig. 1.2. Consider a soft photon with momentum q. We can expand the internal fermion propagator in the limit where q^{μ}/m_e is suppressed. We find

$$\Delta_F = i\frac{\slashed{p} + \slashed{q} + m_e}{(p+q)^2 - m_e^2 + i0} = \frac{1 + \slashed{v}}{2}\frac{i}{v \cdot q + i0} \equiv P_v \frac{i}{v \cdot q + i0} \tag{1.6}$$

where we have defined the projector

$$P_v = \frac{1 + \slashed{v}}{2}, \tag{1.7}$$

which has the properties

$$\slashed{v}P_v = P_v, \qquad P_v^2 = P_v, \qquad P_v \slashed{\varepsilon} P_v = P_v\, \varepsilon \cdot v. \tag{1.8}$$

Using these properties, the outgoing leg part of the diagram in fig. 1.2 can be written as

$$\bar{u}(p)P_v\frac{1}{v \cdot q}(-ie\,\varepsilon \cdot v)P_v\frac{1}{v \cdot q'}(-ie\,\varepsilon' \cdot v).... \tag{1.9}$$

This expansion of soft emissions is called *eikonal approximation*. At this point we should study if this expanded expression can be obtained from an effective Lagrangian. To do this, we need to view the expanded propagator in eq. (1.6) as the propagator in the effective theory and the emissions in the expanded diagram must result from a Feynman rule $-iev^{\mu}$ for the electron-photon vertex. Knowing the Feynman rules ,we need to construct an effective Lagrangian which reproduces them. We consider

$$\mathcal{L}_{\text{eff}}^{v} = \bar{h}_v(x)\,iv \cdot D\,h_v(x), \tag{1.10}$$

where h_v should be considered as an auxiliary fermion field which fulfills $P_v h_v = \not{v} h_v = h_v$. As usual, the propagator can be obtained by inverting the quadratic part of the Lagrangian in Fourier space and multiplying by i. This yields $i/(v \cdot q)$ as obtained in eq. (1.6). The factor P_v arises because the external spinor fulfills the condition $P_v h_v = h_v$ and due to the property $P_v^2 = P_v$ only one projector remains in the result. Due to the fact that $D_\mu = \partial_\mu + ieA_\mu$ the vertex Feynman rule is $-iev^\mu$ as expected. So, the Lagrangian in eq. (1.10) reproduces correctly the eikonal expression in eq. (1.9) obtained by expanding the original QED diagram. Note that the propagator of the field h_v has only a single pole in the energy corresponding to the fermion. This is fine because the field h_v describes a fermion close to its mass-shell with momentum $m_e v^\mu + q^\mu$ where q is the momentum of a soft photon. In this situation anti-fermions cannot arise as external particles and their effects are going to be absorbed into the Wilson coefficients of the theory.

We need more than one of the recently defined fermion fields to describe all the fermions in the problem. So, we should introduce copies of the fermion field h_v to take into account the different velocities of the fermions. Thus, we write the effective Lagrangian as

$$\mathcal{L}_{\text{eff}} = \sum_{i=1}^{4} \bar{h}_{v_i}(x)\, iv_i \cdot D\, h_{v_i}(x) - \frac{1}{4}F_{\mu\nu}F^{\mu\nu} + \mathcal{L}_{\text{int}}, \qquad (1.11)$$

where the velocities are defined as $v_i^\mu = p_i^\mu/m_e$. There are some interesting features of this Lagrangian that will be also present in the SCET one. First of all, the Lagrangian depends on reference vectors along the directions of the energetic particles. In SCET we will see that light-cone vectors in the directions of the massless particles are used. On the other hand, we need different fields to represent fermions in different directions in the effective theory but they are described with the same field as in usual QED. In this case they are modes of the full field used in QED, living in small momentum region around $m_e v_i^\mu$. The same will happen in SCET.

Now we should study the interaction term, $\mathcal{L}_{\text{int}}$, which has the form

$$\mathcal{L}_{\text{int}} = \sum_i C_i(\{v\}, m_e)\, \bar{h}_{v_3}(x)\Gamma_i h_{v_1}(x)\bar{h}_{v_4}(x)\Gamma_i h_{v_2}(x), \qquad (1.12)$$

where Γ_i is a basis of Dirac matrices and $\{v\} = \{v_i, i = 1, ..., 4\}$ is a set of velocity vectors. Terms with only two fermion fields in the interaction Lagrangian are zero when velocities are different. Note that in eq. (1.12) contraction of Dirac indices of the coefficients and the fermion field are implicit.

At this point, the effective Lagrangian is complete. The only object we should calculate are the coefficients C_i (Wilson coefficients). To do this, we should compute the total amplitude in QED and compare with the effective theory. We use the amputated on-shell Green's function for the process in eq. (1.3) calculated in full QED to do the matching.

Thus, our effective theory separates high and low energy energy physics. On one side, the hard scattering of the electrons is calculated in QED and is part of the Wilson coefficient, which depend on the hard scale, m_e. On the other side, low energy diagrams in the effective theory depend only on scales of order of the photon energy. We introduce a very elegant form of the low energy matrix by introducing the *Wilson line* in the direction of v_i

$$S_i(x) = \exp\left[-ie \int_{-\infty}^{0} ds\, v_i \cdot A(x + sv_i)\right]. \qquad (1.13)$$

We can see that the Wilson line introduced in eq. (1.13) reproduces the emission of an incoming electron taking the matrix element with a photon in the final state. To obtain this contribution we expand the Wilson line up to first non-vanishing order,

$$
\begin{aligned}
\langle \gamma(k)|S_i(0)|0\rangle &= -ie \int_{-\infty}^{0} ds\, v_i^{\mu} \langle \gamma(k)|A_{\mu}(sv_i)|0\rangle \\
&= -ie \int_{-\infty}^{0} ds\, v_i \cdot \varepsilon(k) e^{isv_i \cdot k} = e \frac{v_i \cdot \varepsilon(k)}{-v_i \cdot k + i0}.
\end{aligned}
\tag{1.14}
$$

Indeed, we reproduce the *eikonal* rule obtained in eq. (1.9). Analogously, we can define a Wilson line describing the radiation of an outgoing particle

$$
\bar{S}_i^{\dagger}(x) = \exp\left[-ie \int_0^{\infty} ds\, v_i \cdot A(x + sv_i)\right].
\tag{1.15}
$$

It is important to note that the Wilson line fulfills the equation

$$
v_i \cdot D S_i(x) = 0.
\tag{1.16}
$$

Now we redefine the fermion fields in the Lagrangian as

$$
h_{v_i}(x) = S_i(x)h_{v_i}^{(0)}(x),
\tag{1.17}
$$

where $h_{v_i}^{(0)}(x)$ is a new fermion field. So, introducing conditions in eqs. (1.16, 1.17) in the fermion part of the Lagrangian we have

$$
\begin{aligned}
\bar{h}_{v_i}(x)\, iv_i \cdot D h_{v_i}(x) &= \bar{h}_{v_i}^{(0)}(x) S_i^{\dagger}(x)\, iv_i \cdot D[S_i(x)h_{v_i}^{(0)}(x)] \\
&= \bar{h}_{v_i}^{(0)}(x) S_i^{\dagger}(x) S_i(x)\, iv_i \cdot \partial h_{v_i}^{(0)}(x) \\
&= \bar{h}_{v_i}^{(0)}(x)\, iv_i \cdot \partial h_{v_i}^{(0)}(x).
\end{aligned}
\tag{1.18}
$$

This result tell us that the field $h_{v_i}^{(0)}$ is a free field and we were able to remove the interactions with soft photons. The same procedure is used in SCET to decouple soft gluons. Note that while in the fermion Lagrangian the soft photons are decoupled, they are still present in the interaction part, so

$$
\mathcal{L}_{\text{int}} = \sum_i C_i(\{v\}, m_e)\, \bar{h}_{v_3}^{(0)} \bar{S}_3^{\dagger} \Gamma_i S_1 h_{v_1}^{(0)} \bar{h}_{v_4}^{(0)} \bar{S}_4^{\dagger} \Gamma_i S_2 h_{v_2}^{(0)}.
\tag{1.19}
$$

We see that this expression has Wilson lines along the directions of all particles in the scattering process.

Finally, we use the effective Lagrangian recently constructed to compute the scattering amplitude for the process in eq. (1.3), $\mathcal{M}$, where the final state contains n photons, $X_s(k) = \gamma(k_1) + ... + \gamma(k_n)$. Using the interaction Lagrangian obtained in eq. (1.19) the amplitude is written as

$$
\begin{aligned}
\mathcal{M}_{\text{int}} &= \sum_i C_i\, \bar{u}(v_3)\Gamma_i u(v_1)\, \bar{u}(v_4)\Gamma_i u(v_2) \langle X_s(k)|\bar{S}_3^{\dagger} S_1 \bar{S}_4^{\dagger} S_2|0\rangle \\
&= \mathcal{M}_{ee} \langle X_s(k)|\bar{S}_3^{\dagger} S_1 \bar{S}_4^{\dagger} S_2|0\rangle,
\end{aligned}
\tag{1.20}
$$

where $\mathcal{M}_{ee}$ is the amplitude of the process in eq. (1.3) without photons and calculated in full QED. So, we have proven that the amplitude factorizes in a hard part that takes into account purely electron-electron scattering and a soft part that takes

into account the contribution of soft photons. Analogous statements hold for soft gluons in QCD, taking into account that Wilson lines are matrices in color space.

The cross section of this process is obtained squaring the amplitude, so

$$\sigma = \mathcal{H}(m_e, \{v\})\mathcal{S}(E_s, \{v\}),\tag{1.21}$$

where the hard function is the cross section of the process without soft photons

$$\begin{aligned}\mathcal{H}(m_e, \{v\}) &= \frac{1}{2E_1 2E_2|v_1 - v_2|}\\&\times \frac{d^3p_3}{(2\pi)^3 2E_3}\frac{d^3p_4}{(2\pi)^3 2E_4}|\mathcal{M}_{ee}|^2(2\pi)^4\delta^{(4)}(p_1 + p_2 - p_3 - p_4),\end{aligned}\tag{1.22}$$

and the soft function is the Wilson line matrix element squared with the phase space constraints on the soft radiation

$$\mathcal{S}(E_s, \{v\}) = \int_{X_s} |\langle X_s|\bar{S}_3^\dagger S_1 \bar{S}_4^\dagger S_2|0\rangle|^2\theta(E_s - E_{X_s}).\tag{1.23}$$

The integral in eq. (1.23) means that one has to sum over the different multiphoton final states and integrate over their phase space. This kind of Wilson line matrix elements have the very interesting property of *exponentiation*, i.e.

$$\mathcal{S}(E_s, \{v\}) = \exp\left[\frac{\alpha}{4\pi}S^{[1]}(E_s, \{v\})\right],\tag{1.24}$$

so the all order result is obtained by exponentiating the first order result. The derivation of this formula is based in the eikonal identity

$$\frac{1}{v\cdot k_1\, v\cdot(k_1 + k_2)} + \frac{1}{v\cdot k_2\, v\cdot(k_1 + k_2)} = \frac{1}{v\cdot k_1}\frac{1}{v\cdot k_2},\tag{1.25}$$

which allows one to rewrite sums of diagrams with multiple emissions as products of diagrams with single one. In non-abelian gauge theories such as QCD, there are genuine higher order corrections since the different diagrams (and thus the different terms in l.h.s. of eq. (1.25)) have different color factors and cannot be combined. However, these higher order corrections only involve certain maximally non-abelian color structures.

Finally, we should note that the inclusive cross section is finite, but the hard and soft functions contain divergences individually. The soft function contains ultraviolet (UV) divergences which are regularized using dimensional regularization. The renormalization of these divergences gives a finite hard function but introduces a new scale μ, which is called *factorization scale*. After renormalization the factorization theorem takes the form

$$\sigma = \mathcal{H}(m_e, \{v\}, \mu)\mathcal{S}(E_s, \{v\}, \mu),\tag{1.26}$$

where the μ-dependent objects fulfill RG equations.

1.2 The method of regions

In last section we have constructed the effective Lagrangian, $\mathcal{L}_{\text{eff}}$, expanding over the soft photon momenta. This is fine for tree level diagrams but we should pay attention to what happens with loop corrections. In this section we study the part
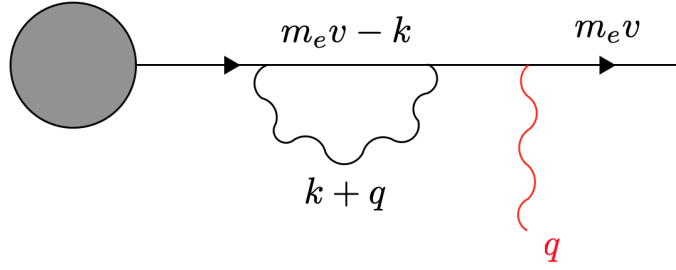
FIGURE 1.3: Loop correction to an outgoing fermion line

that gets lost in the low energy expansion and we will see that it can be recovered by expanding the loop integrals in the region of large loop momentum. This kind of expansions are part of a general technique called the *method of regions* [22, 25, 26] to expand loop integrals about various limits. As this method is used in the construction of SCET we discuss here a simple example based in the computation of the diagram in fig. 1.3. Note that for our discussion we will consider the associated scalar integral because the numerator does not include relevant compications, so we should compute

$$F = \int d^d k \frac{1}{(k+q)^2 \left[(m_e v - k)^2 - m_e^2\right]}, \tag{1.27}$$

where q is a soft photon momentum.

In the low energy theory, we assumed that $k^\mu \sim q^\mu \ll m_e$. Thus, we expand the integral in this region

$$F_{\text{low}} = \int d^d k \frac{1}{(k+q)^2} \frac{1}{-2m_e v \cdot k} \left(1 + \frac{k^2}{2m_e v \cdot k} + \dots \right). \tag{1.28}$$

This expansion produces the propagators $i/(v \cdot k)$ found in the tree-level discussion. As the loop momentum is integrated up to infinity the approximation in eq. (1.28) is no longer valid when $k^\mu \sim m_e$ or longer. Looking at the integral in eq. (1.28) we see that this expansion produces UV divergences stronger than in the original integral in eq. (1.27), but the integral are well defined in dimensional regularization. To correct the problems we consider the difference

$$
\begin{aligned}
F_{\text{high}} &= F - F_{\text{low}} \tag{1.29} \\
&= \int d^d k \frac{1}{(k+q)^2} \left[\frac{1}{(m_e v - k)^2 - m_e^2} - \frac{1}{-2m_e v \cdot k} \left(1 + \frac{k^2}{2m_e v \cdot k} + \dots \right) \right].
\end{aligned}
$$

Note that this integral has support only in the limit $k^\mu \gg q^\mu$ since the square bracket tends to zero for $k^\mu \sim q^\mu$. So, we can expand the integrand around $q^\mu = 0$ by expanding the first propagator denominator

$$
\begin{aligned}
F_{\text{high}} &= \int d^d k \frac{1}{k^2} \left(1 - \frac{q^2}{2q \cdot k} + \dots \right) \tag{1.30} \\
&\quad \times \left[\frac{1}{(m_e v - k)^2 - m_e^2} - \frac{1}{-2m_e v \cdot k} \left(1 + \frac{k^2}{2m_e v \cdot k} + \dots \right) \right].
\end{aligned}
$$

FIGURE 1.4: One loop correction to the Sudakov form factor

Dropping the scaleless integrals we get

$$F_{\text{high}} \quad = \quad \int d^d k \frac{1}{k^2} \left(1 - \frac{q^2}{2q \cdot k} + ... \right) \frac{1}{(m_e v - k)^2 - m_e^2}, \tag{1.31}$$

which is the expansion of the integrand of eq. (1.27) in $k^\mu \sim m_e \gg q^\mu$. The main message of this procedure is that we obtain the full result by performing the expansion of the integrand in two regions, integrating each term and adding the results. In our case, the relevant regions are the hard region ($k^\mu \sim m_e$) and the soft region ($k^\mu \sim q^\mu$).

1.3 SCET$_I$

1.3.1 The Sudakov form factor

The first step to understand the construction of the full effective theory, SCET, will be the study of the simplest object in which soft and collinear particles play a role, the Sudakov form factor. This object is not a physical quantity by itself but it is important and enters in many processes in collider physics. Based in the method of regions explained in section 1.2 we can study this object and explicitly see how collinear modes enter. This generalizes the cases studied in last sections where only soft modes are considered. In fig. 1.4 the one loop correction to the Sudakov form factor is considered. We define the following Lorentz invariants from the different momenta of physical particles in the diagram

$$L^2 = -l^2 - i0, \qquad P^2 = -p^2 - i0, \qquad Q^2 = -(l - p)^2 - i0 \tag{1.32}$$

and we study the form factor in the limit

$$L^2 \sim P^2 \ll Q^2, \tag{1.33}$$

which is the limit of high momentum transferred and small invariant mass. This limit is the used in hadron/jet production processes. We put a small off-shellness in the external lines due to the existence of soft and collinear emissions.

The study of the Sudakov form factor is based on finding which momentum modes are relevant and how the different components of the momenta scale comparing with the external momenta. As a tensor loop integral contains exactly the same momentum regions that its analogous scalar integral we work with the last

one

$$I = i\pi^{-d/2}\mu^{2\epsilon} \int d^d k \frac{1}{(k^2 + i0)[(k+p)^2 + i0][(k+l)^2 + i0]}, \tag{1.34}$$

where we make the usual choice in dimensional regularization for dimensions, $d = 4 - 2\epsilon$.

To perform the expansion of the integral in eq. (1.34) around the limit in eq. (1.33) we introduce two light-like reference vectors along p^μ and l^μ, in analogy with the velocity vectors v_i^μ which we introduced in the case of soft photons. Thus, our light-cone coordinates are

$$\begin{aligned} n^\mu &= (1,0,0,1) \approx p^\mu/p^0, \\ \bar{n}^\mu &= (1,0,0,-1) \approx l^\mu/l^0, \end{aligned} \tag{1.35}$$

with $n^2 = \bar{n}^2 = 0$ and $n \cdot \bar{n} = 2$[1]. Using these light-cone vectors any four vector,p^μ, can be decomposed as

$$p^\mu = n \cdot p \frac{\bar{n}^\mu}{2} + \bar{n} \cdot p \frac{n^\mu}{2} + p_\perp^\mu = p_+^\mu + p_-^\mu + p_\perp^\mu. \tag{1.36}$$

So, $(n \cdot p, \bar{n} \cdot p, p_\perp^\mu)$ are the light-cone components of the vector and we should discuss how they scale. We define a small expansion parameter

$$\lambda^2 \sim P^2/Q^2 \sim L^2/Q^2 \ll 1. \tag{1.37}$$

Note that as $p^2 = n \cdot p\,\bar{n} \cdot p + p_\perp^2$ and due to $p^2 \sim \lambda^2 Q^2$ and $p^\mu = p_-^\mu + \mathcal{O}(\lambda)$ the components of the external momenta scale as

$$\begin{aligned} p^\mu &\sim (\lambda^2, 1, \lambda)Q, \\ l^\mu &\sim (1, \lambda^2, \lambda)Q. \end{aligned} \tag{1.38}$$

Now we perform the region expansion of the integral in eq. (1.34) assigning different scales to the loop momentum k^μ and expanding in each region. The scalings that yield to non-zero contributions are

$$\begin{aligned} \text{hard} \qquad &(h) \quad (1,1,1)Q, \tag{1.39}\\ \text{collinear to } p^\mu \quad &(c) \quad (\lambda^2, 1, \lambda)Q, \\ \text{collinear to } l^\mu \quad &(\bar{c}) \quad (1, \lambda^2, \lambda)Q, \\ \text{soft} \qquad &(s) \quad (\lambda^2, \lambda^2, \lambda^2)Q, \tag{1.40} \end{aligned}$$

where the components of k^μ are $(n \cdot k, \bar{n} \cdot k, k_\perp^\mu)$. From now on, we refer to momenta which are collinear to p^μ as *collinear* and to the ones collinear to l^μ as *anti-collinear*. Since in the soft region all the components of the loop momentum scale as λ^2 we have

$$k_s^2 \sim \lambda^4 Q^2 \sim \frac{P^2 L^2}{Q^2} \ll P^2 \sim L^2, \tag{1.41}$$

that is the hierarchy shown in eq. (1.1). Since $k_s^2 \ll k_c^2$ these modes are sometimes called ultrasoft. This is to differenciate them from soft modes in other observables that scale as $(\lambda, \lambda, \lambda)Q$. The version of SCET for this situation is called SCET$_{\text{II}}$ and

---

[1]Note that in some part of the literature $n \cdot \bar{n} = 1$ is chosen.

it involves the rapidity logarithms that will be present along this thesis and we will study how to treat them. We will study SCET$_\text{II}$ later, however to make clear this introduction we limit ourselves to the present case, SCET$_\text{I}$.

Now we expand the integrand of eq. (1.34) in the different regions up to leading power. To get the leading power in the hard region we simply set all the suppressed components of momenta to zero, i.e. $p^\mu \to p^\mu_-$ and $l^\mu \to l^\mu_+$. So,

$$
\begin{aligned}
I_h &= i\pi^{-d/2}\mu^{2\epsilon}\int d^d k \frac{1}{(k^2+i0)(k^2+2k_-\cdot l_+ + i0)(k^2+2k_+\cdot p_-+i0)}\\
&= \frac{\Gamma(1+\epsilon)}{2l_+\cdot p_-}\frac{\Gamma^2(-\epsilon)}{\Gamma(1-2\epsilon)}\left(\frac{\mu^2}{2l_+\cdot p_-}\right)^\epsilon
\end{aligned} \tag{1.42}
$$

Expanding the integral in the collinear region implies that integration momentum scales as $k^\mu \sim (\lambda^2, 1, \lambda)Q$ and $k^2 \sim \lambda^2 Q^2$. So, we can expand $(k+l)^2 = 2k_-\cdot l_+ + \mathcal{O}(\lambda^2)$. The integral we should compute is

$$
\begin{aligned}
I_c &= i\pi^{-d/2}\mu^{2\epsilon}\int d^d k \frac{1}{(k^2+i0)(2k_-\cdot l_+ + i0)[(k+p)^2+i0]}\\
&= -\frac{\Gamma(1+\epsilon)}{2l_+\cdot p_-}\frac{\Gamma^2(-\epsilon)}{\Gamma(1-2\epsilon)}\left(\frac{\mu^2}{P^2}\right)^\epsilon.
\end{aligned} \tag{1.43}
$$

Note that the contribution to the anticollinear integral is obtained replacing $P^2 \to L^2$ in eq. (1.43).

The only missing contribution is the expansion of the integral in the soft region, where we can expand $(k+l)^2 = 2k_-\cdot l_+ + l^2 + \mathcal{O}(\lambda^3)$ and $(k+p)^2 = 2k_+\cdot l_- + p^2 + \mathcal{O}(\lambda^3)$. Thus, we obtain

$$
\begin{aligned}
I_s &= i\pi^{-d/2}\mu^{2\epsilon}\int d^d k \frac{1}{(k^2+i0)(2k_-\cdot l_+ + i0)(2k_+\cdot p_-+p^2+i0)}\\
&= -\frac{\Gamma(1+\epsilon)}{2l_+\cdot p_-}\Gamma(\epsilon)\Gamma(-\epsilon)\left(\frac{2l_+\cdot p_-\mu^2}{L^2 P^2}\right)^\epsilon.
\end{aligned} \tag{1.44}
$$

Adding the results for the different integrals calculated we find the final result

$$
I_\text{tot} = I_h + I_c + I_{\bar{c}} + I_s = \frac{1}{Q^2}\left(\ln\frac{Q^2}{L^2}\ln\frac{Q^2}{P^2}+\frac{\pi^2}{3}\right), \tag{1.45}
$$

that is finite and reproduces the leading power of the expansion of the full integral in eq. (1.34).

1.3.2 Effective Lagrangian

The exercise done in the last section teaches us to identify the relevant momentum regions for the Sudakov problem. Now we work analogously to section 1.1 to write an effective Lagrangian whose Feynman rules reproduce the diagrams obtained using the method of region expansion.

1.3.2.1 Scaling of the fields

We introduce effective theory fields whose momenta scale as appropriate for each momentum region. Thus, for quark and gluons fields we can substitute

$$\psi \quad \rightarrow \quad \psi_c + \psi_{\bar{c}} + \psi_s, \tag{1.46}$$

$$A^\mu \quad \rightarrow \quad A_c^\mu + A_{\bar{c}}^\mu + A_s^\mu, \tag{1.47}$$

in the QCD Lagrangian, then remove the suppressed terms and read off the effective Lagrangian. Of course this is valid at tree-level. At loop level some matching corrections arise but can be fixed modifying the coefficients of tree-level operators. These matching corrections only affect the terms involving both collinear and anticollinear fields. So, to construct the purely soft and collinear Lagrangian the tree-level substitution for fields is fine.

Both fermion and gauge fields have several components, which scale differently with the expansion parameter λ. To study the scaling of the fields we consider the propagators. We start with the gluon propagator

$$\langle 0|T\{A_\mu^a(x)A_\nu^b(0)\}|0\rangle = \int \frac{d^4p}{(2\pi)^4} \frac{i}{p^2+i0} e^{-ip\cdot x} \left[-g_{\mu\nu} + \xi \frac{p_\mu p_\nu}{p^2}\right] \delta^{ab}, \tag{1.48}$$

where a, b are the color indices of the fields. in the following we work with $A_\mu = A_\mu^a t^a$, where t^a are the generators of $SU(N)$, to keep color implicit. The position x^μ is the Fourier conjugate of the momentum p^μ so $p \cdot x \sim \mathcal{O}(\lambda^0)$. The part of the propagator that involves the gauge parameter ξ scales like $d^4/(p^2)^2 p_\mu p_\nu \sim p_\mu p_\nu$. As gauge symmetry transforms as their associated momentum we expect that in a general gauge $A_\mu \sim p_\mu$. For soft and collinear gluons the field components scale as

$$(n \cdot A_s, \bar{n} \cdot A_s, A_{s\perp}^\mu) \quad \sim \quad (\lambda^2, \lambda^2, \lambda^2), \tag{1.49}$$

$$(n \cdot A_c, \bar{n} \cdot A_c, A_{c\perp}^\mu) \quad \sim \quad (\lambda^2, 1, \lambda). \tag{1.50}$$

From the scaling we see that in terms including soft and collinear gluons, the soft gluons are power suppressed except for the contribution from the $n \cdot A_s$ component.

We do the same exercise with the fermion propagator. For a soft fermion the propagator is written as

$$\langle 0|T\{\psi_s(x)\bar{\psi}_s(0)\}|0\rangle = \int \frac{d^4p}{(2\pi)^4} \frac{i\slashed{p}}{p^2+i0} e^{-ip\cdot x} \sim (\lambda^2)^4 \frac{\lambda^2}{\lambda^4} = \lambda^6. \tag{1.51}$$

From this propagator we see that soft fermions scale as $\psi_s(x) \sim \lambda^3$. The collinear case is more complicated because the numerator of the propagator should be decomposed as

$$\slashed{p} = n \cdot p \frac{\slashed{\bar{n}}}{2} + \bar{n} \cdot p \frac{\slashed{n}}{2} + \slashed{p}_\perp \tag{1.52}$$

and the three terms have different scaling. This implies that different parts of the field scale differently. So, one splits the fermion field into two parts

$$\psi = \xi_c + \eta_c = P_+\psi + P_-\psi, \tag{1.53}$$

where we have define the projectors

$$P_+ = \frac{\not{n}\not{\bar{n}}}{4}, \qquad P_- = \frac{\not{\bar{n}}\not{n}}{4},$$ (1.54)

which fulfills the properties $P_+ + P_- = 1$ and $P_\pm^2 = P_\pm$. Now we can investigate the propagators of these fields, so

$$
\begin{aligned}
\langle 0|T\{\xi_c(x)\bar{\xi}_c(0)\}|0\rangle &= \int \frac{d^4p}{(2\pi)^4} e^{-ip\cdot x} \frac{\not{n}\not{\bar{n}}}{4} \frac{i\not{p}}{p^2 + i0} \frac{\not{\bar{n}}\not{n}}{4} \\
&= \int \frac{d^4p}{(2\pi)^4} e^{-ip\cdot x} \frac{i\bar{n}\cdot p\frac{\not{n}}{2}}{p^2 + i0} \sim \frac{\lambda^4}{\lambda^2} = \lambda^2.
\end{aligned}
$$ (1.55)

Thus, we can observe that $\xi_c \sim \lambda$. Repeating the exercise for η_c we observe that $\eta_c \sim \lambda^2$. From these results we see that soft fermions are suppressed with respect to collinear ones.

1.3.2.2 Effective Lagrangian at leading power

Once we know how the fields scale with the expansion parameter we can insert the decomposition shown in eq. (1.46) into the full QCD action and we get the tree-level effective action and Lagrangian,

$$S = S_s + S_c + S_{\bar{c}} + S_{c+s} + S_{\bar{c}+s} + \dots,$$ (1.56)

where the different terms are collected in terms of their content. S_s contains purely the soft terms, S_c the collinear terms and S_{c+s} describes the collinear-soft interactions. Anticollinear terms are obtained from collinear ones with simple substitutions, thus we suppress a dedicated study on them.

The soft part of the action has the same form that the total QCD action, but replacing the QCD fields by soft ones,

$$S_s = \int d^4x\, \bar{\psi}_s i\not{D}_s \psi_s - \frac{1}{4}(F_{\mu\nu}^{s,a})^2,$$ (1.57)

where the covariant derivative is $iD_s^\mu = i\partial^\mu + A_s^\mu$ and the soft field strength tensor $F_{\mu\nu}^{s,a}$ is built from this derivative. Note that all terms in the action are $\mathcal{O}(\lambda^0)$ since the integration measure $d^4x \sim \mathcal{O}(\lambda^{-8})$.

Next, we consider the collinear part of the action that is again a simple copy of the full QCD one but with $\psi_c = \xi_c + \eta_c$. Thus,

$$
\begin{aligned}
S_c &= \int d^4x(\bar{\xi}_c + \bar{\eta}_c)\left[\frac{\not{n}}{2}i\bar{n}\cdot D_c + \frac{\not{\bar{n}}}{2}in\cdot D_c + i\not{D}_{c\perp}\right](\xi_c + \eta_c) - \frac{1}{4}(F_{\mu\nu}^{c,a})^2 \\
&= \int d^4x\, \bar{\xi}_c\frac{\not{\bar{n}}}{2}in\cdot D_c\xi_c + \bar{\xi}_c i\not{D}_{c\perp}\eta_c + \bar{\eta}_c i\not{D}_{c\perp}\xi_c + \bar{\eta}_c\frac{\not{n}}{2}i\bar{n}\cdot D_c\eta_c - \frac{1}{4}(F_{\mu\nu}^{c,a})^2.
\end{aligned}
$$ (1.58)

This form of the collinear action is not convenient because it includes large and small components of the collinear fermion field, mixing each other. It is simple to avoid this complication integrating over the smallest one. As the action is quadratic in η_c

we can integrate over this field exactly. So, we perform the shift

$$\eta_c \rightarrow \eta_c - \frac{\slashed{\bar{n}}}{2} \frac{1}{i\bar{n} \cdot D_c} i\slashed{D}_{c\perp} \xi_c \tag{1.59}$$

to complete the square in the action S_c. Then, the action takes the form

$$S_c = \int d^4x \bar{\xi}_c \left[in \cdot D_c + i\slashed{D}_{c\perp} \frac{1}{i\bar{n} \cdot D_c} i\slashed{D}_{c\perp} \right] \xi_c - \frac{1}{4}(F^{c,a}_{\mu\nu})^2 + \bar{\eta}_c \frac{\slashed{\bar{n}}}{2} i\bar{n} \cdot D_c \eta_c \tag{1.60}$$

that can be integrated over the field η_c. This integration leaves a $\det \left(\frac{\slashed{\bar{n}}}{2} i\bar{n} \cdot D_c \right)$ that can be done (as the inverse derivative in eq. (1.59)) adopting an $i0$ prescription for the $i\bar{n} \cdot D_c$ operator. The prescription does not introduce physical consequences because it concerns the region close to $\bar{n} \cdot p = 0$, while the effective theory study the region $\bar{n} \cdot p = Q$. The determinant is trivial and this fact can be seen evaluating in light-cone gauge, where $\bar{n} \cdot A_c = 0$, and noting that it is gauge invariant. After dropping the trivial determinant, the collinear SCET action is given by

$$S_c = \int d^4x \bar{\xi}_c \left[in \cdot D_c + i\slashed{D}_{c\perp} \frac{1}{i\bar{n} \cdot D_c} i\slashed{D}_{c\perp} \right] \xi_c - \frac{1}{4}(F^{c,a}_{\mu\nu})^2. \tag{1.61}$$

Finally we consider the soft-collinear effective action, S_{s+c}. The general construction of these type of terms is involved and it is performed in position space formalism in [27] but we restrict ourselves to study the leading power terms. So, we should take into account some considerations: ψ_s is power suppressed compared to the collinear fermion fields, so there are no soft fermion fields in leading power interactions with collinear fields. Also, as $\bar{n} \cdot A_s$ and $A^\mu_{s\perp}$ are power suppressed compared to their collinear counterparts only terms with $n \cdot A_s$ arises. Thus, these conditions imply that the leading power term of S_{s+c} is obtained substituting

$$A^\mu_c \rightarrow A^\mu_c + n \cdot A_s \frac{\bar{n}^\mu}{2} \tag{1.62}$$

in S_c. To get the final result we should perform a derivative expansion in the resulting action which corresponds to the expansion in small momentum components. Thus, we consider the interaction of a soft gluon with a collinear fermion

$$S_{s+c} = \int d^4x \bar{\xi}_c(x) \frac{\slashed{\bar{n}}}{2} n \cdot A_s(x) \xi_c(x), \tag{1.63}$$

which arises from the substitution of the condition in eq. (1.62) in S_c action in eq. (1.61). The momentum is given by a soft and a collinear momentum which scales like a collinear one so x^μ is conjugate to a collinear momentum. Explicitly, this implies the scaling

$$\begin{aligned}
p^\mu_c + p^\mu_s \sim p^\mu_c \quad &\sim \quad (\lambda^2, 1, \lambda), \\
x^\mu \quad &\sim \quad (1, \lambda^{-2}, \lambda^{-1}),
\end{aligned} \tag{1.64}$$

coming from the fact that

$$p_c \cdot x = \frac{1}{2}n \cdot p_c \bar{n} \cdot x + \frac{1}{2}\bar{n} \cdot p_c n \cdot x + p_{c\perp} \cdot x_\perp \sim 1, \tag{1.65}$$

$$p_s \cdot x = \frac{1}{2}n \cdot p_s \bar{n} \cdot x + \frac{1}{2}\bar{n} \cdot p_s \bar{n} \cdot x + p_{s\perp} \cdot x_\perp \tag{1.66}$$

$$= p_{s+} \cdot x_- + p_{s-} \cdot x_+ + p_{s\perp} \cdot x_\perp, \tag{1.67}$$

where only the term involving x_- is leading power. Thus, we expand the action S_{s+c} into a Taylor series

$$S_{s+c} = \int d^4x \, \bar{\xi}_c(x) \frac{\slashed{\bar{n}}}{2} \xi_c(x) \left[1 + x_\perp \cdot \partial_\perp + x_+ \cdot \partial_+ + ... \right] n \cdot A_s(x) \Big|_{x=x_-} \tag{1.68}$$

$$= \int d^4x \, \bar{\xi}_c(x) \frac{\slashed{\bar{n}}}{2} \xi_c(x) n \cdot A_s(x_-) + \mathcal{O}(\lambda),$$

because all the terms with derivatives in eq. (1.68) result in subleading terms. This expansion is called *multipole expansion* in [21]. In the original SCET papers [19, 20] a different method is used to expand in small momentum limit. In this approach, one splits the momentum in a large and a small components and treats the large components in Fourier space and the small ones in position space. This is similar to the procedure used in the study of soft photons, where we split the electron momentum into $p^\mu = m_e v^\mu + k^\mu$ and we expand over the soft residual momentum k^μ. Thus, the position dependence of the field $h_v(x)$ is conjugate to the residual momentum k^μ and the large part $m_e v^\mu$ is used as a label on the field, $h_v(x)$. This hybrid position and space formulation of SCET is called *label formalism*. Further details about this formalism not covered in this introduction can be found in [28].

Once we have studied the different terms of the SCET effective action we arrive to the final expression for the leading power SCET Lagrangian,

$$\mathcal{L}_{\text{SCET}} = \bar{\psi}_s i \slashed{D}_s \psi_s + \bar{\xi}_s \frac{\slashed{\bar{n}}}{2} \left[i n \cdot D + i \slashed{D}_{c\perp} \frac{1}{i \bar{n} \cdot D_c} i \slashed{D}_{c\perp} \right] \xi_c - \frac{1}{4} \left(F_{\mu\nu}^{s,a} \right)^2 - \frac{1}{4} \left(F_{\mu\nu}^{c,a} \right)^2, \tag{1.69}$$

where soft and collinear covariant derivatives are involved

$$i D_\mu^s = i \partial_\mu + g A_\mu^s(x), \qquad i D_\mu^c = i \partial_\mu + g A_\mu^c(x), \tag{1.70}$$

and also the mixed covariant derivative

$$i n \cdot D = i n \cdot \partial + g \, n \cdot A_c(x) + g \, n \cdot A_s(x_-). \tag{1.71}$$

The soft and collinear strength tensors are defined as usual

$$i g F_{\mu\nu}^{s,a} t^a = \left[i D_\mu^s, i D_\nu^s \right], \qquad i g F_{\mu\nu}^{c,a} t^a = \left[i D_\mu, i D_\nu \right], \tag{1.72}$$

where the covariant derivative that appears in the second commutator is defined as

$$D^\mu = n \cdot D \frac{\bar{n}^\mu}{2} + \bar{n} \cdot D_c \frac{n^\mu}{2} + D_{c\perp}^\mu. \tag{1.73}$$

We stated above that we do not consider terms involving $\bar{c}$ fields in the effective Lagrangian, but they can be obtained from the ones involving c fields with the substitutions $n \leftrightarrow \bar{n}$ and $x_- \leftrightarrow x_+$.

1.3.2.3   Gauge transformations

In this section we briefly discuss gauge transformations of the effective Lagrangian recently studied. As we split the gauge field into different soft and collinear components, we consider different gauge transformations

$$\text{soft:} \qquad V_s(x) \;=\; \exp\left[i\alpha_s^a(x)t^a\right], \qquad\qquad (1.74)$$

$$\text{collinear:} \qquad V_c(x) \;=\; \exp\left[i\alpha_c^a(x)t^a\right], \qquad\qquad (1.75)$$

where the gauge transformations scale as their associated fields $\partial\alpha_s^a(x) \sim \lambda^2\alpha_s^a(x)$ and $\partial_\mu\alpha_c^a(x) \sim (\lambda^2, 1, \lambda)\alpha_c^a(x)$. The soft gauge transformation act over the soft fields as usual,

$$\psi_s(x) \;\rightarrow\; V_s(x)\psi_s(x), \qquad\qquad (1.76)$$

$$A_s^\mu(x) \;\rightarrow\; V_s(x)A_s^\mu(x)V_s^\dagger(x) + \frac{i}{g}V_s(x)\partial_\mu V_s^\dagger(x), \qquad\qquad (1.77)$$

so the soft covariant derivative transforms as $D_s^\mu(x) \rightarrow V_s(x)D_s^\mu V_s^\dagger(x)$. On the other hand, the soft gauge transformations act over collinear fields as

$$\psi_c(x) \;\rightarrow\; V_s(x_-)\psi_c(x), \qquad\qquad (1.78)$$

$$A_c^\mu(x) \;\rightarrow\; V_s(x_-)A_c^\mu(x)V_s^\dagger(x_-). \qquad\qquad (1.79)$$

Note that the multipole expansion is used and we have replaced $x \rightarrow x_-$ in the soft fields. Without this expansion a tower of inconvenient power corrections would appear. Also, the gauge collinear field transforms as a matter field, without an inhomogeneous term. This ensures that the mixed covariant derivative transforms at it should be, $D^\mu \rightarrow V_s(x_-)D^\mu(x)V_s^\dagger(x_-)$.

Now we consider the collinear gauge transformation over collinear and soft fields. Soft fields remain invariant under these transformations while collinear fields transform as usual

$$\xi_c(x) \rightarrow V_c(x)\xi_c(x), \qquad D^\mu \rightarrow V_c(x)D^\mu V_c^\dagger(x), \qquad\qquad (1.80)$$

$$\psi_s(x) \rightarrow \psi_s(x), \qquad\qquad D_s^\mu \rightarrow D_s^\mu, \qquad\qquad (1.81)$$

$$A_c^\mu \rightarrow V_c(x)A_c^\mu V_c^\dagger(x) + \frac{1}{g}V_c(x)\left[i\partial^\mu + g\frac{\bar{n}^\mu}{2}n \cdot A_s(x_-), V_c^\dagger(x)\right]. \qquad\qquad (1.82)$$

Once we know the transformation of the covariant derivatives is straightforward to verify that the effective Lagrangian in eq. (1.69) is invariant under both soft and collinear gauge transformations.

1.3.3   The SCET vector current

We have constructed terms in the effective Lagrangian which describe the interaction between soft, (anti)collinear and (anti)collinear-soft fields. What is missing are operators describing the interaction between collinear and anticollinear fields. In the Sudakov problem only the electromagnetic current connects both fields. The necessary hard momentum transferred is provided by the external virtual photon. The tree-level diagram in QCD can be replaced by the SCET operator

$$J^\mu = \bar{\psi}\gamma^\mu\psi \rightarrow \bar{\xi}_c\gamma^\mu\xi_{\bar{c}}. \qquad\qquad (1.83)$$

Due to the projection properties of the collinear fermion fields we simplify the operator in eq. (1.83) as

$$\bar{\xi}_c \gamma^\mu \xi_{\bar{c}} = \bar{\xi}_c \left[n^\mu \frac{\bar{\slashed{n}}}{2} + \bar{n}^\mu \frac{\slashed{n}}{2} + \gamma_\perp^\mu \right] \xi_{\bar{c}} = \bar{\xi}_c \gamma_\perp^\mu \xi_{\bar{c}}. \tag{1.84}$$

However, this operator is insufficient when one wants to make loop calculations or introduce collinear gluons. Usually operators with derivatives are power suppressed but in SCET the derivatives corresponding to the large momentum component of the collinear fields i.e. in general $\bar{n} \cdot \partial \phi_c \sim \lambda^0 Q \phi_c$. So, to construct the more general gauge invariant operator at leading power we consider the series

$$\phi_c(x + t\bar{n}) = \sum_{n=0}^\infty \frac{t^n}{n!} (\bar{n} \cdot \partial)^n \phi_c(x). \tag{1.85}$$

We insert this expansion into a convolution obtaining

$$\int dt C(t) \phi_c(x + t\bar{n}) = \sum_{n=0}^\infty \frac{C_n}{n!} (\bar{n} \cdot \partial)^n \phi_c(x), \tag{1.86}$$

where C_n is the n-th moment of the coefficient function

$$C_n = \int dt C(t) t^n. \tag{1.87}$$

So, instead of including an arbitrary number of derivatives we smear the field ϕ_c along the light-cone as in eq. (1.86). The function $C(t)$ encodes the information about the Wilson coefficients of the higher derivative operators. With the smearing of this field the operator becomes non-local and we should be careful to maintain gauge invariance. We consider the operator that defines the quark parton distribution function

$$\bar{\xi}_c(x + t\bar{n}) [x + t\bar{n}, x] \frac{\slashed{n}}{2} \xi_c(x). \tag{1.88}$$

This operator is not gauge invariant. To solve this problem we need to transport the gauge transformation at point x to the point $x + t\bar{n}$. This can be achieved using the collinear version of the already known Wilson line

$$[x + t\bar{n}, x] = \mathbf{P} \exp \left[ig \int_0^t dt' \, \bar{n} \cdot A_c(x + t\bar{n}) \right]. \tag{1.89}$$

Note that the exponent is a color matrix, so the symbol $\mathbf{P}$ specifies an ordering prescription. The path ordering defines that the color matrix at later time is to the left to the earlier ones. The Wilson line transforms under gauge transformations as

$$[x + t\bar{n}, x] \rightarrow V_c(x + t\bar{n}) [x + t\bar{n}, x] V_c^\dagger(x), \tag{1.90}$$

which renders the operator in eq. (1.88) gauge invariant. In SCET is useful to define a Wilson line running from infinity along $\bar{n}^\mu$ to x^μ as

$$W_c(x) = [x, x - \infty \bar{n}], \tag{1.91}$$

so a Wilson line defined over a finite segment can be written as

$$[x + t\bar{n}, x] = W_c(x + t\bar{n})W_c^\dagger(x).\tag{1.92}$$

This means that to go from x to $x + t\bar{n}$ we first move from x to infinity and then back to $x + t\bar{n}$. The segment that we travel in both directions drops out by unitarity of the matrix, leaving the finite matrix element. With the Wilson line, $W_c(x)$ we can define the *building blocks*

$$\chi_c(x) \equiv W_c^\dagger(x)\xi_c(x),\tag{1.93}$$
$$\mathcal{A}_c^\mu \equiv W_c^\dagger D_c^\mu W_c,\tag{1.94}$$

which are invariant under collinear gauge transformations that vanish at infinity. These building blocks allow us to easily construct gauge-invariant SCET operators. Later, we will introduce the soft Wilson line to decouple soft interactions as we did in eq. (1.13).

Now we can write the more general SCET current operator at leading power. So,

$$J^\mu(0) = \int ds \int dt\, \tilde{C}_V(s,t)\bar{\chi}_c(t\bar{n})\gamma_\perp^\mu\chi_{\bar{c}}(sn).\tag{1.95}$$

Note that at leading order the matching coefficient $\tilde{C}_V(s,t) = \delta(s)\delta(t)$ in order to reproduce eq. (1.84). We should take into account that the Fourier transform of the coefficient encodes a dependence only on the large component of the momentum transferred, $Q^2 = n \cdot l\, \bar{n} \cdot p$. In order to see this, we shift the field to the origin $x = 0$ with the momentum operator and we take the matrix element between a state with an incomng quark with momentum l^μ and a outgoing quark with momentum p^μ,

$$\begin{aligned}\langle q(p)|J^\mu(0)|q(l)\rangle &= \int ds \int dt\, \tilde{C}_V(s,t)e^{-isn\cdot l}e^{it\bar{n}\cdot p}\bar{u}(p)\gamma_\perp^\mu u(l) &(1.96)\\ &= C_V(n \cdot l\, \bar{n} \cdot p)\bar{u}(p)\gamma_\perp^\mu u(l).\end{aligned}$$

We observe that the Fourier transform of the Wilson coefficient, C_V, only depends on $Q^2 = n \cdot l\, \bar{n} \cdot p$ as we notice before. This fact derives also from the fact that SCET is invariant under a rescaling $n^\mu \rightarrow \alpha n^\mu$ and $\bar{n}^\mu \rightarrow 1/\alpha\bar{n}^\mu$, which is known as *reparametrization invariance* [29]. This makes the physics independent of the exact choice of the reference vectors used to set up the effective theory.

1.3.4   Application: one-loop result of C_V

At this point, we briefly discuss the determination of the explicit one-loop contribution of C_V. The Feynman diagrams we should consider are shown in fig. 1.5. In addition to loop diagrams involving (anti)collinear fields and soft exchanges, there is a contribution from the one-loop correction to the Wilson coefficient. The vertices in which an (anti)collinear gluon is emitted from the current are obtained after expanding the Wilson line in the building blocks in terms of the coupling. The diagrams are in one to one correspondence to the diagrams computed when we studied the method of regions for Sudakov factor except for the fact that in that case we left out the numerators of the diagrams, and now we have to include them. Setting the low energy scales P^2 and L^2 to zero the soft and collinear integrals become scaleless. In this way the full theory becomes equal to the hard region and on the effective theory side only the one loop contribution of the Wilson coefficient remains. Thus, we extract the Wilson coefficient computing the on-shell form factor with $P^2 = L^2 = 0$.
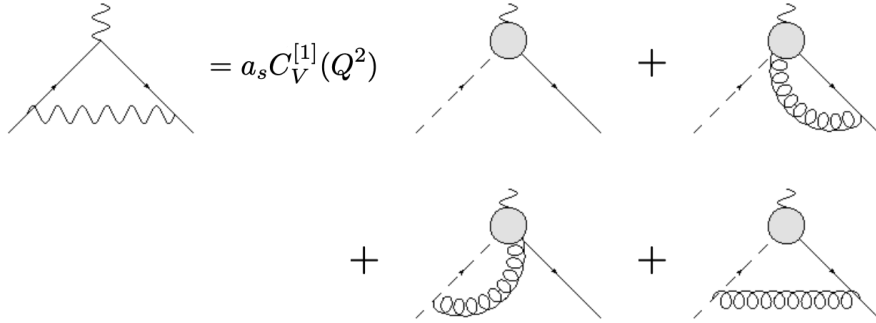
FIGURE 1.5: Diagrams contributing to the one loop Sudakov form factor in SCET. The Feynman rules for gluons emitted from the current are obtained after the expansion of the collinear Wilson lines in the strong coupling, g.

We obtain then the *bare* Wilson coefficient

$$C_V^{\text{bare}}(\epsilon, Q^2) = 1 + a_s(\mu)C_F\left(-\frac{2}{\epsilon^2} - \frac{3}{\epsilon} + \frac{\pi^2}{6} - 8 + \mathcal{O}(\epsilon)\right)\left(\frac{Q^2}{\mu^2}\right)^{-\epsilon} + \mathcal{O}(a_s^2), \quad (1.97)$$

where $a_s(\mu) = \alpha_s(\mu)/(4\pi)$ and the color structure is given by $t^a t^a = C_F \mathbf{1} = (N_c^2 - 1)/(2N_c)\mathbf{1}$. As this is the bare coefficient we still have to renormalize it, absorbing the divergences into a multiplicative $Z-$factor,

$$C_V(Q^2, \mu^2) = Z^{-1}(\epsilon, Q^2, \mu)C_V^{\text{bare}}(\epsilon, Q^2). \quad (1.98)$$

So, we have the renormalized result

$$C_V(Q^2, \mu^2) = 1 + a_s(\mu)C_F\left(-\ln^2\frac{Q^2}{\mu^2} + 3\ln\frac{Q^2}{\mu^2} + \frac{\pi^2}{6} - 8\right) + \mathcal{O}(a_s^2). \quad (1.99)$$

The unusual feature of this calculation in comparison with another analogous calculations in quantum field theory is the emergence of a $1/\epsilon^2$ divergence. This divergence arises because we have both soft and collinear divergences. As a consequence, the Wilson coefficient contains double logarithms and the anomalous dimension that governs the RG equation of the Wilson coefficient contains a logarithmic part,

$$\frac{d}{d\ln\mu}C_V(Q^2, \mu) = \left[\Gamma_{\text{cusp}}(a_s)\ln\frac{Q^2}{\mu^2} + \gamma_V(a_s)\right]C_V(Q^2, \mu). \quad (1.100)$$

The cusp (Γ_{cusp}) and non-cusp (γ_V) anomalous dimensions are known up to $\mathcal{O}(a_s^4)$. Their explicit expressions up to three-loops are given in appendix A and the four-loop result has been recently obtained in [30]. The matching coefficient C_V is also known up to the same accuracy [31, 32] and the explicit results used along this thesis (up to $\mathcal{O}(a_s^2)$) are given in appendix A as well. The presence of this extra logarithm in the anomalous dimension is a distinguishing feature of the RG equation in eq. (1.100). It is important to note that the dependence on this logarithm is only linear, so the expansion of the anomalous dimensions is not spoiled by the presence of large logarithms. We study the origin of this linearity in the next section.

The last point we should study is the decoupling of the soft radiation from the collinear fields. As we did with soft effective theory the soft radiation can be decoupled by considering the soft Wilson line

$$S_n(x) = \mathbf{P} \exp\left[ig \int_{-\infty}^{0} ds\, n \cdot A_s(x + sn) \right], \tag{1.101}$$

which fulfills the equation $n \cdot D_s S_n(x) = 0$. At this point, we can redefine the collinear fields as

$$\xi_c = S_n(x_-)\xi_c^{(0)}, \tag{1.102}$$
$$A_c^\mu = S_n(x_-)A_c^{(0)\mu}S_n^\dagger(x_-). \tag{1.103}$$

So the soft-collinear interaction term becomes

$$\mathcal{L}_{c+s} = \bar{\xi}_c \frac{\bar{\slashed{n}}}{2} in \cdot D\xi_c = \bar{\xi}_c \frac{\bar{\slashed{n}}}{2}(in \cdot D_s + n \cdot A_c)\xi_c \tag{1.104}$$

$$= \bar{\xi}_c^{(0)} \frac{\bar{\slashed{n}}}{2}(in \cdot \partial_s + n \cdot A_c^{(0)})\xi_c^{(0)} = \bar{\xi}_c^{(0)} \frac{\bar{\slashed{n}}}{2}in \cdot D_c^{(0)}\xi_c^{(0)}, \tag{1.105}$$

where the decoupling has removed the soft-collinear interactions from the leading power Lagrangian. Performing an analogous decoupling for the anticollinear fields, the SCET effective Lagrangian takes the form

$$\mathcal{L}_{\text{SCET}} = \mathcal{L}_c^{(0)} + \mathcal{L}_{\bar{c}}^{(0)} + \mathcal{L}_s, \tag{1.106}$$

which tells us that we are dealing with independent theories fo soft and collinear particles. Also, the states separate as

$$|X\rangle = |X_c\rangle \otimes |X_{\bar{c}}\rangle \otimes |X_s\rangle. \tag{1.107}$$

As in the soft photon case, this does not mean that the soft radiation is totally removed. It is manifested as soft Wilson lines along the direction of energetic particles. For example, the vector current is rewritten as

$$\bar{\chi}_c(t\bar{n})\gamma_\perp^\mu \chi_{\bar{c}}(sn) = \bar{\chi}_c^{(0)}(t\bar{n})\bar{S}_n^\dagger(0)\gamma_\perp^\mu S_{\bar{n}}(0)\chi_{\bar{c}}(sn). \tag{1.108}$$

1.3.5   Resummation by renormalization group evolution

In the decoupled theory, the form factor studied above can be written in its factorized form

$$\mathcal{F}(Q^2, L^2, P^2) = C_V(Q^2, \mu)F(P^2, \mu)\bar{F}(L^2, \mu)S(\Lambda_s^2, \mu), \tag{1.109}$$

which can be understood graphically with the help of fig. 1.6. The collinear and anticollinear functions F and $\bar{F}$ are identical and the soft function has a scale $\Lambda_s^2 = L^2P^2/Q^2$.

Each of these objects fulfill individual RG equations. Solving them one can resum the large perturbative logarithms that arise in the fixed order calculations. This is done evaluating each function in eq. (1.109) at its natural scale and evolving them to a common reference scale where they are combined. In this way, logarithms as $\alpha^n \ln^m(Q^2/p^2)$ with $m \leq 2n$ and $p^2 = P^2, L^2, Q^2$ are resummed, preventing us to spoil the standard perturbative expansion of these objects. It is characteristic that in
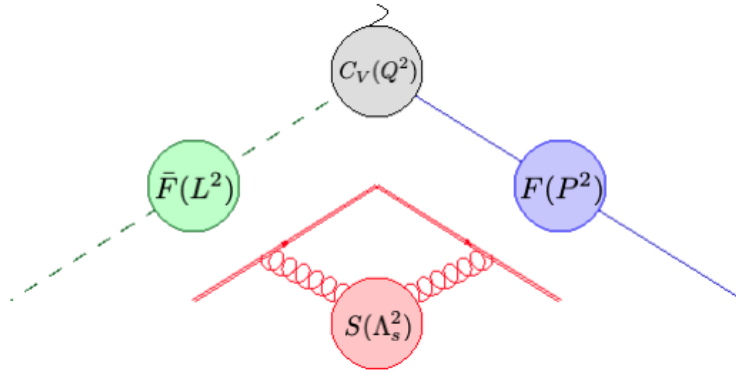
FIGURE 1.6: Factorized form of the Sudakov form factor.

processes as the one presented in fig. 1.6 logarithms with $m = 2n$ appear. They are known as *Sudakov* logarithms and are the result of an interplay of soft and collinear physics.

We have indicated that all the matrix elements in the effective theory depend on the renormalization scale, μ. This dependence must cancel in the product in eq. (1.109), so the sum of the anomalous dimensions of the ingredients should be zero. In eq. (1.100) we gave a RG equation for the Wilson coefficient and here we show the RG equations corresponding to collinear and soft factors,

$$\frac{d}{d\ln\mu}F(P^2, \mu) = -\left[\Gamma_{\text{cusp}}(a_s)\ln\frac{P^2}{\mu^2} + \gamma_F(a_s)\right]F(P^2, \mu), \qquad (1.110)$$

$$\frac{d}{d\ln\mu}S(\Lambda_s^2, \mu) = \left[\Gamma_{\text{cusp}}(a_s)\ln\frac{\Lambda_s^2}{\mu^2} + \gamma_S(a_s)\right]S(\Lambda_s^2, \mu). \qquad (1.111)$$

So, the fact that $\mathcal{F}$ is independent of μ implies

$$\Gamma_{\text{cusp}}(a_s)\ln\frac{Q^2}{\mu^2} + \gamma_V(a_s) - \Gamma_{\text{cusp}}(a_s)\left(\ln\frac{P^2}{\mu^2} + \ln\frac{L^2}{\mu^2}\right) - 2\gamma_F(a_s) \qquad (1.112)$$

$$+\Gamma_{\text{cusp}}(a_s)\ln\frac{\Lambda_s^2}{\mu^2} + \gamma_S(a_s) = 0.$$

In order to obtain a total cancellation of the logarithms we need that all the anomalous dimensions are linear in the logarithms and their coefficient is the same in every case, Γ_{cusp}.

To resum the large logarithms in the form factor, we evaluate every element at its characteristic scale and then we evolve it to a common scale solving the corresponding RG equation. For example, for the hard factor, whose characteristic scale is $\mu_h \sim Q$, the evolution is

$$C_V(Q^2, \mu) = \exp\left\{\int_{\mu_h}^{\mu} d\ln\bar{\mu}\left[\Gamma_{\text{cusp}}(a_s)\ln\frac{Q^2}{\bar{\mu}^2} + \gamma_V(a_s)\right]\right\}C_V(Q^2, \mu_h)$$

$$= U(\mu_h, \mu)C_V(Q^2, \mu_h). \qquad (1.113)$$

1.4 SCET$_{\mathrm{II}}$

Once we have studied the construction of the SCET$_{\mathrm{I}}$ effective Lagrangian, the study of the known as SCET$_{\mathrm{II}}$ can be achieved in a systematic way. The main difference between both effective theories is the scaling of the modes with respect to the expansion parameter. In SCET$_{\mathrm{II}}$ the scaling of collinear and soft modes are

$$p_n \quad \sim \quad (1, \lambda^2, \lambda)Q, \tag{1.114}$$
$$p_s \quad \sim \quad (\lambda, \lambda, \lambda)Q, \tag{1.115}$$

where in this case the expansion parameter is, $\lambda = \Lambda_{\mathrm{QCD}}/Q$. Note that if we change the expansion parameter to $\lambda = \sqrt{\Lambda_{\mathrm{QCD}}/Q}$ the soft modes scale as the soft modes in SCET$_{\mathrm{I}}$ (or ultrasoft modes) did. However collinear modes scale different than they did in SCET$_{\mathrm{I}}$. It is interesting that in SCET$_{\mathrm{II}}$ the collinear modes do not interact with soft ones because they would be off-shell i.e. $p_n + p_s = (1, \lambda, \lambda)$. This difference is crucial with respect to SCET$_{\mathrm{I}}$ and makes the construction of the effective Lagrangian of SCET$_{\mathrm{II}}$ much simpler. Thus, we write the effective Lagrangian of SCET$_{\mathrm{II}}$ as

$$\mathcal{L}_{\mathrm{SCET_{II}}} = \mathcal{L}_c + \mathcal{L}_{\bar{c}} + \mathcal{L}_s, \tag{1.116}$$

where the collinear Lagrangians are the same as the ones derived for SCET$_{\mathrm{I}}$ and the soft Lagrangian is analogous to the one in SCET$_{\mathrm{I}}$ but changing the ultrasoft modes by the soft ones recently defined.

Another important feature in SCET$_{\mathrm{II}}$ is that the invariant mass of both soft and collinear particles scale as $Q^2\lambda^2$, so in a physical process they are only distinguished by their rapidities. Thus, a boost can interchange the roles of both types of particles, letting the physical process invariant. This does not happen in SCET$_{\mathrm{I}}$, where the mass of the collinear particles scales as $Q^2\lambda^2$ while the mass of soft particles scales as $Q^2\lambda^4$.

Due to the fact that the soft modes in SCET$_{\mathrm{II}}$ are basically the same as their corresponding soft modes in SCET$_{\mathrm{I}}$, the matching between both theories is done changing ultrasoft Wilson lines in eq. (1.101) by the corresponding Wilson lines for soft fields. As the functional form of these Wilson lines is exactly the same that the ones for ultrasoft modes, they are written in the same way given in eq. (1.101).

This EFT is particularly useful when one analyses transverse momentum distributions because it allows to separate the perturbative information obtained at the scale of the transverse momentum from the low energy nonperturbative information (see eq. (2.34)).

Chapter 2

Transverse momentum dependent factorization theorems

The main goal of this thesis is the study of the structure of hadrons by extracting information from cross sections of processes which include hadronic sources. In particular, we focus on the extraction of information about the three-dimensional structure of hadrons, i.e., we study processes with a non-vanishing (or unintegrated) transverse momentum, q_T.

The study of processes involving hadrons is involved due to the fact that one cannot calculate their contributions to the cross section with the perturbative approach used in QCD. Hadrons are made of partons (quarks and gluons) distributed inside them and an image of the probability distribution of the partons inside the hadron is given by the so called *parton distribution functions* (PDF). Because of the nonperturbative nature of these objects they cannot be calculated in perturbation theory in QCD and generally they are extracted from the experiments. As in this thesis the interesting processes depend on a non-vanishing transverse momentum we focus on *transverse momentum parton distribution functions* (TMDPDF) giving a three-dimensional information of the probabilistic distribution of partons inside the hadron.

The TMDPDFs are defined in an energy regime $q_T \ll Q$ where Q is the hard scale of the process. Thus, we will see that for $q_T \gg \Lambda_{\text{QCD}}$ (where Λ_{QCD} represents the position of the Landau pole) one will be able to derive some perturbative information which will be complemented by a nonperturbative information extracted from the experiments or Lattice QCD (see e.g. [33–35]). So, having perturbative information of the TMDPDF is crucial in order to reduce theoretical errors and obtaining cleaner information about the nonperturbative physics. In particular, part I of the thesis is devoted to the study of the perturbative information for different TMDPDF depending on their polarization up to the highest known order.

The proper definition of TMDPDFs is given by transverse momentum dependent *factorization theorems*. This issue was considered years ago by Collins, Soper and Sterman [5, 36] where notions of factorization and resummation of large logarithms (in the form $\alpha_s^n \ln^m(q_T^2/Q^2)$) were systematically investigated. Those results yielded the well known *CSS-formalism*. However, in this section we use the principles of SCET revised in chapter 1 to derive factorization theorems for the q_T-differential cross section. Within this framework other observables have been considered in [9, 37–40].

In this section we present the derivation of a factorization theorem for one of the most relevant processes known as Drell-Yan (DY) process. In this process a proton-proton collision leads to a pair of leptons in the final state,

$$p\,p \to l^+ \, l^- + X, \tag{2.1}$$

where X represents all the unidentified particles that are emitted in the process. Let us consider a hard partonic reaction of two incoming partons with momenta p_1 and p_2 along directions n and $\bar{n}$ defined in eq. (1.35), respectively. They are going to generate a virtual photon with virtuality $Q^2 = q^2 > 0$, where q^μ is its four-momentum. A neutral gauge boson, as the Z boson could be generated as well, but for simplicity in the exposition we do not consider this case. The virtual photon has a non-negligible transverse momentum, q_T, defined in light-cone coordinates in the sense of eq. (1.36). The momenta of the initiating partons corresponds to collinear (n) and anticollinear modes ($\bar{n}$) and therefore the momentum of the outgoing photon scales as $Q(1, 1, \lambda)$ where $\lambda \sim q_T/Q$ is the expansion parameter of SCET$_{q_T}$.

The DY cross section factorizes in a very similar way to eq. (1.2)

$$d\sigma = H(Q^2, \mu_H^2) F_n(\mu_F, \zeta) \otimes F_{\bar{n}}(\mu_F, \zeta) \otimes S(\mu_F, \zeta), \qquad (2.2)$$

where the physics at the hard scale is encoded in the hard factor, H, the collinear modes are encoded in the TMDPDF, $F_{n(\bar{n})}$, and the soft modes are encoded in the soft function, S. In next section we will give explicit definitions for these objects. The symbol $\otimes$ represent a multiplication or convolution depending on the space we are working in and μ_H, μ_F play the role of the high-energy and factorization scales, respectively. Finally, the scale ζ is an extra scale that appear as a consecuence of the transverse momentum and it is related with a new type of divergence that appears characteristically in these types of processes. They are a kind of light-cone singularities called *rapidity divergences* and will be studied in detail in section 2.2. Note that in eq. (2.2) the power corrections of order $(q_T^2/Q^2)^n$ are omitted.

In the effective theory approach used to derive factorization theorems, soft particles scale as $Q(\lambda, \lambda, \lambda)$ and collinear particles scale as $Q(1, \lambda^2, \lambda)$ (and $Q(\lambda^2, 1, \lambda)$ for anticollinear ones) where $\lambda \sim q_T/Q$. They are not allowed to interact because the collinear particles would be driven off-shell. This fact is not true in the case of ultrasoft gluons, which scale as $Q(\lambda^2, \lambda^2, \lambda^2)$, but they are not relevant to the kinematical region of interest. The relevant framework to describe soft gluons interacting with collinear particles was named SCET-q_T in [37] and we use here the same denomination. In this theory the virtuality of the particles is of order q_T^2 and it is different from SCET$_{II}$ where it is of order Λ_{QCD}. However, SCET$_{II}$ is needed to perform an operator product expansion (OPE) at the scale q_T to separate the perturbative part of the TMDPDF of the integrated PDF (in q_T). In both theories soft gluons are decoupled from the collinear ones with the effect of the introduction of soft Wilson lines as happened in chapter 1.

As the soft function in eq. (2.2) has a non-vanishing contribution one needs to consider the problem of double counting arising from the overlapping of soft and collinear modes. This fact is important and can affect to the proper definition of the TMDPDFs. In order to cancel the overlapping contributions (known as zero-bin contribution) we rewrite the factorization theorem as

$$d\sigma = H(Q^2, \mu^2) \left[\hat{F}_n \otimes S^{-1} \right] \otimes \left[\hat{F}_n \otimes S^{-1} \right] \otimes S, \qquad (2.3)$$

where hatted quantities represent a perturbative calculation of the collinear elements that still include the contamination from soft radiation region. This version of the factorization theorems is still problematic, because individually the collinear and soft functions are plagued of unregularized and uncancelled divergences which render them ill defined. These divergences appear perturbatively as integrals of the

form

$$\int_0^1 \frac{dt}{t},\tag{2.4}$$

which are manifestations of light-cone singularities. These type of divergences appear for some kind of IR regulators also in the fully integrated PDFs but they are cancelled when real and virtual contributions are combined. But this is not the case for TMDPDFs. These light-cone divergences are a consequence of having soft and collinear Wilson lines defined along light-like trajectories that allow gluons with infinite rapidities to interact with. To avoid these singularities an idea due to Collins and Soper is to tilt the Wilson lines going off-the-light-cone. This trick is used in [41, 42]. However in this thesis a different path is taken. In our approach all the Wilson lines remain on-the-light-cone and we will define the TMDPDF consequently. A more detailed explanation is given in section 2.2 where we explain how to deal with light-cone singularities in our framework.

2.1 Drell-Yan cross section in TMD factorization

The initial form of the cross section for the DY process [11] is

$$
\begin{aligned}
d\sigma &= \frac{4\pi\alpha_{em}^2}{3Q^2 s} \frac{d^4 q}{(2\pi)^4} \frac{1}{4} \sum_{\sigma_1 \sigma_2} \int d^4 y \, e^{-i(q\cdot y)} \\
&\times (-g_{\mu\nu}) \langle N_1(P_1,\sigma_1) N_2(P_2,\sigma_2) | J^{\mu\dagger}(y) J^\nu(0) | N_1(P_1,\sigma_1) N_2(P_2,\sigma_2) \rangle,
\end{aligned}
\tag{2.5}
$$

where $N_{1,2}$ represent the two hadrons in the process with momenta $P_{1,2}$ and $s = (P_1 + P_2)^2$. Note that the scaling of the position variable y is $1/Q(1,1,1/\lambda)$. On the other hand, J^μ is the electromagnetic current

$$J^\mu = \sum_q e_q \bar{\psi} \gamma^\mu \psi,\tag{2.6}$$

with e_q the quark electric charge in units of the electron charge. The full QCD current is matched onto the SCET$_{q_T}$ one

$$J^\mu = C_V(Q^2/\mu^2) \sum_q e_q \bar{\chi}_{\bar{n}} S_{\bar{n}}^{T\dagger} \gamma^\mu S_n^T \chi_n,\tag{2.7}$$

where C_V is the quark form factor introduced in chapter 1 and the n- and $\bar{n}$-collinear fields are described by the *building blocks* $\chi_{n(\bar{n})} = W_{n(\bar{n})}^{T\dagger} \xi_{n(\bar{n})}$. The collinear fields $\xi_{n(\bar{n})}$ were introduced in eq. (1.53). The collinear and soft Wilson lines, $W_{n(\bar{n})}^T$ and $S_{n(\bar{n})}^T$ are defined as presented in chapter 1 with the difference of the introduction of the superscript T, that represent an extra transverse Wilson line. The transverse Wilson lines are essential to ensure gauge invariance of $\chi_{n(\bar{n})}$ among regular and singular gauges [43–46]. In this thesis Feynman gauge is used so transverse Wilson lines are presented in this chapter but they will not be relevant in further calculations. For DY kinematics collinear Wilson lines are defined as

$$W_{n(\bar{n})}^T = T_{n(\bar{n})} W_{n(\bar{n})},\tag{2.8}$$

$$W_n(x) = \bar{P} \exp\left[ig \int_{-\infty}^0 ds\, \bar{n} \cdot A_n(x + s\bar{n}) \right],\tag{2.9}$$

$$T_n(x) = \bar{P}\exp\left[ig\int_{-\infty}^0 d\tau\, l_\perp \cdot A_{n\perp}(x^+,\infty^-,x_\perp+l_\perp\tau)\right], \tag{2.10}$$

$$T_{\bar{n}}(x) = \bar{P}\exp\left[ig\int_{-\infty}^0 d\tau\, l_\perp \cdot A_{\bar{n}\perp}(\infty^+,x^-,x_\perp+l_\perp\tau)\right]. \tag{2.11}$$

Note that $W_{\bar{n}}$ can be obtained from W_n by substitution of $n \leftrightarrow \bar{n}$ and $P \leftrightarrow \bar{P}$. On the other hand soft Wilson lines for DY kinematics are defined as

$$S_{n(\bar{n})}^T = T_{sn(\bar{n})}S_{n(\bar{n})}, \tag{2.12}$$

$$S_n(x) = P\exp\left[ig\int_{-\infty}^0 ds\, n \cdot A_s(x+sn)\right], \tag{2.13}$$

$$T_{sn}(x) = P\exp\left[ig\int_{-\infty}^0 d\tau\, l_\perp \cdot A_{s\perp}(x^+,\infty^-,x_\perp+l_\perp\tau)\right], \tag{2.14}$$

$$T_{s\bar{n}}(x) = P\exp\left[ig\int_{-\infty}^0 d\tau\, l_\perp \cdot A_{s\perp}(\infty^+,x^-,x_\perp+l_\perp\tau)\right], \tag{2.15}$$

where, analogously to the collinear case, $S_{\bar{n}}$ is obtained with the substitutions $n \leftrightarrow \bar{n}$ and $P \leftrightarrow \bar{P}$.

Averaging over nucleon spins and with the help of Fierz transformations we can rewrite the hadronic element in eq. (2.5) as

$$(-g_{\mu\nu})\langle N_1(P_1,\sigma_1)N_2(P_2,\sigma_2)|J^{\mu\dagger}(y)J^\nu(0)|N_1(P_1,\sigma_1)N_2(P_2,\sigma_2)\rangle \rightarrow$$

$$|C_V(Q^2/\mu^2)|^2 \sum_q e_q^2 \frac{1}{N_c}\langle N_1(P_1,\sigma_1)N_2(P_2,\sigma_2)| \left(\bar{\chi}_{\bar{n}}(y)\frac{\slashed{n}}{2}\chi_{\bar{n}}(0)\right) \tag{2.16}$$

$$\left(\bar{\chi}_n(y)\frac{\slashed{\bar{n}}}{2}\chi_n(0)\right)\mathrm{Tr}\left[\bar{T}\left(S_n^\dagger(y)S_{\bar{n}}(y)\right)T\left(S_{\bar{n}}^\dagger(0)S_n(0)\right)\right]|N_1(P_1,\sigma_1)N_2(P_2,\sigma_2)\rangle.$$

The n- and $\bar{n}$-collinear and soft fields act on different Hilbert spaces and one can disentagle the general Hilbert space itself into a direct product of three different Hilbert spaces, corresponding to the different modes [19, 47].

At this point, the cross section in eq. (2.5) is rewritten as

$$d\sigma = \frac{4\pi\alpha_{em}^2}{3Q^2s}\frac{d^4q}{(2\pi)^4}\sum_{\sigma_1\sigma_2}\int d^4y\, e^{-i(q\cdot y)}H(Q^2/\mu^2)\sum_q e_q^2 F_n(y)F_{\bar{n}}(y)S(y) \tag{2.17}$$

where $H(Q^2/\mu^2) = |C_V(Q^2/\mu^2)|^2$ encodes the physics in the hard region and

$$F_n(y) = \frac{1}{2}\sum_{\sigma_1}\langle N_1(P_1,\sigma_1)|\bar{\chi}_n(y)\frac{\slashed{\bar{n}}}{2}\chi_n(0)|N_1(P_1,\sigma_1)\rangle, \tag{2.18}$$

$$F_{\bar{n}}(y) = \frac{1}{2}\sum_{\sigma_2}\langle N_2(P_2,\sigma_2)|\bar{\chi}_{\bar{n}}(y)\frac{\slashed{n}}{2}\chi_{\bar{n}}(0)|N_1(P_2,\sigma_2)\rangle, \tag{2.19}$$

$$S(y) = \langle 0|\mathrm{Tr}\left[\bar{T}\left(S_n^\dagger(y)S_{\bar{n}}(y)\right)T\left(S_{\bar{n}}^\dagger(0)S_n(0)\right)\right]|0\rangle. \tag{2.20}$$

Taylor expanding eq. (2.17) in the physical limit that we are interested in, and taking into account that the derivatives of the fields scale analogously to their correspondent momentum scaling

$$\left(y^-\frac{\partial}{\partial y^-}F_n, y^+\frac{\partial}{\partial y^+}F_n, y_\perp\frac{\partial}{\partial y_\perp}F_n\right) \sim (1,\lambda^2,1) \tag{2.21}$$

$$\left(y^{-}\frac{\partial}{\partial y^{-}}F_{\bar{n}}, y^{+}\frac{\partial}{\partial y^{+}}F_{\bar{n}}, y_{\perp}\frac{\partial}{\partial y_{\perp}}F_{\bar{n}} \right) \quad \sim \quad (\lambda^{2},1,1) \tag{2.22}$$

$$\left(y^{-}\frac{\partial}{\partial y^{-}}S, y^{+}\frac{\partial}{\partial y^{+}}S, y_{\perp}\frac{\partial}{\partial y_{\perp}}S \right) \quad \sim \quad (1,1,\lambda) \tag{2.23}$$

we write the leading power term of the cross section as

$$d\sigma = \frac{4\pi\alpha_{em}^{2}}{3N_{c}Q^{2}s}\frac{d^{4}q}{(2\pi)^{4}}\sum_{\sigma_{1}\sigma_{2}}\int d^{4}y\,e^{-i(q\cdot y)}H(Q^{2}/\mu^{2}) \tag{2.24}$$
$$\times \sum_{q}e_{q}^{2}F_{n}(0^{+},y^{-},y_{\perp})F_{\bar{n}}(y^{+},0^{-},y_{\perp})S(0^{+},0^{-},y_{\perp}) + \mathcal{O}(\lambda).$$

It can be noted that if ultrasoft gluons would be considered instead of soft ones, after the Taylor expansion the soft function would be one to all orders in perturbation theory, as studied in [9]. The fact that the soft function depends only on transverse components is a crucial point in order to have final well defined TMDPDFs.

From now on, we consider the leading power contribution to the partonic cross section but abusing the notation we denote the partonic versions as their hadronic counterparts. So, in momentum space

$$d\sigma = \frac{4\pi\alpha_{em}^{2}}{3N_{c}Q^{2}}\frac{dx_{1}dx_{2}d^{2}q_{T}}{2(2\pi)^{4}}H(Q^{2}/\mu^{2})\sum_{q}e_{q}^{2} \tag{2.25}$$
$$\times \int d^{2}k_{n\perp}d^{2}k_{\bar{n}\perp}d^{2}k_{s\perp}\delta(q_{T}-k_{n\perp}-k_{\bar{n}\perp}-k_{s\perp})F_{n}(x_{1},k_{n\perp})F_{\bar{n}}(x_{2},k_{\bar{n}\perp})S(k_{s\perp}).$$

Note that $x_{1,2}$ are the Bjorken variables defined as

$$x_{1,2} = \frac{\sqrt{Q^{2}+q_{T}^{2}}}{\sqrt{s}}e^{\pm y}, \qquad y = \frac{1}{2}\ln\left(\frac{q^{0}+q^{z}}{q^{0}-q^{z}}\right) \tag{2.26}$$

where y is the rapidity of the photon. Thus, the collinear and soft objects are

$$F_{n}(x_{1},k_{n\perp}) = \frac{1}{2}\int\frac{dr^{-}d^{2}r_{\perp}}{(2\pi)^{3}}e^{-i(r^{-}x_{1}p_{1}^{+}/2-r_{\perp}\cdot k_{n\perp})}F_{n}(0^{+},r^{-},r_{\perp}), \tag{2.27}$$

$$F_{\bar{n}}(x_{1},k_{\bar{n}\perp}) = \frac{1}{2}\int\frac{dr^{+}d^{2}r_{\perp}}{(2\pi)^{3}}e^{-i(r^{+}x_{2}p_{2}^{-}/2-r_{\perp}\cdot k_{\bar{n}\perp})}F_{n}(r^{+},0^{-},r_{\perp}), \tag{2.28}$$

$$S(k_{s\perp}) = \int\frac{d^{2}r_{\perp}}{(2\pi)^{2}}e^{ir_{\perp}\cdot k_{s\perp}}S(0^{+},0^{-},r_{\perp}). \tag{2.29}$$

The cross section in eq. (2.25) has a problem related with the existence of a new type of unregulated and uncancelled divergences in collinear and soft functions which complicate both the renormalization and the nonperturbative interpretation of such elements. These divergences are called *rapidity divergences* and will be studied in detail in section 2.2. In conclusion each of the three elements in eqs. (2.27-2.29) are ill defined and have no physical meaning by themselves. However, considering the combinations

$$F_{n}^{R}(x_{1},k_{n\perp}) = \frac{1}{2}\int\frac{dr^{-}d^{2}r_{\perp}}{(2\pi)^{3}}e^{-i(r^{-}x_{1}p_{1}^{+}/2-r_{\perp}\cdot k_{n\perp})}F_{n}(0^{+},r^{-},r_{\perp})\sqrt{S(0^{+},0^{-},r_{\perp})},$$

$$F_{\bar{n}}^{R}(x_{1},k_{\bar{n}\perp}) = \frac{1}{2}\int\frac{dr^{+}d^{2}r_{\perp}}{(2\pi)^{3}}e^{-i(r^{+}x_{2}p_{2}^{-}/2-r_{\perp}\cdot k_{\bar{n}\perp})}F_{n}(r^{+},0^{-},r_{\perp})\sqrt{S(0^{+},0^{-},r_{\perp})},$$

$$(2.30)$$

can be proved that these quantities are free from rapidity divergences, and we re-name them with the superscript R. This redefinition of the collinear elements is also valid for any considered polarization as we will discuss along chapters 3 and 4 of this thesis.

In the section 2.2 we will discuss that with the regulator used to regulate rapidity divergences, the *modified δ-regulator*, the overlap between collinear and soft regions (known as zero-bin contribution) is analogous to the soft function. With the use of this regulator we can find a simple definition of the TMDPDF in which the zero-bin contribution can be extracted explicitly, i.e. in our notation $F_n \to F_n/S$. Thus,

$$
\begin{aligned}
F_n^R(x_1, k_{n\perp}) &= \frac{1}{2} \int \frac{dr^- d^2 r_\perp}{(2\pi)^3} e^{-i(r^- x_1 p_1^+/2 - r_\perp \cdot k_{n\perp})} \frac{F_n(0^+, r^-, r_\perp)}{\sqrt{S(0^+, 0^-, r_\perp)}}, & (2.31) \\
F_{\bar{n}}^R(x_1, k_{\bar{n}\perp}) &= \frac{1}{2} \int \frac{dr^+ d^2 r_\perp}{(2\pi)^3} e^{-i(r^+ x_2 p_2^-/2 - r_\perp \cdot k_{\bar{n}\perp})} \frac{F_n(r^+, 0^-, r_\perp)}{\sqrt{S(0^+, 0^-, r_\perp)}},
\end{aligned}
$$

where the square root of the soft function is subtracted from the naive collinear matrix elements, affected by rapidity divergences.

Thus, we can rewrite the cross section in eq. (2.25) as

$$
\begin{aligned}
d\sigma &= \frac{4\pi \alpha_{em}^2}{3 N_c Q^2} \frac{dx_1 dx_2 d^2 q_T}{2(2\pi)^4} H(Q^2/\mu^2) \sum_q e_q^2 & (2.32) \\
&\times \int d^2 k_{n\perp} d^2 k_{\bar{n}\perp} d^2 k_{s\perp} \delta(q_T - k_{n\perp} - k_{\bar{n}\perp} - k_{s\perp}) F_n^R(x_1, k_{n\perp}) F_{\bar{n}}^R(x_2, k_{\bar{n}\perp}),
\end{aligned}
$$

where the soft function is absorbed into both collinear matrix elements in order to have a well defined TMDPDF.

To finish this section we study the form of the cross section in the regime $q_T \gg \Lambda_{\text{QCD}}$. This regime is interesting because eq. (2.32) is not the final form of the cross section and the TMDPDFs can be refactorized. This means a second matching of SCET_{q_T}, that describes the physics on the intermediate scale q_T onto SCET_{II}, that studies the nonperturbative physics at the scale Λ_{QCD}. This second matching is very interesting because it allows one to separate the perturbative information computed from TMDPDF from its purely nonperturbative behavior.

Since the scale of this region, q_T, is big enough to be perturbative, its conjugate coordinate, the impact parameter b, is small enough to perform an operator product expansion (OPE) in impact parameter space. Thus, we refactorize the TMDPDF defined in impact parameter space

$$
F_n(x, b, \mu) = \int d^2 k_{n\perp} e^{i k_{n\perp} \cdot b} F_n(x_1, k_{n\perp}, \mu), \tag{2.33}
$$

as

$$
F_n(x, b, \mu) = \int_x^1 \frac{dx'}{x'} C\left(\frac{x}{x'}, b, \mu\right) f_n(x', \mu) + \mathcal{O}(b^2 \Lambda_{\text{QCD}}), \tag{2.34}
$$

where μ is known as the factorization scale and f_n is the integrated PDF defined as

$$
f_n(x, \mu) = \frac{1}{2} \int \frac{dy^-}{2\pi} e^{iy^- x p^+} \langle p | \bar{\chi}_n(0^+, y^-, 0_\perp) \frac{\slashed{\bar{n}}}{2} \chi_n(0) | p \rangle, \tag{2.35}
$$

with p the momentum of the considered parton. On the other hand, the matching coefficients C are the perturbatively calculable part of the TMDPDF and part I of thesis is dedicated to find them up to $\mathcal{O}(a_s^2)$ for different polarizations of TMDPDFs.

Note that along the derivation of the TMDPDF only the factorization scale is explicitly written but due to the existence of rapidity divergences a new scale arises and the TMDPDF has a double-scale dependence that is studied in section 2.3. Also, in section 2.2 we will see how this new scale arises with an explicit one-loop calculation of an unpolarized TMDPDF.

2.2 Rapidity divergences

At the beginning of this chapter, it was pointed out the emergence of rapidity divergences due to some unregulated and uncancelled logarithmic divergences that appear in perturbative calculations of the collinear and soft elements of the factorization theorem in e.g. eq. (2.25). Particularly, these divergences appear in the integration of eikonal propagators given by the Feynman rules of soft and collinear Wilson lines. To regularize these divergences a particular regularization scheme should be chosen. Multiple options in the literature are used in order to regulate rapidity divergences (see e.g. [11, 14, 48–52]) but we will use the known as *modified δ-regularization scheme* developed in [51, 52]. Also, in this section an explicit calculation to see how rapidity divergences are explicitly cancelled is presented.

2.2.1 Modified δ-regularization scheme

The original δ-regularization was proposed in [11] and it is based in an infinitesimal shift of the $i0$-prescriptions that appear in eikonal propagators. So, at the level of diagrams the regularization scheme is based on the substitution (e.g. in the absorption of one gluon by a Wilson line $[\infty^+, 0]$)

$$\frac{1}{k^+ - i0} \rightarrow \frac{1}{k^+ - i\delta^+},\tag{2.36}$$

with $\delta^+ \rightarrow +0$. However, this regularization is not accurate enough to do calculations at higher-orders (in particular from NNLO). Particularly, with this simple substitution the soft function and the zero-bin contribution are only equal to each other at NLO but not for higher-orders. Therefore, eq. (2.30) would not be true at all orders in perturbation theory. In [51, 52] the original δ-regularization scheme was modified to solve this and other issues. Thus, a modified δ-regularization scheme is implemented at operator level and constructed in a way that non-abelian exponentiation and the equality of the soft function and the zero-bin are preserved.

This operator level redefinition consists on a modification of the operational definition of the collinear and soft Wilson lines. In particular, the soft Wilson lines in eq. (2.13) are modified as

$$\tilde{S}_{\bar{n}}(0) = P \exp\left[-ig \int_0^\infty ds A_{s+}(s\bar{n})\right] \quad \rightarrow \quad \tilde{S}_{\bar{n}}(0) = P \exp\left[-ig \int_0^\infty ds A_{s+}(s\bar{n})e^{-i\delta^+ s}\right],$$

$$S_n(0) = P \exp\left[ig \int_{-\infty}^0 ds A_{s-}(sn)\right] \quad \rightarrow \quad S_n(0) = P \exp\left[ig \int_{-\infty}^0 ds A_{s-}(sn)e^{+i\delta^- s}\right],$$

$$\tag{2.37}$$

where $\delta^{\pm} \to +0$. At the level of Feynman diagrams in momentum space the modified expressions for the eikonal propagators are (e.g. for absorption of n gluons by a Wilson line $[\infty^+, 0]$)

$$\frac{1}{(k_1^+ - i0)(k_2^+ - i0)...(k_n^+ - i0)} \rightarrow \frac{1}{(k_1^+ - i\delta^+)(k_2^+ - 2i\delta^+)...(k_n^+ - ni\delta^+)}, \quad (2.38)$$

where the gluons are ordered in the way that k_n is the gluon that fulfills the condition $|k_n^+| \leq |k_i^+| \forall i$. As a consequence of the rescaling invariance of the Wilson lines, now broken by the regulators $\delta^{\pm}$, the expression of the diagrams depend on a unique combination of regulators, $\delta^+\delta^-$. The ordering of the poles in the eikonal propagators is crucial to preserve the non-abelian exponentiation theorem for color factors [53, 54]. Within modified δ-regularization only diagrams with non-abelian color prefactor arise in the exponent. Thus, the soft function can be written as usual

$$\tilde{S}(b) = \exp\left[a_s C_F \left(S^{[1]} + a_s S^{[2]} + ...\right)\right]. \quad (2.39)$$

Analogously to the soft Wilson lines, the collinear Wilson lines are modified, for the TMDPDF as,

$$W_n(x) = P \exp\left[ig \int_{-\infty}^0 ds A_-(x + sn)\right] \quad \rightarrow \quad P \exp\left[ig \int_{-\infty}^0 ds A_-(x + sn)e^{+i\delta^- xs}\right], \quad (2.40)$$

and for the TMDFF as

$$W_n(z) = P \exp\left[ig \int_{-\infty}^0 ds A_-(z + sn)\right] \quad \rightarrow \quad P \exp\left[ig \int_{-\infty}^0 ds A_-(z + sn)e^{+i(\delta^-/z)s}\right]. \quad (2.41)$$

This type of regularization of Wilson lines at operator level is also used in the calculation of multiparticle webs [55–59]. Note that the δ-regularized Wilson line violates the rules of gauge transformations, but this violation is power-suppressed in δ. Therefore, in the calculations δ should be considered as an infinitesimal parameter in order to avoid contributions that violate gauge invariance.

As the soft function is split in order to be combined with the bare definition of the TMDPDF and cancels rapidity divergences (see eq. (2.30)), a new scale is introduced. In the calculation of the soft function the whole dependence on the rapidity regulators appears in terms of a unique function $\ln(\mu^2/(\delta^+\delta^-))$. As each δ regulator represents the rapidity divergences coming form each TMDPDF in the factorization theorem one can separate the soft function introducing new scales, $\zeta_{\pm}$,

$$S\left(b, \ln\left(\frac{\mu^2}{\delta^+\delta^-}\right)\right) = S^{1/2}\left(b, \ln\left(\frac{\mu^2}{(\delta^+/p^+)\zeta_+}\right)\right) S^{1/2}\left(b, \ln\left(\frac{\mu^2}{(\delta^-/p^-)\zeta_-}\right)\right), \quad (2.42)$$

where $\zeta_+\zeta_- = (p^+p^-)^2 = Q^4$, with Q^2 the hard scale of the considered process. In order to introduce this new scale in the calculation of a single TMD, one can do the following substitution

$$\delta^- = \delta^+ \frac{\zeta}{(p^+)^2}, \quad (2.43)$$
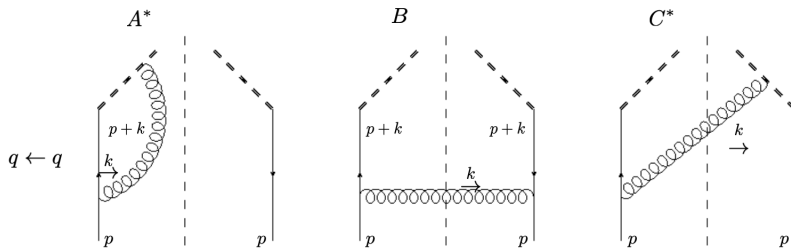
FIGURE 2.1: Feynman diagrams contributing to the TMDPDF at NLO in QCD. The star in a Feynman diagram indicates that its complex conjugate should be added.

where the subscripts $\pm$ are omitted for the variable ζ.

2.2.2 One-loop calculation. Cancellation of rapidity divergences

In this section we present a sketch of a one-loop calculation of an unpolarized quark TMDPDF as in [18] that will help to understand explicitly the cancellation of rapidity divergences between a bare TMDPDF and the soft function, extracting the matching coefficient considered in eq. (2.34) at one-loop accuracy. On the other hand, this calculation helps to understand the way to proceed in the calculation of matching coefficients for polarized TMDs presented in part I of this thesis. Here and along the thesis, Feynman gauge is used.

The Feynman diagrams corresponding to the bare TMDPDF are drawn in fig. 2.1. As we consider massless external particles the only Lorentz invariant present in the calculation is the conjugate coordinate of the transverse momentum, b. This quantity appears only in the diagrams whose left and right parts are connected, so purely virtual diagrams (without any cut propagator) are set to zero. The only relevant piece of the virtual diagrams is the UV-divergent part, that enters in the renormalization constant, Z_q, of the quark TMDPDF[1]. At one loop we have

$$Z_q^{[1]} = -C_F \left(\frac{2}{\epsilon^2} + \frac{4 + 2\mathbf{l}_\zeta}{\epsilon} \right), \tag{2.44}$$

where we introduce the following notation for logarithms, useful along all the thesis,

$$\mathbf{L}_\mu = \ln \left(\frac{X^2 \mathbf{b}^2}{4 e^{-2\gamma_E}} \right), \quad \mathbf{l}_X = \ln \left(\frac{\mu^2}{X} \right), \qquad \lambda_\delta = \ln \left(\frac{\delta^+}{p^+} \right). \tag{2.45}$$

Note that we denote euclidean vectors with bold font, i.e. $\mathbf{b}^2 = -b^2$.

The computation of the non-zero diagrams for the quark TMDPDF provides the quark-to-quark bare matrix element,

$$F^{B[1]}(x, \delta) = 2 C_F \Gamma(-\epsilon) \mathbf{B}^\epsilon \left(\bar{x}(1 - \epsilon) + \frac{2x\bar{x}}{\bar{x}^2 + x^2 \delta^2} \right), \tag{2.46}$$

where $\mathbf{B} = \mathbf{b}^2/4$ and $\bar{x} = 1 - x$. Before combining the collinear and soft matrix elements we should develop our result in the limit $\delta \to 0$. This step implies to

---

[1]More information about the renormalization of the TMDPDF is given in chapter 3, while in this section we introduce only the necessary information to perform this calculation.

proceed from analytical functions to distributions, where the singularity at $x \to 1$ is regularized by the $(..)_+$-distribution

$$[f(x)]_+ = f(x) - \delta(\bar{x}) \int_0^1 dy f(y). \tag{2.47}$$

Within δ-regularization, this transformation can be done as

$$F^{B[1]}(x, \delta) = \left(F^{B[1]}(x, \delta) \right)_+ + \delta(\bar{x}) \int_0^1 dy \, F^{B[1]}(y, \delta) + \mathcal{O}(\delta). \tag{2.48}$$

Using this relation the result in eq. (2.46) is rewritten as

$$F^{B[1]} = 2C_F \Gamma(-\epsilon) \mathbf{B}^\epsilon \left(\left(\frac{2x}{1-x} + \bar{x}(1-\epsilon) \right)_+ + \delta(\bar{x}) \left(-\frac{3}{2} - \frac{\epsilon}{2} - 2\lambda_\delta \right) \right). \tag{2.49}$$

The soft function, necessary to cancel rapidity divergences remaining in eq. (2.48), is calculated up to NNLO within modified δ-regularization scheme in [52]. At NLO the soft function is given by

$$S^{[1]} = -4C_K \mathbf{B}^\epsilon \Gamma(-\epsilon) \left(\mathbf{L}_{\sqrt{\zeta}} + 2\lambda_\delta - \psi(-\epsilon) - \gamma_E \right), \tag{2.50}$$

where the color factor, $C_K = C_F(C_A)$, for quark (gluon) initiating partons. Combining results in eq. (2.49) and eq. (2.50) we find a result free of rapidity divergences. Thus, the final expression for the TMDPDF (ϵ-expanded) is written as

$$F^{[1]} = C_F \left[\left(-\frac{2}{\epsilon} \frac{1+x^2}{1-x} - 2\mathbf{L}_\mu \frac{1+x^2}{1-x} + 2\bar{x} \right)_+ + \delta(\bar{x}) \left(-\mathbf{L}_\mu^2 + 2\mathbf{L}_\mu \mathbf{l}_\zeta + 3\mathbf{L}_\mu + 1 - \zeta_2 \right) \right]. \tag{2.51}$$

This expression is free from rapidity and UV divergences. However, one recognizes the ϵ-pole which is part of the corresponding integrated function. In order to get the result of the matching of the TMDPDF over its corresponding integrated function we have to calculate the matrix elements of the integrated part. The diagrams contributing to this object are all zero, because there is no Lorentz invariant scale. Therefore, the only non-zero contribution is the UV renormalization factor, which is deduced from the DGLAP kernel. For quark-to-quark channel we have

$$f_{q \leftarrow q}^{[1]} = -\frac{2C_F}{\epsilon} \left(\frac{1+x^2}{1-x} \right)_+. \tag{2.52}$$

Finally, we find matching coefficients where ϵ-poles totally cancelled. Up to one loop we find

$$C_{q \leftarrow q}^{[0]} = \delta(\bar{x}), \tag{2.53}$$

$$C_{q \leftarrow q}^{[1]} = C_F \left[-2\mathbf{L}_\mu \frac{1+x^2}{1-x} + 2\bar{x} + \delta(\bar{x}) \left(-\mathbf{L}_\mu^2 + 2\mathbf{L}_\mu \mathbf{l}_\zeta - \zeta_2 \right) \right], \tag{2.54}$$

where the divergent terms at $x \to 1$ should be undestood as $(..)_+$-regularized. In eq. (2.54) we see explicitly how the dependence over the rapidity scale ζ enters due to the procedure to cancel rapidity divergences.

2.3 Evolution of TMD distributions

In this section we discuss the properties of the TMD operator under renormalization scales. From this point, we can derive evolution equations of the TMD distributions, whose solution helps us to obtain the evolution factor which resums logarithms in order to obtain trustable predictions of cross sections. An important point about the evolution of TMD distributions is its spin independence. Thus, the discussion in this section is valid to all the considered TMD distributions. We use the generic notation F for a generic spin (in)dependent TMD.

2.3.1 Double scale evolution

The dependence on renormalization scales is given by the pair of evolution equations

$$\mu^2 \frac{d}{d\mu^2} F(x, \boldsymbol{b}; \mu, \zeta) = \frac{\gamma_F(\mu, \zeta)}{2} F(x, \boldsymbol{b}; \mu, \zeta), \tag{2.55}$$

$$\zeta \frac{d}{d\zeta} F(x, \boldsymbol{b}; \mu, \zeta) = -\mathcal{D}(\mu, \boldsymbol{b}) F(x, \boldsymbol{b}; \mu, \zeta). \tag{2.56}$$

The anomalous dimensions γ_F and $\mathcal{D}$ are defined via the corresponding renormalization constants and are known up to three-loop order [60–63]. Their explicit perturbative expressions can be found in appendix A. As the TMD distributions have two types of divergences renormalized in two different ways, we have a system of two differential equations. A detailed study of this system has been recently presented in ref. [16] and a summary of the main features can be found in the next subsection.

Anomalous dimensions γ_F and $\mathcal{D}$ satisfy the integrability condition (also known as Collins-Soper equation [64])

$$2\mu^2 \frac{d\mathcal{D}(\boldsymbol{b}, \mu)}{d\mu^2} = -\zeta \frac{d\gamma_F(\mu, \zeta)}{d\zeta} = \Gamma_{\text{cusp}}(\mu), \tag{2.57}$$

where Γ_{cusp} is the anomalous dimension for a cusp of two light-like Wilson lines. Due to this equation the expression for γ_F can be rewritten in the form

$$\gamma_F^f(\mu, \zeta) = \Gamma_{\text{cusp}}^f(\mu) \mathbf{l}_\zeta - \gamma_V^f, \tag{2.58}$$

where γ_V^f is anomalous dimension of the vector form factor for quarks ($f = q$) or gluons ($f = g$). The rapidity anomalous dimension $\mathcal{D}$ has not such a simple representation due to the presence of an extra dimensional parameter $\boldsymbol{b}^2$. It generally contains all powers of logarithms $\ln(\mu^2 \boldsymbol{b}^2)$, that at some large values of $\boldsymbol{b}^2$ turns to some non-perturbative function [65].

Due to the integrability condition in eq. (2.57) the system of evolution equations in eqs. (2.55, 2.56) has a unique solution:

$$F_{f \leftarrow h}(x, \boldsymbol{b}; \mu_1, \zeta_1) = R^f[\boldsymbol{b}; (\mu_1, \zeta_1) \to (\mu_2, \zeta_2)] F_{f \leftarrow h}(x, \boldsymbol{b}; \mu_2, \zeta_2), \tag{2.59}$$

where the TMD renormalization factor reads

$$R^f[\boldsymbol{b}; (\mu_1, \zeta_1) \to (\mu_2, \zeta_2)] = \exp\left[\int_P \left(\gamma^f(\mu, \zeta) \frac{d\mu}{\mu} - \mathcal{D}_f(\mu, \boldsymbol{b}) \frac{d\zeta}{\zeta} \right) \right]. \tag{2.60}$$

Here, P is arbitrary path in (μ, ζ)-plane connecting (μ_1, ζ_1) and (μ_2, ζ_2). Eq. (2.60) is in principle independent of the path P, however the truncation of the perturbative series makes some choices more preferable, for a detailed discussion see ref. [16] and next subsection. In particular, we use the special practically-convenient path that corresponds to the ζ-prescription introduced in [16, 66]. We again stress that the TMD evolution equations and their solution of eq. (2.59) do not depend on the polarization.

In eq. (2.34) we pointed out that the small-b limit of the renormalized TMD distribution can be related to the collinear PDF through calculable matching coefficients. So, it is important to know the evolution of collinear PDF with the DGLAP kernel evolution equation

$$\mu^2 \frac{d}{d\mu^2} f^f(x, \mu) = \int_x^1 \frac{dy}{y} P_{q \leftarrow f}\left(\frac{x}{y}\right) f^f(y, \mu), \qquad (2.61)$$

where the DGLAP kernel P is known up to two (or even three) loop order for every polarization in [67–71]. Combining together eqs. (2.55, 2.56) with eq. (2.61) we obtain the evolution properties of the matching kernels. They are

$$\mu^2 \frac{d}{d\mu^2} C_{q \leftarrow f}(x, \mathbf{L}_\mu, \mathbf{l}_\zeta) \qquad (2.62)$$

$$= \sum_{f' = q, \bar{q}} \int_x^1 \frac{dy}{y} C_{q \leftarrow f'}\left(\frac{x}{y}, \mathbf{L}_\mu, \mathbf{l}_\zeta\right) \left(\frac{\gamma_V(\mu, \zeta)}{2} \delta_{ff'} \delta(\bar{y}) - P_{f' \leftarrow f}(y)\right),$$

$$\zeta \frac{d}{d\zeta} C_{q \leftarrow f}(x, \mathbf{L}_\mu, \mathbf{l}_\zeta) = -\mathcal{D}(\mu, b) C_{q \leftarrow f}(x, \mathbf{L}_\mu, \mathbf{l}_\zeta). \qquad (2.63)$$

In perturbation theory, the expression for the coefficient function can be presented as

$$\delta C_{f \leftarrow f'}(x, \mathbf{L}_\mu, \mathbf{l}_\zeta) = \sum_{n=0}^{\infty} a_s^n \sum_{k=0}^{n+1} \sum_{l=0}^{n} \mathbf{L}_\mu^k \mathbf{l}_\zeta^l \delta C_{f \leftarrow f'}^{(n;k,l)}(x). \qquad (2.64)$$

The coefficients $\delta C^{(n;k,l)}$ with $k + l > 0$ are fixed order-by-order with the help of the renormalization group equations in eqs. (2.62, 2.63). Thus, the only non-trivial part to evaluate is $C^{(n;0,0)}$. The expressions for these coefficients in their generic form up to two-loop are given in the chapter 4 of this thesis, devoted to the systematic calculation of matching coefficients of polarized TMD distributions.

2.3.2 ζ-prescription

The implementation of the ζ-prescription leads to the definition of the so-called optimal TMDs. We sketch here the procedure to obtain optimal TMDs referring to the original work [16] for further details. The anomalous dimensions $\gamma_F(\mu, \zeta)$ and $\mathcal{D}(\mu, b)$ governing the evolution can be thought as two components of a vector field in the plane $(\ln\mu^2, \ln\zeta)$. The integrability condition, e.g. eq. (2.57), states that such field is irrotational, i.e. locally conservative. This allows to define a scalar potential and guarantees that the evolution between two points in the $(\ln\mu^2, \ln\zeta)$ space is independent of the path; in particular, no evolution occurs along equipotential lines. However, the perturbative expansion breaks the validity of such statement and in fact it was shown that numerical predictions largely depend on the choice of path. This limit is overcome by the *improved γ solution*, that reinstates path-invariance by
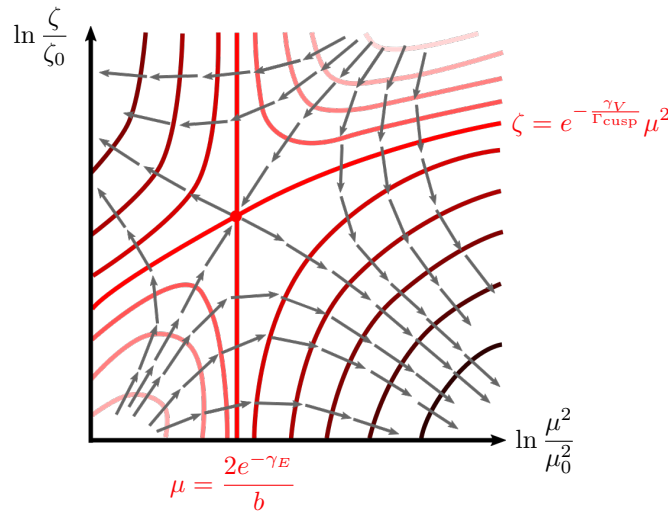
FIGURE 2.2: Sketch of the geometry of the (ζ, μ) plane where the double scale evolution takes place. The anomalous dimensions determine a conservative field (grey arrows) and the evolution is null among equipotential lines (shades of red). The intersection of two special equipotential lines (bright red) determines a saddle point; the zeta-prescription corresponds to running the evolution from this point, after reinstating path invariance. The equations for the special equipotential lines in the figure correspond to the one-loop result.

supplementing γ_F with formally higher-order terms. If we let F be a generic TMD, then the evolution kernel R, implicitly defined as

$$F(x, \boldsymbol{b}, \mu_f, \zeta_f) = R(\boldsymbol{b}; \mu_f, \zeta_f; \mu_i, \zeta_i) F(x, \boldsymbol{b}, \mu_i, \zeta_i) \,, \tag{2.65}$$

within the improved γ solution yields

$$\begin{aligned} R(\boldsymbol{b}; \mu_f, \zeta_f; \mu_i, \zeta_i) &= \exp\left\{ \mathcal{D}(\mu_f, \boldsymbol{b}) \ln\left(\frac{\mu_f^2}{\zeta_f}\right) - \mathcal{D}(\mu_i, \boldsymbol{b}) \ln\left(\frac{\mu_i^2}{\zeta_i}\right) \right. \\ &\quad \left. - \int_{\mu_i}^{\mu_f} \frac{d\mu}{\mu} \left[2\mathcal{D}(\mu, \boldsymbol{b}) + \gamma_V(\mu) \right] \right\} \,, \end{aligned} \tag{2.66}$$

where γ_V is the noncusp anomalous dimension.

Path independence allows one to apply the ζ-*prescription*, the key point of the method. The idea is setting the initial rapidity scale $\zeta_i = \zeta_{\mu_i}$ as a function of μ_i such that the scale-dependence of the initial TMDs vanishes independent of μ_i. At one loop, this simply reads

$$\zeta_\mu = e^{-\frac{\gamma_V}{\Gamma_{\text{cusp}}}} \mu^2 \,, \tag{2.67}$$

and the corrections to higher loops are evaluated in [16].

The relation between ζ and μ draws a line in the $(\ln\zeta, \ln\mu^2)$ plane (fig. 2.2). Since by requirement the TMDs are constant along it, this must be an equipotential line, which is well defined only if path-independence is restored. The remarkable fact with the ζ prescription is that, contrarily to standard evolution, the cancellation of large rapidity logarithms affecting the un-evolved TMDs is an internal mechanism.

The rapidity evolution is still responsible for cancelling the large logarithms in the hard function, but the scale uncertainty of the evolution is now entirely decoupled from the definition of the TMDs (and in particular, from the non-perturbative model that enters their definition).

The definition of *optimal TMDs* requires one more specification, which concerns the choice of initial scale μ_i (and consequently ζ_{μ_i}), and follows from TMD factorization. Considering TMD PDFs for definiteness, we have up to nonperturbative corrections

$$F_{a\leftarrow h}(x, \boldsymbol{b}, \mu, \zeta_\mu) = \sum_b \int_x^1 \frac{dy}{y}\, \mathcal{C}_{a\leftarrow b}(\tfrac{x}{y}, \boldsymbol{b}, \mu, \zeta_\mu, \mu_{\mathrm{OPE}}) f_{b\leftarrow h}(y, \mu_{\mathrm{OPE}}) \left[1 + \mathcal{O}\big(b^2 \Lambda_{\mathrm{QCD}}^2\big)\right],$$

$$(2.68)$$

where $f_{b\leftarrow h}$ are the collinear PDFs, $\mathcal{C}_{a\leftarrow b}$ are transverse momentum matching coefficients known at two loop from ref. [18]. The matching is performed at the scale μ_{OPE}. The choice of μ_{OPE} is in general constrained by μ_i, as they need to lie on the same half-plane with respect to the saddle point. This undesired feature is eliminated by choosing $\mu_i = \mu_{\mathrm{saddle}}$.

Part I

Spin effects in transverse momentum distributions

Chapter 3

Polarized transverse momentum distributions

3.1 Definition of spin dependent transverse momentum distributions

The transverse momentum dependent factorization theorems for semi-inclusive deep inelastic scattering (SIDIS) and Drell-Yan type processes formulated in [10, 11, 13, 14] and revisited in chapter 2 yield a well defined spin (in)dependent transverse momentum dependent distributions (TMDs) free of rapidity divergences. These distributions describe the three-dimensional distribution of quarks and gluons inside a hadron, due to the extra dependence on the transverse momentum in addition to the one-dimensional Bjorken momentum fraction [72].

In chapter 2 we studied the definition of the quark TMD obtained from the factorization theorem. In terms of operators, the quark and gluon component of a TMD can be written as

$$\Phi_{ij}(x, \boldsymbol{b}) = \int \frac{d\lambda}{2\pi} e^{-ixp^+\lambda} \bar{q}_i \left(\lambda n + \boldsymbol{b} \right) \mathcal{W}(\lambda, \boldsymbol{b}) q_j \left(0 \right), \qquad (3.1)$$

$$\Phi_{\mu\nu}(x, \boldsymbol{b}) = \frac{1}{xp^+} \int \frac{d\lambda}{2\pi} e^{-ixp^+\lambda} F_{+\mu} \left(\lambda n + \boldsymbol{b} \right) \mathcal{W}(\lambda, \boldsymbol{b}) F_{+\nu} \left(0 \right), \qquad (3.2)$$

where i, j and μ, ν are Dirac and Lorentz indices, respectively. In addition, n is the lightlike vector and we use the standard notation for the light-cone coordinates. Also, $g_T^{\mu\nu} = g_{\mu\nu} - n^\mu \bar{n}^\nu - \bar{n}^\mu n^\nu$). The operator $\mathcal{W}$ is

$$\mathcal{W}(\lambda, \boldsymbol{b}) = \tilde{W}_n^T \left(\lambda n + \boldsymbol{b} \right) \sum_X |X\rangle \langle X| \tilde{W}_n^{T\dagger} \left(0 \right), \qquad (3.3)$$

with Wilson lines defined in eq. (2.9) taken in the appropriate representation of gauge group. The staple contour of the gauge link (see fig. 3.1) results in the rapidity divergences, the unique feature of TMD operators. The superscript T in Wilson lines indicates that they are incorporated by an additional transverse link at light-cone infinity, which ensures the gauge invariance of the operator. However, transverse links do not give additional contributions in non-singular gauges.

The hadron matrix elements of the TMD operators in eqs. (3.8, 3.9) with open vector and spinor indices are to be decomposed over all possible Lorentz variants, which define all the possible TMDPDFs. In the literature this decomposition is commonly made in momentum space, e.g. see [8, 73] (for quark operators) and [74, 75] (for gluon operators). As in TMD factorization theorems parton distributions are naturally defined in impact parameter space, it is convenient to do the decomposition in this space. The correspondence between decomposition in momentum and
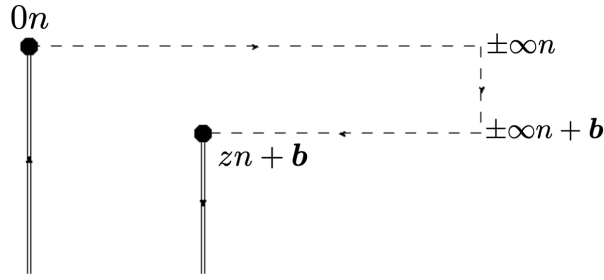
FIGURE 3.1: Staple contour for the gauge link $\mathcal{W}$ of the TMD operator.

impact parameter spaces can be found in e.g.[76, 77]. To study the distributions considered in this thesis we need only a part of the complete decomposition,

$$\Phi_{q\leftarrow h,ij}(x,\boldsymbol{b}) = \langle h|\Phi_{ij}(x,\boldsymbol{b})|h\rangle = \frac{1}{2}\Big(f_1\gamma^-_{ij} + g_{1L}S_L(\gamma_5\gamma^-)_{ij} \tag{3.4}$$

$$+ (S_{T\mu}i\gamma_5\sigma^{+\mu})_{ij}h_1 + (i\gamma_5\sigma^{+\mu})_{ij}\left(\frac{g_{T,\mu\nu}}{2} + \frac{b_\mu b_\nu}{\boldsymbol{b}^2}\right)\frac{S^\nu_T}{2}h^\perp_{1T} + ...\Big),$$

$$\Phi^{\mu\nu}_{g\leftarrow h}(x,\boldsymbol{b}) = \langle h|\Phi^{\mu\nu}(x,\boldsymbol{b})|h\rangle \tag{3.5}$$

$$= \frac{1}{2}\Big(-g^{\mu\nu}_T f^g_1 - i\epsilon^{\mu\nu}_T S_L g^g_{1L} + 2h^{\perp g}_1\left(\frac{g^{\mu\nu}_T}{2} + \frac{b^\mu b^\nu}{\boldsymbol{b}^2}\right) + ...\Big),$$

where the vector b^μ is a 4-dimensional vector of the impact parameter ($b^+ = b^- = 0$ and $-b^2 \equiv \boldsymbol{b}^2 > 0$), and $S_{T,L}$ are components of the hadron spin vector

$$S^\mu = S_L\left(\frac{p^+}{M}\bar{n}^\mu - \frac{M}{2p^+}n^\mu\right) + S^\mu_T, \tag{3.6}$$

and $\epsilon^{\mu\nu}_T = \epsilon^{+-\mu\nu} = n_\alpha\bar{n}_\beta\epsilon^{\alpha\beta\mu\nu}$. On the r.h.s. of eqs. (3.4, 3.5) we omit arguments of TMD distributions $(x,\boldsymbol{b})$, unless they are necessary. Note that in eq. (3.4) we use the normalization for the distribution $h^\perp_{1T}$ different from the traditional one [73]. The traditional definition can be recovered substituting $h^\perp_{1T} \to h^\perp_{1T}\boldsymbol{b}^2 M^2$, with M being the mass of hadron. The dots include non-studied TMDs and the TMD distributions that match the twist-3 and higher parton distribution functions.

Depending on the relation between hadron and quark (gluon) polarization, the different TMD distributions which appear in the decomposition are named as: unpolarized quark (gluon) distribution, $f^{q(g)}_1$, helicity quark (gluon) distribution, $g^{q(g)}_{1L}$, transversity quark distribution, h_1, pretzelosity quark distribution, $h^\perp_{1T}$ and linearly polarized gluon distribution, $h^{\perp g}_1$. To clarify the meaning of the different TMD distributions in terms of quark/gluon and hadron polarization, we can organize the TMD distributions in table 3.1.

The unpolarized TMD distribution is the most studied case and it has been treated using different regularization schemes at the next-to-leading order (NLO) [9–11, 13, 78–80], the next-to-next-to-leading order (NNLO) [18, 51, 81, 82] and recently at next-to-next-to-next-to-leading order (N^{3}LO) [**?**]. For polarized distributions there were calculations performed only for helicity, transversity and linearly polarized gluon distributions at NLO [77, 83]. However, these works miss a systematic discussion on the relevant renormalization schemes, which are fundamental to establish their

	U	L	T
U	$f_1^{q,g}$		$h_1^{\perp,q}$
L		$g_1^{q,g}$	$h_{1L}^{\perp,q}$
T	$f_{1T}^{\perp,q,g}$	$g_{1T}^{q,g}$	$h_1^q,\ h_{1T}^{\perp,q}$

TABLE 3.1: Overview of leading-twist unpolarized (U), longitudinally polarized (L) or transversely polarized (T) quark/gluon (row) TMDs for unpolarized, longitudinally polarized and transversely polarized hadrons (column). The distributions marked in bold also also appear in its collinear version, the ones marked in red are T-odd and not studied in this thesis.

calculation and to provide a path to higher order analysis. In this thesis NNLO results for some polarized TMD distributions are presented and discussed [84–86]. The importance of using highest available perturbative inputs for TMD distributions is important for the successful description of the experimental data, and significantly increases the predictive power of the framework [16, 66]. In this way, we reduce the theoretical error of the proper TMD distributions, allowing a better description of the interesting non-perturbative physics. Also as a consequence of performing high order perturbative calculation, the evolution of TMD distributions has been calculated at two and three loops [52, 62, 63]. This fact make possible to obtain phenomenological predictions up to N^{3}LL [17, 87].

For convenience we introduce the universal notation

$$\Phi_q^{[\Gamma]} = \frac{\text{Tr}(\Gamma\Phi)}{2}, \qquad \Phi_g^{[\Gamma]} = \Gamma^{\mu\nu}\Phi_{\mu\nu}. \tag{3.7}$$

Thus, we can write the spin (in)dependent quark and gluon TMD distribution definition in a process-independent way,

$$\Phi_{q\leftarrow h}^{[\Gamma]}(x, \boldsymbol{b}) = \frac{1}{2}\int\frac{d\lambda}{2\pi}e^{-ixp^+\lambda} \tag{3.8}$$
$$\langle P, S|\bar{T}\{\bar{q}(\lambda n + \boldsymbol{b})\tilde{W}_n^T(\lambda n + \boldsymbol{b})\}\,\Gamma\,T\{\tilde{W}_n^{T\dagger}(0)q(0)\}|P, S\rangle,$$

$$\Phi_{g\leftarrow h}^{[\Gamma]}(x, \boldsymbol{b}) = \frac{1}{xp^+}\int\frac{d\lambda}{2\pi}e^{-ixp^+\lambda} \tag{3.9}$$
$$\langle P, S|\bar{T}\{F_{+\mu}(\lambda n + \boldsymbol{b})\tilde{W}_n^T(\lambda n + \boldsymbol{b})\}\,\Gamma^{\mu\nu}\,T\{\tilde{W}_n^{T\dagger}(0)F_{+\nu}(0)\}|P, S\rangle,$$

where Γ represents the different Dirac or Lorentz variants for each polarization. We will investigate the Dirac or Lorentz variants allowed in order to have well defined spin dependent with cancellation of rapidity divergences in section 3.3.

3.2 Renormalization of TMD operator

The TMD operator defined in eqs. (3.8, 3.9) are affected by ultraviolet (UV) and rapidity divergences. In these sense, the TMD distributions obtained from the hadronic matrix elements of these operators are the *unsubstracted* TMD distributions. Both these divergences are renormalized by appropriate renormalization constants [15]. Consequently, the renormalized, and hence physical, TMD distributions depends on two scales. Traditionally, UV renormalization scale is denoted by μ and the rapidity

renormalization scale is denoted by ζ. The renormalized TMDPDF has the form

$$\Phi^{\text{ren}}(x, \boldsymbol{b}; \mu, \zeta) = Z(\mu, \zeta|\epsilon)R(\boldsymbol{b}, \mu, \zeta|\epsilon, \delta)\Phi^{\text{unsub.}}(x, \boldsymbol{b}|\epsilon, \delta), \tag{3.10}$$

where we explicitly show the dependence on regularization parameters. In particular, ϵ is the parameter of dimensional regularization ($d = 4 - 2\epsilon$) and regularizes UV divergences, which are renormalized by the factor Z. The δ is the parameter of δ-regularization [18, 52], and R is the rapidity renormalization factor. The singularities in ϵ and δ cancels in the product of eq. (3.10). The renormalization factors are independent of the Lorentz structure but they change according the parton color representation. The renormalization factors Z and R are intertwined and it is important to specify in which order the divergences are subtracted. Here we work in the scheme where renormalization of rapidity divergences is made prior to the renormalization of UV divergences. The final result for Φ^{ren} is of course independent of the subtraction order.

The renormalization factors are scheme dependent. For the UV renormalization we use the $\overline{\text{MS}}$-scheme. To specify the renormalization scheme for rapidity divergences we recall that within the TMD factorization theorem the rapidity divergences are compensated by the soft factor [10, 11, 15]. As before, the soft factor is defined as a product of soft Wilson lines

$$S(\boldsymbol{b}) = \frac{\text{Tr}_{\text{color}}}{N_c} \langle 0| \left[S_n^{T\dagger} \tilde{S}_{\bar{n}}^T \right] (\boldsymbol{b}) \left[\tilde{S}_{\bar{n}}^{T\dagger} S_n^T \right] (0)|0\rangle. \tag{3.11}$$

In perturbation theory, the soft function is calculated up to two-loop accuracy in δ-regularization scheme in [52]. An example of the Feynman diagrams that should be evaluated to obtain the first non-trivial result (NLO) for the soft function are given in fig. 3.2. The factors R introduced in eq. (3.10) also renormalize the soft factor, such that the whole factorization expression is finite, see the proof and detailed derivation in [15]. It can be shown that within a properly defined scheme the renormalized soft factor is trivial, i.e.

$$R(b, \mu, \zeta|\epsilon, \delta^+)S(\boldsymbol{b}|\epsilon, \delta^+, \delta^-)R(b, \mu, \bar{\zeta}|\epsilon, \delta^+) = 1, \tag{3.12}$$

where $\delta^{\pm}$ regularize rapidity divergences in the corresponding direction. In this scheme the rapidity renormalization factor has an exceptionally simple form [12, 15, 52]

$$R(b, \mu, \zeta|\epsilon, \delta^+) = S^{-1/2}\left(\boldsymbol{b}|\epsilon, \frac{\delta^+}{2p^+}\sqrt{\zeta}, \frac{\delta^+}{2p^+}\sqrt{\zeta} \right). \tag{3.13}$$

Such a scheme is very natural since it does not leave any remnant of soft factor in the factorization theorem, and therefore, coincides with other popular schemes of rapidity renormalization, e.g. with the one suggested in [10]. Although here we adopt the δ-regularization notation, these expressions could be translated to other regularization schemes, e.g. the translation dictionary of δ-regularization to the regularization by tilted Wilson lines is given in [88].
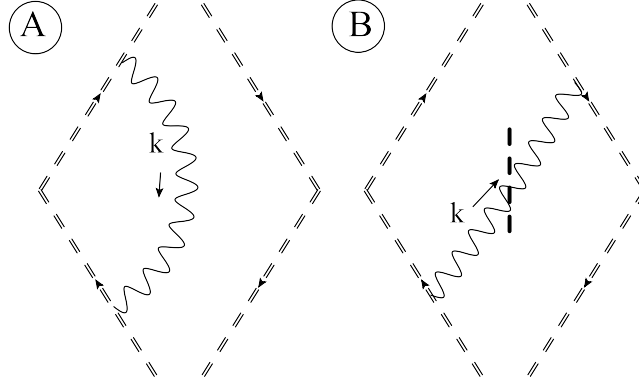
FIGURE 3.2: Feynman diagrams contributing to the TMD soft function at NLO in QCD.

3.3 Small-b OPE. Leading dynamical twist TMDs

Regardless of the non-perturbative nature of the TMD distributions, the large-q_T (or small-b) matching of TMD distributions on the corresponding integrated functions can be evaluated. Such consideration is practically very important because the resulting matching coefficients serve as an initial input to a model or a phenomenological ansatz for TMD distributions.

The small-b operator product expansion (OPE) is the relation between TMD operators and lightcone operators. Its leading order can be written as

$$\Phi_{ij}(x, \boldsymbol{b}) = \tag{3.14}$$
$$\left[\left(C_{q\leftarrow q}(\boldsymbol{b}) \right)^{ab}_{ij} \otimes \phi_{ab} \right](x) + \left[\left(C_{q\leftarrow g}(\boldsymbol{b}) \right)^{\alpha\beta}_{ij} \otimes \phi_{\alpha\beta} \right](x) + ...,$$
$$\Phi_{\mu\nu}(x, \boldsymbol{b}) = \tag{3.15}$$
$$\left[\left(C_{g\leftarrow q}(\boldsymbol{b}) \right)^{ab}_{\mu\nu} \otimes \phi_{ab} \right](x) + \left[\left(C_{g\leftarrow g}(\boldsymbol{b}) \right)^{\alpha\beta}_{\mu\nu} \otimes \phi_{\alpha\beta} \right](x) + ...,$$

where symbol $\otimes$ denotes the Mellin convolution in the variable x, i.e.

$$(f \otimes g)(x) = \int_x^1 \frac{dz}{z} f(z) g\left(\frac{x}{z}\right). \tag{3.16}$$

The functions $C(\boldsymbol{b})$ are dimensionless, i.e. they depend on $\boldsymbol{b}$ only logarithmically. The dots represent the power suppressed contributions, which presently have been studied only for the unpolarized case (see discussion in [65]). At this order of OPE, the functions $\phi(x)$ are the formal limit of the TMD operators $\Phi(x, \boldsymbol{0})$. The hadronic matrix elements of ϕ are the PDFs

$$
\begin{aligned}
\phi_{q\leftarrow h, ij}(x) &= \langle h | \phi_{ij}(x) | h \rangle \tag{3.17}\\
&= \frac{1}{2} \Big(f_{1,q}(x) \gamma_{ij}^- + g_{1L,q}(x) S_L (\gamma_5 \gamma^-)_{ij} \\
&\quad + (S_{T\mu} i \gamma_5 \sigma^{+\mu})_{ij} h_1 \Big) + \mathcal{O}\left(\frac{M}{p^+}\right),\\
\phi_{g\leftarrow h}^{\mu\nu}(x) &= \langle h | \phi^{\mu\nu}(x) | h \rangle \tag{3.18}\\
&= \frac{1}{2} \left(-g_T^{\mu\nu} f_{1,g}(x) - i\epsilon_T^{\mu\nu} S_L g_{1L,g} \right) + \mathcal{O}\left(\frac{M}{p^+}\right),
\end{aligned}
$$

where M is the mass of hadron. Both sides of eqs. (3.14, 3.15) should be supplemented by the ultraviolet renormalization constants.

The matching coefficients defined above should be free of rapidity divergences when the TMD distribution is renormalized. But the cancellation of rapidity divergences for the spin-dependent distributions is a non-trivial statement. Let us consider the small-b OPE for a generic TMD quark operator. At one loop we find

$$\Phi_q^{[\Gamma]} = \Gamma^{ab}\phi_{ab} + a_s C_F \mathbf{B}^\epsilon \Gamma(-\epsilon) \Big[\tag{3.19}$$

$$- (\gamma^+\gamma^-\Gamma + \Gamma\gamma^-\gamma^+)^{ab} + \bar{x} \left(\frac{g_T^{\alpha\beta}}{2} - \frac{b^\alpha b^\beta}{4\mathbf{B}}\epsilon \right) (\gamma^\mu\gamma_\alpha\Gamma\gamma_\beta\gamma_\mu)^{ab}$$

$$+ \left(\frac{1}{1-x} - \ln\left(\frac{\delta}{p^+}\right) \right) \left(\gamma^+\gamma^-\Gamma + \Gamma\gamma^-\gamma^+ + \frac{i\epsilon\gamma^+\slashed{b}\Gamma}{2\mathbf{B}} + \frac{i\epsilon\Gamma\slashed{b}\gamma^+}{2\mathbf{B}} \right)^{ab}$$

$$- \frac{i\pi}{2} \left(\gamma^+\gamma^-\Gamma - \Gamma\gamma^-\gamma^+ + \frac{i\epsilon\gamma^+\slashed{b}\Gamma}{2\mathbf{B}} - \frac{i\epsilon\Gamma\slashed{b}\gamma^+}{2\mathbf{B}} \right)^{ab} \Big] \otimes \phi_{ab} + \mathcal{O}(a_s^2),$$

where the divergent part at $x \to 1$ should be understood as $(..)_+$-distributed. Along this thesis, all the divergent contributions at $x \to 1$ should be understood as $(..)_+$ regularized. In eq. (3.19), we omit the gluon operator contribution for simplicity. The complex term in the last line of eq. (3.19) is the artifact of δ-regularization. The logarithm of δ represents the rapidity divergence which is to be eliminated by the factor R defined in eq. (3.13) which at this perturbative order reads

$$R = 1 + 2a_s C_F \mathbf{B}^\epsilon \Gamma(-\epsilon)$$

$$\times \left(\mathbf{L}_{\sqrt{\zeta}} + 2\ln\left(\frac{\delta}{p^+}\right) - \psi(-\epsilon) - \gamma_E \right) + \mathcal{O}(a_s^2). \tag{3.20}$$

The rapidity divergence cancels in the product $R\Phi$ if and only if

$$\gamma^+\Gamma = \Gamma\gamma^+ = 0\,, \tag{3.21}$$

yielding

$$R\Phi_q^{[\Gamma]} = \Gamma^{ab}\phi_{ab} + a_s C_F \mathbf{B}^\epsilon \Gamma(-\epsilon) \tag{3.22}$$

$$\times \Big[\left(-4 + \frac{4}{1-x} + 2\delta(\bar{x})(\mathbf{L}_{\sqrt{\zeta}} - \psi(-\epsilon) - \gamma_E) \right) \Gamma^{ab}$$

$$+ \bar{x} \left(\frac{g_T^{\alpha\beta}}{2} - \frac{b^\alpha b^\beta}{4\mathbf{B}}\epsilon \right) (\gamma^\mu\gamma_\alpha\Gamma\gamma_\beta\gamma_\mu)^{ab} \Big] \otimes \phi_{ab} + \mathcal{O}(a_s^2)\,.$$

The cancellation of rapidity divergences is the fundamental pre-requisite to obtain the matching coefficients of the renormalized operator Φ and ϕ.

The conditions analogue to eq. (3.21) for the gluon operator are

$$\Gamma^{+\mu} = \Gamma^{-\mu} = \Gamma^{\mu+} = \Gamma^{\mu-} = 0. \tag{3.23}$$

They follow from OPE for a generic gluon TMD operator $\Phi^{\mu\nu}$ similar to eq. (3.19), which we do not present here, since it is rather lengthy and not instructive. The conditions in eqs. (3.21, 3.23) are satisfied only for the following Dirac and Lorentz

structures

$$\Gamma^q = \{\gamma^+, \gamma^+ \gamma^5, \sigma^{+\mu}\}, \qquad \Gamma^g = \{g_T^{\mu\nu}, \epsilon_T^{\mu\nu}, b^\mu b^\nu / \boldsymbol{b}^2\}, \qquad (3.24)$$

which exactly correspond to the Lorentz structures for the so called "leading dynamical twist" TMD distributions. In this way, the relations eqs. (3.21, 3.23) provide a definition of the leading dynamical twist for TMD operators that can be used with no reference to a particular cross-section. On the other hand, our work shows that TMD operators of non-leading dynamical twist have rapidity singularities that are not canceled by the soft factor in eq. (3.11). While we have no knowledge of a calculation of the correction to the leading order of TMD factorization, our finding demonstrates that it has a different structure of rapidity divergences (which can spoil the factorization). The relation in eq. (3.21) will be used in chapter 4 to fix the definition of γ_5 in the dimensional regularization.

In order to calculate the matching coefficients, we consider the quark and gluon matrix elements with the momentum of parton set to $p^\mu = p^+ \bar{n}^\mu$. This choice of kinematic is allowed for consideration of twist-2 contribution only (which is the case of this thesis). Then, the calculations are greatly simplified. In particular, the perturbative corrections to the parton matrix element of ϕ's are zero, due to the absence of a scale in the dimensional regularization. Therefore, such matrix elements are equal to their renormalization constant, i.e., they have not finite ϵ-terms. In practice, it implies that the matching coefficient is the ϵ-finite part of the parton matrix element of the renormalized TMD operator (3.10). The evaluation of OPE for a general Lorentz structure (as in eq. (3.22)) is not very representative because one needs only the components associated with the TMDPDFs. Therefore, we project out the required components and present the expressions for each particular distribution.

Chapter 4

Matching of polarized transverse momentum distributions

This chapter is devoted to the study of the perturbative information which can be derived from the TMDPDFs. By means of the small-b limit of the TMDPDF we can isolate the perturbative information inside the matching coefficients, target of our calculations for the different polarizations of TMDs we consider. In order to find the expression for the matching coefficients, we evaluate the matrix elements with free quark or gluon states. The spinor and Lorentz indices of the in/out-going quarks and gluons can be contracted with the different Lorentz variants allowed for the leading dynamical twist quark or gluon TMDs considered. Schematically, we deal with the equation

$$\Phi_{f \leftarrow f'}(x, \boldsymbol{b}) = \sum_{r = q, \bar{q}, g} C_{f \leftarrow r} \otimes \phi_{r \leftarrow f'}(x), \tag{4.1}$$

where $\phi_{f \leftarrow f'}(x)$ represents the different polarized PDFs evaluated on free-quark states. This equation can be solved recursively starting from the first non-zero contribution. We obtain expressions for the matching coefficients up to second order in perturbation theory (NNLO). Then, the leading order expression is

$$C^{[0]}_{f \leftarrow f'} = C^{(0;0,0)}_{f \leftarrow f'}(x) = \delta_{ff'} \Phi^{[0]}_{f \leftarrow f'}. \tag{4.2}$$

Using it as a starting expression for iteration we obtain

$$C^{[1]}_{f \leftarrow f'} = \Phi^{[1]}_{f \leftarrow f'}(x, \boldsymbol{b}) - \phi^{[1]}_{f \leftarrow f'}(x), \tag{4.3}$$

$$C^{[2]}_{f \leftarrow f'} = \Phi^{[2]}_{f \leftarrow f'}(x, \boldsymbol{b}) - \sum_r C^{[1]}_{f \leftarrow r} \otimes \phi^{[1]}_{r \leftarrow f'}(x) - \phi^{[2]}_{f \leftarrow f'}(x). \tag{4.4}$$

The evaluation of TMD is made using the δ-regularization, which is described in details in chapter 2. Evaluating Feynman diagrams in fig. 4.1 we keep the momentum of quark collinear, $p^\mu = p^+ \bar{n}^\mu$. This choice of kinematics significantly simplifies the calculation. In particular, it implies that $\boldsymbol{b}^2$ is the only (Lorentz invariant) scale that is present in the diagrams. Since the scaleless loop-integrals are zero in the dimensional regularization, many diagrams vanish. For example, this is the case of all pure virtual correction diagrams. Thus, the outcome of each diagram up to NNLO has a generic form

$$\text{diag.} = (\boldsymbol{b}^2)^{2\epsilon} \left[f_1(x, \epsilon) + \left(\frac{\delta^+}{p^+} \right)^\epsilon f_2(x, \epsilon) + \left(\frac{\delta^+}{p^+} \right)^{-\epsilon} f_3(x, \epsilon) \right] \tag{4.5}$$
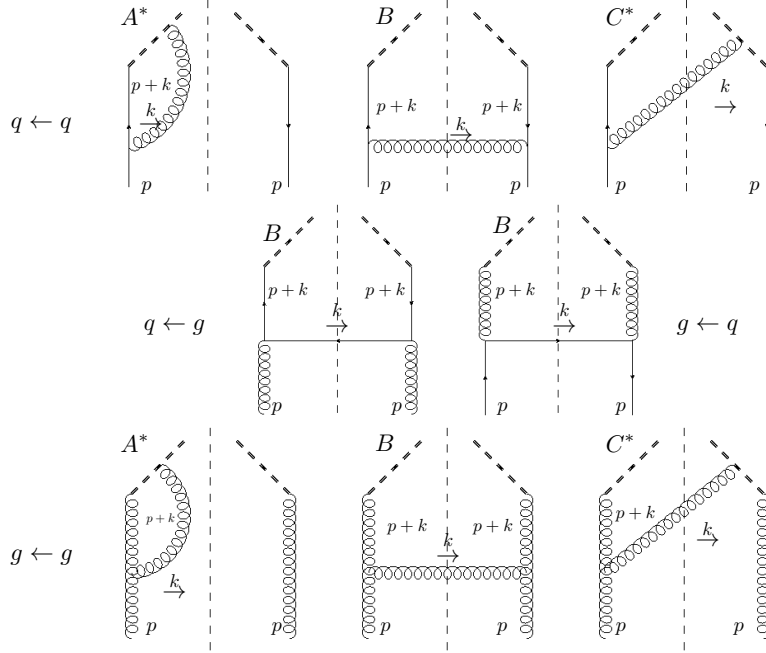
FIGURE 4.1: Feynman diagrams contributing to the TMDPDF at NLO in QCD. The external lines represent the final states. The dashed lines represent the quark or gluon Wilson lines. The star in a diagram indicates that its complex conjugate should be added.

$$+\ln\left(\frac{\delta^+}{p^+}\right) f_4(x,\epsilon) + \ln^2\left(\frac{\delta^+}{p^+}\right) f_5(x,\epsilon)\bigg].$$

where the functions f_i are regulated in the limit $x \to 1$ with $(..)_+$-distributions and at NLO only functions f_1, f_3, f_4 are present. The second and the third terms here represent the IR divergence. Therefore, the functions f_2 and f_3 exactly cancel in the sum of all the diagrams (and this fact can be also traced in the sum of sub-classes of diagrams). The last two terms represent the rapidity diverging pieces and thus the functions f_4 and f_5 are canceled by the rapidity renormalization factor. Altogether these cancellations serve as a good intermediate check of the computation.

Summing together the diagrams we obtain the un-subtracted expression for TMD-PDF on free-quark or gluon states. Let us denote it as

$$\Phi_{f\leftarrow f'}^{\text{unsub.}} = \Phi_{f\leftarrow f'}^{[0]\text{unsub.}}\delta_{ff'} + a_s\Phi_{f\leftarrow f'}^{[1]\text{unsub.}}\delta_{ff'} + a_s^2\Phi_{f\leftarrow f'}^{[2]\text{unsub.}} + \mathcal{O}(a_s^3), \qquad (4.6)$$

and it is UV and rapidity divergent. Starting from eq. (3.10) the renormalization procedure reads (for quarks)

$$\Phi_{f\leftarrow f'}^{[0]} = \Phi_{f\leftarrow f'}^{[0]\text{unsub.}} \qquad (4.7)$$

$$\Phi_{f\leftarrow f'}^{[1]} = \Phi_{f\leftarrow f'}^{[1]\text{unsub.}} - \frac{S^{[1]}\Phi_{f\leftarrow f'}^{[0]\text{unsub.}}}{2} + \left(Z_q^{[1]} - Z_2^{[1]}\right)\Phi_{f\leftarrow f'}^{[0]\text{unsub.}}. \qquad (4.8)$$

$$\Phi^{[2]}_{f \leftarrow f'} = \Phi^{[2]\text{unsub.}}_{f \leftarrow f'} - \frac{S^{[1]}\Phi^{[1]\text{unsub.}}_{f \leftarrow f'}}{2} - \frac{S^{[2]}\Phi^{[0]\text{unsub.}}_{f \leftarrow f'}}{2} + \frac{3S^{[1]}S^{[1]}\Phi^{[0]\text{unsub.}}_{f \leftarrow f'}}{8}$$
$$+ \left(Z^{[1]}_q - Z^{[1]}_2\right)\left(\Phi^{[1]\text{unsub.}}_{f \leftarrow f'} - \frac{S^{[1]}\Phi^{[0]\text{unsub.}}_{f \leftarrow f'}}{2}\right)$$
$$+ \left(Z^{[2]}_q - Z^{[2]}_2 - Z^{[1]}_2 Z^{[1]}_q + Z^{[1]}_2 Z^{[1]}_2\right)\Phi^{[0]\text{unsub.}}_{f \leftarrow f'}, \tag{4.9}$$

where superscript in square brackets indicates the perturbative order of a quantity. In this expression we have $Z = Z_2^{-1} Z_q$ with Z_2 the quark-field renormalization constant, and Z_q the quark TMD renormalization constant. Note that for gluons we have the same expressions for the renormalized TMD but $Z = Z_3^{-1} Z_g$ with Z_3 the gluon-field renormalization constant, and Z_q the gluon TMD renormalization constant The expression for them can be found e.g. in [18]. The soft function up to NNLO in δ-regularization can be found in the appendix A.

On the other hand, all loop-integrals contributing to collinear PDFs are zero. Thus the only non-zero part of $\phi(x)$ is the renormalization constant. That is, the needed expression for PDF evaluated on quarks or gluons is a pure singularity, which can be found using renormalization group equations. It reads

$$\phi^{[0]}_{f \leftarrow f'}(x) = P^{[0]}_{f \leftarrow f'}, \qquad \phi^{[1]}_{f \leftarrow f'}(x) = -\frac{\delta_{ff'}}{\epsilon} P^{[1]}_{f \leftarrow f'}(x), \tag{4.10}$$
$$\phi^{[2]}_{f \leftarrow f'}(x) = \frac{1}{2\epsilon^2}\left(\sum_r P^{[1]}_{f \leftarrow r} \otimes P^{[1]}_{r \leftarrow f'} + \frac{\beta_0}{2} P^{[1]}_{f \leftarrow f'}\right)(x) - \frac{1}{2\epsilon} P^{[2]}_{f \leftarrow f'}(x),$$

where $P^{[n]}$ are perturbative coefficients of DGLAP kernel at a_s^n-order for each polarization, and $\beta_0 = \frac{11}{3}C_A - \frac{2}{3}N_f$ is the QCD β-function.

With this information we can calculate the matching coefficients for different polarizations using the different Lorentz variants related to each case. Depending on the distributions studied we achieve different levels of precision in each calculation.

4.1 Helicity TMD distribution

We begin studying the distribution of longitudinally polarized quarks or gluons inside a longitudinally polarized hadron, the helicity distribution. In this case the Lorentz structures for quark and gluon operators are

$$\Gamma = \gamma^+ \gamma^5, \quad \Gamma^{\mu\nu} = i\epsilon^{\mu\nu}_T. \tag{4.11}$$

The corresponding "orthogonal" projectors are

$$\overline{\Gamma} = \mathcal{N}_{\text{sch.}}\frac{\gamma^- \gamma^5}{2}, \quad \overline{\Gamma}^{\mu\nu} = i\mathcal{N}_{\text{sch.}}\frac{\epsilon^{\mu\nu}_T}{2}, \tag{4.12}$$

where the factor $\mathcal{N}_{\text{sch.}}$ depends on the definition of γ^5 matrix in dimensional regularization. The definition of the γ^5 in dimensional regularization is a crucial point to make a systematic calculation of the perturbative part of this distribution at different orders in perturbation theory. Historically the most popular schemes (for QCD calculations) are 't Hooft-Veltman-Breitenlohner-Maison (HVBM) [89, 90], and Larin

scheme [91, 92]. In both schemes the combination $\gamma^+ \gamma^5$ can be presented as

$$\gamma^+ \gamma^5 = \frac{i}{3!} \epsilon^{+\nu\alpha\beta} \gamma_\nu \gamma_\alpha \gamma_\beta, \tag{4.13}$$

where $\epsilon^{\mu\nu\alpha\beta}$ is the antisymmetric Levi-Civita tensor. The difference between schemes is hidden in the definition of Levi-Civita tensor. In HVBM the $\epsilon^{\mu\nu\alpha\beta}$ is defined only for 4-dimensional set of indices. I.e. $\epsilon^{\mu\nu\alpha\beta} = 1$ if $\{\mu\nu\alpha\beta\}$ is even permutation of $\{0,1,2,3\}$, $\epsilon^{\mu\nu\alpha\beta} = -1$ if the permutation is odd, and $\epsilon^{\mu\nu\alpha\beta} = 0$ for any another case.

Due to the fact that in dimensional regularization the integration over loop momenta are done in $d \neq 4$ but the γ_5 matrix is four dimensional we should split the quantities which enter into the calculation in a 4-dimensional part and in a $(d-4)$-dimensional part. For example, the metric tensor in d-dimensions is written as,

$$g^{\mu\nu} = \bar{g}^{\mu\nu} + \hat{g}^{\mu\nu}, \tag{4.14}$$

where $\bar{g}^{\mu\nu}$ is the part of the tensor with $\mu, \nu = 0, 1, 2, 3$ and $\hat{g}^{\mu\nu}$ is the part with $\mu, \nu = 4, ..., d-4$. Consequently, for a general d-dimensional vector p^μ, we have the notation $\bar{g}^{\mu\nu} p_\nu = \bar{p}^\mu$ and $\hat{g}^{\mu\nu} p_\nu = \hat{p}^\mu$ for physical and unphysical components, respectively. Note that $\hat{v}^+ = \hat{v}^- = 0$, i.e. the unphyisical components are transverse. Thus, one can see that the relation of the Dirac matrices γ^μ with γ^5 are

$$\{\bar{\gamma}^\mu, \gamma^5\} = 0, \qquad [\hat{\gamma}^\mu, \gamma^5] = 0, \tag{4.15}$$

so, the well known 4-dimensional relation $\{\gamma^\mu, \gamma^5\} = 0$ is replaced by its analogous expression in d dimensions

$$\{\gamma^\mu, \gamma^5\} = 2\hat{\gamma}^\mu \gamma^5. \tag{4.16}$$

Also we conserve that $\gamma^5 \gamma^5 = 1$. The relation in eq. (4.16) allows to make the calculation os the diagrams in an analogous way to a case without γ^5 matrices. The only difference is an extra $(d-4)$-dimensional piece that can be calculated using derivatives with respect to the impact parameter of the 1-loop integrals presented in the appendix B. To see another way to apply the HVBM scheme to calculation in dimensional regularization see [88].

In Larin scheme the ϵ-tensor is non-zero for all set of d-dimensional indices, so we do not need to split our quantities in 4 and $(d-4)$-dimensional ones. The value of individual components are undefined, however, the product of two ϵ-tensors is defined as,

$$\epsilon^{\mu_1\nu_1\alpha_1\beta_1} \epsilon^{\mu_2\nu_2\alpha_2\beta_2} = -g^{\mu_1\mu_2} g^{\nu_1\nu_2} g^{\alpha_1\alpha_2} g^{\beta_1\beta_2} + g^{\mu_1\nu_2} g^{\nu_1\mu_2} g^{\alpha_1\alpha_2} g^{\beta_1\beta_2} - ..., \tag{4.17}$$

where the dots mean all 4! permutations of indices with alternating signs.

The drawback of both schemes is the violation of Adler-Bardeen theorem for the non-renormalization of the axial anomaly. This must be fixed by an extra finite renormalization constant Z_{qq}^5, derived from an external condition. A detailed discussion about this point can be found in [91, 93, 94]. The NNLO calculation of polarized deep-inelastic-scattering and Drell-Yan process in refs.[93, 94] made in (HVBM) have shown that the finite renormalization is required only for the the quark-to-quark part (both singlet and non-singlet cases). The same finite renormalization constant can be used for Larin scheme up to ϵ-singular terms at NNLO [69]. However, it seems that for higher order terms (in ϵ or in the coupling constant) the constant should be modified [69].

Needless to say, that Larin scheme is far more convenient then HVBM, because it does not violate Lorentz invariance. However, the Larin scheme, as it is originally formulated and used in modern applications [69], is inapplicable for TMD calculations. The point is that it does violate the definition of the leading dynamical twist eq. (3.21). Indeed, in the Larin scheme we have

$$\gamma^+ \Gamma = \gamma^+ \left(\gamma^+ \gamma^5\right)_{\text{Larin}} = \frac{i}{3!} \epsilon^{+\nu\alpha\beta} \gamma^+ \gamma_\nu \gamma_\alpha \gamma_\beta \neq 0, \tag{4.18}$$

because there is a contribution when all indices $\{\nu\alpha\beta\}$ are transverse. Note, that in HVBM scheme there is not such problem, since in the 4-dimensional $\epsilon^{+\nu\alpha\beta}$, one of the indices is necessarily "$-$". To ensure the existence of eq. (3.21) we perform a small modification of Larin scheme, and call it *Larin$^+$* scheme. We define

$$\left(\gamma^+ \gamma^5\right)_{\text{Larin}^+} = \frac{i\epsilon^{+-\alpha\beta}}{2!} \gamma^+ \gamma_\alpha \gamma_\beta = \frac{i\epsilon_T^{\alpha\beta}}{2!} \gamma^+ \gamma_\alpha \gamma_\beta. \tag{4.19}$$

The ϵ_T-tensor is d-dimensional, and for calculations it should be supplemented by the relation

$$\epsilon_T^{\alpha_1\beta_1} \epsilon_T^{\alpha_2\beta_2} = -g_T^{\alpha_1\alpha_2} g_T^{\beta_1\beta_2} + g_T^{\alpha_1\beta_2} g_T^{\beta_1\alpha_2}. \tag{4.20}$$

In the case the ϵ-tensor is 4-dimensional, the definition eq. (4.19) coincides with HVBM. The normalization factors presented in the eq. (4.12) are

$$\mathcal{N}_{\text{sch.}} = \begin{cases} 1 & \text{HVBM,} \\ (1-\epsilon)^{-1}(1-2\epsilon)^{-1} & \text{Larin}^+. \end{cases} \tag{4.21}$$

Due to the fact that the helicity distribution is present in all the quark and gluon channels at leading twist and to the extra complications that the treatment of γ^5 matrix in dimensional regularization introduces in the calculation it is done only up to NLO.

The expression of the matching of quark and gluon helicity distribution onto integrated functions are

$$\begin{aligned} g_{1L}(x,\boldsymbol{b}) &= [\Delta C_{q\leftarrow q}(\boldsymbol{b}) \otimes g_{1L}](x) + [\Delta C_{q\leftarrow g}(\boldsymbol{b}) \otimes g_{1L}^g](x) + \mathcal{O}(\boldsymbol{b}^2), \\ g_{1L}^g(x,\boldsymbol{b}) &= [\Delta C_{g\leftarrow q}(\boldsymbol{b}) \otimes g_{1L}](x) + [\Delta C_{g\leftarrow g}(\boldsymbol{b}) \otimes g_{1L}^g](x) + \mathcal{O}(\boldsymbol{b}^2), \end{aligned} \tag{4.22}$$

where ΔC are the helicity matching coefficient we calculate. We can write their expressions up to NLO as

$$\Delta C_{q\leftarrow q} = \delta(\bar{x}) + a_s C_F \Bigg\{ 2\boldsymbol{B}^\epsilon \Gamma(-\epsilon) \Big[\frac{2}{1-x} - 2$$

$$+ \bar{x}(1+\epsilon)\mathcal{H}_{\text{sch.}} + \delta(\bar{x})\left(\mathbf{L}_{\sqrt{\zeta}} - \psi(-\epsilon) - \gamma_E\right) \Big] \Bigg\}_{\epsilon\text{-finite}},$$

$$\Delta C_{q\leftarrow g} = a_s C_F \Bigg\{ 2\boldsymbol{B}^\epsilon \Gamma(-\epsilon) \Big[x - \bar{x}\mathcal{H}_{\text{sch.}} \Big] \Bigg\}_{\epsilon\text{-finite}},$$

$$\Delta C_{g\leftarrow q} = a_s C_F \Bigg\{ 2\boldsymbol{B}^\epsilon \Gamma(-\epsilon) \Big[1 + \bar{x}\mathcal{H}_{\text{sch.}} \Big] \Bigg\}_{\epsilon\text{-finite}},$$

$$\Delta C_{g \leftarrow g} = \delta(\bar{x}) + a_s C_A \Bigg\{ 2\boldsymbol{B}^\epsilon \Gamma(-\epsilon) \frac{1}{x} \Big[\frac{2}{1-x} - 2 \tag{4.23}$$

$$- 2x^2 + 2x\bar{x}\mathcal{H}_{\text{sch.}} + \delta(\bar{x}) \left(\boldsymbol{L}_{\sqrt{\zeta}} - \psi(-\epsilon) - \gamma_E \right) \Big] \Bigg\}_{\epsilon\text{-finite}},$$

where the subscript "ϵ-finite" implies the removal of ϵ-singular terms. The terms divergent in the limit $x \to 1$ should be understood as $(..)_+$-distributed, see eq. (2.47). The coefficient $\mathcal{H}_{\text{sch.}}$ accumulates the difference between HVBM and Larin$^+$ schemes,

$$\mathcal{H}_{\text{sch.}} = \begin{cases} 1 + 2\epsilon & \text{HVBM}, \\ \dfrac{1+\epsilon}{1-\epsilon} & \text{Larin}^+. \end{cases} \tag{4.24}$$

One can see that the expressions within HVBM and Larin$^+$ schemes coincide up to ϵ-suppressed parts at this perturbative accuracy.

In the regime of large-q_T, the TMD factorization reproduces the collinear factorization. Therefore, it is natural to normalize the helicity TMDPDF such that at large-q_T it reproduces the cross-section for polarized Drell-Yan, which in turn is normalized onto cross-section of unpolarized Drell-Yan process [94]. The TMD equivalent of this statement is the requirement of equality between helicity and unpolarized matching coefficients

$$\left[Z_{qq}^5(\boldsymbol{b}) \otimes \Delta C_{q \leftarrow q}(\boldsymbol{b}) \right](x) = C_{q \leftarrow q}(x, \boldsymbol{b}). \tag{4.25}$$

The constant Z_{qq}^5 is universal, in the sense that it is independent on the rapidity regularization scheme. We find the following finite renormalization constant for the TMD matching

$$Z_{qq}^5 = \delta(\bar{x}) + 2a_s C_F \boldsymbol{B}^\epsilon \Gamma(-\epsilon) \left(1 - \epsilon - (1+\epsilon)\mathcal{H}_{\text{sch.}} \right) \bar{x}. \tag{4.26}$$

Note, that HVBM version of Z_{qq}^5 coincides with the NLO part of the one presented in [94] up to logarithmic terms (which are dependent on the kinematics of process) .

Concluding the section we present the expressions for the helicity TMD distribution in the regime of small-b where the matching coefficients are taken in the limit $\epsilon \to 0$,

$$\Delta C_{q \leftarrow q} \equiv C_{q \leftarrow q} = \delta(\bar{x}) + a_s C_F \Big(-2\boldsymbol{L}_\mu \Delta p_{qq} + 2\bar{x}$$
$$+ \delta(\bar{x}) \left(-\boldsymbol{L}_\mu^2 + 2\boldsymbol{L}_\mu \boldsymbol{l}_\zeta - \zeta_2 \right) \Big) + \mathcal{O}(a_s^2),$$
$$\Delta C_{q \leftarrow g} = a_s T_F \left(-2\boldsymbol{L}_\mu \Delta p_{qg} + 4\bar{x} \right) + \mathcal{O}(a_s^2),$$
$$\Delta C_{g \leftarrow q} = a_s C_F \left(-2\boldsymbol{L}_\mu \Delta p_{gq} - 4\bar{x} \right) + \mathcal{O}(a_s^2),$$
$$\Delta C_{g \leftarrow g} = \delta(\bar{x}) + a_s C_A \Big(-2\boldsymbol{L}_\mu \Delta p_{gg} - 8\bar{x}$$
$$+ \delta(\bar{x}) \left(-\boldsymbol{L}_\mu^2 + 2\boldsymbol{L}_\mu \boldsymbol{l}_\zeta - \zeta_2 \right) \Big) + \mathcal{O}(a_s^2), \tag{4.27}$$

with $\boldsymbol{l}_\zeta = \ln\mu^2/\zeta$. The functions Δp are the combination of helicity evolution kernel (which can be found e.g. in [69]) and the TMD anomalous dimension. They are

$$\Delta p_{qq}(x) = \frac{2}{1-x} - 1 - x,$$

$$\Delta p_{qg}(x) = 2x - 1, \quad \Delta p_{gq}(x) = 2 - x,$$
$$\Delta p_{gg}(x) = \frac{2}{1-x} + 2 - 4x. \tag{4.28}$$

The coefficients $\Delta C_{q\leftarrow q}$ and $\Delta C_{q\leftarrow g}$ have been evaluated in [83]. Our expressions agree with ones presented in [83] apart of ζ_2 term in $\Delta C_{q\leftarrow q}$. This disagreement is the result of different renormalization schemes. We use the conventional $\overline{\text{MS}}$ scheme with $e^{\epsilon \gamma_E}$ factor, while MS-scheme of [83] is defined with $\Gamma^{-1}(1 + \epsilon)$ factor. The coefficients $\Delta C_{g\leftarrow q}$ and $\Delta C_{g\leftarrow g}$ have been evaluated in [77] and we agree with them. To see an older calculation in which helicity TMDs are used see e.g. [95].

4.2 Transversely polarized distribution

In this section, we consider the transversely polarized TMD distribution and we focus on the leading twist distributions in which it can be decomposed. These distributions are the so called transversity and pretzelosity (also called quadrupole) TMD distributions. Our aim is the evaluation of their twist-2 matching up to two loop order, in order to do a calculation of a polarized TMD distribution at the same level of the unpolarized TMD distribution. Both these distributions have been recently subject of experimental, phenomenological and theoretical investigations. The SIDIS data relevant for this extractions come mainly from HERMES [96] and COMPASS [97, 98]. Recently also RHIC has provided data in this direction [99] and it is expected that transversity will be one of the central measurements in future EIC and LHC-Spin. The transverse momentum dependent transversity has been extracted using SIDIS data by Anselmino et al. in [100–102] with Gaussian models without taking into account the TMD evolution. In refs. [103, 104] the lowest order evolution has been considered. An issue of these extractions is the size of the theoretical error. The reduction of it essentially requires the inclusion of the higher order perturbative information. Let us also mention here the attempts to extract the transversity distribution making use of lattice input [105]. Also, the integral of the transversity distribution over the light-cone momentum is related to the tensor charge of the nucleon. This quantity is relevant because it can be computed by lattice QCD, offering a chance to test lattice results and it is an useful quantity to search for physics beyond the Standard Model [106]. The transversity TMDFF is also an interesting and practically important object (see [107] for a recent review) and we show a calculation of it twist-2 matching up to NNLO. For what concerns pretzelosity, we mention here the recent analysis made in [108, 109]. According to this analysis, the pretzelosity distribution is very small and practically consistent with a null value.

The transversely polarized TMD distribution is parameterized in terms of four TMDPDFs, which were originally introduced in momentum space [7, 73]. For our purposes we need the equivalent parametrization in the position space. It reads

$$\Phi_{q\leftarrow h}^{[i\sigma^{\alpha+}\gamma_5]}(x, \boldsymbol{b}) = S_T^\alpha h_1(x, \boldsymbol{b}) - i\lambda b^\alpha M h_{1L}^\perp(x, \boldsymbol{b}) \tag{4.29}$$

$$+ i\epsilon_T^{\alpha\mu} b_\mu M h_1^\perp(x, \boldsymbol{b}) + \frac{M^2 \boldsymbol{b}^2}{2} \left(\frac{g_T^{\alpha\mu}}{2} + \frac{b^\alpha b^\mu}{\boldsymbol{b}^2} \right) S_{T\mu} h_{1T}^\perp(x, \boldsymbol{b}),$$

where s_T is the transverse part of the hadron spin, λ is helicity, M is the mass of hadron and $\boldsymbol{b}^2 = -b^2 > 0$. The detailed relation between momentum and position space definitions can be found in [76, 110]. The function h_1, is known as TMD

transversity distribution, and the function $h_{1T}^\perp$, is known as the pretzelosity distribution. Note that the general Lorentz structure for a transversely polarized operator is usually addressed as $i\sigma^{+\alpha}\gamma^5 = \epsilon_T^{\alpha\nu}\sigma^{+\nu}$. However, at leading twist the transversity and pretzelosity distributions have no mixture with gluon distributions and the common practice is to eliminate the γ^5 or ϵ_T from the definition of these operators. Thus, the Lorentz structure for these two distributions is simply expressed using $\sigma^{\alpha+}$. On the contrary, in a longitudinally polarized operator there is mixture with gluons at leading twist and the γ^5 cannot be dropped nor in definition nor in computations (see [84] for a discussion of the different schemes for γ^5 used in a NLO calculation of the helicity distribution).

The small-b operator product expansion (OPE) allows the systematic expansion of the TMD operator in powers of b. The operators that are associated to the powers of b are then classified by twists. The evaluation of the matrix element of the small-b OPE results into an expression of the form

$$\Phi_{q\leftarrow h}^{[i\sigma^{\alpha+}\gamma^5]}(x,\boldsymbol{b}) = \sum_f \left[C_{q\leftarrow f;\text{tw-2}}^{\alpha\beta}(\boldsymbol{b}) \otimes h_{f\leftarrow h}^{\beta;\text{tw-2}} \right](x) \tag{4.30}$$

$$+ b_\beta \sum_f \left[C_{q\leftarrow f;\text{tw-3}}^{\alpha\beta\gamma}(\boldsymbol{b}) \otimes h_{f\leftarrow h}^{\gamma;\text{tw-3}} \right](x) + \dots,$$

where h are collinear distributions, C are coefficient functions and $\otimes$ is the integral convolution in the momentum fractions. The terms in eq. (4.30) incorporate all tensor structures of the TMD distribution parametrization in eq. (4.29). Extracting particular tensors, one can find the matching of individual TMDPDFs onto collinear functions. In particular, the tensor structure of h_1 and $h_{1T}^\perp$ appears in the twist-2 term, while the tensor structure for $h_{1L}^\perp$ and $h_1^\perp$ can be produced only at the twist-3 [110]. In this thesis we only concentrate in twist-2 distribution so we only study the first line on eq. (4.30).

The OPE in transversely polarized case has an exceptionally simple structure, since there are no gluon operators. The only PDF that contribute to the matching of these twist-2 distributions is the collinear transversity PDF. Its expression reads [111]

$$S_T^\alpha h_1(x) = \frac{1}{2} \int \frac{d\lambda}{2\pi} e^{-ixp^+\lambda} \langle P,S|\bar{T}\{\bar{q}(\lambda n)[\lambda n,0]\, i\sigma^{\alpha+}\gamma^5\, q(0)\}|P,S\rangle. \tag{4.31}$$

The PDF $h_1(x)$ can also be interpreted as the probability distribution to find a transversely polarized quark in a hadron.

The coefficient functions of the OPE are dimensionless and the dependence on b enters only via logarithms, or via dimensionless tensors. Generally, the twist-2 coefficient functions can have structures $\sim g_T^{\alpha\beta}$ and $\sim b^\alpha b^\beta / \boldsymbol{b}^2$. It is natural to decompose it as

$$C_{q\leftarrow f;\text{tw-2}}^{\alpha\beta}(x,\boldsymbol{b}) = g_T^{\alpha\beta}\delta C_{q\leftarrow f}(x,\mathbf{L}_\mu) + \left(\frac{g_T^{\alpha\beta}}{2(1-\epsilon)} + \frac{b^\alpha b^\beta}{\boldsymbol{b}^2} \right) \delta^\perp C_{q\leftarrow f}(x,\mathbf{L}_\mu), \tag{4.32}$$

where $\delta C_{q\leftarrow f}$ and $\delta^\perp C_{q\leftarrow f}$ are the twist-2 matching coefficients for transversity and pretzelosity TMD distributions respectively. Note that the normalizations are take in $d = 4 - 2\epsilon$ dimensions. In this way, the pieces of this decomposition do not mix. In particular, the tensor in the second term of eq. (4.32) has zero trace (in $d = 4 - 2\epsilon$ dimensions). Comparing the parametrization in eq. (4.32) with the parametrization

for TMD distributions we find that the matching for individual TMDPDFs are

$$
h_1^q(x, \boldsymbol{b}) = \int_x^1 \frac{dy}{y} \sum_{f=q,\bar{q}} \delta C_{q \leftarrow f} \left(\frac{x}{y}, \mathbf{L}_\mu \right) h_1^f(y) + \mathcal{O}(\boldsymbol{b}^2), \tag{4.33}
$$

$$
h_{1T}^{\perp,q}(x, \boldsymbol{b}) = \frac{2}{\boldsymbol{b}^2 M^2} \int_x^1 \frac{dy}{y} \sum_{f=q,\bar{q}} \delta^\perp C_{q \leftarrow f} \left(\frac{x}{y}, \mathbf{L}_\mu \right) h_1^f(y) + \mathcal{O}(\boldsymbol{b}^2), \tag{4.34}
$$

where we explicitly express the Mellin convolution integral. In these formulas we also suppress the scale dependence of functions because it is common to all the TMD distributions independently on their polarization. The sum over flavors runs only over non-singlet combinations, since there are no gluon operator with transverse polarized configuration that could mix with the quarks.

The coefficient functions δC and $\delta^\perp C$ can be evaluated perturbatively. At tree order, $\sim a_s^0$, the coefficient function in eq. (4.32) is proportional to $g_T^{\alpha\beta}$, and thus only δC is non-zero. The terms proportional to $\sim b^\alpha b^\beta / b^2$ are generated by loop-diagrams and appear already at one-loop level [84].

4.2.1 Transversity TMDPDF

The evaluation of the transversity matching coefficient is very similar to the evaluation of the unpolarized matching coefficient made in [18]. The main technical details to perform this calculation (an also the unpolarized one) up to NNLO are expained in the appendix B. The main difference, which only simplifies the evaluation, is the absence of the mixing with the gluon operator.

The LO contribution expression for transversity TMDPDF is

$$
h_{1 f \leftarrow f'}^{[0]}(x) = \delta(1-x)\delta_{ff'}. \tag{4.35}
$$

Substituting it in eq. (4.1), we find the LO matching coefficient

$$
\delta C_{f \leftarrow f'}^{[0]} = \delta C_{f \leftarrow f'}^{(0;0,0)}(x) = \delta_{ff'}\delta(1-x). \tag{4.36}
$$

The NLO expression for matching coefficient reads

$$
\delta C_{f \leftarrow f'}^{[1]}(x, \boldsymbol{b}) = C_F \delta_{ff'} \left(-\frac{4x \mathbf{L}_\mu}{1-x} + \delta(\bar{x}) \left(-\mathbf{L}_\mu^2 + 2\mathbf{L}_\mu \mathbf{l}_\zeta - \zeta_2 \right) \right). \tag{4.37}
$$

This result agrees[1] with the ones obtained in refs. [83, 84, 88]. It is easy to see that logarithmic part of eq. (4.37) satisfies renormalization group equations eqs. (2.62, 2.63). The finite part is

$$
\delta C_{f \leftarrow f'}^{(1;0,0)}(x) = -C_F \zeta_2 \delta_{ff'}\delta(\bar{x}). \tag{4.38}
$$

Note, that in order to evaluate NNLO matching coefficient one needs the terms suppressed by ϵ, since they interfere with the singularities of the PDF, and produce a non-zero finite and $1/\epsilon$ contribution to eq. (4.4). The complete expression at all orders of ϵ can be found in [84].

Now we focus on the expression for $\delta C^{[2]}$. Firstly we present the only non-trivial part that is the finite part $\delta C^{(2;0,0)}$. At NNLO we have the mixing with anti-quark

---

[1]The calculation made in [83] is made in a non-standard $\overline{\text{MS}}$-scheme. And for this reason, the coefficient presented in [83] is different from eq. (4.37) by $\zeta_2 \delta(\bar{x})$ term.

operator, therefore, the matching is split into two channels

$$\delta C^{(2;0,0)}_{f \leftarrow f'}(x) = \delta_{ff'} \delta C^{(2;0,0)}_{q \leftarrow q}(x) + \delta_{f\bar{f}'} \delta C^{(2;0,0)}_{q \leftarrow \bar{q}}(x), \tag{4.39}$$

where

$$\begin{aligned}
\delta C^{(2;0,0)}_{q \leftarrow q}(x) = & \; C_F^2 \Big\{ \delta p(x) \Big[4\mathrm{Li}_3(\bar{x}) - 20\mathrm{Li}_3(x) - 4\ln\bar{x}\,\mathrm{Li}_2(\bar{x}) + 12\ln x\,\mathrm{Li}_2(x) \tag{4.40} \\
& + 2\ln^2\bar{x}\ln x + 2\ln\bar{x}\ln^2 x + \frac{3}{2}\ln^2 x + 8\ln x + 20\zeta_3 \Big] - 2\ln\bar{x} + 4\bar{x} \Big\} \\
& + C_F C_A \Big\{ \delta p(x) \Big[8\mathrm{Li}_3(x) - 4\mathrm{Li}_3(\bar{x}) + 4\ln\bar{x}\,\mathrm{Li}_2(\bar{x}) - 4\ln x\,\mathrm{Li}_2(x) \\
& - \frac{\ln^3 x}{3} - \frac{11}{6}\ln^2 x - \frac{76}{9}\ln x + 6\zeta_3 - \frac{404}{27} \Big] + 2\ln\bar{x} + \frac{14}{3}\bar{x} \Big\} \\
& + C_F N_f \Big\{ \delta p(x) \Big[\frac{\ln^2 x}{3} + \frac{10}{9}\ln x + \frac{56}{27} \Big] - \frac{2\bar{x}}{3} \Big\} \\
& + \delta(\bar{x}) \Big[C_F^2 \frac{5\zeta_4}{4} + C_F C_A \Big(5\zeta_4 - \frac{77}{9}\zeta_3 - \frac{67}{6}\zeta_2 + \frac{1214}{81} \Big) \\
& + C_F N_f \Big(\frac{14}{9}\zeta_3 + \frac{5}{3}\zeta_2 - \frac{164}{81} \Big) \Big],
\end{aligned}$$

$$\begin{aligned}
\delta C^{(2;0,0)}_{q \leftarrow \bar{q}}(x) = & \; \Big(C_F^2 - \frac{C_F C_A}{2} \Big) \Big\{ \delta p(-x) \Big[8\mathrm{Li}_3 \Big(\frac{1}{1+x} \Big) - 8\mathrm{Li}_3 \Big(\frac{x}{1+x} \Big) \tag{4.41} \\
& + 4\mathrm{Li}_3(x^2) - 4\ln x\mathrm{Li}_2(x^2) + 4\ln^2 x\ln(1+x) - 4\ln x\ln^2(1+x) \\
& - \frac{2}{3}\ln^3 x - 4\zeta_3 \Big] + 2\bar{x} \Big\}.
\end{aligned}$$

Here,

$$\delta p(x) = \frac{2x}{1-x}, \tag{4.42}$$

is the regular part of LO DGLAP kernel.

It is intriguing to observe that the parts of eqs. (4.40, 4.41) enclosed by the square brackets literally coincide with corresponding parts for the unpolarized matching coefficient, see [18] eqs. (7.3, 7.8). In other words, the matching coefficient for both unpolarized and transversity distributions has the form

$$C^{(2;0,0)}(x) = P^{[1]}(x)F_1(x) + F_2(x) + \delta(\bar{x})F_3, \tag{4.43}$$

where $P^{[1]}(x)$ is the corresponding LO DGLAP kernel, for the corresponding PDF. Then we observe that the function $F_1(x)$ and the constant F_3 are the same for unpolarized and transversity kernels (for both flavor channels). Such behavior is expected since the contributions proportional to $1/(1-x)$, as well as $\delta(\bar{x})$ contributions, that primary form the LO DGLAP kernel, come from the diagrams where the quarks interact with the Wilson lines. Such diagrams are insensitive to the polarization structure of the operator. The rest of diagrams are not singular in the limit $x \to 1$, and thus form a regular contribution. For more detailed discussion on the internal structure of transversity kernel see [71].

For completeness, we present here the non-zero logarithmic terms of the matching coefficients. These terms can be calculated from the renormalization group equations and serve as a strong check of our calculation. So,

$$\delta C_{q\leftarrow q}^{(2;4,2)}(x) = -\delta C_{q\leftarrow q}^{(2;4,1)}(x) = 4\delta C_{q\leftarrow q}^{(2;4,0)}(x) = 2C_F^2\delta(\bar{x}), \tag{4.44}$$

$$\delta C_{q\leftarrow q}^{(2;3,0)}(x) = 2C_F^2\delta p(x) + C_F\left(-\frac{22}{9}C_A + \frac{4}{9}N_f\right)\delta(\bar{x}), \tag{4.45}$$

$$\delta C_{q\leftarrow q}^{(2;3,1)}(x) = 4C_F^2\delta p(x) + C_F\left(\frac{11}{3}C_A - \frac{2}{3}N_f\right)\delta(\bar{x}), \tag{4.46}$$

$$\delta C_{q\leftarrow q}^{(2;2,0)}(x) = 4C_F^2\delta p(x)(2\ln\bar{x} - \ln x) + C_F\delta p(x)\left(\frac{2}{3}N_f - \frac{11}{3}C_A\right) \tag{4.47}$$
$$+\delta(\bar{x})\left[-7C_F^2\zeta_2 + C_F C_A\left(-\frac{67}{9} + 2\zeta_2\right) + \frac{10}{9}C_F N_f\right],$$

$$\delta C_{q\leftarrow q}^{(2;2,1)}(x) = \delta(\bar{x})\left[-2C_F^2\zeta_2 + C_F C_A\left(\frac{134}{9} - 4\zeta_2\right) - \frac{20}{9}C_F N_f\right], \tag{4.48}$$

$$\delta C_{q\leftarrow q}^{(2;1,0)}(x) = C_F^2\left[2\delta p(x)\left((3 + 4\ln\bar{x})\ln x + \zeta_2\right) - 4\bar{x}\right] \tag{4.49}$$
$$C_F C_A\left[2\delta p(x)\left(-2\ln x\left(\frac{11}{3} + \ln x\right) - \frac{134}{9} + 4\zeta_2\right) + 2\bar{x}\right]$$
$$+C_F N_f\,\delta p(x)\frac{8}{9}(5 + 3\ln x) + C_F\delta(\bar{x})\left[-\frac{22}{3}C_A\zeta_2 + \frac{4}{3}\zeta_2 N_f\right],$$

$$\delta C_{q\leftarrow q}^{(2;1,1)}(x) = C_F\delta(\bar{x})\left[-\frac{112}{27} + C_A\left(\frac{404}{27} - 14\zeta_3\right)\right], \tag{4.50}$$

$$\delta C_{q\leftarrow\bar{q}}^{(2;1,0)}(x) = 4\left(C_F^2 - \frac{C_F C_A}{2}\right)\left\{\delta p(-x)\left[4\text{Li}_2(-x) + 4\ln x\ln(1 + x)\right. \tag{4.51}$$
$$\left.-\ln^2 x + 2\zeta_2\right] + \bar{x}\right\}.$$

4.2.2 Transversity TMDFF

In the case of the transversity TMDFF the calculation of the matching coefficients can be done with the available tools developed for the calculation of the TMDPDF. This is because despite the different origin and interpretation of these distributions, their perturbative treatment is analogous. Thus, in this section we discuss the fundamental definitions to translate the theory developed for PDFs to FFs and we present the results up to the same order of unpolarized TMDFF calculated in [18].

The unsubtracted transversity TMDFFs are defined with the following hadronic matrix elements,

$$\Delta_{q\to N}^{[i\sigma^{\alpha+}\gamma^5]}(z,\boldsymbol{b}) = \frac{1}{4zN_c}\sum_X \int \frac{d\lambda}{2\pi}e^{-ip^+\lambda/z}$$

$$\times \langle 0|T\left[\tilde{W}_n^{T\dagger}q_j\right]_a(n\lambda+\boldsymbol{b})|P,S;X\rangle i\sigma^{\alpha+}\gamma^5\langle P,S;X|\bar{T}\left[\bar{q}_i\,\tilde{W}_n^T\right]_a(0)|0\rangle,$$

where z represents the momentum fraction of the final state parton fragmenting into a hadron. The hadronic matrix element can be parameterized in a similar way that in eq. (4.29)

$$\Delta_{q\to h}^{[i\sigma^{\alpha+}\gamma_5]}(z,\boldsymbol{b}) = S_T^\alpha H_1(z,\boldsymbol{b}) - i\lambda b^\alpha M H_{1L}^\perp(z,\boldsymbol{b}) \tag{4.52}$$

$$+i\epsilon_T^{\alpha\mu}b_\mu M H_1^\perp(z,\boldsymbol{b}) + \frac{M^2\boldsymbol{b}^2}{2}\left(\frac{g_T^{\alpha\mu}}{2}+\frac{b^\alpha b^\mu}{\boldsymbol{b}^2}\right)S_{T\mu}H_{1T}^\perp(z,\boldsymbol{b}),$$

where again S_T is the transverse part of the hadron spin, λ is helicity, M is the mass of hadron and $\boldsymbol{b}^2 = -b^2 > 0$. We recall that the parametrization presented here is valid for produced hadrons with spin-1/2. For the scalar or pseudo-scalar hadrons, the functions, H_1, $H_{1L}^\perp$ and $H_{1T}^\perp$ are absent. The transversity TMDFF, or Collins function, is represented by the function H_1. The matching onto the fragmentation function is done as

$$H_1^q(z,\boldsymbol{b}) = \int_z^1 \frac{dy}{y^{3-2\epsilon}}\sum_{f=q,\bar{q}}\delta\mathbb{C}_{q\to f}\left(\frac{z}{y},\mathbf{L}_\mu\right)H_1^f(y) + \mathcal{O}(\boldsymbol{b}^2). \tag{4.53}$$

The factor $z^{2-2\epsilon}$ is added to meet the common normalization of collinear FF function, that is defined as

$$S_T^\alpha H_1(x) = \frac{z^{1-2\epsilon}}{4N_c}\sum_X \int \frac{d\lambda}{2\pi}e^{-ip^+\lambda/z} \tag{4.54}$$

$$\times \langle 0|T\left[\tilde{W}_n^{T\dagger}q_j\right]_a(n\lambda)|P,S;X\rangle i\sigma^{\alpha+}\gamma^5\langle P,S;X|\bar{T}\left[\bar{q}_i\,\tilde{W}_n^T\right]_a(0)|0\rangle,$$

where the γ^5 can be dropped as in the TMDPDF case. The evolution kernels for the collinear FFs are known at two loops [70, 71].

The main difference in evaluation of TMDFFs in comparison to TMDPDFs is the origin of parton momentum in diagrams, which is incoming in the PDF case, and outgoing in the FF case. Therefore, the expressions for TMDFFs could be obtained by the application of the crossing symmetry $x \to z^{-1}$ at the diagram level. This, however, should be done with caution since there is a brunch cut for $x > 1$, which should be transformed into a branch cut for $z > 1$. Additionally, one should take into account the z^ϵ factors that are present in definitions of FFs, and that mix in the ϵ-expansions with various contributions. For the detailed discussion on relation between PDFs and FFs see [112] and references within. To avoid these complications, we re-evaluate the PDF master integrals with $x \to z^{-1}$ and reassemble the final result. The LO matching of transversity TMDFF is elementary

$$\delta\mathbb{C}_{f\to f'}^{[0]} = \delta_{ff'}\delta(\bar{z}). \tag{4.55}$$

Therefore, the renormalization properties of the FF case are similar to the case of PDFs and the matching procedure follows the same pattern as in the unpolarized

case [18]. For this reason we skip the details of evaluation and present the final result.

For the presentation of the NLO and NNLO coefficient functions we introduce again logarithmic decomposition (see eq. (2.64))

$$\delta \mathbb{C}_{f \to f'}(z, \mathbf{L}_\mu, \mathbf{l}_\zeta) = \sum_{n=0}^{\infty} a_s^n \sum_{k=0}^{n+1} \sum_{l=0}^{n} \mathbf{L}_\mu^k \, \mathbf{l}_\zeta^l \, \delta \mathbb{C}_{f \to f'}^{(n;k,l)}(z). \tag{4.56}$$

The terms accompanied by logarithms, i.e. with $k + l > 0$ can be restored with renormalization group equation. The NLO matching coefficient is given by

$$z^2 \delta C_{f \leftarrow f'}^{[1]}(x, \boldsymbol{b}) = C_F \delta_{ff'} \left(2\delta p(z) \left(2\ln z - \mathbf{L}_\mu \right) + \delta(\bar{x}) \left(-\mathbf{L}_\mu^2 + 2\mathbf{L}_\mu \mathbf{l}_\zeta - \zeta_2 \right) \right). \tag{4.57}$$

At NNLO we have the same mixing with anti-quark operator. The matching is split into two channels

$$\delta \mathbb{C}_{f \to f'}^{(2;0,0)}(z) = \delta_{ff'} \delta \mathbb{C}_{q \to q}^{(2;0,0)}(z) + \delta_{f\bar{f}'} \delta \mathbb{C}_{q \to \bar{q}}^{(2;0,0)}(z), \tag{4.58}$$

where,

$$
\begin{aligned}
z^2 \delta \mathbb{C}_{q \to q}^{(2;0,0)}(z) = {}& C_F^2 \bigg\{ \delta p(z) \bigg[40\mathrm{Li}_3(z) - 4\mathrm{Li}_3(\bar{z}) + 4\ln\bar{z}\mathrm{Li}_2(\bar{z}) - 16\ln z\mathrm{Li}_2(z) \\
& - \frac{40}{3}\ln^3 z + 18\ln^2 z\ln\bar{z} - 2\ln^2\bar{z}\ln z + \frac{15}{2}\ln^2 z \\
& - 8\left(1 + \zeta_2\right)\ln z - 40\zeta_3 \bigg] + 4\bar{z}(1 + \ln z) + 2z(\ln\bar{z} - \ln z) \bigg\} \\
& + C_F C_A \bigg\{ \delta p(z) \bigg[4\mathrm{Li}_3(\bar{z}) + 12\mathrm{Li}_3(z) - 4\ln\bar{z}\mathrm{Li}_2(\bar{z}) - 8\ln z\mathrm{Li}_2(z) + 3\ln^3 z \\
& - 4\ln\bar{z}\ln^2 z - \frac{11}{6}\ln^2 z - 12\zeta_2\ln z + \frac{70}{3}\ln z + 2\zeta_3 - \frac{404}{27} \bigg] \\
& + \frac{14}{3}\bar{z} - 2z\ln\bar{z} - 2(1 - 2z)\ln z \bigg\} \\
& + C_F N_f \bigg\{ \delta p(z) \bigg[\frac{\ln^2 z}{3} - \frac{10}{3}\ln z + \frac{56}{27} \bigg] - \frac{2}{3}\bar{z} \bigg\} + \delta(\bar{z}) \bigg\{ \frac{5}{4}\zeta_4 C_F^2 \\
& + C_F C_A \bigg[\frac{1214}{81} - \frac{67}{6}\zeta_2 + 65\zeta_4 - \frac{77}{9}\zeta_3 \bigg] + C_F N_f \bigg[-\frac{164}{81} + \frac{5}{3}\zeta_2 + \frac{14}{9}\zeta_3 \bigg] \bigg\},
\end{aligned}
\tag{4.59}
$$

$$
\begin{aligned}
z^2 \delta \mathbb{C}_{q \to \bar{q}}^{(2;0,0)}(z) = {}& \left(C_F^2 - \frac{C_F C_A}{2} \right) \bigg\{ \delta p(-z) \bigg[8\mathrm{Li}_3\left(\tfrac{1}{1+z}\right) - 8\mathrm{Li}_3\left(\tfrac{z}{1+z}\right) \\
& - 4\mathrm{Li}_3\left(z^2\right) + 16\ln z\mathrm{Li}_2\left(z\right) - 4\ln z\mathrm{Li}_2\left(z^2\right) - 4\ln z\ln^2(1+z) \\
& - 12\ln^2 z\ln(1+z) + 6\ln^3 z + 4\zeta_3 \bigg] + 2\bar{z} \bigg\}.
\end{aligned}
\tag{4.60}
$$

The singularity at $z \to 1$ is understood as a $(..)_+$-distribution (see eq. (2.47)). Similarly to the PDF case, the expressions enclosed by square brackets in eqs. (4.59, 4.60) literally coincide with the ones of the unpolarized fragmenting function case, (see eqs. (7.11, 7.17) in [18]). In other words, it can be written in the form of eq. (4.43), and the functions $F_1(z)$ and F_3 coincide for polarized and unpolarized cases.

For completeness, we present here the non-zero logarithmic terms of the matching coefficients as in the TMDPDF case,

$$z^2 \delta \mathbf{C}_{q \leftarrow q}^{(2;4,2)}(z) = -z^2 \delta \mathbf{C}_{q \leftarrow q}^{(2;4,1)}(z) = 4z^2 \delta \mathbf{C}_{q \leftarrow q}^{(2;4,0)}(z) = 2C_F^2 \delta(\bar{z}), \tag{4.61}$$

$$z^2 \delta \mathbf{C}_{q \leftarrow q}^{(2;3,0)}(z) = 2C_F^2 \delta p(z) + C_F \left(-\frac{22}{9} C_A + \frac{4}{9} N_f \right) \delta(\bar{z}), \tag{4.62}$$

$$z^2 \delta \mathbf{C}_{q \leftarrow q}^{(2;3,1)}(z) = -4C_F^2 \delta p(z) + C_F \left(\frac{11}{3} C_A - \frac{2}{3} N_f \right) \delta(\bar{z}), \tag{4.63}$$

$$z^2 \delta \mathbf{C}_{q \leftarrow q}^{(2;2,0)}(z) = -8C_F^2 \delta p(z)(\ln z - \ln \bar{z}) + C_F \delta p(z) \left(\frac{2}{3} N_f - \frac{11}{3} C_A \right) \tag{4.64}$$
$$+ \delta(\bar{z}) \left[-7 C_F^2 \zeta_2 + C_F C_A \left(-\frac{67}{9} + 2\zeta_2 \right) + \frac{10}{9} C_F N_f \right],$$

$$z^2 \delta \mathbf{C}_{q \leftarrow q}^{(2;2,1)}(z) = 8C_F^2 \delta p(z) \ln z + \delta(\bar{x}) \left[-2 C_F^2 \zeta_2 + C_F C_A \left(\frac{134}{9} - 4\zeta_2 \right) \tag{4.65}$$
$$-\frac{20}{9} C_F N_f \right],$$

$$z^2 \delta \mathbf{C}_{q \leftarrow q}^{(2;1,0)}(z) = C_F^2 \left[4\delta p(x) \left(-3(1 + 4\ln \bar{z}) \ln z + 8\ln^2 z + \zeta_2 \right) - 2\bar{z} \right] \tag{4.66}$$
$$+ C_F C_A \left[2\delta p(x) \left(\frac{22}{3} \ln z - 2\ln^2 z - \frac{134}{9} + 4\zeta_2 \right) + 2\bar{z} \right]$$
$$+ C_F N_f \, \delta p(z) \frac{8}{9} (5 - 3\ln z) + C_F \delta(\bar{z}) \left[-\frac{22}{3} C_A \zeta_2 + \frac{4}{3} \zeta_2 N_f \right],$$

$$z^2 \delta \mathbf{C}_{q \leftarrow q}^{(2;1,1)}(z) = C_F \delta(\bar{z}) \left[-\frac{112}{27} + C_A \left(\frac{404}{27} - 14\zeta_3 \right) \right], \tag{4.67}$$

$$z^2 \delta \mathbf{C}_{q \leftarrow \bar{q}}^{(2;1,0)}(z) = 4 \left(C_F^2 - \frac{C_F C_A}{2} \right) \left\{ \delta p(-z) \left[4\text{Li}_2(-z) \right. \right. \tag{4.68}$$
$$\left. \left. -\ln z (\ln z - 4\ln(1 + z)) + 2\zeta_2 \right] + \bar{z} \right\}.$$

4.3 Pretzelosity TMDPDF

The calculation for the matching of the pretzelosity TMDPDF over the transversity integrated PDF is in principle similar to the one of the transversity TMDPDF. In this case one has a different projector, see eq. (4.32),

$$\frac{b^\mu b^\nu}{b^2} + \frac{g_T^{\mu\nu}}{2(1 - \epsilon)}, \tag{4.69}$$

to be compared to $g_T^{\mu\nu}$ used in the transversity calculation. Moreover the relation

$$\sigma^{\mu+} \left(\frac{b^\mu b^\nu}{b^2} + \frac{g_T^{\mu\nu}}{2(1-\epsilon)} \right) \sigma^{-\nu} = 0 \qquad (4.70)$$

allows a simplification of many diagrams. In particular, the diagrams with a non-interacting quark line are exactly zero, according to the expression (4.70). This feature reduces the number of diagrams that we have to calculate for the pretzelosity TMD distribution. The pretzelosity projector is built as a sum of two terms. The first one is $g_T^{\mu\nu}$ and it is the same as in the transversity calculation. As the topology of the diagrams is the same in both cases the integrals that appear in the calculation of the diagrams are also the same. The second term of the projector is $b^\mu b^\nu / b^2$ and this implies new types of master integrals, that has scalar products $(b \cdot q)^2$ in the numerator (here, q^μ is a loop-momentum). The explicit expressions for these integrals can be found in the appendix B. Such structures appear due to the convolution of a generic diagram with open indices with the projector (4.69).

The small-b expression for the matching of the pretzelosity distribution is written in a form equivalent to the transversity case,

$$h_{1T,f\leftarrow f'}^\perp(x,b) \quad = \sum_{r=q,\bar{q},q'} \left[\delta^\perp C_{f\leftarrow r}(b) \otimes \delta f_{r\leftarrow f'} \right](x) + \mathcal{O}(b^2). \qquad (4.71)$$

Note, that the collinear function in eq. (4.71) is the transversity PDF. As in the transversity case, at NLO we have only the quark-to-quark channel, and at NNLO we have quark-to-quark and quark-to-antiquark channels.

Due to eq. (4.70), the un-subtracted pretzelosity distribution is zero at LO, i.e. $\delta^\perp \Phi^{[0]}(x) = 0$. Consequently, the LO matching coefficient is also zero, i.e.

$$\delta^\perp C_{q\leftarrow q}^{[0]}(x) = 0. \qquad (4.72)$$

This fact induces a simplification in the renormalization of the pretzelosity TMDPDF at NLO, demanding the absence of any divergences at this order. Moreover, due to the absence of the tree order collinear counterpart for the matching procedure the pretzelosity is suppressed by a_s. As a result, the expression for the matching coefficient is given solely by the one-loop TMD matrix element

$$\delta^\perp C_{q\leftarrow q}^{[1]}(x,b) = \delta^\perp \Phi_{q\leftarrow q}^{[1]}(x,b) = -4C_F B^\epsilon \Gamma(-\epsilon) \bar{x} \epsilon^2. \qquad (4.73)$$

We see that the obtained matching coefficient is ϵ-suppressed, so, in the limit $\epsilon \to 0$ it is zero, i.e. $\delta^\perp C_{q\leftarrow q}^{[1]}(x,b) = 0$. According to eq. (4.73), the perturbative part of the pretzelosity distribution is suppressed numerically. This result coincides with the estimation made in [8]. This observation is indeed supported by the measurements of $\sin(3\phi_h - \phi_S)$-asymmetries by HERMES and COMPASS, see e.g.[108] and references within. We also mention that it is not possible to obtain the small-b matching at the helicity distribution. The helicity distribution as a part of pretzelosity distribution is suggested by various model calculations (see [113] and references within).

The nullity of the LO pretzelosity distribution and the ϵ-suppressed behavior of the NLO contribution yields in a simple expression for the renormalized pretzelosity TMDPDF at NNLO

$$h_{1T,f\leftarrow f}^{\perp[2]} = \delta^\perp \Phi_{f\leftarrow f'}^{[2]} - \frac{S^{[1]} \delta^\perp \Phi_{f\leftarrow f'}^{[1]}}{2} + \left(Z_q^{[1]} - Z_2^{[1]} \right) \delta^\perp \Phi_{f\leftarrow f'}^{[1]} \qquad (4.74)$$

In this expression it is important to keep all ϵ-terms of $\delta^\perp \Phi^{[1]}_{f \leftarrow f''}$, since they are multiplied by factors with leading $1/\epsilon^2$-behavior (the TMD renormalization factor, and soft factor). Thus, these terms produce $1/\epsilon$ singularities, despite the suppressed behavior of $\delta^\perp \Phi^{[1]}_{f \leftarrow f'}$. Naturally, these terms cancel the corresponding ultraviolet singularities of the un-subtracted TMD matrix element. We have also checked the exact cancellation of infrared divergences, and rapidity divergences. It is interesting to trace the distribution of the contributions between diagrams with different color factor. There are four types of contribution

$$\delta^\perp \Phi^{[2]}_{f \leftarrow f'} = C_F^2 A_F + C_F \left(C_F - \frac{C_A}{2} \right) A_{FA} + \frac{C_F C_A}{2} A_A + C_F N_f A_N. \tag{4.75}$$

The contribution A_N is ϵ-suppressed in a similar manner as the one-loop expression. The contribution A_F is canceled by the renormalization factor entirely up terms suppressed in ϵ. Thus, the only non-zero contribution to the TMD matrix element comes from A_{FA} and A_A, which we find to be equal up to higher powers of ϵ. So, concluding we have found

$$A_F = \frac{S^{[1]} \delta^\perp \Phi^{[1]}_{f \leftarrow f'}}{2} - \left(Z_q^{[1]} - Z_2^{[1]} \right) \delta^\perp \Phi^{[1]}_{f \leftarrow f'} + \mathcal{O}(\epsilon), \tag{4.76}$$

$$A_{FA} = A_A + \mathcal{O}(\epsilon), \qquad A_N = \mathcal{O}(\epsilon). \tag{4.77}$$

Therefore, the contribution proportional to C_A disappears from the final expression, despite only these diagram are non-trivial. The resulting TMD matrix element in the pretzelosity channel is proportional to C_F^2 only, and it reads

$$h^{\perp[2]}_{1T,q \leftarrow q} = -4 C_F^2 \left(\bar{x} \left(3 + 4 \ln \bar{x} \right) + 4 x \ln x \right) + \mathcal{O}(\epsilon), \tag{4.78}$$

$$h^{\perp[2]}_{1T,q \leftarrow \bar{q}} = 0. \tag{4.79}$$

Expanding eq. (4.71) up to order a_s^2 we obtain the following expressions for matching coefficient

$$\delta^\perp C^{[2]}_{q \leftarrow q}(x, \boldsymbol{b}) = h^{[2]}_{1T,q \leftarrow q}(x, \boldsymbol{b}) - \left[\delta^\perp C^{[1]}_{q \leftarrow q}(\boldsymbol{b}) \otimes \delta f^{[1]}_{q \leftarrow q} \right](x) \tag{4.80}$$

$$\delta^\perp C^{[2]}_{q \leftarrow \bar{q}}(x, \boldsymbol{b}) = 0. \tag{4.81}$$

The convolution term that appears in eq. (4.80) is different from zero because the NLO matching coefficient is ϵ-suppressed but the NLO transversity integrated PDF is ϵ-divergent. So, the result for the convolution term is finite,

$$\left[\delta^\perp C^{[1]}_{q \leftarrow q}(\boldsymbol{b}) \otimes \delta f^{[1]}_{q \leftarrow q} \right](x) = -4 C_F^2 \left(\bar{x} \left(3 + 4 \ln \bar{x} \right) + 4 x \ln x \right), \tag{4.82}$$

which is the same that we get in eq. (4.78). Using eq. (4.80) we obtain a null value for the NNLO pretzelosity to transversity matching coefficient. So,

$$\delta^\perp C^{[2]}_{q \leftarrow f}(x, \boldsymbol{b}) = 0 + \mathcal{O}(\epsilon), \tag{4.83}$$

where $f = q, \bar{q}$.

We stress once more that the cancellation that leads to the zero result has a non-trivial structure. Because the topologies of diagrams that contribute to convolution

term in eq. (4.80) and to the TMD matrix element eq. (4.78) are completely different. In the first case, these are ladder diagrams, while in the second case we have diagrams with tree-gluon vertex and non-planar diagrams. All this indicates the presence of a not yet understood concept behind these cancellations, and it suggests that such cancellations take a place at higher orders as well. Therefore we conjecture that

$$\delta^\perp C_{q \leftarrow f}(x, \boldsymbol{b}) = 0, \tag{4.84}$$

at all orders of perturbation theory. Recently, this conjecture has been confirmed in [114], where the first non-zero matching of the pretzelosity distribution has been found at twist-3.

4.4 Linearly polarized gluon TMDPDF

The definition of the linearly polarized gluon TMDPDF (lpTMDPDF) comes from the definition of the global gluon TMDPDF distribution and its decomposition over independent Lorentz structures. This decomposition contains 8 components [74, 77]. If we constraint ourselves to the case of a unpolarized hadron only two of these structures survive,

$$\Phi^{\mu\nu}_{g \leftarrow h}(x, \boldsymbol{b}) = -\frac{g_T^{\mu\nu}}{2(1-\epsilon)} f_{1, g \leftarrow h}(x, \boldsymbol{b}) + h^\perp_{1, g \leftarrow h}(x, \boldsymbol{b}) \left(\frac{g_T^{\mu\nu}}{2(1-\epsilon)} + \frac{b^\mu b^\nu}{\boldsymbol{b}^2} \right), \tag{4.85}$$

where f_1 is the unpolarized gluon TMDPDF and $h_1^\perp$ is known as linearly polarized gluon TMDPDF. Its name results from the fact that this distribution study the distribution of linearly polarized gluons inside an unpolarized hadron. Both f_1 and $h_1^\perp$ contribute to the gluon-induced TMD processes on equal foot. Although these functions share some common properties, they are completely independent non-perturbative functions that are to be extracted from the experiment. Both these functions have a lot of interest because they participate of processes of the standing of Higgs boson production by gluon-gluon fusion. The study of the lpTMDPDF at the same level of accuracy of the unpolarized TMDPDF is important in order to study its effect in the transverse momentum spectrum of the Higgs boson. A detailed study of this process is discussed in the chapter 5 of this thesis.

The usage of a d-dimensional definition for the decomposition in eq. (4.85) is important for the following two-loop calculation because the ϵ-dependent parts influence the result. The definition in eq. (4.85) is the standard one [81, 84] written such that the unpolarized part coincides with the standard definition of the unpolarized TMDPDF, see e.g. [10, 18, 81],

$$f_{1, g \leftarrow h}(x, \boldsymbol{b}) = -g_T^{\mu\nu} \Phi_{g \leftarrow h, \mu\nu}(x, \boldsymbol{b}), \tag{4.86}$$

whereas the linearly-polarized tensor is orthogonal to it. In turn the lpTMDPDF is given by

$$h^\perp_{1, g \leftarrow h}(x, \boldsymbol{b}) = \frac{1}{1 - 2\epsilon} \left(g_T^{\mu\nu} + 2(1-\epsilon) \frac{b^\mu b^\nu}{\boldsymbol{b}^2} \right) \Phi_{g \leftarrow h, \mu\nu}(x, \boldsymbol{b}). \tag{4.87}$$

Sometimes, one would like to use TMD distributions defined in the momentum space. The relation between coordinate and momentum representation is the usual

one [74, 77] (here in $d = 4$ dimensions),

$$\Phi_{g \leftarrow h, \mu\nu}(x, \mathbf{k}) = \int \frac{d^2\mathbf{b}}{(2\pi)^2} e^{i(bk)} \Phi_{g \leftarrow h, \mu\nu}(x, \mathbf{b}) \tag{4.88}$$

$$= -\frac{g_T^{\mu\nu}}{2} f_{1, g \leftarrow h}(x, \mathbf{k}) + h_{1, g \leftarrow h}^{\perp}(x, \mathbf{k}) \left(\frac{g_T^{\mu\nu}}{2} + \frac{k^\mu k^\nu}{\mathbf{k}^2} \right),$$

where

$$f_{1, g \leftarrow h}(x, \mathbf{k}) = \int_0^\infty \frac{|\mathbf{b}| d|\mathbf{b}|}{2\pi} J_0(|\mathbf{b}||\mathbf{k}|) f_{1, g \leftarrow h}(x, \mathbf{b}), \tag{4.89}$$

$$h_{1, g \leftarrow h}^{\perp}(x, \mathbf{k}) = -\int_0^\infty \frac{|\mathbf{b}| d|\mathbf{b}|}{2\pi} J_2(|\mathbf{b}||\mathbf{k}|) h_{1, g \leftarrow h}^{\perp}(x, \mathbf{b}). \tag{4.90}$$

As with the other distributions studied, a small-b expansion can be performed in order to obtain perturbative calculable matching coefficients. In the present case, it results into the following expressions

$$f_{1, g \leftarrow h}(x, \mathbf{b}; \mu, \zeta) = \sum_f \int_x^1 \frac{dy}{y} C_{g \leftarrow f}(y, \mathbf{b}; \mu, \zeta; \tilde{\mu}) f_{1, f \leftarrow h}\left(\frac{x}{y}, \tilde{\mu} \right) + \mathcal{O}(b^2) \tag{4.91}$$

$$h_{1, g \leftarrow h}^{\perp}(x, \mathbf{b}; \mu, \zeta) = \sum_f \int_x^1 \frac{dy}{y} \delta^L C_{g \leftarrow f}(y, \mathbf{b}; \mu, \zeta; \tilde{\mu}) f_{1, f \leftarrow h}\left(\frac{x}{y}, \tilde{\mu} \right) + \mathcal{O}(\mathbf{b}^2), \tag{4.92}$$

where the sum runs over the active parton flavors (quarks and gluon), and $f_1(x, \mu)$ is unpolarized collinear distributions defined as usual

$$f_{1, q \leftarrow h}(x, \mu) = \int \frac{d\lambda}{2\pi} e^{-ixp^+\lambda} \langle P | \bar{T} \{ \bar{q}(\lambda n) \tilde{W}_n(\lambda n) \} \frac{\gamma^+}{2} T\{ \tilde{W}_n^\dagger(0) q(0) \} | P \rangle, \tag{4.93}$$

$$f_{1, g \leftarrow h}(x, \mu) = \frac{1}{xp^+} \tag{4.94}$$

$$\times \int \frac{d\lambda}{2\pi} e^{-ixp^+\lambda} \langle P | \bar{T} \left\{ F_{+\mu}(\lambda n) \tilde{W}_n(\lambda n) \right\} T \left\{ \tilde{W}_n^\dagger(0) F_{+\mu}(0) \right\} | P \rangle.$$

The scales μ and ζ in eqs. (4.91, 4.92) are the scales of TMD evolution discussed in the chapter 2. The scale $\tilde{\mu}$ is the scale of OPE, that is not related to the TMD evolution scales and whose dependence cancels in the convolution of coefficient function and collinear distribution.

The tree-order of matching coefficients, C and $\delta^L C$, are to be calculated in QCD perturbation theory.

$$C_{g \leftarrow f}(x, \mathbf{b}; \mu, \zeta; \tilde{\mu}) = \delta_{gf} \delta(1-x) + \mathcal{O}(a_s), \tag{4.95}$$

$$\delta^L C_{g \leftarrow f}(x, \mathbf{b}; \mu, \zeta; \tilde{\mu}) = \mathcal{O}(a_s), \tag{4.96}$$

Nowadays, the coefficients $C_{f \leftarrow h}(x, \mathbf{b})$ are known at a_s^2-order (NNLO) [18, 51, 81, 82], whereas coefficients $\delta^L C_{f \leftarrow h}(x, \mathbf{b})$ are known at a_s-order (NLO). Note that in literature related to TMD calculations, e.g. in refs. [77, 84], the orders of $\delta^L C_{f \leftarrow h}$ are traditionally counted alike the unpolarized case. So, the linear a_s-terms are denoted as NLO. Here we use the same convention. In this thesis we present expression for $\delta^L C_{g \leftarrow f}$ up to NNLO.

The higher order coefficient function for OPE at twist-2 level can be deduced

from the calculation of matrix elements with free parton states with subsequent matching of the result on the desired OPE structures eq. (4.92). Therefore, the task is naturally split into two steps: the evaluation of parton-matrix element and the matching as explained at the beginning of this chapter. The evaluation of parton matrix elements of the TMD operators at two-loop level is the most complicated part of this calculation because it has some extra difficulties than in the analogous calculation for the unpolarized case. In the case of lpTMDPDF the main complication comes from the rich vector structure, which is reduced to scalar products by projection factor in eq. (4.87), and the use of unpolarized parton states with momentum $p^\mu = p^+ \bar{n}^\mu$. In this aspect the current computation is similar to evaluation of the pretzelosity distribution [85] albeit with significantly larger number of loop-integrals. The reduction of integrals to master integrals and some details of their evaluation is presented in the appendix B.

The NLO expression of the matching coefficients read

$$\delta^L C^{[1]}_{g\leftarrow g}(x, \mathbf{b}) = \left(4C_A \mathbf{B}^\epsilon \Gamma(-\epsilon) \frac{\bar{x}}{x} \epsilon \right)_{\epsilon\text{-finite}}, \tag{4.97}$$

$$\delta^L C^{[1]}_{g\leftarrow q}(x, \mathbf{b}) = \left(4C_F \mathbf{B}^\epsilon \Gamma(-\epsilon) \frac{\bar{x}}{x} \epsilon \right)_{\epsilon\text{-finite}}, \tag{4.98}$$

We write the full ϵ-dependent NLO expressions here because they are needed in the calculation of the NNLO matching coefficients. Using the same notation introduced in eq. (2.64), the finite parts of these results are

$$\delta^L C^{(1;0,0)}_{g\leftarrow g}(x) = -4C_A \frac{\bar{x}}{x}, \tag{4.99}$$

$$\delta^L C^{(1;0,0)}_{g\leftarrow q}(x) = -4C_F \frac{\bar{x}}{x}, \tag{4.100}$$

The results in eqs. (4.99, 4.100) agree with [77, 84, 115].

The NNLO calculation has a more involved expression but we can write it in terms of its finite and logarithmic parts in a simple form as

$$\delta^L C^{[2]}_{g\leftarrow f}(x, \mathbf{b}; \mu, \zeta, \mu) = \left(-\frac{1}{2}\mathbf{L}^2_\mu + \mathbf{L}_\mu \mathbf{l}_\zeta \right) \delta^L C^{(2,1,1)}_{g\leftarrow f}(x) + \mathbf{L}_\mu \delta^L C^{(2,1,0)}_{g\leftarrow f}(x) \tag{4.101}$$
$$+ \delta^L C^{(2,0,0)}_{g\leftarrow f}(x).$$

The finite part result for the two available channels is,

$$\delta^L C^{(2;0,0)}_{g\leftarrow g}(x) = C_A^2 \left[-16\frac{\bar{x}}{x}\left(\text{Li}_2(x) - \ln x \right) + \frac{124}{3}\ln x + \left(\frac{148}{9} + 20\zeta_2 \right)\frac{\bar{x}}{x} \right. \tag{4.102}$$
$$\left. -8\ln^2 x - \frac{100}{9}\bar{x} - \frac{4}{9}x(11x - 14) \right]$$
$$+ C_F N_f \cdot 4\left[\ln^2 x - 2\frac{(\bar{x}^3)}{x} \right] + C_A N_f \cdot \frac{4}{9}\left[17\frac{\bar{x}}{x} + 1 - 3x - x^2 + 6\ln x \right],$$

$$\delta^L C^{(2;0,0)}_{g\leftarrow q}(x) = C_F(C_F - C_A)\left[8\frac{\bar{x}}{x}(\ln\bar{x} + \ln^2\bar{x}) - 20\ln x + 4\ln^2 x + 8\bar{x} \right] \tag{4.103}$$
$$+ C_F C_A\left[16\frac{\bar{x}}{x}\left(\frac{11}{18} + \frac{5}{4}\zeta_2 - \frac{\ln\bar{x}}{3} - \text{Li}_2(x) \right) \right.$$

$$+4\frac{\ln x}{x}\left(4+5x-x\ln x\right)\Big]+C_F N_f\cdot\frac{16}{9}\frac{\bar{x}}{x}[2+3\ln\bar{x}].$$

These results have been recently obtained in ref. [116] with an independent calculation using the exponential regulator of ref. [50] to regularize rapidity divergences. We find full agreement with the final results presented.

Due to fact that the logarithmic terms can be calculated solving the renormalization group eqs. (2.55, 2.56) they can be written in terms of the NLO finite part and anomalous dimensions as

$$
\begin{aligned}
\delta^L C^{(2,1,1)}_{g\leftarrow f}(x) &= \frac{\Gamma^g_0}{2}\delta^L C^{(1,0,0)}_{g\leftarrow f}(x), \\
\delta^L C^{(2,1,0)}_{g\leftarrow f}(x) &= 2\beta_0\delta^L C^{(1,0,0)}_{g\leftarrow f}(x)-\sum_{f'=g,q,\bar{q}}[\delta^L C^{(1,0,0)}_{g\leftarrow f'}\otimes P^{[1]}_{f'\leftarrow f}](x),
\end{aligned}
\tag{4.104}
$$

where $\Gamma^g_0 = 4C_A$ is LO cusp anomalous dimension, $\beta_0 = 11/3C_A - 2/3N_f$ is LO β−function, and we have used that $\gamma^{g[1]}_V = -2\beta_0$. The explicit expressions for these coefficients are given here for completeness,

$$
\begin{aligned}
\delta^L C^{(2,1,1)}_{g\leftarrow g}(x) &= -8C_A^2\frac{\bar{x}}{x}, \tag{4.105} \\
\delta^L C^{(2;1,0)}_{g\leftarrow g}(x) &= -16C_A^2\left\{\frac{1+x}{x}\ln x+\frac{\bar{x}}{x}\left[\frac{x}{6}(2-x)+\frac{15}{4}-\ln\bar{x}\right]\right\} \tag{4.106} \\
&\quad +16C_F T_r N_f\left[\frac{1}{3}\frac{\bar{x}}{x}\left(2+(2-x)x\right)+\ln x\right]+\frac{16}{3}C_A T_r N_f\frac{\bar{x}}{x},
\end{aligned}
$$

$$
\begin{aligned}
\delta^L C^{(2,1,1)}_{g\leftarrow q}(x) &= -8C_F C_A\frac{\bar{x}}{x}, \tag{4.107} \\
\delta^L C^{(2;1,0)}_{g\leftarrow q}(x) &= -4C_F C_A\left[\frac{\bar{x}}{x}\left(\frac{43}{3}+x\right)+4\frac{1+x}{x}\ln x\right] \tag{4.108} \\
&\quad +4C_F^2\left[\frac{\bar{x}}{x}(x+4\ln\bar{x})+2\ln x\right]+\frac{32}{3}C_F T_r N_f\frac{\bar{x}}{x}.
\end{aligned}
$$

In the expressions above we have set $\tilde{\mu} = \mu$, which is a poor choice. In particular, due to this choice one obtains the double-logarithms in the coefficient function and, as the result, a badly convergent perturbative series. A much better behaved coefficient function can be achieved by distinguishing the scales of evolution and OPE. For example, this is realized by applying the ζ-prescription, which consists in the selection of TMD evolution scales along the null-evolution line in the plane (μ,ζ) (for further information see chapter 2). This line is parameterized as $\zeta = \zeta_\mu(\boldsymbol{b})$, and it is defined by the boundary condition that it passes through the saddle point of the evolution potential [16]. The expression for the coefficient function can be obtained by the substitution (here for gluon distributions)

$$\text{in }\zeta\text{-prescription:}\qquad \mathbf{l}_\zeta = \frac{\mathbf{L}_\mu}{2}-\frac{2\beta_0}{\Gamma^g_0}+\mathcal{O}(a_s).\tag{4.109}$$

The higher order terms and the derivation of this expression can be found in ref. [16, 66]. The coefficient function in ζ-prescription satisfies DGLAP equation, and thus

the remaining scale is the OPE scale $\tilde{\mu}$. In other words, we have

$$\delta^{l}C_{g\leftarrow f}(x, \boldsymbol{b}; \mu, \zeta_{\mu}(b), \tilde{\mu}) = \delta^{l}C_{g\leftarrow f}(x, \boldsymbol{b}; \tilde{\mu}), \qquad (4.110)$$

where the logarithmic part has simple form

$$\delta^{l}C^{[2]}_{g\leftarrow f}(x, \boldsymbol{b}; \tilde{\mu}) = \left(\beta_0 \delta^{l}C^{(1,0,0)}_{g\leftarrow f}(x) \right. \qquad (4.111)$$

$$\left. - \sum_{f'=g,q,\bar{q}} [\delta^{l}C^{(1,0,0)}_{g\leftarrow f'} \otimes P^{[1]}_{f'\leftarrow f}](x) \right) \mathbf{L}_{\tilde{\mu}} + \delta^{l}C^{(2,0,0)}_{g\leftarrow f}(x).$$

The finite part $\delta^{l}C^{(2,0,0)}_{g\leftarrow f}(x)$ remains unaffected. Note that, generally the ζ-prescription also modifies the finite part of NNLO expression, as it is happens e.g. for the unpolarized TMDPDF. The use of the expression of matching coefficients with the elections of scales provided by ζ-prescription is important in order to do phenomenological predictions because the software `artemide` [117] needs as an input the coefficient functions in this scheme.

Chapter 5

Higgs transverse momentum spectrum

Gluon-gluon fusion is the leading channel for Higgs boson production in hadron-hadron collisions [118–120]. The transverse momentum dependent (TMD) factorization of Higgs production has been demonstrated to follow the same pattern as the Drell-Yan/vector boson case studied in chapter 2 in different frameworks [10, 11, 13, 15, 121] and in this sense it has been reviewed in [77]. Within the TMD factorization theorem, which describes the Higgs production at small transverse momentum, there are two dominant terms in the factorized cross-section. Those terms correspond to the fusion of unpolarized and the linearly polarized gluons [115, 122, 123]. Schematically, it reads

$$\frac{d\sigma}{dy d^2\boldsymbol{q}_T} = \sigma_{gg\to H} \int \frac{d^2\boldsymbol{b}}{(2\pi)^2} \, e^{-i(\boldsymbol{b}\boldsymbol{q}_T)} \Big(f_{1,g}(x_A, \boldsymbol{b}) f_{1,g}(x_B, \boldsymbol{b}) + h_{1,g}^{\perp}(x_A, \boldsymbol{b}) h_{1,g}^{\perp}(x_B, \boldsymbol{b}) \Big),$$

(5.1)

where $\sigma_{gg\to H}$ is the factorized gluon-gluon-Higgs cross-section, $x_{A,B}$ are the collinear fractions of gluon momenta, f_1 is the unpolarized gluon traverse momentum dependent parton distribution function (TMDPDF) and $h_{1,g}^{\perp}$ is the linearly polarized gluon TMDPDF (lpTMDPDF) that was proposed as an independent distribution long ago by Mulders and Rodrigues [74] and whose matching is presented in chapter 4. Eq. (5.1) allows to understand the importance of having information of the lpTMDPDF at same order of the unpolarized TMDPF to study of the Higgs transverse momentum spectrum. In this chapter we study the impact of considering the lpTMDPDF at different orders of accuracies in the calculation of the Higgs production cross section.

The modern state-of-the-art of perturbative calculations is the next-to-next-to-leading order as we have studied in chapter 4. However, phenomenological applications for the NNLO Higgs transverse momentum spectrum only use the matching coefficients for the linearly polarized gluons up to NLO. The counting in many phenomenological applications is different from the one required by TMD factorization. In fact, using standard resummation, see e.g. [37, 115, 124–127], the small-b expansion is incorporated into the factorization formula, ignoring the non-perturbative TMD effects and one worries only about the perturbative expansion of the cross section. The TMD factorization includes the resummation for large enough q_T, however one has different requirements in the realization of the perturbative series. So, while in the usual resummation the whole bracketed factor in eq. (5.1) should be given at a certain perturbative order, in TMD factorization each distribution should be matched independently to its collinear counterpart at the same given order. Both approaches are consistent with computing the small-b expansion at the same order.

The case of linearly polarized gluon contribution to eq. (5.1) is special because the tree-level matching accidentally vanishes.

In this chapter we use the calculation of $h_{1,g}^\perp$ at two loops presented in chapter 4 and we estimate the impact of this correction on the Higgs transverse momentum spectrum.

The result presented in this chapter is relevant for many cases beyond Higgs boson production. In particular, there are processes that are also sensitive to lpTMD-PDF and that are addressed in the literature [128–132]. Among these it is worth a special mentioning the case of heavy-quark production [133–139], which is relevant at LHC, future Electron-Ion Collider (EIC) or the LHeC.

In TMD factorization each TMD distribution ($f_{1,g}$ and $h_{1,g}^\perp$ in this case) is an independent fundamental non-perturbative function. In order to sensibly construct a TMD for any practical purpose it is fundamental to include the asymptotical small-b limit, where each TMD distribution match to collinear parton distributions and the matching coefficient calculated up to NNLO in chapter 4. In practice, for the description of the TMD distributions one typically uses a phenomenological ansatz that matches the OPE results at small-b to a non-perturbative input at large-b. It can be written in the form

$$h_{1,g\leftarrow h}^\perp(x, \boldsymbol{b}) \;\; = \;\; \sum_f \int_x^1 \frac{dy}{y} \delta^l C_{g\leftarrow f}(y, \boldsymbol{b})\, f_{1,f\leftarrow h}\left(\frac{x}{y}\right) h_{1\mathrm{NP}}^\perp(x, \boldsymbol{b}^2), \qquad (5.2)$$

and a similar expression can be used for $f_1(x, \boldsymbol{b})$ with a different $f_{1\mathrm{NP}}(x, \boldsymbol{b}^2)$ and the corresponding matching coefficient. In eq. (5.2) we omit scale variables, and the function $h_{1\mathrm{NP}}^\perp$ is an arbitrary function with the only constraint

$$\lim_{\boldsymbol{b}^2 \to 0} h_{1\mathrm{NP}}^\perp(x, \boldsymbol{b}^2) \simeq 1 + \mathcal{O}(\boldsymbol{b}^2), \qquad (5.3)$$

which is necessary to be consistent with the small-b limit of the TMD. A similar ansatz has been used also for the quark TMD, and the respective non-perturbative correction has been called

$$f_{NP}(x, \boldsymbol{b}) = \exp\left(-\frac{\lambda_1 \bar{x} + \lambda_2 x + \lambda_3 x\bar{x}}{\sqrt{1 + \lambda_3 x^{\lambda_4} \boldsymbol{b}^2}} \boldsymbol{b}^2\right) \qquad (5.4)$$

where the values of the parameters λ_i, $i = 1, ..., 5$ used are the same obtained in the study of the extraction of the unpolarized TMDPDF form experimental data in refs. [17, 140]. In order to have some phenomenological result here we also choose $f_{NP} = f_{1NP} = h_{1NP}^\perp$. We will comment about the consistency of this choice later in this chapter, making a comparison of our result with the one obtained with Pythia.

5.1 Contribution of lpTMDPDF to Higgs production

The lpTMDPDF and the unpolarized gluon TMDPDF use to be present at the same time in many processes. A particularly important place to study the effect of lpT-MDPDF is Higgs production in hadron-hadron collision. The dominating channel for Higgs production is gluon-gluon fusion via the top-quark loop [118], which can be written via an effective interaction term in the Lagrangian [141]

$$\mathcal{L}_{ggH} = \frac{a_s(\mu) C_t(\mu)}{3v} F_{\mu\nu}^A F^{A,\mu\nu} H, \qquad (5.5)$$

where H is the Higgs field, $F_{\mu\nu}$ is the gluon field strength tensor, and v is the Higgs vacuum expectation value. The effective coupling constant at NNLO is derived in [142, 143]. Using the effective vertex in eq. (5.5) one can derive the TMD factorization theorem for Higgs production following the same steps as in the Drell-Yan case (see chapter 2 of this thesis). The resulting expression is

$$\frac{d\sigma}{dyd^2\boldsymbol{q}_T} = \frac{2\sigma_0(\mu)}{\pi}C_t^2(\mu)U(\mu,-\mu)|C_H(-m_H^2,-\mu^2)|^2 \tag{5.6}$$
$$\int \frac{d^2\boldsymbol{b}}{4\pi}e^{i(\boldsymbol{b}\boldsymbol{q}_T)}\Phi_{g\leftarrow h_1}^{\mu\nu}(x_1,\boldsymbol{b};\mu,\zeta_1)\Phi_{g\leftarrow h_2}^{\mu\nu}(x_2,\boldsymbol{b};\mu,\zeta_2),$$

where y is the Higgs boson rapidity and $x_{1,2} = \sqrt{(m_H^2+\boldsymbol{q}_T^2)/s}e^{\pm y}$. The function C_H is the gluon scalar form-factor (the NNLO expression can be found in [61]). The coefficient function $|C_H|^2$ in Drell-Yan like cross section is evaluated at a space like momentum$(-q^2)$. Thus, some contributions of order π^2 which could be large, especially in the case of Higgs boson production (see refs. [144, 145]) appear. These corrections can be resummed by the technique introduced in [145], so,

$$|C_H(-q^2)|^2 \rightarrow U|C_H(q^2)|^2, \tag{5.7}$$

where U is the so called "π^2-resummation" exponent. At LO it reads [145]

$$U = \exp\left(\frac{\Gamma_0}{2a_s\beta_0^2}\left[2a\arctan a - \ln(1+a^2)\right]\right), \qquad a = \pi a_s. \tag{5.8}$$

The TMD distributions $\Phi^{\mu\nu}$ are defined in eq. (3.9). The scale μ is of the order of the hard scale, m_H in this case, and $\zeta_1\zeta_2 = m_H^4$.

With the decomposition in eq. (4.85) the product of TMD distributions turns into

$$\Phi_{g\leftarrow h_1}^{\mu\nu}(x_1,\boldsymbol{b})\Phi_{g\leftarrow h_2}^{\mu\nu}(x_2,\boldsymbol{b}) = \frac{1}{2}\Big(f_{1,g\leftarrow h_1}(x_1,\boldsymbol{b})f_{1,g\leftarrow h_2}(x_2,\boldsymbol{b})$$
$$+h_{1,g\leftarrow h_1}^{\perp}(x_1,\boldsymbol{b})h_{1,g\leftarrow h_2}^{\perp}(x_2,\boldsymbol{b})\Big) \tag{5.9}$$

Therefore, for a consistent phenomenological application of this formula one should consider f_1 and $h_1^{\perp}$ at the same perturbative order. The perturbative inputs up to NNLO are reported in tab. 5.1.

Function	H	$C_{g\leftarrow f}, \delta^L C_{g\leftarrow f}$	Γ_{cusp}	$\mathcal{D}$	γ_F	α_s running	PDF evolution
NLO	α_s	α_s	α_s^2	α_s resummed	α_s^2	NLO provided by NNPDF3.1 [146]	
NNLO	α_s^2	α_s^2	α_s^3	α_s^2 resummed	α_s^3	NNLO provided by NNPDF3.1 [146]	

TABLE 5.1: Summary of perturbative orders used for each part of the cross section. The symbol H stands for the first line of eq. (5.6).

It is interesting to mention that if the Higgs boson were a pseudo-scalar particle, then the main change in the structure of cross-section in eq. (5.6) would be a sign of $h_1^{\perp}h_1^{\perp}$ term in eq. (5.9). In this case, the expressions for perturbative corrections in C_t and C_H are also changed although their LO remains the same [123].

In order to study the numerical impact of the NLO and NNLO matching for lpT-MDPDF together with the cross-section in eq. (5.6) a new module has been added to `artemide` [117]. The non-perturbative parts of gluon TMD distributions and gluon rapidity anomalous dimension are unknown, and nowadays the data are not sufficient to fix it. In order to provide some value for a cross section we use the inputs in eqs. (5.2-5.3) with $f_{NP} = f_{1NP} = h_{1NP}^{\perp}$, where f_{NP} is the non-perturbative function for quarks extracted from a fit of Drell-Yan and Z-boson production data using `artemide 2.01`, see eq. (5.4). The perturbative calculable parts of the evolution kernel differ in quark and gluon case (at the order that we work) by the Casimir scaling factor C_A/C_F. Here we have assumed the same scaling for the un-calculable non-perturbative pieces of the evolution kernel. The error band of our prediction come from scale variations of a factor of 2, consistently with the ζ-prescription [16].

In order to check the validity of the model assumptions we have compared the cross section in eq. (5.6), integrated in rapidity, with PYTHIA [147, 148]. The agreement of our prediction at NNLO and PYTHIA is shown in fig. 5.1 and it is extremely good in the range of q_T where the TMD factorization theorem is expected to hold. In that figure we have also included the error provided by PYTHIA, although it is not clearly visible and we have not used any normalization factor.
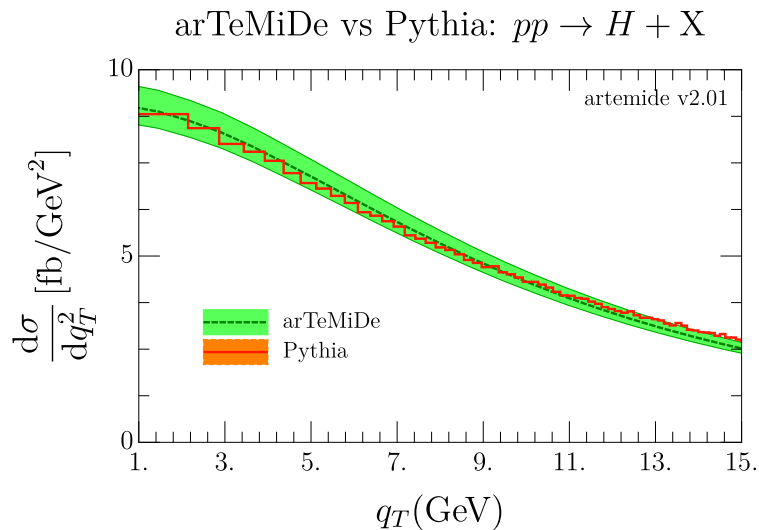

FIGURE 5.1: The cross section in eq. (5.6) integrated over all rapidity range with `artemide2.01` at NNLO and PYTHIA. The errors of PYTHIA are included, although not clearly visible. The shaded area shows the variation band in $\tilde{\mu}$, see eq. (4.110).

In fig. 5.2 we have plotted the lpTMDPDF, eq. (5.2-5.3), as a function of b at $x = 0.01$ at NLO and at NNLO. The NNLO includes the perturbative correction to the first non-trivial order (which is NLO). This correction appears to be large, almost a factor 2. The bands show the sensitivity of the distribution to the change of the OPE scale $\tilde{\mu} \to c_4\tilde{\mu}$ with $c_4 \in (0.5, 2)$, see eq. (4.110). The relative size of the band decreases between NLO and NNLO. Altogether, this figure points to the fact that the lpTMDPDF effects could have been underestimated up to now.

The experimental data on the Higgs differential cross section are still affected by big errors. For a demonstration we have considered the cross section in eq. (5.6) measured at CMS collaboration, where the rapidity is integrated in the interval indicated by that experiment [149]. Because the experimental cross section just uses the data from one particular decay of the Higgs boson we have normalized our cross
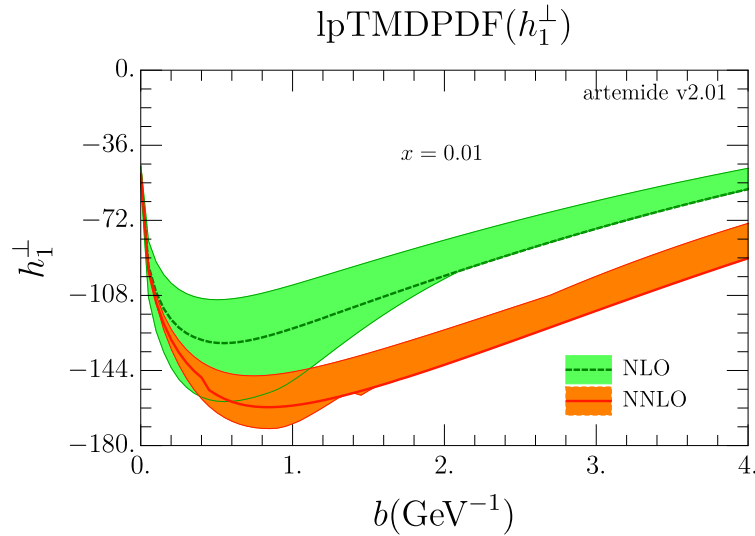
FIGURE 5.2: The lpTMDPDF, eq. (5.2-5.3), as a function of b at $x = 0.01$. The shaded area shows the variation band in $\tilde{\mu}$, see eq. (4.110).
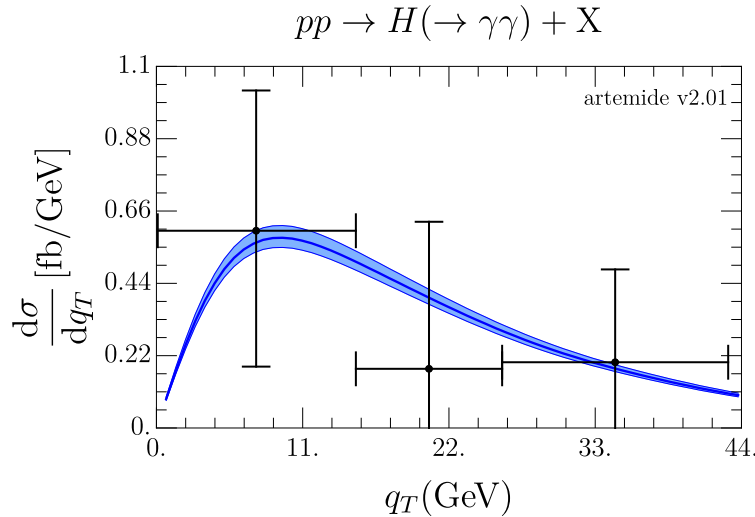

FIGURE 5.3: Comparison of Higgs-production cross-section with variation band to the measurement presented in [149] by CMS collaboration.

section with the experimental one integrating in the interval of transverse momenta shown in fig. 5.3. From this figure it is clear that currently the data are not sensitive to the TMD structures.

In the Higgs production cross-section the lpTMDPDF mainly affects the low-q_T region, as it is demonstrated in fig. 5.4. Practically, the lpTMDPDF can be distinguished from the unpolarized TMDPDF at $q_T \lesssim$ 5-8GeV, where it modifies the values of cross-section by about 5%. Such value of variation band is typical for NNLO approximation, see e.g. [127]. In fig. 5.4 (right) we compare the NNLO cross sections the size of the variation band, which is the maximum deviation value obtained from the variation of all three scales (in ζ-prescription) by factors $c_i \in (0.5, 2)$ [16]. The variation band is of the order of few percents and the main contribution to it is the μ-band (the scale between hard part and the TMD-evolution factor). Nowadays, these factors can be pushed to N³LO reducing the variation band further, if necessary.
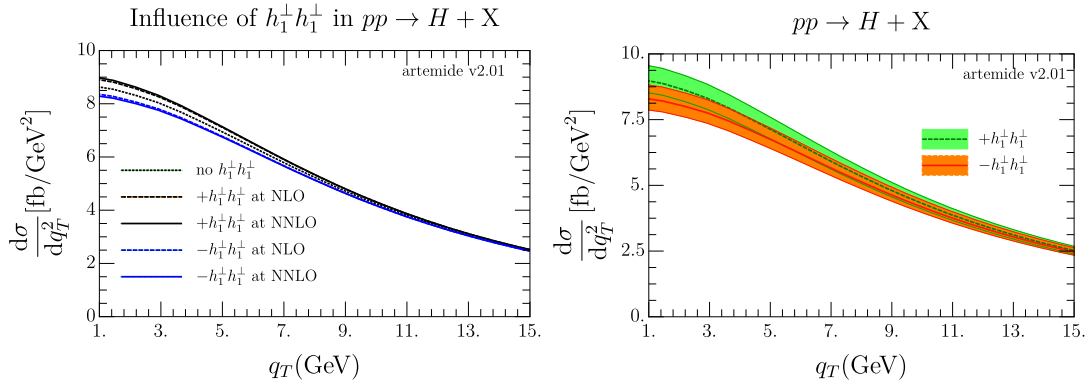
FIGURE 5.4: Cross section for Higgs production including linearly polarized gluon effects at different orders. (left)The variation of cross-section integrated over all rapidities at different perturbative orders for lpTMDPDF. The black (blue) lines correspond the case of positive (negative) contribution for $h_1^\perp h_1^\perp$-term in eq. (5.9). (right) The scale-variation band for the cross section at NNLO. The parity even (odd) Higgs case is represented with a green (orange) band. In both figures the center of mass energy is set as in [149] and rapidity is integrated over its complete range.

5.2 Positivity relations

Finally, we comment on the positivity relation formulated in ref. [74]:

$$|f_1(x, \boldsymbol{q}_T)| - |h_1^\perp(x, \boldsymbol{q}_T)| > 0. \tag{5.10}$$

This relation is a consequence of positive definiteness of the gluon-polarization matrix in a free theory, and certainty holds at LO. However, it does not need to be accomplished at higher order in perturbation theory. The positivity bound is formulated in momentum space, whereas all perturbative calculation are performed in coordinate space. This causes an additional problem since the Hankel transform of a positive function is not necessary a positive function.
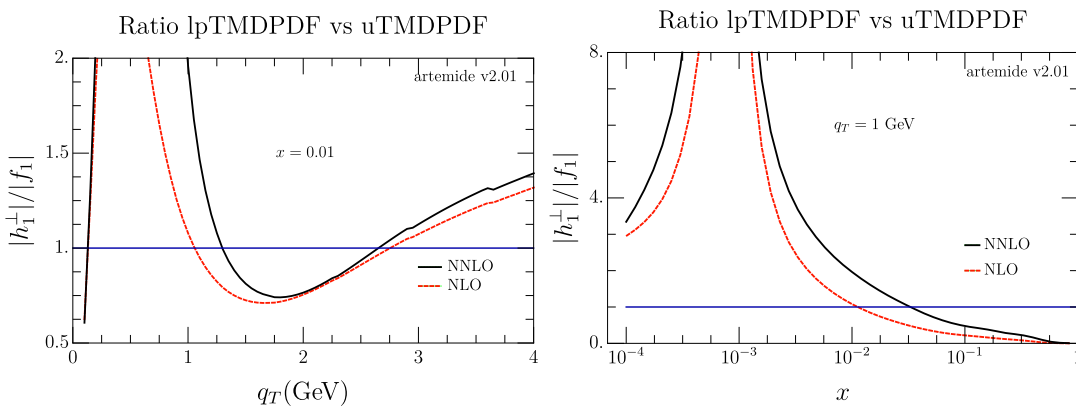

FIGURE 5.5: (left) Ratio of linearly polarized and unpolarized gTMD to check eq. (5.10) as a function of q_T at fixed $x = 0.01$. (right) Ratio of linearly polarized and unpolarized gTMD to check eq. (5.10) as a function of q_T at fixed $q_T = 1$ GeV.

Within our model we have checked that it is easy to get a violation of this bound,

for any fixed value of x and q_T. Typically, the violation happens in the vicinity of sign change point of f_1 (note, that our realization of f_1 is positive-definite in b-space). Outside of this point the inequality in eq. (5.10) is respected. The situation is exemplified in fig. 5.5, where we plot the ratio of $|f_1|/|h_1^\perp|$ at different values of q_T with fixed x (left) and viceversa (right).

We also note that the positions of zeros in TMDPDFs strongly depends on the non-perturbative input. In particular, selecting some appropriate model one can, possibly, remove the zero from unpolarized TMDPDF, or fix positions of zeros equal in both gluon TMDPDFs. In other words eq. (5.10) can be used as a serious constraint on non-perturbative part of the TMD distributions. However, we do not see enough justification for such an approach at the moment.

We have also observed that the ratio $|h_1^\perp|/|f_1|$ tends to saturate at smaller values of x as it is suggested for instance by [150]. Then for extreme small values of $x \sim 10^{-4}$ it is violated again. However, such values can be outside the applicability region of our calculation since the perturbative expressions for f_1 [18] and $h_1^\perp$ eqs. (4.103, 4.104) have contributions $\sim a_s^{n+1} \ln^n(x)/x$ that should be resummed for a proper comparison.

Part II

Transverse momentum distributions with jets

Chapter 6

TMD factorization theorems for processes with jets

The part I of this thesis was focused on the improving of perturbative information of the TMD distributions that enter in the factorization theorems defined for processes where the transverse momentum of partons in the proton is probed. Since a transverse momentum measurement can also be thought of as the measurement of an angle, it is natural that TMD factorization theorems generically involve two TMD distributions. Traditionally, the relative transverse momentum of two hadrons in e^+e^-, the transverse momentum of a hadron semi-inclusive deep-inelastic scattering (SIDIS), $ep \rightarrow ehX$, and the transverse momentum of a γ^*/Z boson in pp collisions have been considered.

In general the extraction of non-perturbative effects in such processes with final-state hadrons is harder, due to the fact that the behavior of the nonperturbative parts of hadronic TMD fragmentation functions is less studied than its analogues for initial states. Thus, in this section we propose to replace individual final-state hadrons by jets in e^+e^- or SIDIS measurements [151]. The geometry of these events is sketched in fig. 6.1. Jets are collimated sprays of hadrons, that appear in high-energy collisions because of the collinear singularity of quantum chromodynamics (QCD). In practice they are identified by clustering particles according to a specified algorithm. The advantage of this new approach is that the TMD jet functions that should be defined are perturbatively calculable, thus removing an important source of uncertainty. Specifically, the intrinsically nonperturbative distribution of the momentum fraction of individual hadrons is removed by using jets. This improvement allows one to reduce the theoretical uncertainties in phenomenological predictions. Due to this fact, the channel to investigate the non-perturbative effects of the TMD distributions and then to improve the knowledge about structure of hadrons is simplified.

On the theoretical side, we should demonstrate that similar factorization theorems holding in the hadronic cases hold when they are substituted by jets. One of the key ingredients to probe these factorization theorems is the axis selection in the calculation of the TMD jet functions. We discuss two different axis selections and clustering algorithms commonly used: standard jet axis (SJA) and Winner-Take-All (WTA) recombination scheme [152]. They works as follows: as long as at least one pair of particles exists whose angular distance is smaller than R, the two particles with the smallest distance are selected and merged. The rule to merge two particles of four-momenta p_1, p_2 into a new "particle" with momentum $p_{(12)}$ reads

$$\text{SJA} : E_{(12)} = E_1 + E_2, \quad \boldsymbol{p}_{(12)} = \boldsymbol{p}_1 + \boldsymbol{p}_2, \tag{6.1}$$

$$\text{WTA} : E_{(12)} = E_1 + E_2, \quad \boldsymbol{p}_{(12)} = E_{(12)} \Big[\frac{\boldsymbol{p}_1}{|\boldsymbol{p}_1|} \theta(E_1 - E_2) + \frac{\boldsymbol{p}_2}{|\boldsymbol{p}_2|} \theta(E_2 - E_1) \Big],$$
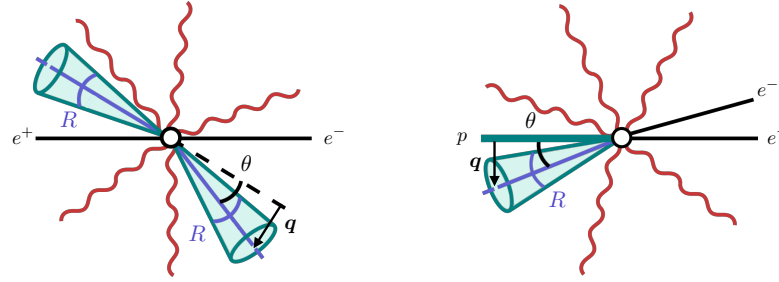
FIGURE 6.1: Geometry of the event for $e^+e^- \to$ dijet (left) and SIDIS (right). The horizontal direction represents the beam axis. For dijets the relevant quantities q and θ are the transverse momentum decorrelation and angular decorrelation of the system, defined with respect to the relative orientation of the two jets. We consider almost back-to-back jets, $\theta \ll 1$, and study different hierarchies between θ and the jet radius R. In SIDIS q represents the transverse mometum of the jet, and the corresponding angle is measured with respect to the beam axis. We work in the Breit frame, where the jet recoils almost in the direction of the incoming proton, $\theta \ll 1$.

i.e. with the SJA the two four-momenta are added, while with the WTA the new pair is massless by definition, and its direction coincides with the one of the most energetic particle. The algorithm stops when the angular separation between each pair of remaining particles exceeds R. Once the algorithm stops, the resulting particles are defined to be the final jets. We will discuss how they affect to the factorization.

In the context of SIDIS experiments, replacing the nonperturbative TMD fragmentation functions with calculable jet functions would allow one to increase the sensitivity to initial-state nonperturbative physics. It could be interesting to see whether this can be investigated with existing HERA data, and exciting to explore at the electron-ion collider (EIC), which will enable the extraction of PDFs with unmatched precision, with SIDIS experiments playing an important role [153]. Of course, for small transverse momenta, the jet functions themselves will also receive nonperturbative corrections. However, this can be addressed by exploiting the universality of the nonperturbative structure of the TMD jet function, with $e^+e^- \to$ dijet providing a useful testing ground. In principle, data from e^+e^- collisions could be used to fit a model for nonperturbative corrections to the jet function to be later applied to SIDIS.

A number of other jet observables that account for transverse momentum dependence have recently been considered. The main focus has been on the transverse momentum of hadrons fragmenting in jets, in both inclusive [154] and semi-inclusive [155, 156] processes. In the same context, we will do a similar study to this one in chapter 7 using soft drop jet grooming to reduce sensitivity to soft radiation within the jet in the same line of refs. [157–159] . These studies consider the transverse momentum with respect to the standard jet axis (SJA); instead, as an alternative way to reduce sensitivity to soft radiation, refs. [160, 161] performed a similar analysis for the transverse momentum with respect to the Winner-Take-All (WTA) axis. The transverse momentum of the jet itself was also recently considered in photon + jet production [162] and lepton-jet correlation in deep-inelastic scattering [163].

6.1 Regimes of application. The TMD jet function and choice of axis

To probe factorization theorems we focus on e^+e^- annihilation process because the application of the framework is simpler. However, from this discussion the probe of factorization for a SIDIS process is straightforward and we only give some kinematical information.

In the case of $e^+e^- \to$ dijet, the main physical quantity we consider is the transverse momentum decorrelation. It is defined as

$$\boldsymbol{q}_T = \frac{\boldsymbol{p}_{T1}}{z_1} + \frac{\boldsymbol{p}_{T2}}{z_2}, \qquad (e^+e^- \to \text{dijet}) \qquad (6.2)$$

where $\boldsymbol{p}_{Ti}$ are the jet transverse momenta measured with respect to a common direction and $z_i = 2E_i/\sqrt{s}$ are their energy fractions, $\sqrt{s}$ is the center-of-mass energy of the collision. Since factorization requires a small transverse momentum decorrelation, we will always assume

$$q_T \equiv |\boldsymbol{q}_T| \ll \frac{\sqrt{s}}{2}. \qquad (6.3)$$

A related quantity is the angular decorrelation, shown in the left panel of fig. 6.1,

$$\theta = \arctan\left(\frac{2q_T}{\sqrt{s}}\right) \approx \frac{2q_T}{\sqrt{s}}, \qquad (6.4)$$

where the final expression exploits eq. (6.3). This makes it explicit that we consider configurations where jets are almost back to back. Another interesting small-angle configuration occurs for two jets moving in almost the same direction, which we do not study in this thesis. The angular decorrelation is similar to the azimuthal decorrelation in hadronic collisions, calculated at next-to-leading logarithmic accuracy in refs. [164–167].

In principle, the definitions in eqs. (6.2, 6.4) depend on the choice of axis with respect to which the jet transverse momenta are measured. However, differences induced by this choice are suppressed by powers of q_T^2/s. Of course, the definition *is* sensitive to the details of the jet algorithm. We use the so called k_T-type algorithms [168] that introduce an specific definition of the distance between two particles i and j,

$$d_{ij} = \min\left(p_{Ti}^{2p}, p_{Tj}^{2p}\right) \frac{\Delta R_{ij}^2}{R^2}, \qquad (6.5)$$

and a distance between each particle and the beam,

$$d_{iB} = p_{Ti}^{2p}. \qquad (6.6)$$

In each case, $p = 1, 0, -1$ correspond to the k_T, Cambridge/Aachen, and anti-k_T algorithm, respectively. R is the jet radius understood as an angular distance and

$$\Delta R_{ij} = \sqrt{(\Delta \eta_{ij})^2 + (\Delta \phi_{ij})^2}, \qquad (6.7)$$

where $\Delta \eta_{ij}$ and $\Delta \phi_{ij}$ the rapidity and azimuthal differences between both particles i and j. The algorithm identifies the smallest distance between d_{ij} and d_{iB}. If it is

the beam distance, d_{iB}, the particle is defined as a jet and removed from the list of particles. If the smallest distance is d_{ij} the two particles are merged into a single one. The procedure is repeated until no particles are left in the event. Our default throughout this chapter will be the WTA axis with anti-k_T [169], but we will also consider the SJA and other clustering algorithms of the k_T family.

In SIDIS, shown in the right panel of fig. 6.1, we choose to work in the Breit frame and define the transverse momentum as

$$q_T = \frac{P_{TJ}}{z} + q_{Tin}, \qquad \text{(SIDIS)} \qquad (6.8)$$

where P_{TJ} is the transverse momentum of the jet with respect to the beam axis, q_{Tin} is the transverse momentum of the initial-state quark in the proton, and $z = 2E_J/Q$ is the jet energy normalized to (minus) the virtuality of the photon Q^2. In analogy with eq. (6.4) we define a corresponding angle θ and require

$$\theta = \arctan\left(\frac{2q_T}{Q}\right) \simeq \frac{2q_T}{Q} \ll 1. \qquad (6.9)$$

We use the same symbols q_T and θ for analog quantities in different processes since they play the same role in factorization formulae, and their meaning should be clear from the context.

The other relevant quantity that enters in the factorization of the cross section is

$$\mathcal{R} \equiv 2\tan\frac{R}{2}. \qquad (6.10)$$

For small values, $\mathcal{R}$ is just the jet radius parameter R, but in general the parameter $\mathcal{R}$ allows us to capture some power corrections. In the following we will use $\mathcal{R}$ when considering transverse momenta, while we use R when considering angles. In this section we discuss the factorization formulas for all possible hierarchies between θ and R.

Our factorization analysis is carried out using Soft-Collinear Effective Theory (SCET) (see chapter 1), in which the jets are described by collinear modes and the radiation outside the jets is described by a soft mode. In the framework of this effective field theory we begin introducing the jet function, which is the main new ingredient of our analysis, providing its definition and briefly discussing its renormalization.

The jet function, that enters the factorization theorem for $\theta \sim R$, is written in $\boldsymbol{b}$-space as the following collinear matrix element

$$J_q(z, \boldsymbol{b}, E\mathcal{R}) = \frac{z}{2N_c} \qquad (6.11)$$
$$\times \text{Tr}\left[\frac{\bar{\slashed{n}}}{2} \langle 0| \left[\delta\left(2E/z - \bar{n}\cdot P\right)e^{i\boldsymbol{b}\cdot P}\chi_n(0)\right] \sum_X |J_{\text{alg},R}X\rangle\langle J_{\text{alg},R}X|\bar{\chi}_n(0)|0\rangle\right.$$

Here, z is the light-cone momentum fraction of the jet with respect to the initiating quark, E is the energy of the initiating quark, and P is the momentum operator. The trace in eq. (6.11) is over Dirac indices, and $\chi_n(y) = W_n^\dagger(y)\xi_n(y)$, where ξ_n is the collinear quark field in the light-like direction n^μ and W_n is a collinear Wilson line as the defined in eq. (2.9), ensuring collinear gauge invariance. The subscript *alg* serves as a reminder that the jet function depends on the jet axis selection discussed in eq. (6.1).

Mode	$R \ll \theta \ll 1$	$\theta \sim R \ll 1$	$\theta \ll R$ (WTA)	$\theta \ll R \ll 1$ (SJA)	$\theta \ll R \sim 1$ (SJA)
hard	$(1,1,1)$	$(1,1,1)$	$(1,1,1)$	$(1,1,1)$	$(1,1,1)$
n-coll.	$(1,\theta^2,\theta)$	$(1,\theta^2,\theta)$	$(1,\theta^2,\theta)$		
$\bar{n}$-coll.	$(\theta^2,1,\theta)$	$(\theta^2,1,\theta)$	$(\theta^2,1,\theta)$		
n-coll$_2$	$(1,R^2,R)$			$(1,R^2,R)$	
$\bar{n}$-coll$_2$	$(R^2,1,R)$			$(R^2,1,R)$	
n-csoft				$\theta/R(1,R^2,R)$	
$\bar{n}$-csoft				$\theta/R(R^2,1,R)$	
soft	(θ,θ,θ)	(θ,θ,θ)	(θ,θ,θ)	(θ,θ,θ)	(θ,θ,θ)

TABLE 6.1: The parametric scaling of the momenta $(p^-, p^+, \boldsymbol{p})$ corresponding to the modes in SCET, for the various hierarchies between θ and R. For $\theta \ll R$ the modes differ between the Winner-Take-All and standard jet axis.

Gluon-initiated jets do not enter for e^+e^- and SIDIS, but we give the corresponding definition for completeness,

$$J_g(z,\boldsymbol{b},E\mathcal{R}) \;=\; \frac{zE}{N_c^2-1}$$
$$\times \langle 0| \left[\delta\big(2E/z - \bar{n}\cdot P\big)e^{i\boldsymbol{b}\cdot\boldsymbol{P}} \mathcal{B}_{n\perp\mu}(0)\right] |J_{\mathrm{alg},R}X\rangle \, \langle J_{\mathrm{alg},R}X| \, \mathcal{B}_{n\perp\mu}(0) |0\rangle, \tag{6.12}$$

where

$$\mathcal{B}_{n\perp\mu} = \frac{1}{\bar{n}\cdot\mathcal{P}}\, i\bar{n}_\alpha g_{\perp\mu\beta} W_n^\dagger F_n^{\alpha\beta} W_n \tag{6.13}$$

is the collinear gluon field, with $F_n^{\alpha\beta}$ the collinear field strength tensor. In this section we will perform the calculation in both momentum and impact parameter spaces. To go from one to another simply involves replacing

$$e^{i\boldsymbol{b}\cdot\boldsymbol{P}} \quad \rightarrow \quad \int \frac{\mathrm{d}^2\boldsymbol{b}}{(2\pi)^2}\, e^{i\boldsymbol{b}\cdot(\boldsymbol{P}-\boldsymbol{q}_T)} = \delta^{(2)}(\boldsymbol{q}_T - \boldsymbol{P})\,. \tag{6.14}$$

in eqs. (6.11, 6.12).

The above definitions are for the bare jet functions, as indicated by the absence of renormalization scales. A perturbative calculation shows that both ultraviolet (UV) and rapidity divergences affect these distributions, so that one should consider the renormalized quantities

$$J_q(z,\boldsymbol{b},E\mathcal{R},\mu,\zeta) = Z_q(\zeta,\mu)R_q(\zeta,\mu)J_q(z,\boldsymbol{b},E\mathcal{R}) \tag{6.15}$$

and similarly for J_g. Here Z_q is the UV renormalization factor, R_q is the rapidity renormalization factor, and rapidity divergences are removed first, as in the hadronic TMD case. A key observation is that these renormalization factors are the same as in the case of TMDs, as we discuss in section 6.2.2.

6.1.1 $R \sim \theta \ll 1$

We turn to the factorization analysis, starting with dijet production in e^+e^- scattering at a center-of-mass energy $\sqrt{s}$, where $\theta \approx 2q_T/\sqrt{s} \sim R \ll 1$. This is the simplest case since there are only two scales, $\sqrt{s}$ and q_T. The cross section differential in the

momentum decorrelation $\boldsymbol{q}$ and the jet energy fractions $z_i = 2E_{J,i}/\sqrt{s}$ factorizes as

$$
\frac{d\sigma_{e^+e^- \to JJX}}{dz_1\, dz_2\, d^2\boldsymbol{q}_T} = \sigma_0^{e^+e^-}(s)\, H_{e^+e^-}(s,\mu) \tag{6.16}
$$

$$
\times \int \frac{d^2\boldsymbol{b}}{(2\pi)^2}\, e^{-i\boldsymbol{b}\cdot\boldsymbol{q}_T} J_q(z_1,\boldsymbol{b},\tfrac{\sqrt{s}}{2}\mathcal{R},\mu,\zeta)\, J_{\bar{q}}(z_2,\boldsymbol{b},\tfrac{\sqrt{s}}{2}\mathcal{R},\mu,\zeta)
$$

$$
\times \left[1 + \mathcal{O}\!\left(\frac{q_T^2}{s}\right)\right].
$$

The hard function $H_{e^+e^-}$ encodes the hard scattering process, in which a quark-anti-quark pair is produced. It contains virtual corrections, but no real radiation because that would result in $q_T \sim \sqrt{s}$. For convenience we have extracted the tree-level cross section $\sigma_0^{e^+e^-}$, which contains a sum over quark flavors. The jet functions describe the fraction z_i of energy of the initial (anti-)quark that goes into the jet, as well as their transverse momentum through the impact parameter $\boldsymbol{b}$ (its Fourier conjugate). They depend on the jet algorithm, as indicated by the argument $\frac{\sqrt{s}}{2}\mathcal{R}$, but this does not affect their anomalous dimension, as required by RG consistency. Soft radiation does not resolve the jet because its typical angle is order 1, whereas $R \ll 1$. Consequently, we do not have to consider clustering soft radiation in the jet algorithm, and we can simply include its effect as an overall recoil of the system, as indicated in eq. (6.16). The soft function has been absorbed into the jet functions in the above expression, as we will discuss in sec. 6.2.2. There we will also show that the RG evolution between the hard scale $\mu_H \sim \sqrt{s}$ and jet scale $\mu_J \sim q_T$ in eq. (6.16) resums invariant mass logarithms of $\mu_H/\mu_J \sim \sqrt{s}/q_T$, and similarly that ζ is related to the resummation of invariant rapidity logarithms of $\sqrt{s}/q_T$ [16, 66], see also refs. [9, 10, 14, 36, 49].

The corresponding factorization theorem for the cross section of semi-inclusive deep-inelastic scattering is given by

$$
\frac{d\sigma_{ep \to eJX}}{dQ^2\, dx\, dz\, d^2\boldsymbol{q}_T} = \sum_q \sigma_{0,q}^{\mathrm{DIS}}(x,Q^2)\, H_{\mathrm{DIS}}(Q^2,\mu) \tag{6.17}
$$

$$
\times \int \frac{d^2\boldsymbol{b}}{(2\pi)^2}\, e^{-i\boldsymbol{b}\cdot\boldsymbol{q}} F_q(x,\boldsymbol{b},\mu,\zeta)\, J_q\!\left(z,\boldsymbol{b},\frac{Q\mathcal{R}}{2},\mu,\zeta\right)
$$

$$
\times \left[1 + \mathcal{O}\!\left(\frac{q_T^2}{Q^2}\right)\right],
$$

which is differential in the photon virtuality Q^2, Bjorken x, the energy fraction z of the jet generated by the splitting of the quark, and the jet transverse momentum q_T. We work in the Breit frame, where $z = 2E_J/Q$, and apply an e^+e^- jet algorithm. The modification to the factorization theorem compared to eq. (6.16) is fairly modest: the hard function is replaced by the one for SIDIS, one of the jet functions is replaced by a TMD PDF, and the sum over quark flavors must be explicitly included because both $\sigma_{0,q}^{\mathrm{DIS}}$ and F_q depend on it (J_q does not, as long as we can treat quarks as massless). The hard function is slightly different,

$$
H_{e^+e^-}(Q^2,\mu) = |C_V(Q^2,\mu)|^2 = 1 + 2a_s C_F\left(-\mathbf{l}_{Q^2}^2 - 3\mathbf{l}_{Q^2} - 8 + \frac{7\pi^2}{6}\right) + \mathcal{O}(a_s^2),
$$

$$
H_{\mathrm{DIS}}(Q^2,\mu) = |C_V(-Q^2,\mu)|^2 = 1 + 2a_s C_F\left(-\mathbf{l}_{Q^2}^2 - 3\mathbf{l}_{Q^2} - 8 + \frac{\pi^2}{6}\right) + \mathcal{O}(a_s^2),
$$

$$\tag{6.18}$$

$$(6.19)$$

where C_V is the Wilson coefficient for the hard matching, $\mathbf{l}_{Q^2} = \ln(\mu^2/Q^2)$ and $a_s = g^2/(4\pi)^2$. The NNLO and NNNLO expression can be found in ref. [61], taking into account that $H_{e^+e^-}(Q^2,\mu)$ is the same as for the Drell-Yan process. The two loop expressions are provided in eqs. (A.6, A.7) of the appendix A.

6.1.2 $R \ll \theta \ll 1$

We now consider the case where we have an additional hierarchy due to the small size of the jet radius, $R \ll \theta \ll 1$. This regime will be of limited phenomenological interest to us but we discuss it because it allows us to make contact between our framework and TMD measurements with final state hadrons, corresponding to the $R \to 0$ limit. The modes are again listed in table 6.1, and involve additional collinear modes whose scaling is set by R.

The factorization in this case is an extension of eqs. (6.16, 6.17). The jet function contains two scales $\sqrt{s}\mathcal{R} \ll q_T$, which can be separated through a further collinear factorization,

$$J_i(z,\boldsymbol{b},E\mathcal{R},\mu,\zeta) = \sum_j \int_z^1 \frac{dz'}{z'} \left[(z')^2 \mathbb{C}_{i \to j}(z',\boldsymbol{b},\mu,\zeta) \right] \mathcal{J}_j\left(\frac{z}{z'},E\mathcal{R},\mu\right) \quad (6.20)$$
$$\times \left[1 + \mathcal{O}(b_T^2 E^2 \mathcal{R}^2) \right].$$

Only collinear radiation at angular scales θ, encoded in $\mathbb{C}_{i \to j}$ (matching coefficient for unpolarized hadronic TMDFF) can affect q_T. However, subsequent splittings down to angles of order R will change the parton j with momentum fraction z' into a jet with momentum fraction z. This is described by the semi-inclusive jet function $\mathcal{J}_j$, which has been calculated to $\mathcal{O}(\alpha_s)$ in refs. [170, 171] (our notation matches that of ref. [170]). Explicitly, the one-loop result of the semi-inclusive quark jet function given by [170] is

$$\mathcal{J}_q^{[1]}(z,2zE\mathcal{R},\mu) = 2C_F\left[\delta(1-z)\left(\tfrac{13}{2} - \tfrac{2\pi^2}{3} + \tfrac{3}{2}L_R\right) + (L_R - 2\ln z)\left(p_{qq}(z) + p_{gq}(z)\right) \right.$$
$$\left. -2p_{gq}(z)\ln(1-z) - 2(1+z^2)\mathcal{L}_1(1-z) - 1 \right]. \quad (6.21)$$

The distinction between WTA vs. standard jet axis is irrelevant, since $\theta \gg R$. The additional RG evolution between $\mu_J \sim q_T$ and $\mu_{\mathcal{J}} \sim E\mathcal{R}$ sums single logarithms of $\mu_J/\mu_{\mathcal{J}} \sim q_T/(E\mathcal{R}) \sim \theta/R$.

The $(z')^2$ in front of $\mathbb{C}_{i \to j}$ was chosen to ensure that these matching coefficients coincide with those for TMD fragmentation, given to $\mathcal{O}(\alpha_s^2)$ in refs. [18, 51]. It is not surprising that same matching coefficients enter here, since for $R \to 0$ the semi-inclusive jet function becomes the fragmentation function (summed over hadron species) [172]. Thus in this limit we reproduce the known results for TMD fragmentation to hadrons.

6.1.3 $\theta \ll R$ **for the Winner-Take-All axis**

We now consider $\theta \ll R$ for the Winner-Take-All axis. For $R \sim 1$, the modes in table 6.1 are expected and factorization takes on a rather simple form. Even if soft radiation sees the jet boundary, it does not affect the position of the jet axis, due to the

WTA recombination scheme. Specifically, the merging prescription in eq. (6.1) implies that soft radiation never affects the direction of the jet (it always "loses" against collinear radiation), while its contribution to the jet energy is power suppressed. The only effect of soft radiation, either inside or outside the jet, is thus therefore a total recoil of the two collinear sectors, which is therefore described by the standard TMD soft function. In particular, the observable is insensitive to the distinction between soft radiation inside and outside the jet. Since $\theta \ll R$, the collinear modes do not resolve the jet boundary, so $z = 1$ and the $E\mathcal{R}$ dependence drops out,

$$J_i^{\text{WTA}}(z, \boldsymbol{b}, E\mathcal{R}, \mu, \zeta) = \delta(1-z) \mathscr{J}_i^{\text{WTA}}(\boldsymbol{b}, \mu, \zeta) \left[1 + \mathcal{O}\left(\frac{1}{b_T^2 E^2 \mathcal{R}^2} \right) \right]. \tag{6.22}$$

For completeness we also provide a definition of $\mathscr{J}_q^{\text{WTA}}$,

$$\mathscr{J}_q^{\text{WTA}}(\boldsymbol{b}) = \frac{1}{2N_c} \text{Tr}\left[\frac{\bar{\slashed{n}}}{2} \langle 0| \left(\frac{1}{\bar{n}P} e^{i\boldsymbol{b}\cdot\boldsymbol{P}} \chi_n(0) \right) \sum_X |J_{\text{WTA}}\rangle \langle J_{\text{WTA}}| \bar{\chi}_n(0) |0\rangle \right], \tag{6.23}$$

and a similar formula can be written for the gluon case.

For $\theta \ll R \ll 1$, one would expect the same modes as are listed for the standard jet axis in table 6.1. In this case the soft function does not resolve the jet boundary, because $R \ll 1$, but collinear-soft modes with scaling

$$(p^-, p^+, \boldsymbol{p}_T) \sim \theta/R(1, R^2, R), \quad \theta/R(R^2, 1, R), \tag{6.24}$$

resolve the jet boundary and contribute to q_T. However, by the same reasoning as before, their only effect is a total recoil on the system, independent of whether emissions are inside or outside the jet. Consequently, these additional modes do not need to be considered, since they will simply be removed by the zero-bin subtraction [173], due to their overlap with the soft mode. This leads to the interesting conclusion that, **for the WTA axis, the cross section for $\theta \ll R$ is independent of R.**

6.1.4 $\theta \ll R$ for the standard jet axis

For completeness we also discuss $\theta \ll R$ for the standard jet axis. We do not present any numerical results for this case, and therefore limit our discussion to the dijet momentum decorrelation in e^+e^- collisions. First we consider the case $\theta \ll R \sim 1$, for which the modes are given in table 6.1. Energetic emissions outside the jet are not allowed because these would lead to $\theta \sim R$. Because the standard jet axis is along the total momentum of the jet, momentum conservation implies that q_T is simply determined by the transverse momentum of soft radiation outside the jets. In particular, the angle of energetic emissions inside the jet is unrestricted. Since $R \sim 1$, these emissions are hard, explaining the absence of a collinear mode. Each of these hard emissions induces a soft Wilson line, implying the presence of non-global logarithms (NGLs) [174] of $\sqrt{s}\mathcal{R}/q_T$. The corresponding cross section can be described using the framework of refs. [175, 176] (see also refs. [177, 178])

$$\frac{d\sigma_{e^+e^-\to JJX}^{\text{SJA}}}{d^2\boldsymbol{q}_T} = \sum_{m=2}^{\infty} \text{Tr}_c[\mathcal{H}_m(\{n_i\}, \sqrt{s}, \mathcal{R}) \otimes \mathcal{S}_m(\{n_i\}, \boldsymbol{q}, \mathcal{R})] \left[1 + \mathcal{O}\left(\frac{q_T^2}{Q^2} \right) \right]. \tag{6.25}$$

We have eliminated the measurement of the momentum fractions of the jets, since $z_i = 1$ in this limit. $\mathcal{H}_m$ denotes the hard function with m real emissions inside the jets, along the light-like directions n_i. The soft function $\mathcal{S}_m$ describes the transverse momentum q_T of soft radiation outside the jets, produced by the Wilson lines along

the directions n_i. The color indices describing the representation of the hard emissions/Wilson lines connects the hard and soft function, and Tr_c denotes the trace over these color indices. Finally, $\otimes$ denotes integrals over the light-like directions n_i.

Moving on to $\theta \ll R \ll 1$, we have collinear modes whose angular size is set by R, and additional collinear-soft modes with scaling

$$(p^-, p^+, \boldsymbol{p}) \sim \theta/R(1, R^2, R), \quad \theta/R(R^2, 1, R),$$ (6.26)

which are fixed by the requirement that they resolve the jet boundary and contribute to q_T. Because $R \ll 1$, no hard real emissions are allowed, and the soft function does not resolve the jet. However, each collinear emission produces a collinear-soft Wilson line, in direct analogy to the soft Wilson lines generated by hard emissions for $R \sim 1$. Using again the framework of refs. [175, 176], the corresponding cross section is given by

$$
\begin{aligned}
\frac{d\sigma^{\text{SJA}}_{e^+e^- \to JJX}}{d^2\boldsymbol{q}_T} \;=\; & \sigma_0^{e^+e^-}(s)\, H_{e^+e^-}(s, \mu) \int \frac{d^2\boldsymbol{b}}{(2\pi)^2}\, e^{-i\boldsymbol{b}\cdot\boldsymbol{q}}\, S(\boldsymbol{b}) \\
& \times \left[\sum_{m=2}^{\infty} \text{Tr}_c[\mathcal{J}_m(\{n_i\}, \tfrac{\sqrt{s}}{2}\mathcal{R}) \otimes \mathcal{U}_m(\{n_i\}, \boldsymbol{b}, \mathcal{R})] \right]^2 \\
& \times \left[1 + \mathcal{O}\!\left(\frac{q_T^2}{Q^2}\right) \right].
\end{aligned}
$$ (6.27)

The hard and soft function are the same as for $\theta \sim R$. The jet function $\mathcal{J}_m$ describes m collinear emissions inside a jet along light-like directions n_i, and the collinear-soft function $\mathcal{U}_m$ describes the resulting q_T from collinear-soft emissions of these Wilson lines.

To summarize: when using the WTA axis, the same factorization formulae valid for hadrons hold for jets, independently of the hierarchy between the angle θ and the jet radius parameter R. Because the factorization theorem ensures that hadronization effects in the jets are universal, they can be estimated in e^+e^- and then used in the analysis of SIDIS experiments. We anticipate that the main nonperturbative effects come from the evolution factor. These effects are universal (i.e. the same in e^+e^-, SIDIS, and Drell-Yan experiments and independent of the polarization of the hadrons) and their estimation is one of the major goals of TMD analyses. In this context we note the vital role played by the ζ-prescription [16], which ensures that the nonperturbative contribution to the evolution factor (that is responsible for the resummation) is uncorrelated with other nonperturbative effects.

Another observation has lead us to focus on the large radius regime of the jets. In fact, at one-loop order we notice that our jet function is well described by its large-R limit. In this limit the jet functions simplify considerably, and are determined by renormalization group evolution (RGE) up to a constant. We exploit this fact to numerically extract the two-loop, large-radius jet function from `Event2` and push the accuracy of the calculation to N^3LL in this case. Surprisingly, the validity of this regime extends down to fairly small values of the jet radius, allowing us to get precise results across the whole range in transverse momentum. This brings the perturbative precision of TMDs with jets on par with TMDs with final-state hadrons. We will discuss further about numerical results in the section 6.4.
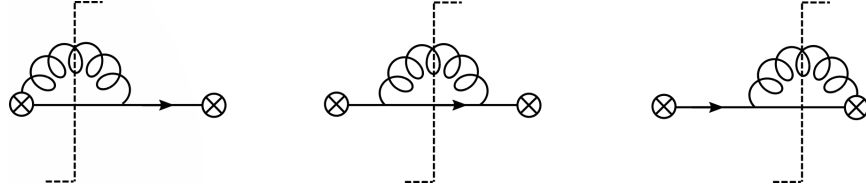
FIGURE 6.2: Cut diagrams that contribute to the one-loop quark jet function in SCET. Here $\otimes$ represents the collinear (anti-)quark field χ_n ($\bar{\chi}_n$), which contains a collinear Wilson line that can emit gluons. A sum over cuts is understood, where cuts through loops describe real emissions, while only cutting the quark line corresponds to virtual corrections. The latter vanish for our choice of regulators.

6.2 Quark jet function at one loop

In this section we present a detailed calculation of the one-loop quark jet function that enters the factorization formula in eqs. (6.16, 6.17). We use dimensional regularization with $d = 4 - 2\epsilon$ to handle UV divergences, and the modified δ-regulator for the rapidity divergences [51, 179]. We present a detailed calculation in momentum space in section 6.2.1.1 and in impact-parameter space in section 6.2.1.2, that provides a cross check of our results. The advantage of performing the calculation in momentum space is that this is the space in which the jet algorithm is defined. On the other hand, the renormalization and resummation are simpler in impact-parameter space.

6.2.1 Unsubstracted jet function

The one-loop diagrams that contribute to the quark function are given in fig. 6.2. This leads to the following expression for the bare jet function up to one loop,

$$
\begin{aligned}
J_q^{\mathrm{alg}}(z, \boldsymbol{q}, ER) &= \sum_n a_s^n J_q^{[n]}(z, \boldsymbol{q}, ER) \frac{1}{\pi} \delta(q_T^2) \delta(1-z) + g^2 \sum_{\mathrm{cases}} C_F \left(\frac{\mu^2 e^{\gamma_E}}{4\pi} \right)^\epsilon \\
&\times \int_0^\infty \frac{\mathrm{d}\ell^+}{2\pi \ell^+} \int \frac{\mathrm{d}^d k}{(2\pi)^d} \left[2 \frac{2E - k^-}{k^- - i\delta^-} + (1-\epsilon)\left(1 - \frac{k^+}{\ell^+}\right) + \mathrm{h.c.} \right] \\
&\times (2\pi)\delta^+(k^2)\,(2\pi)\delta^+\left[(\ell-k)^2\right] \Theta_{\mathrm{case}} \frac{1}{\pi} \delta(q_T^2 - q_{T\mathrm{case}}^2) \\
&\times \delta\left(z - \frac{E_{J\,\mathrm{case}}}{E}\right) + \mathcal{O}(a_s^2).
\end{aligned}
\tag{6.28}
$$

Here E is the energy of the quark field initiating the jet, and its small light-cone component ℓ^+ (and thus virtuality) is integrated over. The phase space of the outgoing gluon, with momentum k^μ, and quark, with momentum $\ell^\mu - k^\mu$ is integrated over, subject to the q_T and z measurement. The $\delta^+(k^2) \equiv \delta(k^2)\theta(k_0)$ and $\delta^+[(k-\ell)^2]$ denote the corresponding on-shell conditions. The coupling has been replaced by the renormalized one in the $\overline{\mathrm{MS}}$ scheme.

There are three different cases we need to consider:

(a) both partons are inside the jet,
(b) the gluon is outside the jet,
(c) the quark is outside the jet.

These cases are identified by Θ_{case}, and the transverse momentum $q_{T\mathrm{case}}^2$ and jet energy $E_{J,\mathrm{case}}$ depend on the case and jet algorithm, and are given in table 6.2 in terms

case	algorithm	Θ_{case}	$E_{J\,\text{case}}$	$q^2_{T\text{case}}$
(a) both in	SJA	$\theta\big(x(1-x)E\mathcal{R}-k_T\big)$	E	0
	WTA			$\dfrac{k_T^2}{\max^2(x,1-x)}$
(b) gluon out	SJA/WTA	$\theta\big(k_T-x(1-x)E\mathcal{R}\big)$	Ex	$\dfrac{k_T^2}{x^2}$
(c) quark out	SJA/WTA	$\theta\big(k_T-x(1-x)E\mathcal{R}\big)$	$E(1-x)$	$\dfrac{k_T^2}{(1-x)^2}$

TABLE 6.2: The Θ_{case} that encodes the various regions of phase space, and the corresponding jet energy $E_{J\,\text{case}}$ and transverse momentum $q^2_{T\text{case}}$. At this order the only difference between jet algorithms is the recombination scheme, i.e. standard jet axis vs. Winner-Take-All.

of the energy fraction of the quark

$$x \equiv 1 - \frac{k^-}{2E} \tag{6.29}$$

and of the jet size $\mathcal{R}$, defined in eq. (6.10).

At one loop, there are only two partons, so every distance measure gives the same clustering condition (as we will see in section 6.3, this is no longer true at two loops). There are differences between the standard and WTA recombination scheme that directly follow from the different rules in eq. (6.1). This distinction is only relevant when both partons are inside the jet, in which case the standard jet axis is along their total momentum while the WTA axis is along the most energetic one.

Switching from k^- to the quark energy fraction x, using the on-shell conditions, and exploiting azimuthal symmetry, we rewrite the one-loop term of eq. (6.28) as

$$
\begin{aligned}
J_q^{\text{alg}\,[1]}(z,\boldsymbol{q},E\mathcal{R}) &= \sum_{\text{cases}} \frac{4C_F}{\pi} \frac{(\mu^2 e^{\gamma_E})^\epsilon}{\Gamma(1-\epsilon)} \int_0^1 \mathrm{d}x \int_0^\infty \frac{\mathrm{d}k_T}{k_T^{1+2\epsilon}} \Theta_{\text{case}}\, \delta(q_T^2 - q^2_{T\text{case}}) \\
&\quad \times \delta\Big(z - \frac{E_{J\,\text{case}}}{E}\Big)\Big[\frac{(1+x^2)(1-x)}{(1-x)^2 + (\delta_E^-)^2} - (1-x)\epsilon \Big].
\end{aligned}
\tag{6.30}
$$

Here we replaced the δ^- regulator by its dimensionless counterpart

$$\delta_E^\pm \equiv \frac{\delta^\pm}{2E}. \tag{6.31}$$

After similar manipulations, the corresponding one-loop gluon jet function is

$$
\begin{aligned}
J_g^{\text{alg}\,[1]}(z,\boldsymbol{q},E\mathcal{R}) &= \sum_{\text{cases}} \frac{4}{\pi} \frac{(\mu^2 e^{\gamma_E})^\epsilon}{\Gamma(1-\epsilon)} \int_0^1 \mathrm{d}x \int_0^\infty \frac{\mathrm{d}k_T}{k_T^{1+2\epsilon}} \Theta_{\text{case}}\, \delta(q_T^2 - q^2_{T\text{case}}) \\
&\quad \delta\Big(z - \frac{E_{J\,\text{case}}}{E}\Big) \times \Big\{ C_A(1-x)\Big[x + \frac{1}{x} + \frac{x}{(1-x)^2 + (\delta_E^-)^2} \Big] \\
&\quad + \frac{n_f}{2}\Big[1 - \frac{2x(1-x)}{1-\epsilon} \Big] \Big\}.
\end{aligned}
\tag{6.32}
$$

From this expression one can obtain the one-loop result for the gluon jet function presented in ref. [151], following step by step the calculation of the quark function

detailed below.

6.2.1.1   Result in momentum space

In order to perform the calculation in transverse momentum space we directly solve the two integrals in eq. (6.30), inserting the measurements for the various cases in table 6.2. We start with the case of both partons inside the jet.

In the case of the standard jet axis, the dependence on the transverse momentum is trivial and the calculation reduces to the one performed in ref. [170] for the semi-inclusive quark jet function. After integration over the transverse momentum,

$$
\begin{aligned}
J_{q(a)}^{\mathrm{SJA}\,[1]} &= -\frac{2C_F}{\pi}\left(\frac{\mu^2}{E^2\mathcal{R}^2}\right)^{\epsilon}\frac{e^{\epsilon\gamma_E}}{\epsilon\,\Gamma(1-\epsilon)}\,\delta(1-z)\,\delta(q_T^2) \\
&\quad \times \int_0^1 \mathrm{d}x\,x^{-2\epsilon}(1-x)^{1-2\epsilon}\left[\frac{1+x^2}{(1-x)^2}-\epsilon\right].
\end{aligned}
\tag{6.33}
$$

Here we set the rapidity regulator δ_E^- to zero because the endpoint $x=1$ is already regulated by dimensional regularization. The remaining integral over the energy fraction is a combination of Euler Beta functions, whose expansion up to $\mathcal{O}(\epsilon^0)$ yields

$$
J_{q(a)}^{\mathrm{SJA}\,[1]} = \frac{2C_F}{\pi}\,\delta(1-z)\,\delta(q_T^2)\left[\frac{1}{\epsilon^2}+\frac{1}{\epsilon}\left(L_R+\frac{3}{2}\right)+\frac{1}{2}L_R^2+\frac{3}{2}L_R+\frac{13}{2}-\frac{3\pi^2}{4}\right], \tag{6.34}
$$

where

$$
L_R = \ln\left(\frac{\mu^2}{E^2\mathcal{R}^2}\right). \tag{6.35}
$$

For the WTA axis, the transverse momentum dependence becomes nontrivial. The condition $\max(x,1-x)$ reduces to $x>\frac{1}{2}$ if we symmetrize the integrand,

$$
\begin{aligned}
J_{q(a)}^{\mathrm{WTA}\,[1]} &= \frac{2C_F}{\pi}\frac{e^{\epsilon\gamma_E}}{\Gamma(1-\epsilon)}\frac{\mu^{2\epsilon}}{(q_T^2)^{1+\epsilon}}\,\delta(1-z)\int_{\frac{1}{2}}^{1}\mathrm{d}x\,x^{-2\epsilon}\theta\big((1-x)E\mathcal{R}-q_T\big) \\
&\quad \times\left[\left(-3+\frac{2}{x}-\epsilon\right)+2\frac{1-x}{(1-x)^2+(\delta_E^-)^2}\right].
\end{aligned}
\tag{6.36}
$$

Performing the remaining integral requires to treat the integrand as a two-dimensional distribution. We should expand

$$
\begin{aligned}
&\frac{\mu^{2\epsilon}}{q_T^{2+2\epsilon}}\frac{1-z}{(1-z)^2+(\delta_E^-)^2}\,\theta\left(z-1+\frac{q_T}{E\mathcal{R}}\right) \\
&= \delta(q_T^2)\left\{\delta(1-z)\left[-\frac{1}{2\epsilon^2}+\frac{1}{\epsilon}\left(\ln\delta_E^--\frac{1}{2}L_R\right)-\frac{1}{4}L_R^2\right]\right. \\
&\quad \left.+L_R\mathcal{L}_0(1-z)-2\mathcal{L}_1(1-z)\right\}+\mathcal{L}_0(q_T,\mu)\left[-\delta(1-z)\ln\delta_E^-+\mathcal{L}_0(1-z)\right] \\
&\quad -\mathcal{L}_0^{\mathrm{cut}}\big(q_T,E\mathcal{R}(1-z)\big)\mathcal{L}_0(1-z),
\end{aligned}
\tag{6.37}
$$

where the last term involves a genuine two-dimensional distribution. This identity was obtained by switching to cumulative distributions in both variables, then expanding in δ_E^-, and finally expanding in ϵ. At this point, some notation used in this

part of the thesis, and closer to the used in jet community should be clarified. We define plus distributions in a compact form as

$$\mathcal{L}_n(x) = \left[\frac{\ln^n x}{x}\right]_+, \tag{6.38}$$

which satisfy

$$\int_0^1 dx\, \mathcal{L}_n(x) = 0. \tag{6.39}$$

Plus distributions in terms of the transverse momentum q_T are needed in momentum space calculation and can be derived from eq. (6.38),

$$\mathcal{L}_n(q_T, q_0) = \frac{1}{q_0^2}\, \mathcal{L}_n\left(\frac{q_T^2}{q_0^2}\right), \tag{6.40}$$

such that

$$\int_0^{p_T^2} dq_T^2\, f(q_T^2)\mathcal{L}_n(q_T, q_0) = \int_0^{p_T^2/q_0^2} dx\, f(q_0^2 x)\mathcal{L}_n(x). \tag{6.41}$$

The related "cut" distribution that appear in eq. (6.37) is defined as

$$\mathcal{L}_n^{\text{cut}}(q_T, q_0) = \mathcal{L}_n(q_T, q_0)\theta(q_0 - q_T). \tag{6.42}$$

Thus, solving the integral in eq. (6.36) we have

$$
\begin{aligned}
J_{q(a)}^{\text{WTA}\,[1]} &= \frac{2C_F}{\pi}\delta(1-z)\left\{\delta(q_T^2)\left[\frac{1}{\epsilon^2} + \frac{1}{\epsilon}\left(L_R + \frac{3}{2}\right) + \frac{1}{2}L_R^2 + \frac{3}{2}L_R + \frac{7}{2} - 2\ln^2 2 - \frac{5\pi^2}{12}\right]\right. \\
&\quad - \mathcal{L}_1^{\text{cut}}\left(q_T, \frac{E\mathcal{R}}{2}\right) + \left(2\ln 2 - \frac{3}{2}\right)\mathcal{L}_0^{\text{cut}}\left(q_T, \frac{E\mathcal{R}}{2}\right) \\
&\quad \left. + \theta\left(\frac{E\mathcal{R}}{2} - q_T\right)\frac{1}{q_T^2}\left[3\frac{q_T}{E\mathcal{R}} + 2\ln\left(1 - \frac{q_T}{E\mathcal{R}}\right)\right]\right\}.
\end{aligned}
\tag{6.43}
$$

Finally we consider the cases where only one particle is inside the jet, that are independent of the jet algorithm. We use $x \to 1 - x$ to combine the case where the gluon is outside the jet with the case where the quark is outside. Both the integrals over transverse momentum and energy fraction are fixed by the δ functions enforcing the measurement, resulting in

$$
\begin{aligned}
J_{q(b)+(c)}^{[1]} &= \frac{2C_F}{\pi}\frac{\mu^{2\epsilon}}{(q_T^2)^{1+\epsilon}}\frac{e^{\epsilon\gamma_E}}{\Gamma(1-\epsilon)}\theta\left(z - 1 + \frac{q_T}{E\mathcal{R}}\right) \\
&\quad \times \left[\left(-3 + \frac{2}{z} - \epsilon\right) + \frac{2(1-z)}{(1-z)^2 + (\delta_E^-)^2}\right]z^{-2\epsilon}.
\end{aligned}
\tag{6.44}
$$

Expanding the result in ϵ and δ_E^- we obtain

$$
\begin{aligned}
J_{q(b)+(c)}^{[1]} &= \frac{2C_F}{\pi}\left\{\delta(q_T^2)\delta(1-z)\left[-\frac{1}{\epsilon^2} + \frac{1}{\epsilon}\left(2\ln\delta_E^- - L_R\right) - \frac{1}{2}L_R^2 + \frac{\pi^2}{12}\right]\right. \\
&\quad + \left(-3 + \frac{2}{z} + 2\mathcal{L}_0(1-z)\right)\left[\mathcal{L}_0(q_T, \mu) - \mathcal{L}_0^{\text{cut}}(q_T, E\mathcal{R}(1-z))\right] \\
&\quad \left. + L_R\delta(q_T^2)\right] - 2\ln\delta_E^-\,\mathcal{L}_0(q_T, \mu)\delta(1-z)
\end{aligned}
$$

$$-2\delta(q_T^2)\Big[\Big(-3+\frac{2}{z}\Big)\ln(1-z)+2\mathcal{L}_1(1-z)\Big]\Big\}. \tag{6.45}$$

We now combine the expressions in eqs. (6.34, 6.43) with eq. (6.45), to obtain the bare quark jet function at one loop

$$
\begin{aligned}
J_q^{\text{axis}\,[1]} &= \frac{2C_F}{\pi}\Big\{\delta(1-z)\Big[\delta(q_T^2)\Big(\frac{2}{\epsilon}\ln\delta_E^- +\frac{3}{2\epsilon}+\frac{3}{2}L_R\Big)-2\ln\delta_E^-\,\mathcal{L}_0(q_T,\mu)+\Delta_q^{\text{axis}}(q_T^2)\Big] \\
&\quad +(p_{qq}(z)+p_{gq}(z))\Big[\delta(q_T^2)L_R+\mathcal{L}_0(q_T,\mu)-\mathcal{L}_0^{\text{cut}}(q_T,E\mathcal{R}(1-z))\Big] \\
&\quad -2\Big[\Big(-3+\frac{2}{z}\Big)\ln(1-z)+2\mathcal{L}_1(1-z)\Big]\delta(q_T^2)\Big\}.
\end{aligned}
\tag{6.46}
$$

The dependence on the algorithm occurs via the functions Δ_q^{axis}, that explicitly read

$$\Delta_q^{\text{SJA}}(q_T^2)=\delta(q_T^2)\Big(\frac{13}{2}-\frac{2\pi^2}{3}\Big), \tag{6.47}$$

$$
\begin{aligned}
\Delta_q^{\text{WTA}}(q_T^2) &= \delta(q_T^2)\Big(\frac{7}{2}-2\ln^2 2-\frac{\pi^2}{3}\Big)+\theta\Big(\frac{E\mathcal{R}}{2}-q_T\Big)\frac{1}{q_T^2}\Big[\frac{3q_T}{E\mathcal{R}}+2\ln\Big(1-\frac{q_T}{E\mathcal{R}}\Big)\Big] \\
&\quad +\Big(2\ln 2-\frac{3}{2}\Big)\mathcal{L}_0^{\text{cut}}\Big(q_T,\frac{E\mathcal{R}}{2}\Big)-\mathcal{L}_1^{\text{cut}}\Big(q_T,\frac{E\mathcal{R}}{2}\Big).
\end{aligned}
\tag{6.48}
$$

The expression for the WTA axis is more involved because it introduces the threshold $z>\frac{1}{2}$. We notice that

$$\Delta_q^{\text{WTA}}(q_T^2)=\Delta_q^{\text{SJA}}(q_T^2)\Big[1+\mathcal{O}\Big(\frac{E^2\mathcal{R}^2}{q_T^2}\Big)\Big]. \tag{6.49}$$

This implies that the dependence on the jet algorithm vanishes in the regime $R\ll\theta$, as predicted from the factorization formula in eq. (6.20) (the semi-inclusive jet function $\mathcal{J}$ that enters there is independent of the jet axis).

6.2.1.2 Result in impact-parameter space

The calculation of the quark jet function at one loop can also directly be performed in impact-parameter space. This calculation provides a check of the results in the previous section. We perform the same two integrals of eq. (6.30) with the cases shown in the table 6.2 as in the momentum-space calculation, but first carry out the Fourier transform of the jet function

$$J_q^{\text{alg}[1]}(z,\boldsymbol{b},E\mathcal{R})=\int d\boldsymbol{q}\,e^{i\boldsymbol{b}\cdot\boldsymbol{q}}\,J_q^{\text{alg}[1]}(z,\boldsymbol{q},E\mathcal{R}). \tag{6.50}$$

The case with both partons inside the jet is the only one that depends on the choice of axis. The result for SJA has a trivial dependence on the transverse momentum and can be written as

$$J_{q(a)}^{\text{SJA}\,[1]}=2C_F\,\delta(1-z)\Big[\frac{1}{\epsilon^2}+\frac{1}{\epsilon}\Big(L_R+\frac{3}{2}\Big)+\frac{1}{2}L_R^2+\frac{3}{2}L_R+\frac{13}{2}-\frac{3\pi^2}{4}\Big]. \tag{6.51}$$

Note that for this calculation the IR divergences are regulated by ϵ and we can safely neglect the δ_E^- regulator.

The WTA axis choice introduces a non trivial dependence on the transverse momentum of the jet function. Symmetrizing the integral over x, as in eq. (6.36), we rewrite the jet function as

$$J_{q(a)}^{\text{WTA}\,[1]} = 8\pi C_F \left(\frac{\mu^2 e^{\gamma_E}}{4\pi}\right)^{\epsilon} \delta(1-z) \int_{1/2}^1 dx \left[\frac{1+x^2}{1-x} - \epsilon(1-x) + \frac{1+(1-x)^2}{x} - \epsilon x\right]$$
$$\int \frac{d^{d-2}\boldsymbol{k}_T}{(2\pi)^{d-2}} \frac{1}{k_T^2} \theta\big(x(1-x)E\mathcal{R} - k_T\big) e^{i\boldsymbol{b}\cdot\boldsymbol{k}/x} . \tag{6.52}$$

Integration over the transverse momentum allows us to rewrite eq. (6.52) as

$$J_{q(a)}^{\text{WTA}\,[1]} = 2C_F \frac{(\mu^2 e^{\gamma_E})^{\epsilon}}{\Gamma^2(1-\epsilon)} \delta(1-z)(E\mathcal{R})^{-2\epsilon}\Gamma(-\epsilon) \int_{1/2}^1 dx\, x^{-2\epsilon}(1-x)^{-2\epsilon}$$
$$\times \left[\frac{1+x^2}{1-x} - \epsilon(1-x) + \frac{1+(1-x)^2}{x} - \epsilon x\right]$$
$$-2C_F \delta(1-z) B_{ER}^2 \int_{1/2}^1 dx \left[(1+x^2)(1-x) + \frac{(1+(1-x)^2)}{x}(1-x)^2\right]$$
$$\times {}_2F_3\Big(1,1;2,2,2;-B_{ER}^2(1-x)^2\Big) + \mathcal{O}(\epsilon). \tag{6.53}$$

The jet function depends on the transverse position in terms of the dimensionless combination

$$B_{ER} = \frac{1}{2} b_T E\mathcal{R}. \tag{6.54}$$

The remaining step is the integration over x. The integral in the first term (first two lines) is straightforward to perform analytically. On the other hand, the second integral has a part for which we were unable to obtain a closed analytical expression. The result of this second integral is given by the function $\mathcal{G}(B_{ER})$, whose explicit expression is

$$\mathcal{G}(B_{ER}) = -11 - \frac{5}{8} B_{ER}^2 \, {}_2F_3\left(1,1;2,2,2;-\frac{B_{ER}^2}{4}\right) - 2B_{ER}^2 \, {}_2F_3\left(1,1;2,2,2;-B_{ER}^2\right) \ln 2$$
$$+ \left(4\pi B_{ER}^2 H_0^S(B_{ER}) + \frac{3}{2}\pi H_0^S(B_{ER}) - 8B_{ER}\right) J_1(B_{ER})$$
$$+ \left(-4\pi B_{ER}^2 H_1^S(B_{ER}) + 8B_{ER}^2 - \frac{3}{2}\pi H_1^S(B_{ER}) + 11\right) J_0(B_{ER}) + \mathcal{S} \tag{6.55}$$

where H_n^S are the Struve functions of order n. $\mathcal{S}$ is a remainder that we did not manage to simplify further,

$$\mathcal{S} = 2B_{ER}^2 \sum_{n=0}^{\infty} \frac{\Gamma(1+n)}{\Gamma^3(2+n)} (-B_{ER}^2)^n \left[H_{2n} - n\, {}_3F_2\left(1,1,1-2n;2,2;\frac{1}{2}\right)\right] \tag{6.56}$$

with H_n the n-th harmonic number.

Thus we have

$$J_{q(a)}^{\text{WTA}\,[1]} = 2C_F \delta(1-z) \left[\frac{1}{\epsilon^2} + \frac{1}{\epsilon}\left(L_R + \frac{3}{2}\right) + \frac{1}{2}L_R^2 + \frac{3}{2}L_R + \frac{13}{2} - \frac{3\pi^2}{4} + \mathcal{G}(B_{ER})\right]. \tag{6.57}$$

Note that the only difference between the SJA and WTA results is $\mathcal{G}$. When $B_{ER} \ll 1$ the function $\mathcal{G}$ is zero, as required by the axis independence in this limit.

Next we consider the case when only one parton is inside the jet. By using $x \to 1 - x$, we can combine case (b) and (c). As we now have an explicit dependence on the momentum fraction of the jet, the rapidity regulator δ_E^- needs to be kept. We find,

$$
\begin{aligned}
J_{q(b)+(c)}^{[1]} &= 2C_F \Bigg\{ \left(p_{qq}(z) + p_{gq}(z) \right) \bigg[L_R - L_\mu - 2\ln(1-z) \\
&\quad + B_{ER}^2 (1-z)^2 \, {}_2F_3 \Big(1,1;2,2,2; -B_{ER}^2(1-z)^2 \Big) \bigg] \\
&\quad + \delta(1-z) \Big[\frac{2}{\epsilon}\ln\delta_E^- + 2L_\mu \ln\delta_E^- \Big] + \delta(1-z) \Big[\frac{3}{2\epsilon} + \frac{3}{2}L_R + \frac{13}{2} - \frac{2\pi^2}{3} \Big] \\
&\quad - \delta(1-z) \Big[\frac{1}{\epsilon^2} + \frac{1}{\epsilon}\Big(L_R + \frac{3}{2} \Big) + \frac{1}{2}L_R^2 + \frac{3}{2}L_R + \frac{13}{2} - \frac{3\pi^2}{4} \Big] \Bigg\}.
\end{aligned}
\tag{6.58}
$$

The terms with a divergent behavior in the limit $z \to 1$ should be understood as regulated under the +-prescription. For clarity we have split the $\delta(1-z)$ contribution into three pieces: the first term will be eliminated after the renormalization of rapidity divergences, and the third term is exactly cancelled by the corresponding part of the case with both particles inside the jet, removing IR divergences presented here as double poles in ϵ.

The final result for the quark jet function for both choices of axis is obtained summing eq. (6.51) (SJA) or (6.57) (WTA) with (6.58),

$$
\begin{aligned}
J_q^{\text{axis}\,[1]} &= 2C_F \Bigg\{ \left(p_{qq}(z) + p_{gq}(z) \right) \bigg[L_R - L_\mu - 2\ln(1-z) \\
&\quad + B_{ER}^2 (1-z)^2 \, {}_2F_3 \Big(1,1;2,2,2; -B_{ER}^2(1-z)^2 \Big) \bigg] \\
&\quad + \delta(1-z) \Big(\frac{2}{\epsilon}\ln\delta_E^- + 2L_\mu \ln\delta_E^- \Big) + \delta(1-z) \Big(\frac{3}{2}L_R + \frac{3}{2\epsilon} + \tilde{\Delta}_q^{\text{axis}}(B_{ER}) \Big) \Bigg\},
\end{aligned}
\tag{6.59}
$$

where

$$
\tilde{\Delta}_q^{\text{SJA}}(B_{ER}) = \frac{13}{2} - \frac{2\pi^2}{3}, \qquad \tilde{\Delta}_q^{\text{WTA}}(B_{ER}) = \frac{13}{2} - \frac{2\pi^2}{3} + \mathcal{G}(B_{ER}).
\tag{6.60}
$$

We have checked that these expressions agree with those obtained in section 6.2.1.1, which is partially numerical for the WTA axis. For the numerical implementation, we use the above expressions when a closed analytic expression is available, while we find it more convenient to estimate the sum $\mathcal{S}$, defined in eq. (6.56), by numerically Fourier transforming its momentum-space counterpart.

6.2.2 Renormalization and resummation

6.2.2.1 Renormalized jet function

The jet function in eq. (6.11) has the same renormalization as in the case of TMDs as it was pointed out in eq. (6.15). As in all the cases where factorization with jets holds the soft function is the same that the one of the hadronic TMD case. Thus, the rapidity renormalization factor is the same that the one used in eq. (3.13). As the

operators in the jet function are the same that for hadronic TMDs, the UV renormalization constants are the same as well.

Then, we can easily compute the renormalized NLO quark jet functions from the unsubstracted expressions obtained in the section 6.2.1. The final expression for the renormalized jet function in transverse momentum space is given by

$$
\begin{aligned}
J_q^{[1],\,\mathrm{axis}}(z, \boldsymbol{q}, E\mathcal{R}, \mu, \zeta) \; = \; & 2C_F\Bigg\{\delta(1-z)\Big[\frac{3}{2}L_R\delta(q_T^2) - \mathbf{l}_\zeta\,\mathcal{L}_0(q_T, \mu) \\
& -\mathcal{L}_1(q_T, \mu) + d_q^{\mathrm{axis}}(q_T^2)\Big] + \Big(p_{qq}(z) + p_{gq}(z)\Big) \\
& \times \Big[L_R\delta(q_T^2) + \mathcal{L}_0(q_T, \mu) - \mathcal{L}_0^{\mathrm{cut}}\big(q_T, E\mathcal{R}(1-z)\big)\Big] \\
& -2\Big[\Big(-3 + \frac{2}{z}\Big)\ln(1-z) + 2\mathcal{L}_1(1-z)\Big]\delta(q_T^2)\Bigg\},
\end{aligned}
\tag{6.61}
$$

where the axis-dependent functions are simply related to eqs. (6.47, 6.48) by $d_q^{\mathrm{axis}} = \Delta_q^{\mathrm{axis}} - \frac{\pi^2}{12}$ and the $\pi^2/12$ difference comes from the soft function at NLO,

$$
d_q^{\mathrm{SJA}}(q_T^2) \; = \delta(q_T^2)\Big(\tfrac{13}{2} - \tfrac{3\pi^2}{4}\Big),
\tag{6.62}
$$

$$
\begin{aligned}
d_q^{\mathrm{WTA}}(q_T^2) \; = \; & \delta(q_T^2)\Big(\frac{7}{2} - 2\ln^2 2 - \frac{5\pi^2}{12}\Big) + \theta\Big(\frac{E\mathcal{R}}{2} - q_T\Big)\frac{1}{q_T^2}\Big[\frac{3q_T}{E\mathcal{R}} + 2\ln\Big(1 - \frac{q_T}{E\mathcal{R}}\Big)\Big] \\
& + \Big(2\ln 2 - \frac{3}{2}\Big)\mathcal{L}_0^{\mathrm{cut}}\Big(q_T, \frac{E\mathcal{R}}{2}\Big) - \mathcal{L}_1^{\mathrm{cut}}\Big(q_T, \frac{E\mathcal{R}}{2}\Big).
\end{aligned}
\tag{6.63}
$$

In impact-parameter space the renormalized jet function reads

$$
\begin{aligned}
J_q^{[1],\,\mathrm{axis}}(z, \boldsymbol{b}, E\mathcal{R}, \mu, \zeta) \; = \; & 2C_F\Bigg\{\delta(1-z)\Big[\frac{3}{2}L_R - \frac{1}{2}L_\mu^2 + L_\mu\mathbf{l}_\zeta + \tilde{d}_q^{\mathrm{axis}}(B_{ER})\Big] \\
& + \Big(p_{qq}(z) + p_{gq}(z)\Big)\Big[L_R - L_\mu - 2\ln(1-z) \\
& + B_{ER}^2(1-z)^2 \, _2F_3\big(1, 1; 2, 2, 2; -B_{ER}^2(1-z)^2\big)\Big]\Bigg\},
\end{aligned}
\tag{6.64}
$$

where the axis-dependent functions are again related to eq. (6.60) by $\tilde{d}_q^{\mathrm{axis}} = \tilde{\Delta}_q^{\mathrm{axis}} - \frac{\pi^2}{12}$,

$$
\begin{aligned}
\tilde{d}_q^{\mathrm{SJA}} \; &= \; \frac{13}{2} - \frac{3\pi^2}{4}, \\
\tilde{d}_q^{\mathrm{WTA}} \; &= \; \frac{13}{2} - \frac{3\pi^2}{4} + \mathcal{G}(B_{ER}).
\end{aligned}
\tag{6.65}
$$

From eq. (6.61) one can take the limits $\mathcal{R} \to 0$ and $\mathcal{R} \to \infty$, to approach the factorization regimes described respectively in section 6.1.2 and in sections 6.1.3, 6.1.4. In the small-R limit the two axes give the same result, and we explicitly checked that the jet function factorizes further as in eq. (6.20). The large-R limit is particularly interesting for the WTA axis, where the jet function simplifies as in eq. (6.22). We verified that the dependence on the jet radius drops out in this limit, obtaining

$$
\mathscr{J}^{\mathrm{WTA}[1]}(\boldsymbol{b}, \mu, \zeta) = 2C_F\Big(\frac{7}{2} - \frac{5\pi^2}{12} - 3\ln 2 - \frac{1}{2}L_\mu^2 + L_\mu\mathbf{l}_\zeta + \frac{3}{2}L_\mu\Big).
\tag{6.66}
$$

6.2.2.2   Resummation and ζ-prescription

The renormalization group equations (RGEs) of the TMD jet function are the same as for the standard hadronic TMD,

$$
\begin{aligned}
\mu \frac{\mathrm{d}}{\mathrm{d}\mu} J_q(\boldsymbol{b}; \mu, \zeta) &= \gamma_q(\mu, \zeta) J_q(\boldsymbol{b}; \mu, \zeta) \\
\zeta \frac{\mathrm{d}}{\mathrm{d}\zeta} J_q(\boldsymbol{b}; \mu, \zeta) &= -\mathcal{D}_q(\mu; \boldsymbol{b}) J_q(\boldsymbol{b}; \mu, \zeta)
\end{aligned} \tag{6.67}
$$

where $\mathcal{D}_q$ and γ_q are the rapidity and UV anomalous dimension, respectively. We only consider the quark jet function, because the gluon does not enter in our phenomenological results. As in the hadronic TMD case we have that the rapidity anomalous dimension is

$$
\mathcal{D}_q = -\left.\frac{\mathrm{d}\ln R_q}{\mathrm{d}\ln\zeta}\right|_{f.p.} = -\frac{1}{2}\left.\frac{\mathrm{d}\ln R_q}{\mathrm{d}\ln\delta^+}\right|_{f.p.}, \tag{6.68}
$$

where $|_{f.p.}$ denotes the finite parts.

Since the order of derivatives can be interchanged, one obtains [49, 52],

$$
\mu \frac{\mathrm{d}}{\mathrm{d}\mu}\left(-\mathcal{D}_q(\mu^2, \boldsymbol{b})\right) = \zeta \frac{\mathrm{d}}{\mathrm{d}\zeta}\gamma_q(\mu, \zeta) = -\Gamma_q^{\mathrm{cusp}}. \tag{6.69}
$$

where Γ_q^{cusp} is the quark cusp anomalous dimension. Consequently,

$$
\gamma_q = \Gamma_q^{\mathrm{cusp}} \mathbf{l}_\zeta - \gamma_{V,q}, \tag{6.70}
$$

where

$$
\mathbf{l}_\zeta \equiv \ln\left(\frac{\mu^2}{\zeta}\right), \tag{6.71}
$$

and γ_V is the finite part of the renormalization of the vector form factor. Both γ_V and $\mathcal{D}$ are the same that the used in hadronic TMD analysis and their perturbative expressions are known up to $\mathcal{O}(a_s^3)$ are collected in appendix A.

The high energy scale value for μ is always set at the hard scale, i.e. $\sqrt{s}$ for e^+e^- and Q for SIDIS. As for the TMD case, the evolution of the jet function in the plane (μ, ζ) is governed by eq. (6.67). A systematic treatment of this case has been provided in ref. [16] and a revision of the main features of evolution are studied in the chapter 2 of this thesis. In our results we have implemented the *optimal* solution suggested in [16]. At this point we are left to choose an initial equipotential line $\zeta_\mu(\boldsymbol{b})$, which is known as the ζ-prescription. A special line is provided by the saddle point of the evolution potential. This line exists for all values of $\boldsymbol{b}$ (at least for $b_T < 1/\Lambda_{QCD}$) and covers all the ranges on μ and ζ, providing the optimal solution

$$
J_q(\boldsymbol{b}; \mu, \zeta_\mu(\boldsymbol{b})) = J_q(\boldsymbol{b}). \tag{6.72}
$$

Explicitly, at two-loop order

$$
\begin{aligned}
\mathbf{l}_{\zeta_\mu} \equiv \ln\frac{\mu^2}{\zeta_\mu} = {} & \frac{1}{2}L_\mu - \frac{3}{2} + a_s\left[\frac{11C_A - 2T_F}{36}L_\mu^2 + C_F\left(-\frac{3}{4} + \pi^2 - 12\zeta_3\right)\right. \\
& \left. + C_A\left(\frac{649}{108} - \frac{17\pi^2}{12} + \frac{19}{2}\zeta_3\right) + T_F\left(-\frac{53}{54} + \frac{\pi^2}{6}\right)\right].
\end{aligned} \tag{6.73}
$$

The evolution of the optimal distribution to a generic set of scales (μ, ζ) is then simply given by

$$J_q(\boldsymbol{b}; \mu, \zeta) = J_q(\boldsymbol{b}) U_R^q[\boldsymbol{b}; (\mu, \zeta), (\mu_0, \zeta_{\mu_0}(\boldsymbol{b}))], \qquad (6.74)$$

where $(\mu_0, \zeta_{\mu_0}(\boldsymbol{b}))$ is a point on the special line and U_R^q is the TMD evolution factor

$$U_R^q[\boldsymbol{b}; (\mu_1, \zeta_1), (\mu_2, \zeta_2)] = \exp\left[\int_P \left(\gamma_q(\mu, \zeta)\frac{\mathrm{d}\mu}{\mu} - \mathcal{D}_q(\mu, \boldsymbol{b})\frac{\mathrm{d}\zeta}{\zeta}\right)\right]. \qquad (6.75)$$

Choosing the simplest possible line which connects the initial and final point of the evolution in the improved-γ scheme, eq. (6.75) reduces to

$$U_R^q[\boldsymbol{b}; (\mu, \zeta), (\mu, \zeta_\mu(\boldsymbol{b}))] = U_R^q[\boldsymbol{b}; (\mu, \zeta)] = \left(\frac{\zeta}{\zeta_\mu(\boldsymbol{b})}\right)^{-\mathcal{D}_q(\mu, \boldsymbol{b})}, \qquad (6.76)$$

which is convenient for numerical calculations.

The rapidity anomalous dimension $\mathcal{D}_q$ has a nonperturbative part, which is independent of other nonperturbative inputs of the jet distribution and should be estimated by itself. The ζ-prescription (unlike e.g. the b^*-prescription) allows this separation theoretically. The extractions of the nonperturbative part of the evolution factor from data within this prescription has been carried out in ref. [17, 140, 180]. In our phenomenological analysis we use the parametrization of [140] for the nonperturbative contribution to the rapidity anomalous dimension,

$$\mathcal{D}_q(\mu, \boldsymbol{b}) = \mathcal{D}_q^{\text{res}}(\mu, b^*(\boldsymbol{b})) + g(\boldsymbol{b}). \qquad (6.77)$$

Here $\mathcal{D}_q^{\text{res}}$ is the resummed perturbative part of $\mathcal{D}_q$, and

$$b^*(\boldsymbol{b}) = \sqrt{\frac{b_T^2 B_{\text{NP}}^2}{b_T^2 + B_{\text{NP}}^2}}, \qquad g(\boldsymbol{b}) = c_0 \, b_T \, b^*(\boldsymbol{b}), \qquad (6.78)$$

where the constants B_{NP} and c_0 parametrize the nonperturbative effects. The perturbative expansion of the resummed rapidity anomalous dimension $\mathcal{D}_q^{\text{res}}$ is

$$\mathcal{D}_q^{\text{res}}(\mu, \boldsymbol{b}) = \sum_{n=0}^{\infty} a_s^n(\mu) \mathcal{D}_q^{\text{res}[n]}(X) \qquad (6.79)$$

where $X = \beta_0 a_s(\mu) \ln(\mu^2 b_T^2 e^{2\gamma_E}/4)$, β_0 is the leading coefficients of the QCD beta function and $a_s = g^2/(4\pi)^2$. The leading term reads

$$\mathcal{D}_q^{\text{res}[0]}(X) = -\frac{\Gamma_q^{[0]}}{2\beta_0}\ln(1 - X), \qquad (6.80)$$

and we have used this expansion up to third order in a_s, which incorporates the four-loop anomalous dimension. The complete expression up this order can be found in ref. [16, 181]. The unresummed expression for the rapidity anomalous dimension is reported in the appendix A.
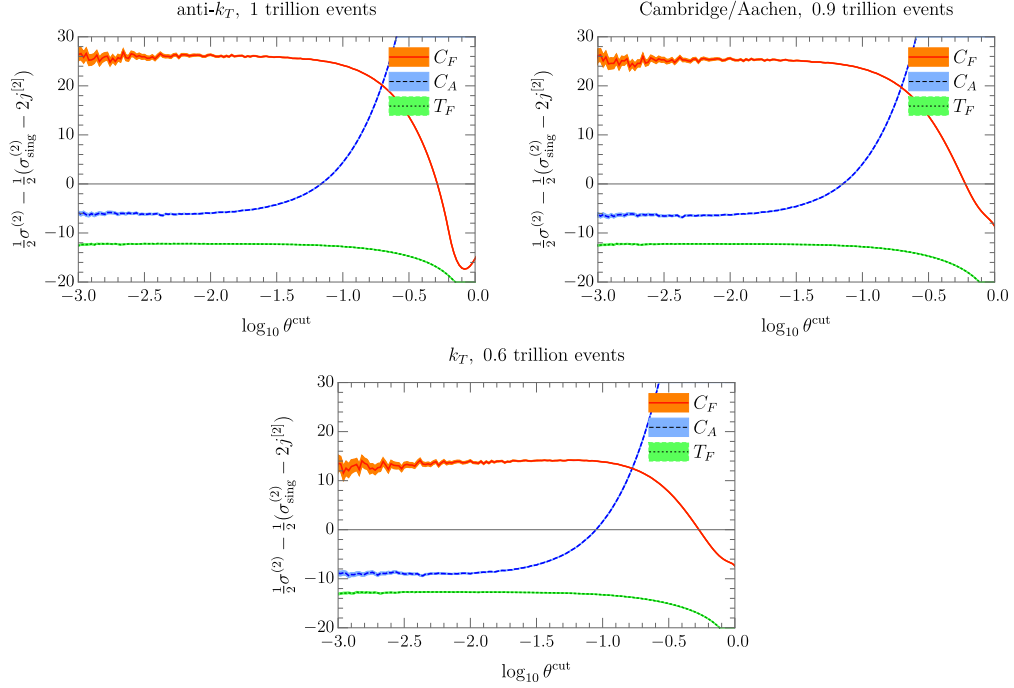
FIGURE 6.3: The difference between the $\mathcal{O}(\alpha_s^2)$ contribution to e^+e^- cross section with a cut on the angular decorrelation $\theta \leq \theta^{\text{cut}}$, obtained from `Event2` and from our factorization theorem. The panels correspond to the (e^+e^- version of) anti-k_T, Cambridge/Aachen and k_T jet algorithm, and the curves correspond to the different color structures, see eq. (6.82). The uncertainty bands indicate the statistical uncertainty. The missing two-loop constant in the quark jet function is the value of the plateau at small θ^{cut}.

6.3   Quark jet function for large R at two loops

As we will see in our numerical analysis, the large-R limit captures the dominant part of the perturbative corrections. This justifies focusing on the quark jet function in the large-R limit, $\mathscr{J}_q^{\text{WTA}}$, which is completely determined at two loops by known anomalous dimensions, except for a constant $j^{[2]}$. Explicitly,

$$
\begin{aligned}
\mathscr{J}_q^{[2],\text{WTA}}(\boldsymbol{b},\mu,\zeta) &= C_F\bigg\{ C_F\bigg[\frac{1}{2}L_\mu^4 - (3+2\mathbf{l}_\zeta)L_\mu^3 + \Big(2\mathbf{l}_\zeta^2 + 6\mathbf{l}_\zeta - \frac{5}{2} + 6\ln2 + \frac{5\pi^2}{6}\Big)L_\mu^2 \\
&\quad + \bigg(\Big(14 - 12\ln2 - \frac{5\pi^2}{3}\Big)\mathbf{l}_\zeta + \frac{45}{2} - 18\ln2 - \frac{9\pi^2}{2} + 24\zeta_3\bigg)L_\mu\bigg] \\
&\quad + C_A\bigg[-\frac{22}{9}L_\mu^3 + \Big(\frac{11}{3}\mathbf{l}_\zeta - \frac{35}{18} + \frac{\pi^2}{3}\Big)L_\mu^2 + \Big(\frac{404}{27} - 14\zeta_3\Big)\mathbf{l}_\zeta \\
&\quad + \bigg(\Big(\frac{134}{9} - \frac{2\pi^2}{3}\Big)\mathbf{l}_\zeta + \frac{57}{2} - 22\ln2 - \frac{11\pi^2}{9} - 12\zeta_3\bigg)L_\mu\bigg] + \frac{n_f}{2}\bigg[\frac{8}{9}L_\mu^3 \\
&\quad + \Big(\frac{2}{9} - \frac{4}{3}\mathbf{l}_\zeta\Big)L_\mu^2 - \frac{112}{27}\mathbf{l}_\zeta + \Big(-\frac{40}{9}\mathbf{l}_\zeta - 10 + 8\ln2 + \frac{4\pi^2}{9}\Big)L_\mu\bigg]\bigg\} \\
&\quad + j^{[2]}.
\end{aligned} \tag{6.81}
$$

We extract this constant using the `Event2` generator [182], which we run with $n_f = 5$ and an infrared cutoff $\rho = 10^{-12}$, generating about a trillion events. Specifically, we consider the difference at $\mathcal{O}(a_s^2)$ between the the cross section with a cut on the angular decorrelation $\theta \leq \theta^{\text{cut}}$ obtained from `Event2` and our factorization theorem, extracting the overall factor of a_s^2. This is shown in fig. 6.3, where the different panels correspond to the (e^+e^- version of) anti-k_T [169], Cambridge/Aachen [183, 184] and k_T [185] jet algorithm. The different curves in each panel correspond to the C_F^2, $C_F C_A$ and $C_F T_F$ color structure, with the bands indicating the statistical uncertainty. From varying the infrared cutoff we conclude that the cross section obtained from `Event2` can be trusted for $\log_{10} \theta^{\text{cut}} > -3$, corresponding to the plotted range.

The clear plateau at small values for θ^{cut} shows that our factorization theorem predicts the singular part of the cross section correctly. The value of the plateau corresponds to the missing two-loop constant $j^{[2]}$ (the overall factor of $1/2$ was chosen to cancel the factor of 2 from the two jet functions in the factorization theorem). The decomposition of $j^{[2]}$ in terms of the C_F^2, $C_F C_A$ and $C_F T_F$ color structures is given by

$$j^{[2]} = j_{C_F}^{[2]} + j_{C_A}^{[2]} + \frac{n_f}{5} j_{T_F}^{[2]} , \tag{6.82}$$

i.e. the color structures are inside the constants. We extracted the result by fitting the plateau to a constant, assuming $n_f = 5$, and the generalization to arbitrary number of flavors only involves rescaling $j_{T_F}^{[2]}$. The best range for this fit is not a priori clear, since we have no control over the power corrections, corresponding to contributions to the cross section not included our factorization theorem. These become more relevant as θ^{cut} increases; on the other hand, lowering θ^{cut} increases the statistical uncertainties. We choose to consider the fit range $-3 \leq \log_{10} \theta^{\text{cut}} \leq \log_{10} \theta_{\text{max}}^{\text{cut}}$, where we vary $\log_{10} \theta_{\text{max}}^{\text{cut}}$ between -2.9 and -2 in steps of 0.02 (this corresponds to the size of our binning). We perform a different fit in each window, including the uncertainty from the `Event2` integration. We take the lowest and highest value obtained in this way as the error, and their average as the central value, leading to

$$\text{anti-}k_T: \qquad j_{C_F}^{[2]} = 25.3 \pm 0.6 \,, j_{C_A}^{[2]} = -6.3 \pm 0.2 \,, j_{T_F}^{[2]} = -12.5 \pm 0.3 \,,$$

$$C/A: \qquad j_{C_F}^{[2]} = 24.5 \pm 0.6 \,, j_{C_A}^{[2]} = -6.7 \pm 0.2 \,, j_{T_F}^{[2]} = -12.5 \pm 0.2 \,,$$

$$k_T: \qquad j_{C_F}^{[2]} = 12.2 \pm 1.1 \,, j_{C_A}^{[2]} = -9.3 \pm 0.2 \,, j_{T_F}^{[2]} = -13.0 \pm 0.3 \,. \tag{6.83}$$

While these constants are remarkably similar for anti-k_T and Cambridge/Aachen, they differ substantially for k_T.

6.4 Numerical results

This section is focused on the obtention of phenomenological predictions for current and future experiments. A comparison of this type of predictions with future data would allow us to extract nonperturbative information about the jet functions recently defined and due to the universality of these function, information about nonperturbative effects of hadronic TMDs. The region of interest for TMDs is small q_T, for which the regimes $\theta \sim R$ and $\theta \ll R$ are most relevant. This leads us to exclusively focus on the WTA axis, which is well behaved in the large-R limit. We start by considering the transverse momentum decorrelation in e^+e^- collisions, obtaining numerical predictions for the Belle II and LEP experiments. We use e^+e^- to test the perturbative convergence, and explore the dependence on the jet radius R and cut
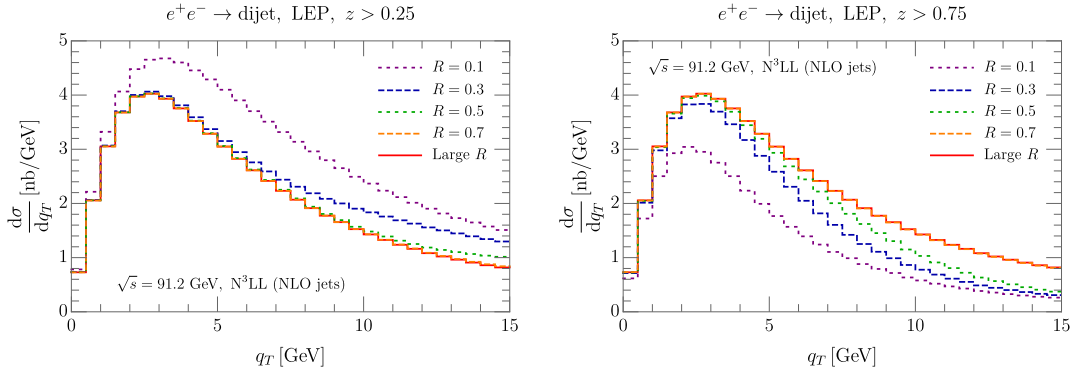
FIGURE 6.4: Dependence of the cross section differential in the transverse momentum decorrelation on the jet radius parameter R, for cuts on jet energy fraction $z > 0.25$ (left) and $z > 0.75$ (right). We use the NLO jet function computed in the regime $R \sim \theta$, and show the large-R result (red solid) for comparison.

on the jet energy fraction z. This process is a perfect playground for this kind of studies because only the jet functions are involved. In the case of SIDIS we provide numerical predictions for HERA and the EIC, and investigate the sensitivity of our cross section to nonperturbative effects.

In our numerical implementation we build on the `arTeMiDe` code [16, 66] to obtain resummed predictions for TMD cross sections. The original version of `arTeMiDe` [186] provides cross sections for Drell-Yan and SIDIS with fragmentation into hadrons. However, its modular structure allowed us to extend it to processes involving jets with a modest amount of modification. Specifically, we have added $e^+e^- \to$ dijet and jet-SIDIS high-level modules, and a jet TMD low-level module that provides our perturbative input for the quark jet functions in $\boldsymbol{b}$-space at the initial scale.

A key point at the time of obtaining reliable phenomenological predictions is the implementation of the double scale evolution share by TMD jet function/PDF. We should run the evolution factor in eq. (6.76) from the initial scale

$$(\mu_0, \zeta_0) = \left(\frac{2e^{-\gamma_E}}{b_T} + 2\,\mathrm{GeV}, \zeta_{\mu_0} \right),\qquad (6.84)$$

where μ_0 is frozen at 2 GeV to avoid the Landau pole and (μ_0, ζ_0) belongs to the special line, to the hard scale

$$(\mu_H, \zeta_H) = \begin{cases} (\sqrt{s}, s) & e^+e^- \\ (Q, Q^2) & \mathrm{SIDIS} \end{cases} \qquad (6.85)$$

The rapidity resummation is the dominant source of uncertainty. Consistently we use the nonperturbative parameters extracted in ref. [140] and we will always use the highest known order in the evolution (N³LL), even though the jet function for generic R is only calculated at one-loop order. The nonperturbative parameters of the evolution kernel in eqs. (6.77, 6.78) are set to

$$B_{NP} = 2.5\,\mathrm{GeV}^{-1}, \qquad c_0 = 0.037\,. \qquad (6.86)$$

6.4.1 Momentum decorrelation in e^+e^- collisions

In our analysis of the e^+e^- cross section, differential in the transverse momentum decorrelation, we consider two experiments:

- Belle II: $\sqrt{s} = 10.52$ GeV, 4 quark flavors.

- LEP: $\sqrt{s} = 91.1876$ GeV, 5 quark flavors.

We account for both the photon and Z-boson contribution, and restrict the plotted q_T range to a region where the power corrections to the factorization theorem can be neglected. In the Belle analysis we omit b-jets, since we do not include quark mass effects in our calculation of the jet function. (Experimentally, these are of course relatively easy to distinguish from light quark jets.)

We start our analysis by studying the dependence on the jet radius parameter R in fig. 6.4 for LEP. The cross section is shown for various jet radii, ranging from $R = 0.1$ to 0.7, using the factorization formulae for $\theta \sim R$ in section 6.1.1. We consider two representative cuts on the jet energy fraction: $z > 0.25$ (left panel) and $z > 0.75$ (right panel). For comparison we also show the large-R limit, discussed in section 6.1.3. We use the one-loop jet function (since we only have the one-loop result for $\theta \sim R$), but include the hard function at two-loop order and perform the resummation at N³LL accuracy.

As expected, as R increases the results approach the $R \to \infty$ limit. In both cases, the cross section for $R = 0.7$ is indistinguishable from the large-R result, and for $z > 0.25$ the difference is even minimal for $R = 0.5$. This means that in the factorization in eq. (6.22) the power corrections $\mathcal{O}(\theta/R) \sim \mathcal{O}(1/b_T^2 E^2 \mathcal{R}^2)$ have a limited impact even for $\theta \lesssim R$. This observation will be used in the rest of our analysis, to justify including the two-loop jet function in the large-R limit, as this will capture the dominant two-loop contribution. Explicitly, we will combine results according to

$$\left(\frac{\mathrm{d}\sigma}{\mathrm{d}q_T}\right)^{\mathrm{N}^3\mathrm{LL}} = \left(\frac{\mathrm{d}\sigma}{\mathrm{d}q_T}\right)^{\mathrm{NLO}} + \left(\frac{\mathrm{d}\sigma}{\mathrm{d}q_T}\right)^{\mathrm{NNLO}}_{\mathcal{R}\to\infty} - \left(\frac{\mathrm{d}\sigma}{\mathrm{d}q_T}\right)^{\mathrm{NLO}}_{\mathcal{R}\to\infty}, \qquad (6.87)$$

where NLO and NNLO indicate the order of the jet function. In each term we use the NNLO hard function and include the resummation at N³LL accuracy. The above approximation contains all large logarithms of θ (or equivalently, q_T) at N³LL accuracy. It reduces to NNLL accuracy for $\theta \sim R \ll 1$, since it misses some $\mathcal{O}(\theta/R)$ corrections. We have shown that their effect is small, except in the tail region.

Next we study the perturbative convergence of the TMD cross section in fig. 6.5. We take $R = 0.5$, $z > 0.25$ and show results for the cross section for Belle II (left panel) and LEP (right panel) at NLL, NNLL and N³LL. The ingredients that enter in the various perturbative orders are summarized in table A.1. The perturbative uncertainty is estimated by varying the scales μ_i in eqs. (6.84, 6.85) up and down by a factor 2 around their central value and taking the envelope. The band obtained by this procedure at NLL is artificially small and not shown. As expected, the N³LL correction is small compared to the NNLL one, and the uncertainty bands overlap and are reduced at higher order.

In fig. 6.6 we investigate the dependence of the cross section on the cut on the jet energy fraction $z > z_{\mathrm{cut}}$ for a fixed value of the jet radius, which provides a complementary picture to fig. 6.4. We show results for Belle II with $R = 0.7$ (left panel) and LEP with $R = 0.3$ (right panel), imposing $z > z_{\mathrm{cut}}$ and varying $z_{\mathrm{cut}} = 0.01$ to $z_{\mathrm{cut}} = 0.75$. As in fig. 6.4, we use NLO jet functions. For $R = 0.7$ the dependence on the cut on z is relatively mild, which reflects the fact that in the large-R limit
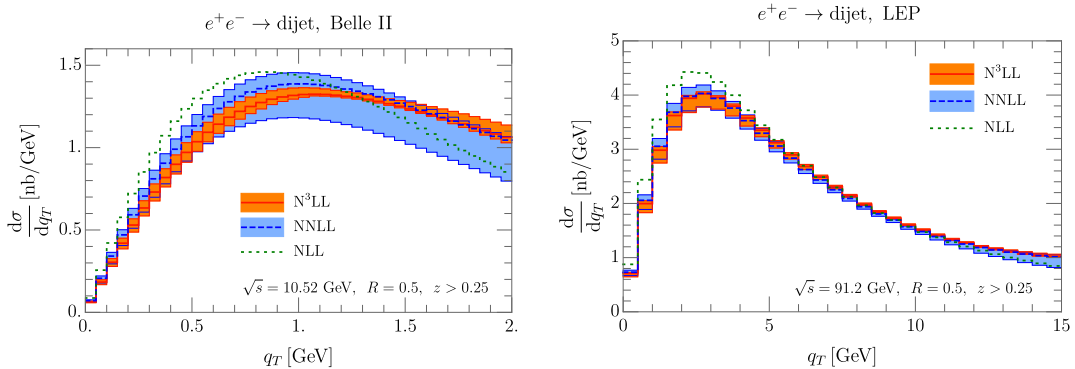
FIGURE 6.5: Perturbative convergence of the cross section differential in transverse momentum decorrelation, for Belle II (left) and LEP (right), for jet radius $R = 0.5$ and jet energy fraction $z > 0.25$. The N^3LL result is obtained with the prescription in eq. (6.87). The bands encode the perturbative uncertainty, as described in the text.
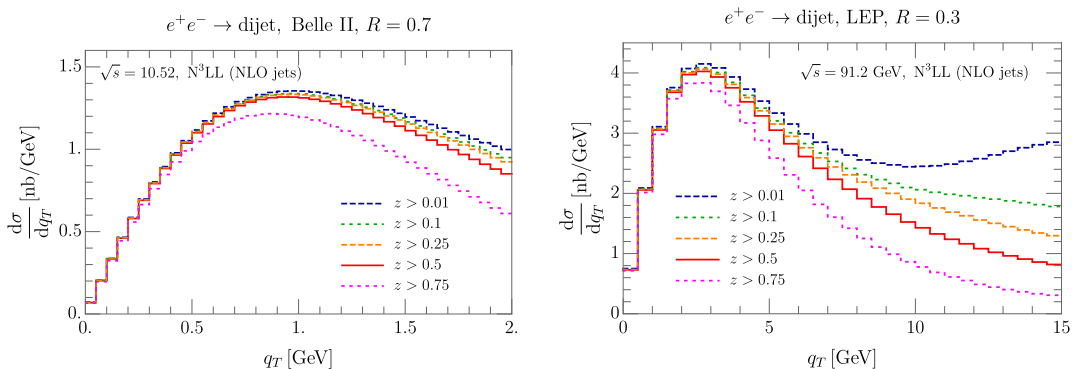

FIGURE 6.6: Dependence of the transverse momentum decorrelation distribution on the cut on jet energy fraction z, for Belle II with $R = 0.7$ (left panel) and LEP with $R = 0.3$ (right panel). The dependence on this cut is larger for smaller R, as discussed in the text. In both cases, the results for $z > 0.5$ (solid red curve) exactly coincide with the large-R limit, see footnote.

the jet function is proportional to $\delta(1 - z)$, and thus independent of this cut. For $R = 0.3$ there is a stronger dependence, and at very small (large) values of z the cross section shows unphysical features. This is not surprising, since the cross section diverges as $z_{cut} \to 0$ (every single low-energy particle originates a different jet) and has large logarithms of $1 - z_{cut}$ for $z_{cut} \to 1$. We found that, regardless of the jet radius, for $z_{cut} = 0.5$ the cross section coincides with the large-R result. This is due to a one-loop accident. At this perturbative order, the initial quark undergoes a single splitting, see fig. 6.2. When integrating over $0.5 < z < 1$, each phase-space configuration contributes to the cross section with exactly one jet (either a jet containing two particles or a jet containing the most energetic particle). Due to the WTA recombination prescription, the resulting jet axis is the same in either case, independent of R. Thus it must in particular coincide with the large-R limit.

As a next step, we study how sensitive these cross sections are to B_{NP} and c_0 that parametrize the nonperturbative contribution to the rapidity evolution, see eqs. (6.77, 6.78). We considered both the "fixed B_{NP}" and "variable B_{NP}" schemes used in the fit in ref. [140], and varied the parameters within the statistical errors listed in their table 4. In practice, we found that the B_{NP} variation is subdominant, so in
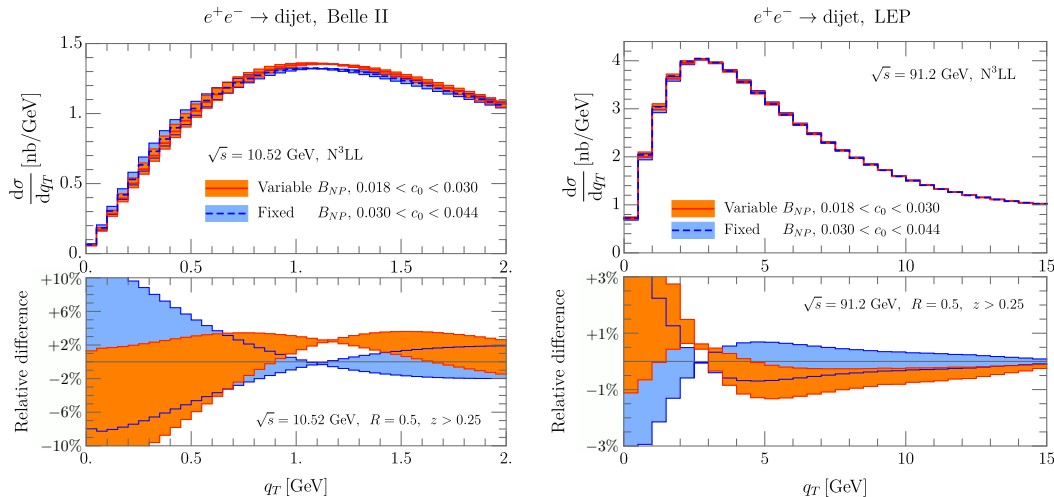
FIGURE 6.7: Estimate of the sensitivity of the TMD to nonpertur-
bative effects in the rapidity resummation at Belle II (left) and LEP
(right). We vary the parameter c_0 in the range of its statistical uncer-
tainty, testing both the fixed and variable B_{NP} schemes of ref. [140].
Results are obtained with the prescription in eq. (6.87).

fig. 6.7 we simply plot variations of c_0. As one would expect, the sensitivity to non-
perturbative effects is much larger at Belle, commensurate with its smaller center-
of-mass energy, and increases at low transverse momenta. The conclusions obtained
from the two schemes are compatible with each other. The situation is similar for
LEP, though the relative variation is substantially lower (below 1% for most of the
range in q_T).

Finally, we have investigated the impact of the choice of jet algorithm, specif-
ically, the impact of the different two-loop constants in eq. (6.83). We found the
difference with respect to anti-k_T to be negligible for Cambridge-Aachen ($< 0.1\%$)
and very small for the k_T algorithm ($< 1\%$).

6.4.2 Transverse momentum dependent distributions in SIDIS

In this section we show representative results for TMD measurements with jets in
SIDIS, showing results for

- HERA: $\sqrt{s} = 318$ GeV,

- EIC: $\sqrt{s} = 100$ GeV.

The EIC is a future facility for the study of TMD distributions, and the above value
for its center-of-mass energy is an assumption. We take $10 \leq Q \leq 25$ GeV and
study the transverse momentum distribution for $q_T \leq 3$ GeV, ensuring that power
corrections of order q_T^2/Q^2 to the factorization theorem can be neglected. In this
kinematic range we expect quark mass effects to be negligible, so we ignore them.
We work in the Breit frame, impose a cut on the jet energy fraction $z > 0.25$ and set
the jet radius to $R = 0.5$. Our e^+e^- analysis in the left panel of fig. 6.4 shows that in
this case the large-R approximation works extremely well, so we again include the
two-loop, large-R jet function of sec. 6.3, using eq. (6.87).

We use the quark TMD PDFs obtained in ref. [140]. In this fit the matching of the
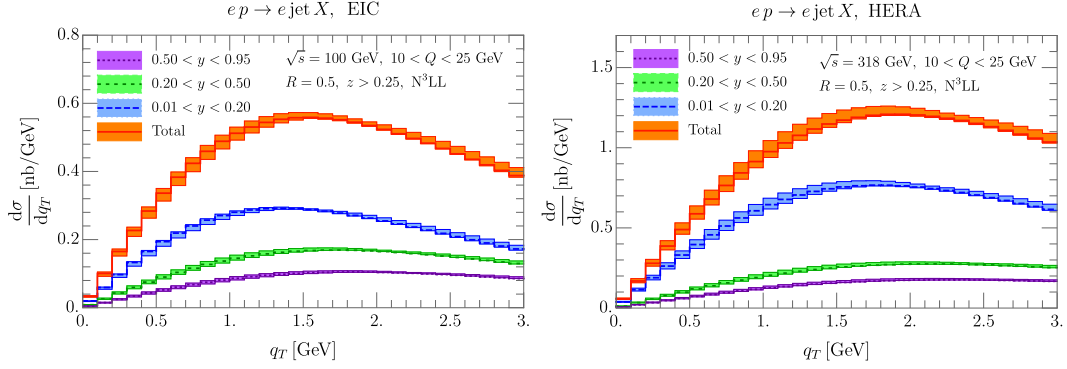TMDs onto PDF is incorporated at NNLO, using the NNPDF 3.1 PDFs [146] with

FIGURE 6.8: TMD cross section for SIDIS with jets at the EIC (left) and at HERA (right), with $10 < Q < 25$ GeV and different intervals in elasticity within the range $0.01 < y < 0.95$. Results are obtained with the prescription in eq. (6.87).
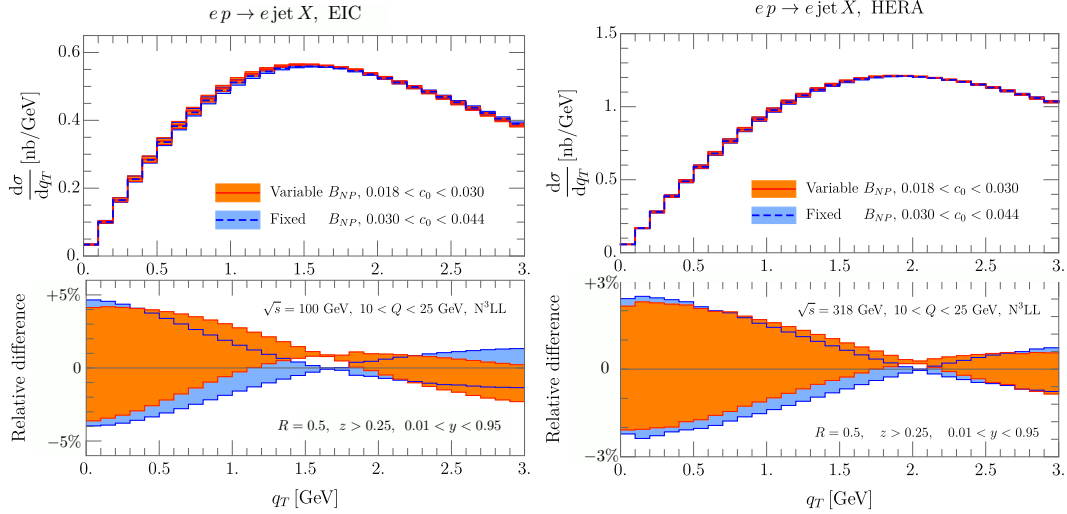

FIGURE 6.9: Sensitivity of the cross section to nonperturbative effects at the EIC (left) and HERA (right). This is estimated by varying the parameter c_0, that controls the nonperturbative contribution to the evolution kernel, within its current statistical uncertainty [140]. Results are obtained with the prescription in eq. (6.87).

$\alpha_s(M_Z) = 0.118$. The additional nonperturbative component of the TMD PDFs is modeled with the ansatz

$$f_{NP} = \exp\left(- \frac{\lambda_1(1-x) + \lambda_2 x + \lambda_3 x(1-x) b_T^2}{\sqrt{1 + \lambda_4 x^{\lambda_5} b_T^2}} \right), \qquad (6.88)$$

where the values for λ_i were fit in ref. [140].

Our results are shown in fig. 6.8, for which we consider different intervals in the elasticity y in the range $0.01 < y < 0.95$. In each case, we obtained the uncertainty band by independently varying the scales μ_H and μ_0 up and down by a factor of 2 around their central values, and taking the envelope. We find that roughly half of the contribution to the cross section comes from low elasticity ($y < 0.2$). The variation in shape between the different elasticity intervals is modest; at high elasticity the peak of the distribution is shifted towards larger transverse momenta.

We now investigate the sensitivity of our observable to nonperturbative hadronic physics. A rough impression can be obtained by varying the parameters B_{NP}, c_0 and λ_i (see eqs. (6.77, 6.78, 6.88)) that enter our nonperturbative model. In principle, these parameters are highly correlated and a full error estimate would require taking data with a large number of replicas, along the lines of the original analysis in ref. [140]. In practice, we observe that the nonperturbative uncertainty is dominated by the variation of the single parameter c_0. Therefore, we obtain a realistic estimate of the size of NP effects by simply varying c_0 within its statistical uncertainty, which we show in fig. 6.9. The effect of varying c_0 is not large (below 5% at the EIC and 3% at HERA), but non-negligible, and grows for small q_T. This plot suggests that such a measurement can likely be used to improve our knowledge of the nonperturbative part of the evolution kernel, parametrized by c_0, which is very relevant because it is universal. We have explored the dependence on R, z_{cut} and the range in Q and y, finding similar sensitivity to nonperturbative effects.

Chapter 7

TMD factorization theorems for processes with groomed jets

In chapter 6 of this thesis we considered the possibility of studying processes with jets in final states defining a jet-TMD. Thus, we replace a final state hadron with a jet [151, 160, 187] in SIDIS and e^+e^- processes. The check of this possibility has revealed that standard jet definitions are compatible with a factorization theorem only in the case of small enough radii, which is a not obvious experimental condition in the planned electron-hadron collider like EIC or LHeC. Instead large jet-radii need a specific definition of jet, which allows soft radiation to be independent of radius. It was achieved using the winner-take-all (WTA) axis [152], and the perturbative calculations were done with a precision similar to the case of fragmenting hadrons.

In this chapter we consider the possibility of groomed jets in SIDIS or $e^+e^- \to$ 2 jets. Developments in jet substructure have shown that applying a grooming algorithm to a jet, using for example the so called "soft-drop" procedure, robustly removes the contamination from both underlying event and non-global correlations. Since this process essentially removes wide angle soft radiation, retaining only a collinear core, it also dramatically reduces hadronization effects (see fig. 7.1), thus allowing an easier access to the TMD non-perturbative physics which we want to probe. Groomed jets with an identified light/heavy hadron in the jet were also proposed as probes of TMD evolution and distribution in [157, 158]. The residual non-perturbative effects contain pieces that depend on the soft-drop grooming procedure and require careful analysis as was pointed out in [188]. In addition, with the use of soft-drop we can derive factorization theorems for large jet radius ($R \sim 1$), which we consider to be the relevant case for low energy experiments, such as EIC. So, in the case of groomed jets we do not need an extra discussion for large-radius jets as with the definition used along chapter 6.

In order to focus on collimated jet configurations, we also impose an upper cutoff in the groomed jet invariant mass. Note that the small transverse momentum constraint does not necessarily ensure collimated configurations since topologies with two or more widely separated sub-jets are also permitted. This constraint allows us to derive a factorization theorem involving the same universal soft function that appears in traditional hadronic TMD, and which is independent of the jet radius for $R \sim 1$. This is a key feature for groomed jets and it is necessary for the universality of TMDs and for this reason, in this chapter, we only consider $R \sim 1$. The cutoff is imposed using groomed jet-thrust, $e \equiv (m/Q)^2$, where m is the groomed invariant mass and Q is the center of mass energy. This allows us to introduce a single cutoff parameter, e_{cut}, independent of the jet energy or transverse momentum. We shall see that imposing this constraint still allows us to capture a majority of events and hence does not significantly impact the cross-section.
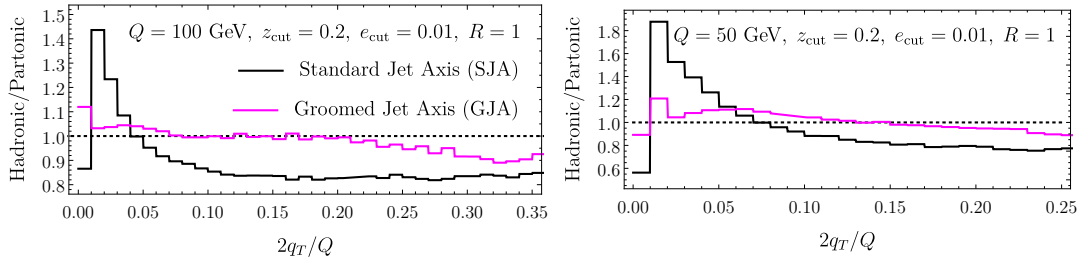
FIGURE 7.1: Hadronization effects in a typical $e^+e^- \to 2$ jets from PYTHIA 8 [147, 148]. at center of mass values, LEFT: $Q = 100$ GeV, RIGHT: $Q = 50$ GeV.

As in chapter 6 the measurement that we are considering is a generalization of the di-hadron momentum de-correlation,

$$\boldsymbol{q}_T = \frac{\boldsymbol{p}_{Th_1}}{z_1} + \frac{\boldsymbol{p}_{Th_2}}{z_2} \tag{7.1}$$

where one or both of the identified hadrons is replaced by a jet, defined through an infrared-safe jet algorithm. Here $\boldsymbol{p}_{Th_i}$ and z_i are the transverse momentum and energy fraction of the hadron i respectively. The factorization theorem is usually written for this normalized vector sum of the transverse momenta rather than just the sum of the transverse momenta. It can be verified by momentum conservation and simple geometry that the quantity $\boldsymbol{p}_{Th_1}/z_1$ represents the transverse momentum of the radiation recoiling against the hadron with respect to the axis defined by the hadron itself. This makes it convenient to write a factorization theorem which matches onto the standard hadron fragmentation function as explained in [157].

We consider three possible scenarios as illustrated in fig. 7.2 and we refer to them as di-hadron, hadron-jet, and di-jet momentum de-correlation. To simplify the discussion we focus on the case of di-jets (fig. 7.2c) and we briefly comment how our results are generalized for the case of hadron-jet de-correlation where the Breit frame in eq. (6.8) is used.

For the case of groomed jets the observable $\boldsymbol{q}_T$ is defined with the groomed quantities, i.e., p_{jet}^μ is the *groomed* jet four-momentum and $z_{\text{jet}} = 2p_{\text{jet}}^0/Q$. The transverse component $\boldsymbol{p}_{T\,\text{jet}}$ is measured with respect to an axis close to the full or groomed jet axes. The exact choice of the axis only differs by power corrections. For concreteness in the results that follow we make the choice of the axis to lie along one of the groomed jets.

Since we want to probe the non-perturbative physics, we wish to work in the small transverse momentum regime ($q_T \ll \sqrt{s}$ where $q_T \equiv |\boldsymbol{q}_T|$).

7.1 Grooming procedure: Soft-drop

The grooming procedure that we use is the soft-drop algorithm. We give here a brief review of the soft-drop groomer and eventually discuss the various hierarchies, the relevant modes and the factorization of the cross section in the next sections.

Soft-drop grooming [159] removes contaminating soft radiation from the jet by constructing an angular ordered tree of the jet, and removing the branches at the widest angles which fail an energy requirement. The angular ordering of the jet is constructed through the Cambridge/Aachen (C/A) clustering algorithm [183, 184, 189–191]. As soon as a branch is found that passes the test, it is declared the groomed
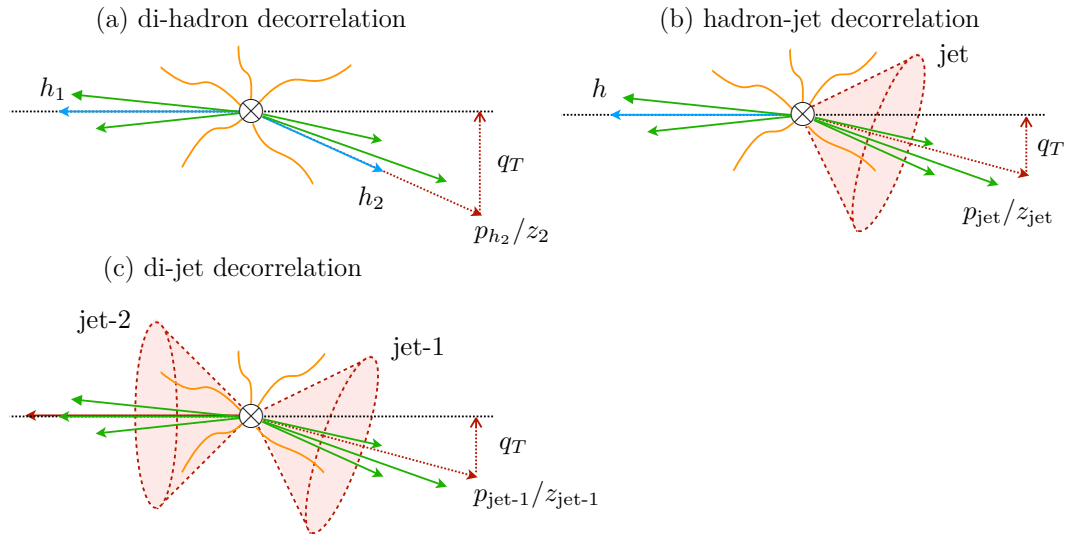
(a) di-hadron decorrelation

(b) hadron-jet decorrelation

(c) di-jet decorrelation

FIGURE 7.2: Three possible transverse momentum de-correlation measurements in e^+e^- annihilation: (a) Identify two hadrons h_1 and h_2 with momenta p_{h_1}, p_{h_2} and energy fractions z_{h_1}, z_{h_2} respectively, (b) Identify a jet and a hadron with momentum p_{jet}, p_h with energy fractions z_{jet}, z_h, (c) Identify two jets with momenta p_{jet_1}, p_{jet_2} and energy fractions z_{jet_1}, z_{jet_2}.

jet, and all the constituents of the branch are the groomed constituents. At the end of the grooming procedure only the narrow energetic core remains from the original jet. Since at large angles all collinear energetic radiation is to be found at the center of the jet, no cone is actually imposed to enclose this core. One simply finds the branch whose daughters are sufficiently energetic. Formally the daughters could have any opening angle, though their most likely configuration is collinear.

The strict definition of the algorithm is as follows. Given an ungroomed jet (which itself is identified first using a suitable algorithm such as the anti-k_T, [169]), first we build the clustering history by starting with a list of particles in the jet. At each stage we merge the two particles within the list that are closest in angle. This merging is usually taken to be summing the momenta of the particles, though one could use winner-take-all schemes [152, 192, 193]. This gives a pseudo-particle, and we remove the two daughters from the current list of particles, replacing them with the merged pseudo-particle. This is repeated until all particles are merged into a single parent. Then we open the tree back up working backwards so that at each stage of the declustering, we have two branches available, label them i and j. We require:

$$\frac{\min\{E_i, E_j\}}{E_i + E_j} > z_{cut}\left(\frac{\theta_{ij}}{R}\right)^\beta, \tag{7.2}$$

where z_{cut} is the modified mass drop parameter, β is the parameter which controls the angularities, θ_{ij} is the angle between i^{th} and j^{th} particle, R is the jet radius and E_i is the energy of the branch i. If the two branches fail this requirement, the softer branch is removed from the jet, and we decluster the harder branch, once again testing eq. (7.2) within the hard branch. The pruning continues until we have a branch that when declustered passes the condition eq. (7.2). All particles contained within this branch whose daughters are sufficiently energetic constitute the groomed jet. Intuitively we have identified the first genuine collinear splitting.

For a hadron-hadron collision, one uses the transverse momentum (p_T) with respect to the beam for the condition of eq. (7.2),

$$\frac{\min\{p_{Ti}, p_{Tj}\}}{p_{Ti} + p_{Tj}} > z_{\text{cut}} \left(\frac{\theta_{ij}}{R}\right)^{\beta}. \tag{7.3}$$

We formally adopt the power counting $z_{\text{cut}} \ll 1$, though typically one chooses $z_{\text{cut}} \sim 0.1$. See [194] for a study on the magnitude of the power corrections with respect to z_{cut} for jet mass distributions. To be specific, in this thesis we consider only the case $\beta = 0$. Note that for $\beta = 0$ the energy of the groomed jet constituents is a collinear unsafe observable [159, 195], however, the additional constraint of the measured transverse momentum $\mathbf{q}_T$ provides a physical collinear cutoff in a similar way a jet shape measurement does.

7.2 Factorization. Hierarchies and modes

In order to compute the transverse momentum de-correlation $\mathbf{q}_T$, defined in eq. (7.1), for two groomed jets in di-jet events in e^+e^- annihilation (fig. 7.2 (c)) we are going to impose a normalized jet mass measurement on both jets through $e = (m_{\text{jet}}/Q)^2$. The other parameters that enter our cross section are the soft-drop parameters $z_{\text{cut}} \sim 0.1$, $\beta = 0$. Ultimately we are going to integrate over the jet mass measurement up to an appropriate (but still small) cut-off value e_{cut}.

We have a rich spectrum of possible hierarchies of momenta, which are all consistent with maintaining $q_T/Q, e_{\text{cut}}, z_{\text{cut}} \ll 1$. We have that $q_T/Q, e_{\text{cut}}, z_{\text{cut}}$ are now expansion parameters in the effective field theory (EFT), and they should be taken into account in the factorization of the process. We first list and briefly discuss these hierarchies and the corresponding factorization theorems within an EFT. The general modes that we will consider will fall into three classes. Modes that explicitly pass soft drop (usually the highly energetic collinear modes), modes that explicitly fail soft-drop (the global soft function modes) and finally those which can live on the border and need to be tested, as to whether they pass or fail. Only the modes that pass soft-drop will contribute to e, while $\mathbf{q}_T$ receives contributions from all radiation that fails soft-drop.

The first regime in which we are interested is $Q \gg Q z_{\text{cut}} \gg q_T \gtrsim Q\sqrt{e} \gg Q\sqrt{e z_{\text{cut}}}$. Here we have low values of q_T which are of the order of $Q\sqrt{e}$. We identify the following modes to be relevant to the cross section:

$$\begin{aligned}
\text{soft:} \quad & p_s^{\mu} \sim q_T(1,1,1); \\
\text{collinear:} \quad & p_c^{\mu} \sim Q(\lambda_c^2, 1, \lambda_c), \ \lambda_c = \sqrt{e},
\end{aligned} \tag{7.4}$$

and the factorization of the cross section in this region is schematically

$$\frac{d\sigma}{de_1 de_2 d^2\mathbf{q}_T} = H_2^{ij}(Q; \mu) \times S(\mathbf{q}_T) \otimes \mathcal{J}_i^{\perp}(e_1, Q, z_{\text{cut}}, \mathbf{q}_T) \otimes \mathcal{J}_j^{\perp}(e_2, Q, z_{\text{cut}}, \mathbf{q}_T). \tag{7.5}$$

Apart from the hard factor H all the other terms in this equation are affected by rapidity divergences. The global soft function S that appears in the factorization theorem in eq. (7.5) (and later in the SIDIS case eq. (7.18)) is the universal function that is also present in the factorization theorem of Drell-Yan, di-hadron production in electron-positron annihilation, and semi-inclusive DIS with TMDs. The operator

definition of the soft function is given by

$$S(\boldsymbol{q}_T) = \frac{1}{N_R}\text{tr}\,\langle[S_n^\dagger S_{\bar{n}}](0)\delta^{(2)}(\boldsymbol{q}_T - \boldsymbol{\mathcal{P}}_\perp)[S_{\bar{n}}^\dagger S_n](0)\rangle\,, \tag{7.6}$$

where $N_R = N_c$ for $S_{n/\bar{n}}$ in the fundamental and $N_c^2 - 1$ for the adjoint representation of $SU(N_c)$. This function has been calculated at NNLO in [52] in b-space and the main results are presented in the appendix A. This function is responsible for the TMD evolution which is actually known up to third order [62, 63]. Because of the universality of this soft function the non-perturbative corrections that it generates in the TMD-evolution factor are process independent [10, 11, 65].

The soft factor provides finally a rapidity renormalization factor for the jets which is totally analogous to the TMD case in eq. (3.13). So, in this sense we can re-write eq. (7.5) as

$$\frac{d\sigma}{de_1 de_2 d^2\boldsymbol{q}_T} = H_2^{ij}(Q;\mu) \times \mathcal{J}_i^\perp(e_1, Q, z_{\text{cut}}, \boldsymbol{q}_T; \mu, \zeta_A) \otimes \mathcal{J}_j^\perp(e_2, Q, z_{\text{cut}}, \boldsymbol{q}_T; \mu, \zeta_B)\,, \tag{7.7}$$

with $\zeta_A\zeta_B = Q^4 z_{\text{cut}}^4$, which recalls clearly the all-order factorization for the di-hadron fragmentation case using TMD. The hadronization corrections to eqs. (7.5-7.7) are discussed in more detail in section 7.7.

The jet-TMD of eq. (7.7) can be re-factorized depending on the relative magnitudes of the effective scales which define it so that one can identify the more complete set of modes

$$\begin{aligned}
\text{soft:} \quad & p_s^\mu \sim q_T(1,1,1); \\
\text{collinear:} \quad & p_c^\mu \sim Q(\lambda_c^2, 1, \lambda_c),\ \lambda_c = \sqrt{e}; \\
\text{soft-collinear:} \quad & p_{sc}^\mu \sim Qz_{\text{cut}}(\lambda_{sc}^2, 1, \lambda_{sc}),\ \lambda_{sc} = q_T/(Qz_{\text{cut}}); \\
\text{collinear-soft:} \quad & p_{cs}^\mu \sim Qz_{\text{cut}}(\lambda_{cs}^2, 1, \lambda_{cs}),\ \lambda_{cs} = \sqrt{e/z_{\text{cut}}}
\end{aligned} \tag{7.8}$$

and we illustrate this in fig. 7.3. We start considering the limit $q_T \gtrsim Q\sqrt{e} \gg Q\sqrt{ez_{\text{cut}}}$, which corresponds to region II in fig. 7.3, when the unintegrated and unsubtracted jet function, $\mathcal{J}_i^\perp$, in eq. (7.5) can be re-factorized into three terms,

$$\mathcal{J}_i^\perp(e, Q, z_{\text{cut}}, \boldsymbol{q}_T) = S_{sc,i}^\perp(Qz_{\text{cut}}, \boldsymbol{q}_T) \times \int de'\, S_{cs,i}(e - e', Qz_{\text{cut}})J_i(e', Q) \tag{7.9}$$

where all the rapidity divergent part and transverse momentum dependence is contained in the calculable $S_{sc,i}^\perp$. The subtracted and unsubtracted jet-TMD are related by

$$\mathcal{J}_i^\perp(e, Q, z_{\text{cut}}, \boldsymbol{b}, \mu, \zeta) = \sqrt{S(\boldsymbol{b})}\mathcal{J}_i^\perp(e, Q, z_{\text{cut}}, \boldsymbol{b}) \tag{7.10}$$

where we have expressed all the subtraction in $\boldsymbol{b}$-space. Throughout this chapter we will interchange between $\boldsymbol{q}_T, \boldsymbol{b}$ spaces for the transverse spectrum and between e, s spaces for the jet mass. We use the same symbol for any function in either space. The variable we are working in should be clear from the argument of the function. A dictionary to translate between spaces is given in the appendix C. For smaller values of q_T: $Q \gg Qz_{\text{cut}} \gtrsim Q\sqrt{e} \gg q_T \sim Q\sqrt{ez_{\text{cut}}}$, the collinear-soft and soft-collinear merge into the same mode which we still refer to as collinear-soft. The soft and collinear modes remain unchanged in their scaling compared to region II. The form of factorization theorem in eq. (7.5) does not change but now the corresponding
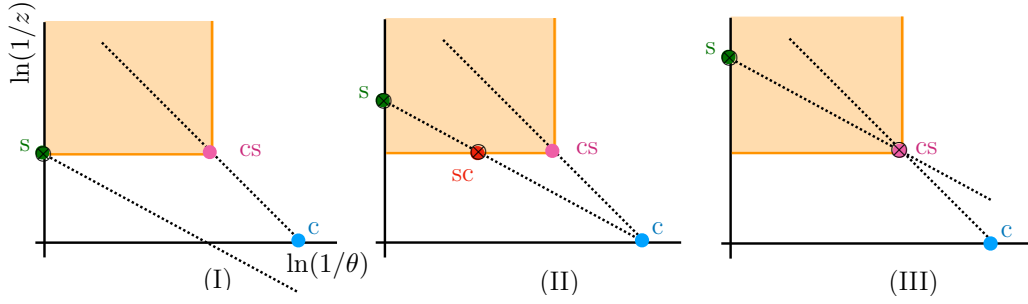
$\otimes$ = contributes to the transverse momentum measurement

FIGURE 7.3: Three possible hierarchies for q_T. Shaded region is one that fails Soft-Drop. (I) Largest $q_T \sim Q z_{\text{cut}}$. The cross section is factorized into 3 function s, cs and c. (II) The soft function s splits into two s and sc.(III) The sc function merges with the cs function.

jet TMDs are re-factorized as (see region III in fig. 7.3),

$$\mathcal{J}_i^\perp(e, Q, z_{\text{cut}}, \boldsymbol{q}_T) = \int de' \, S_{cs,i}^\perp(e - e', Q z_{\text{cut}}, \boldsymbol{q}_T) J_i(e', Q). \tag{7.11}$$

Several of the parameters in the differential cross-secion in eq. (7.7) are in practice integrated in experiments, so that it is convenient to explicitly write the cumulant (or partially integrated) distribution

$$\frac{d\sigma}{d^2\boldsymbol{q}_T}(e_{\text{cut}}) = \int_0^{e_{\text{cut}}} de_1 de_2 \frac{d\sigma}{de_1 de_2 d^2\boldsymbol{q}_T} \,. \tag{7.12}$$

For this cross section we work with the integrated jet function which depends on e_{cut} rather than e,

$$\mathcal{J}_j^\perp(e_{\text{cut}}, Q, z_{\text{cut}}, \boldsymbol{q}_T; \mu, \zeta) = \int_0^{e_{\text{cut}}} de \, \mathcal{J}_j^\perp(e, Q, z_{\text{cut}}, \boldsymbol{q}_T; \mu, \zeta) \,. \tag{7.13}$$

and the factorization theorem for electron-positron annihilation is

$$\frac{d\sigma}{d^2\boldsymbol{q}_T}(e_{\text{cut}}) = H_2^{ij}(Q; \mu) \int \frac{d^2\boldsymbol{b}}{4\pi} e^{i\boldsymbol{b}\cdot\boldsymbol{q}_T} \mathcal{J}_i^\perp(e_{\text{cut}}, Q, z_{\text{cut}}, \boldsymbol{b}; \mu, \zeta) \mathcal{J}_j^\perp(e_{\text{cut}}, Q, z_{\text{cut}}, \boldsymbol{b}; \mu, \zeta) \,. \tag{7.14}$$

The resummation of logarithms inside the jet-TMD implied by eqs. (7.9-7.11) is taken into account defining the cumulant jet function as

$$\mathcal{J}_i^\perp(e_{\text{cut}}, Q, z_{\text{cut}}, \boldsymbol{b}; \mu, \zeta) = \sqrt{S(\boldsymbol{b})} \mathcal{J}_i^\perp(e_{\text{cut}}, Q, z_{\text{cut}}, \boldsymbol{b}) \,, \tag{7.15}$$

$$\mathcal{J}_i^\perp(e_{\text{cut}}, Q, z_{\text{cut}}, \boldsymbol{b}) = S_{sc,i}^\perp(Q z_{\text{cut}}, \boldsymbol{b}) \mathcal{J}_i(e_{\text{cut}}, Q, z_{\text{cut}}; \mu), \tag{7.16}$$

$$\mathcal{J}_i(e_{\text{cut}}, Q, z_{\text{cut}}; \mu) = \int_0^{e_{\text{cut}}} de \int de' \, S_{cs,i}(e - e', Q, z_{\text{cut}}; \mu) J_i(e', Q; \mu) \tag{7.17}$$

and we recall that the rapidity divergences are present only in S and $S_{sc,i}^\perp$, canceling in their product in eq. (7.15). With the exception of the soft-collinear function, $S_{sc}^\perp$, all other ingredients of the factorization are already known at least up to NLO accuracy. In section 7.4 we report the defining matrix elements of each function, we summarize

the NLO results and we perform the NLO calculation of $S_{sc}^{\perp}$. We have performed the calculation using analytic η rapidity regulator, so in section 7.4 we present the NLO result of the soft function with this regulator, despite it is presented in the appendix A in modified δ-regularization scheme. The connection between rapidity regulator obtained in this calculation and the ζ-parameter we used in the part I of this thesis is outlined in the section 7.5.

The factorization for DIS-like processes is analogous, with the difference that here we demand that the hard scattering of the lepton on the proton produces a single jet. In the Breit frame we measure the transverse component, $\boldsymbol{q}_T$, of the transferred momentum, $q^{\mu} = k'^{\mu} - k^{\mu}$ with respect to the single groomed jet. As before, we impose a jet mass cut-off e_{cut} and the grooming parameter z_{cut}. In this framework the initial state proton is moving along the $-z$ direction and the final state jet is moving in the opposite $+z$-direction, so that we can assign the directions n and $\bar{n}$ to the beam and jet definition. The contribution to this transverse momentum measurement comes from the initial state radiation which forms part of the TMDPDF and the radiation that fails soft-drop in the final state jet. We demand that there is a single energetic jet with $E_J \sim Q/2 = \sqrt{-q^2}/2$ with accompanying soft radiation.

Since we are working with two back-to-back directions, our usual definition of the soft function holds: in other words the change from future pointing to past pointing Wilson lines does not affect its value [10, 11, 13, 15, 196].

Since we still impose the same jet mass measurement on the final state jet, we have all the modes that we had in the e^+e^- case. The main difference is that now the initial hadronic state is a TMDPDF. The form of the factorized cross section follows again the hierarchy $Q \gg Q z_{\text{cut}} \gg q_T$, $R \sim 1$ and

$$\frac{d\sigma}{dx dQ^2 d^2\boldsymbol{q}_T} = \frac{\sigma_0(x, Q)}{xs} H_2(Q, \mu) \times S(\boldsymbol{q}_T) \otimes B_{i \leftarrow h}(x, Q, \boldsymbol{q}_T) \otimes \mathcal{J}_j^{\perp}(e_{\text{cut}}, Q, z_{\text{cut}}, \boldsymbol{q}_T) \,,$$
(7.18)

where $x = -q^2/(2P \cdot k)$, k is the momentum of the incoming electron, and $\sigma_0(x, Q)$ is the Born cross section of this process given in the appendix A. The un-subtracted TMDPDF is $B_{i \leftarrow h}$. In our rapidity regularization scheme the (subtracted) TMDPDF is defined as

$$F_{i \leftarrow h}(x, \boldsymbol{b}; \mu, \zeta) = \sqrt{S(\boldsymbol{b})} B_{i \leftarrow h}(x, Q, \boldsymbol{b}).$$
(7.19)

At perturbative values of q_T, the $F_{i \leftarrow h}$ can be matched onto the collinear PDF as is discussed in the part I of this thesis. The matching coefficients at NNLO are the unpolarized ones evaluated in [18, 81].

Once the subtracted quantities are included we can write

$$\frac{d\sigma}{dx dQ^2 d^2\boldsymbol{q}_T} = \frac{\sigma_0(x, Q)}{xs} H_2(Q, \mu)$$
(7.20)
$$\times \int \frac{d^2\boldsymbol{b}}{(2\pi)^2} e^{i\boldsymbol{b} \cdot \boldsymbol{q}_T} F_{i \leftarrow h}(x, Q, \boldsymbol{b}, \mu, \zeta_A) \mathcal{J}_j^{\perp}(e_{\text{cut}}, Q, z_{\text{cut}}, \boldsymbol{b}; \mu, \zeta_B) \,.$$

Finally we observe that using monte-carlo simulations (particularly PYTHIA 8 [147, 148]) most of the events fall in the kinematic regime

$$Q \gg Q z_{\text{cut}} \gg q_T \sim Q\sqrt{e_{\text{cut}}} \,.$$
(7.21)

An important consequence of the jet function refactorization in eq. (7.9) is that the transverse momentum dependent elements decouple from the jet mass elements.
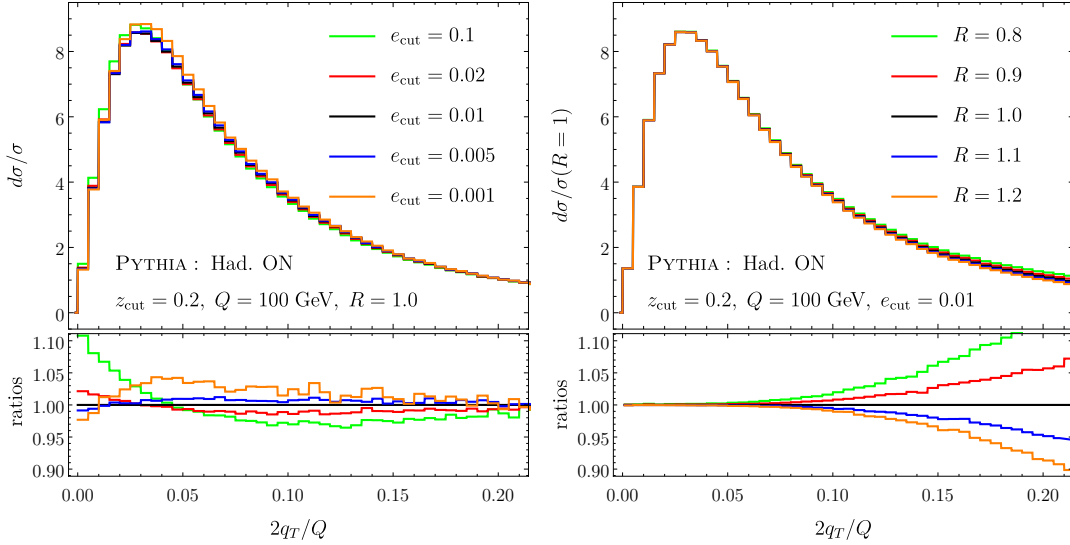
FIGURE 7.4: LEFT: The normalized cross sections for different values of the jet mass cutoff parameter e_{cut}. We also include the corresponding ratios with respect to the case $e_{\text{cut}} = 0.01$. RIGHT: The *relatively* normalized cross section for fixed $e_{\text{cut}} = 0.01$ and for different value of the jet radius R. The corresponding ratios are with respect to $R = 1$.

This suggests that, as long as we remain within the hierarchy of eq. (7.21), then the exact mass cutoff on the invariant mass will only influence the overall normalization and not the shape of the TMD distribution. We test this observation against the monte-carlo simulations by comparing the normalized TMD distributions for various values of e_{cut}. We show the results in fig. 7.4 (left). The jet algorithm is implemented through FASTJET-3 [168]. In addition we note that as long as we measure $q_T \ll Q z_{\text{cut}}$ and for $R \sim 1$ the shape and normalization of the cross section is independent of the choice of R. We also demonstrate this with the help of simulations. We simulate events at $Q = 50$ GeV and we analyze them for different values of $R \gtrsim 1$. We show the resulting distributions in fig. 7.4 (right). Note that for that plot we preserve the relative normalizations of the curves.

7.3   Renormalization group evolution

7.3.1   Solution of renormalization group equations

The main quantity involved in the factorization procedure carried out in previous section is the subtracted jet-TMD for which we have

$$\mu \frac{d}{d\mu} \mathcal{J}^{\perp}(e, Q, z_{\text{cut}}, \boldsymbol{b}, \mu, \zeta) = \gamma_F^q(\mu, \zeta) \mathcal{J}^{\perp}(e, Q, z_{\text{cut}}, \boldsymbol{b}, \mu, \zeta), \tag{7.22}$$

$$\zeta \frac{d}{d\zeta} \mathcal{J}^{\perp}(e, Q, z_{\text{cut}}, \boldsymbol{b}, \mu, \zeta) = -\mathcal{D}^q(\mu, \boldsymbol{b}) \mathcal{J}^{\perp}(e, Q, z_{\text{cut}}, \boldsymbol{b}, \mu, \zeta), \tag{7.23}$$

where on the r.h.s. we have considered just quark initiated jets and we have Fourier transformed with respect to $\boldsymbol{q}_T$ the jet functions appearing in eq. (7.7). Of course this result recalls literally the standard TMD case.

However, because of the refactorization of $\mathcal{J}^{\perp}$ (see eqs. (7.9-7.11)) this resummation is not complete and large logarithms can still spoil the convergence of the

perturbative series. Defining s as the variable conjugate to e in Laplace space (see appendix C) and

$$G \in \left\{ S_{sc}^{sub}(Qz_{\text{cut}}, \boldsymbol{b}), S_{cs}(s, Qz_{cut}), J(s, Q) \right\}; \quad S_{sc}^{sub}(Qz_{\text{cut}}, \boldsymbol{b}) = \sqrt{S(\boldsymbol{b})} S_{sc}(Qz_{\text{cut}}, \boldsymbol{b}),$$
(7.24)

we have

$$\mu \frac{d}{d\mu} G = \gamma^G(\mu, \alpha_s) G = \left(\Gamma^G[\alpha_S] \mathbf{l}_{m_G^2} + \Delta \gamma^G[\alpha_S] \right) G,$$
(7.25)

which are formally similar to the TMD case. Note that $\mathbf{l}_{m_G^2} = \ln \left(\mu^2 / m_G^2 \right)$ and the values of m_G are reported in table 7.1. The only function in G which has a rapidity evolution equation is S_{sc}^{sub} and it scales like $\mathcal{J}^\perp$ in eq. (7.23). The cusp part of eq. (7.25) is proportional to the standard cusp anomalous dimension

$$\Gamma_\mu^G[a_s] = \frac{\Gamma_0^G}{\Gamma_0^{\text{cusp}}} \Gamma^{\text{cusp}} = \frac{\Gamma_0^G}{\Gamma_0^{\text{cusp}}} \sum_{n=0}^{\infty} a_s^{1+n} \Gamma_n^{\text{cusp}},$$
(7.26)

For the non-cusp part we have also a perturbative expansion

$$\Delta \gamma^G[\alpha_S] = \sum_{n=0}^{\infty} a_s^{1+n} \gamma_n^G.$$
(7.27)

The anomalous dimensions that enter in the calculations for each case are given in the appendix A. The evolution in rapidity and factorization scales of all quantities can be implemented using the the ζ-prescription whose general framework can be found in ref. [16] and sketched in chapter 2 of this thesis.

The solution to the RGE in eq. (7.25) is

$$G(\mu) = \mathcal{U}_G(\mu, \mu_0) G(\mu_0), \quad \mathcal{U}_G(\mu, \mu_0) = \exp \left(K_G(\mu, \mu_0) \right) \left(\frac{\mu_0}{m_G} \right)^{2 \, \omega_G(\mu, \mu_0)},$$
(7.28)

with

$$K_G(\mu, \mu_0) = 2 \int_{\alpha(\mu_0)}^{\alpha(\mu)} \frac{d\alpha}{\beta[\alpha]} \Gamma^G[\alpha] \int_{\alpha(\mu_0)}^{\alpha} \frac{d\alpha'}{\beta[\alpha']} + \int_{\alpha(\mu_0)}^{\alpha(\mu)} \frac{d\alpha}{\beta[\alpha]} \Delta \gamma^G[\alpha],$$
(7.29)

$$\omega_G(\mu, \mu_0) = \int_{\alpha(\mu_0)}^{\alpha(\mu)} \frac{d\alpha}{\beta[\alpha]} \Gamma^G[\alpha].$$
(7.30)

Since we are interested only in the NLL and NLL′ result we may keep only the first two terms in the perturbative expansion of the cusp part (i.e., Γ_0^G, Γ_0^{cusp}, and Γ_1^{cusp}) and only the first term form the non-cusp part (γ_0^G). Performing this expansion we get,

$$K_G(\mu, \mu_0) = -\frac{\gamma_0^G}{2\beta_0} \ln r - \frac{2\pi \Gamma_0^G}{(\beta_0)^2} \left[\frac{r - 1 - r\ln r}{\alpha_s(\mu)} + \left(\frac{\Gamma_1^{\text{cusp}}}{\Gamma_0^{\text{cusp}}} - \frac{\beta_1}{\beta_0} \right) \frac{1 - r + \ln r}{4\pi} + \frac{\beta_1}{8\pi\beta_0} \ln^2 r \right],$$
(7.31)

$$\omega_G(\mu, \mu_0) = -\frac{\Gamma_0^G}{2\beta_0} \left[\ln r + \left(\frac{\Gamma_{\text{cusp}}^1}{\Gamma_{\text{cusp}}^0} - \frac{\beta_1}{\beta_0} \right) \frac{\alpha_s(\mu_0)}{4\pi} (r - 1) \right],$$
(7.32)

Function	Γ_0^G	γ_0^G	m_G
H_{ij}	$-4(C_i + C_{\bar{j}})$	$-4\bar{\gamma}_i(C_i + C_j)$	Q
S_{cs}	$-8C_i$	0	$Q\sqrt{z_{\text{cut}}/\tilde{s}}$
J_i	$8C_i$	$4\bar{\gamma}_i C_i$	$Q/\sqrt{\tilde{s}}$
$B_{i/h}$	0	$4\bar{\gamma}_i C_i + \gamma_{sc}^0$	0
S	$4(C_i + C_j)$	0	ν_s
$S_{sc}^{\perp}$	0	γ_0^{sc}	n.a

TABLE 7.1: Anomalous dimensions coefficients for up to NLL accuracy: $\bar{\gamma}_q = 3/2$, $\bar{\gamma}_g = \beta_0/(2C_A)$, and $\gamma_0^{sc} = 2\alpha_s(\mu)C_F/\pi\ln(\nu/Qz_{\text{cut}})$.

where $r = \alpha(\mu)/\alpha(\mu_0)$ and β_n are the coefficients of the QCD β-function,

$$\beta[\alpha_s] = \mu\frac{d\alpha_s}{d\mu} = -2\alpha_s \sum_{n=0}^{\infty} \left(\frac{\alpha_s}{4\pi}\right)^{1+n} \beta_n . \tag{7.33}$$

The expressions for all ingredients necessary to perform the evolution of any function that appears in the factorization theorems we considered in this paper are given in tab. 7.1. The two loop non-cusp anomalous dimensions we need to NNLL RGEs are given by ref. [197]

$$\frac{1}{2}\gamma_1^s + \gamma_1^{sc} = \frac{C_i}{2}\left[34.01C_F + \left(\frac{1616}{27} - 56\zeta_3 - 9.31\right)C_A - \left(\frac{448}{27} + 14.04\right)n_f T_R - \frac{2}{3}\pi^2\beta_0\right],$$

$$\gamma_1^{cs} = C_i\left[-17.00C_F + \left(-55.20 + \frac{22}{9}\pi^2 + 56\zeta_3\right)C_A + \left(23.61 - \frac{8}{9}\pi^2\right)n_f T_R\right]$$

$$\gamma_1^q = C_F\left[\left(3 - 4\pi^2 + 48\zeta_3\right)C_F + \left(\frac{1769}{27} + \frac{22}{9}\pi^2 - 80\zeta_3\right)C_A\right.$$
$$\left. + \left(-\frac{484}{27} - \frac{8}{9}\pi^2\right)n_f T_R\right],$$

$$\gamma_1^s + \gamma_1^{sc} + \gamma_1^B = C_i\left[\left(20 - 4\pi^2 + 48\zeta_3\right)C_F + \left(60.87 + \frac{22}{9}\pi^2 - 80\zeta_3\right)C_A\right.$$
$$\left. + \left(-24.94 - \frac{8}{9}\pi^2\right)n_f T_R\right]. \tag{7.34}$$

The resummation of potentially large logarithms inside the jet-TMD is done performing the evolution in Laplace space and then integrating such that we get the cumulant before we take the inverse transform. In this way we resum logarithms which are associated to e_{cut}. All this works as follows. Starting from eq. (7.17), then taking the Laplace and consecutively the inverse transform with respect to e we find

$$\mathcal{J}_i(e_{\text{cut}}, Q, z_{\text{cut}}; \mu) = \frac{1}{2\pi i}\int_{\gamma-i\infty}^{\gamma+i\infty} ds\frac{\exp(se_{\text{cut}}) - 1}{s} S_{cs,i}(s, Q, z_{\text{cut}}; \mu)J_i(s, Q; \mu) . \tag{7.35}$$

Then solving the RGE equations for the collinear-soft and jet function as described

before, and performing the last remaining integral over the Laplace conjugate variable s we get

$$\mathcal{J}_i(e_{\text{cut}}, Q, z_{\text{cut}}; \mu) = \exp\left(K_{cs}(\mu, \mu_{cs}) + K_J(\mu, \mu_J)\right) S_{cs,i}(L_{cs} \to \partial_{\omega_{cs}}; \mu_{cs}) J_i(L_J \to \partial_{\omega_J}; \mu_J)$$

$$\left(\frac{\mu_{cs}}{Q\sqrt{z_{\text{cut}}e_{\text{cut}}}}\right)^{2\omega_{cs}(\mu,\mu_{cs})} \left(\frac{\mu_J}{Q\sqrt{e_{\text{cut}}}}\right)^{2\omega_J(\mu,\mu_J)} \frac{\exp(\gamma_E(\omega_{cs}(\mu, \mu_{cs}) + \omega_J(\mu, \mu_J)))}{\Gamma(1 - \omega_{cs}(\mu, \mu_{cs}) - \omega_J(\mu, \mu_J))} . \quad (7.36)$$

This is our final result for the resummed cumulant jet function. The order of logarithmic accuracy is then determined by the order of which the kernels K_F, ω_F, and the fixed order collinear-soft and jet functions are evaluated. At this stage of the calculation the canonical scales, μ_{cs} and μ_J, are not yet fixed. This allows us to choose the scales such that potentially large logarithms are minimized in momentum space. From the above is clear that the canonical choice of scales such as the fixed order logarithms are minimized are,

$$\mu_{cs} = Q\sqrt{z_{\text{cut}}e_{\text{cut}}} , \qquad\qquad \mu_J = Q\sqrt{e_{\text{cut}}} . \qquad (7.37)$$

In numerical applications one needs to perform variations around these scales in order to obtain an estimate of the theoretical uncertainty.

7.4 Operator definitions and one-loop results

In this section we give the operator definitions of the factorization elements discussed in section 7.2 and their NLO expansions. From those we determine the renormalization functions, group equations, and corresponding anomalous dimensions. Many of the results presented here are already known and found in literature.

7.4.1 Jet functions

The quark and gluon jet function definitions, one loop calculation, and the corresponding Laplace transforms can be found in ref. [197]. Here we summarize their results. The quark jet function is given by,

$$J_q(e, Q) = \frac{(2\pi)^3}{N_c} \text{tr} \langle \frac{\not{\bar{n}}}{2} \chi_n(0) \delta(Q - \mathcal{P}^-) \delta^{(2)}(\mathcal{P}_\perp) \delta(e - \mathcal{E}) \bar{\chi}_n \rangle , \qquad (7.38)$$

and the gluon

$$J_q(e, Q) = \frac{(2\pi)^3}{N_c} \text{tr} \langle \frac{\not{\bar{n}}}{2} \mathcal{B}_{n\perp}^\mu(0) \delta(Q - \mathcal{P}^-) \delta^{(2)}(\mathcal{P}_\perp) \delta(e - \mathcal{E}) \mathcal{B}_{n\perp\mu} \rangle , \qquad (7.39)$$

where N_c is the number of colors and $\mathcal{B}_{n\perp}^\mu$ is the gauge invariant gluon building block of the effective field theory,

$$\mathcal{B}_{n\perp}^\mu = \frac{1}{g}[W_n^\dagger(\mathcal{P}_\perp^\mu + gA_{n,\perp}^\mu)W_n] . \qquad (7.40)$$

As demonstrated earlier when working with the cumulant distribution (i.e., when integrating out to e_{cut}) it is useful to work in Laplace space. The renormalized

groomed jet function up to NLO contributions in Laplace space is given by

$$J_i(s, Q; \mu) = 1 + \frac{\alpha_s C_i}{2\pi} \left\{ L_J^2 + \bar{\gamma}_i L_J - \frac{\pi^2}{3} + c_i \right\} + \mathcal{O}(\alpha_s^2) , \tag{7.41}$$

where for quark initiated jets we have

$$C_q = C_F = \frac{N_c^2 - 1}{2N_c} , \bar{\gamma}_q = \frac{3}{2} , c_q = \frac{7}{2} , \tag{7.42}$$

and for gluon initiated jets we have

$$C_g = C_A = N_c , \bar{\gamma}_g = \frac{\beta_0}{2C_A} , c_g = \frac{67}{18} - \frac{10}{9} \frac{n_f T_R}{C_A} , \tag{7.43}$$

The logarithms, L_J that appear in eq. (7.41) and the corresponding one loop anomalous dimensions are

$$L_J = \ln\left(\frac{\mu^2 \tilde{s}}{Q^2}\right) , \gamma^J = \frac{\alpha_s C_i}{\pi} \left(2L_J + \bar{\gamma}_i\right) + \mathcal{O}(\alpha_s^2) . \tag{7.44}$$

The anomalous dimension is defined through the RG equation satisfied by renormalized jet functions. In Laplace space this is

$$\frac{d}{d\ln\mu} J_i(s, Q; \mu) = \gamma^J(s, Q; \mu) J_i(s, Q; \mu) . \tag{7.45}$$

In momentum space the above equation is written as convolution (in the invariant mass variable e), of the anomalous dimension and the renormalized jet function.

7.4.2   Collinear-soft function

The operator definition of the invariant equation mass measurement collinear soft function is given by

$$S_{cs}(e, Q z_{cut}) = \frac{1}{N_R} \text{tr} \langle T \left(U_n^\dagger W_t \right) \mathcal{M}_e^{SD} \bar{T} \left(W_t^\dagger U_n \right) \rangle , \tag{7.46}$$

where $\mathcal{M}_e^{SD}$ is the invariant measurement function,

$$\mathcal{M}_e^{SD} = \delta \left(e - (1 - \Theta_{SD}) \mathcal{E} \right) . \tag{7.47}$$

Here we dropped the jet flavor (quark/anti-quark or gluon) for simplicity of notation and the normalization constant N_R is simply the size of the representation for SU(N_c) of the W_t and U_n Wilson lines. For quark jets (fundamental representation) we have $N_R = N_c$ and for gluon jets (adjoint representation) we have $N_R = N_c^2 - 1$. At NLO the bare collinear soft function is given by

$$\begin{aligned} S_{cs,\text{bare}}(e, Q z_{\text{cut}}) &= \delta(e) \\ &+ \frac{\alpha_s C_i}{\pi} \left\{ -\frac{1}{\epsilon^2} \delta(e) + \frac{1}{\epsilon} \mathcal{L}_0(e, \xi) - \mathcal{L}_1(e, \xi) + \frac{\pi^2}{12} \delta(e) \right\} + \mathcal{O}(\alpha_s^2) , \end{aligned} \tag{7.48}$$

where

$$\xi \equiv \frac{\mu^2}{Q^2 z_{\text{cut}}} . \tag{7.49}$$

Therefore we have for the renormalized function

$$S_{cs}(e, Qz_{cut}) = \delta(e) + \frac{\alpha_s C_i}{\pi}\left\{-\mathcal{L}_1(e, \xi) + \frac{\pi^2}{12}\delta(e)\right\} + \mathcal{O}(\alpha_s^2)\,, \tag{7.50}$$

where

$$S_{cs,bare}(e, Qz_{cut}) = Z_{cs} \otimes S_{cs}(e, Qz_{cut})\,, \tag{7.51}$$

with

$$Z_{cs}(e) = \delta(e) + \frac{\alpha_s C_i}{\pi}\left\{-\frac{1}{\epsilon^2}\delta(e) + \frac{1}{\epsilon}\mathcal{L}_0(e, \xi)\right\} + \mathcal{O}(\alpha_s^2)\,. \tag{7.52}$$

In Laplace space for the renormalized collinear-soft function we get,

$$S_{cs}(s, Qz_{cut}; \mu) = 1 - \frac{\alpha_s C_i}{2\pi}L_{cs}^2 + \mathcal{O}(\alpha_s^2)\,, \tag{7.53}$$

which satisfies the following RGE

$$\frac{d}{d\ln\mu}S_{cs}(s, Qz_{cut}; \mu) = \gamma^{cs}(s, \mu)S_{cs}(s, Qz_{cut}; \mu)\,. \tag{7.54}$$

The logarithm L_{cs} and the corresponding anomalous dimension are

$$L_{cs} = \ln(\xi\tilde{s})\,, \gamma^{cs}(s, \mu) = -2\frac{\alpha_s C_i}{\pi}L_{cs} + \mathcal{O}(\alpha_s^2)\,. \tag{7.55}$$

7.4.3 Soft function

The soft function that appears in the factorization theorems in eqs. (7.14, 7.18) is defined in eq. (7.6) and it has been calculated in several schemes at higher orders in QCD, as reported in sec. 7.2. Here we report a one loop expression using the analytic regulator in momentum space,

$$S_{bare} = \delta^{(2)}(\boldsymbol{q}_T) + \frac{\alpha_s(\mu)C_i}{\pi}\left\{\frac{4}{\eta}\left[\mathcal{L}_0(q_T^2, \mu^2) - \frac{1}{2\epsilon}\delta^{(2)}(\boldsymbol{q}_T)\right] + \frac{1}{\epsilon}\left[\frac{1}{\epsilon} - 2\ln\left(\frac{\nu}{\mu}\right)\right]\delta^{(2)}(\boldsymbol{q}_T)\right.$$
$$\left. + 4\mathcal{L}_0(q_T^2, \mu^2)\ln\left(\frac{\nu}{\mu}\right) - 2\mathcal{L}_1(q_T^2, \mu^2) - \frac{\pi^2}{12}\delta^{(2)}(\boldsymbol{q}_T)\right\} + \mathcal{O}(\alpha_s^2)\,. \tag{7.56}$$

The renormalized soft function, S, is defined through

$$S_{bare} = Z_s^{\perp}(\mu, \nu) \otimes S(\mu, \nu)\,, \tag{7.57}$$

and satisfies the following renormalization group equations

$$\frac{d}{d\ln\mu}S(\mu, \nu) = \gamma^s(\mu, \nu)S(\mu, \nu)\,, \frac{d}{d\ln\nu}S(\mu, \nu) = \gamma_\nu^s(\mu, \nu) \otimes S(\mu, \nu)\,. \tag{7.58}$$

Therefore we find for the one-loop corresponding impact parameter space quantities

$$S(\mu, \nu) = 1 + \frac{\alpha_s(\mu)C_i}{\pi}\left\{4\ln\left(\frac{\mu_E}{\mu}\right)\ln\left(\frac{\nu}{\mu}\right) - 2\ln^2\left(\frac{\mu_E}{\mu}\right) - \frac{\pi^2}{12}\right\} + \mathcal{O}(\alpha_s^2)\,, \tag{7.59}$$
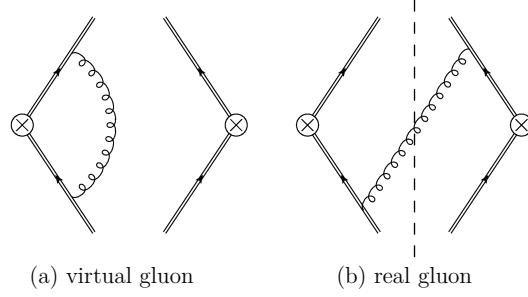
(a) virtual gluon   (b) real gluon

FIGURE 7.5: The order $\mathcal{O}(\alpha_s)$ diagrams that contribute to the soft-collinear function.

$$Z_s^\perp(\mu,\nu) = 1 + \frac{\alpha_s(\mu)C_i}{\pi}\left\{\frac{4}{\eta}\left[\ln\left(\frac{\mu_E}{\mu}\right) - \frac{1}{2\epsilon}\right] + \frac{1}{\epsilon}\left[\frac{1}{\epsilon} - 2\ln\left(\frac{\nu}{\mu}\right)\right]\right\} + \mathcal{O}(\alpha_s^2), \quad (7.60)$$

with

$$\gamma^s(\mu,\nu) = -4\frac{\alpha_s(\mu)C_i}{\pi}\ln\left(\frac{\nu}{\mu}\right) + \mathcal{O}(\alpha_s^2), \gamma_\nu^s(\mu,\nu) = 4\frac{\alpha_s(\mu)C_i}{\pi}\ln\left(\frac{\mu_E}{\mu}\right) + \mathcal{O}(\alpha_s^2). (7.61)$$

The rapidity and renormalization scales used to produce our result are fixed using the ζ-prescription [16] adapted for this case. Later in section 7.5 we give a description of how one can use the rapidity regulated objects that have ν dependence to construct the subtracted rapidity divergences free objects but yet keep trace of the rapidity logs using the ζ parameter.

7.4.4 Soft-collinear function

The soft-collinear function is defined by the matrix element

$$S_{sc}^\perp(Qz_{cut}) = \frac{1}{N_R}\text{tr}\langle T\left(U_n^\dagger W_t\right)\mathcal{M}_\perp^{SD}\bar{T}\left(W_t^\dagger U_n\right)\rangle, \quad (7.62)$$

and the groomed jet measurement function, $\mathcal{M}_\perp^{SD}$ is given in terms of the label momentum operator, $\mathcal{P}$,

$$\mathcal{M}_\perp^{SD} = \Theta_{SD} \times \delta^2\left(\boldsymbol{q}_T - \Theta_{SD}\mathcal{P}_\perp\right), \quad (7.63)$$

where Θ_{SD} denotes the soft drop groomer. The collinear-soft modes only contribute to the invariant mass measurement if they pass soft-drop, which is implemented by the Θ_{SD} term. The NLO calculation involves one real and one virtual diagram shown in fig. 7.5. While the virtual diagram is scaleless. The diagram with a real gluon needs to be integrated over the phase-space of soft gluon. This then yields non-vanishing contribution from when the soft gluon fails the grooming,

$$S_{sc,\text{NLO}}^\perp(Qz_{cut}) = 4g^2 C_i\tilde{\mu}^{2\epsilon}\,\nu^\eta\int\frac{d^dk}{(2\pi)^{d-1}}\frac{\delta(k^2)\,\delta^{(2)}(\boldsymbol{q}_T - \boldsymbol{k}_\perp)}{k^+\,(k^-)^{1+\eta}}\theta(Qz_{\text{cut}} - k^-). \quad (7.64)$$

Performing the integrals we find for the bare quantity

$$S_{sc,\text{bare}}^\perp(Qz_{\text{cut}}) = \delta^{(2)}(\boldsymbol{q}_T) + \frac{\alpha_s C_i}{\pi}\left\{-\frac{2}{\eta}\left[\mathcal{L}_0(q_T^2,\mu^2) - \frac{1}{2\epsilon}\delta^{(2)}(\boldsymbol{q}_T)\right]\right. \quad (7.65)$$

$$+\frac{1}{\epsilon}\ln\left(\frac{\nu}{Qz_{\text{cut}}}\right)\delta^{(2)}(\boldsymbol{q}_T) - 2\ln\left(\frac{\nu}{Qz_{\text{cut}}}\right)\mathcal{L}_0(q_T^2, \mu^2)\right\} + \mathcal{O}(\alpha_s^2) ,$$

and for the renormalized quantity, $S_{sc,}^{\perp}(Qz_{\text{cut}}; \mu, \nu)$ we have

$$S_{sc,\text{bare}}^{\perp}(Qz_{\text{cut}}) = Z_{sc}^{\perp}(\mu, \nu) \otimes S_{sc}^{\perp}(Qz_{\text{cut}}; \mu, \nu) , \tag{7.66}$$

and satisfies the following renormalization group equations

$$\frac{d}{d\ln\nu}S_{sc}^{\perp}(\mu, \nu) = \gamma_{\nu}^{sc}(\mu, \nu) \otimes S_{sc}^{\perp}(\mu, \nu) , \frac{d}{d\ln\mu}S_{sc}^{\perp}(\mu, \nu) = \gamma^{sc}(\mu, \nu)S_{sc}^{\perp}(\mu, \nu) , \tag{7.67}$$

where the Qz_{cut} dependence is suppressed to improve readability. In $\overline{\text{MS}}$ scheme the corresponding Fourier transform can be obtained using eq. (C.5)

$$\tilde{S}_{sc}^{\perp}(Qz_{\text{cut}}; \mu, \nu) = 1 + \frac{\alpha_s C_i}{\pi}\left\{ - 2\ln\left(\frac{\nu}{Qz_{\text{cut}}}\right)\ln\left(\frac{\mu_E}{\mu}\right)\right\} + \mathcal{O}(\alpha_s^2) , \tag{7.68}$$

$$\tilde{Z}_{sc}^{\perp}(\mu, \nu) = 1 + \frac{\alpha_s C_i}{\pi}\left\{ - \frac{2}{\eta}\left[\ln\left(\frac{\mu_E}{\mu}\right) - \frac{1}{2\epsilon}\right] + \frac{1}{\epsilon}\ln\left(\frac{\nu}{Qz_{\text{cut}}}\right)\right\} + \mathcal{O}(\alpha_s^2) , \tag{7.69}$$

and thus for the one-one-loop anomalous dimensions we get

$$\gamma_{\nu}^{sc}(\mu, \nu) = -2\frac{\alpha_s(\mu)C_i}{\pi}\ln\left(\frac{\mu_E}{\mu}\right) + \mathcal{O}(\alpha_s^2) \tag{7.70}$$

$$\gamma^{sc}(\mu, \nu) = 2\frac{\alpha_s(\mu)C_F}{\pi}\ln\left(\frac{\nu}{Qz_{\text{cut}}}\right) + \mathcal{O}(\alpha_s^2). \tag{7.71}$$

7.5 The connection between ζ-parameter and rapidity regulator

In the standard EFT approach one used the rapidity renormalization group (RRG) equations in order to resum large logarithms at the level of individual rapidity regulated terms [14, 49]. A more recent approach for performing the resummation of large logarithms in the TMD evolution, known as ζ-prescription, was introduced in ref. [16] and scketched in section 2. Here we rewrite the fixed order results using the rapidity regulator in the past sections in the form appropriate for implementing the ζ-prescription. In the framework of ref. [16] one works with the rapidity divergent free quantity,

$$S_{sc}^{sub}(b; \mu, \zeta) \equiv \sqrt{S_2^{\perp}(\boldsymbol{b}; \mu, \nu_s)} \, S_{sc}^{\perp}(\boldsymbol{b}, Qz_{\text{cut}}; \mu, \nu_{sc}) , \tag{7.72}$$

where we have explicitly show the dependence on the rapidity regulator parameters ν_s and ν_{sc}. In the RRG approach this combination does not acquire rapidity evolution thus here in order to establish the rapidity evolution we fix the rapidity scales at two different values. Particularly we evaluate the soft-collinear rapidity scale at its canonical value, $\nu_{sc} = Qz_{\text{cut}}$, and we allow for the corresponding soft scale to float through a parameter ζ: $\nu_s = \sqrt{\zeta}$. Note that this is not a unique choice of scales since any choice for which $\nu_s/\nu_{sc} = \sqrt{\zeta}/(Qz_{\text{cut}})$ will give the same result. With this choice

of scales we have,

$$S_{sc}^{sub}(b; \mu, \zeta) = 1 + \frac{\alpha_s(\mu)C_i}{2\pi} \left\{ 2\ln\left(\frac{\mu_E}{\mu}\right)\ln\left(\frac{\zeta}{\mu^2}\right) - 2\ln^2\left(\frac{\mu_E}{\mu}\right) - \frac{\pi^2}{12} \right\} + \mathcal{O}(\alpha_s^2) , \quad (7.73)$$

and according to the notation of eqs. (7.22, 7.23) satisfies the following equations

$$\mu^2 \frac{d}{d\mu^2} S_{sc}^{sub}(b; \mu, \zeta) = \frac{1}{2}\gamma^{sc/sub}(\mu, \zeta)S_{sc}^{sub}(b; \mu, \zeta) , \quad (7.74)$$

$$\zeta \frac{d}{d\zeta} S_{sc}^{sub}(b; \mu, \zeta) = -\mathcal{D}(\mu)S_{sc}^{sub}(b; \mu, \zeta) . \quad (7.75)$$

Its easy to show that the anomalous dimensions $\gamma^{sc/sub}$ and $\mathcal{D}$ are related to the RG and RRG anomalous dimensions of the global soft and soft-collinear function as follows,

$$\gamma^{sc/sub}(\mu, \zeta) = \frac{1}{2}\gamma^s + \gamma^{sc} = \Gamma^{\text{cusp}}[\alpha_s]\ln\left(\frac{\mu^2}{\zeta}\right) + \frac{1}{2}\Delta\gamma^s[\alpha_s] + \Delta\gamma^{sc}[\alpha_s] , \quad (7.76)$$

and

$$\mathcal{D}(\mu) = \Gamma^{\text{cusp}}[\alpha_s]\ln\left(\frac{\mu}{\mu_E}\right) - \frac{1}{4}\Delta\gamma_\nu^s[\alpha_s] , \quad (7.77)$$

where

$$\Delta\gamma_\nu^s = -\left(\frac{\alpha_s(\mu)}{4\pi}\right)^2 C_i \left[\left(\frac{128}{9} - 56\zeta_3\right)C_A + \frac{112}{9}\beta_0\right] + \mathcal{O}(\alpha_s^3). \quad (7.78)$$

It is easy to confirm by looking the above equations that the anomalous dimensions $\gamma^{sc/sub}$ and $\mathcal{D}$ satisfy the following differential equations,

$$\frac{d}{d\ln\zeta}\gamma^{sc/sub}(\mu, \zeta) = -\Gamma_{\text{cusp}} , \qquad \frac{d}{d\ln\mu}\mathcal{D}(\mu) = +\Gamma_{\text{cusp}} . \quad (7.79)$$

Also comparing against the notation of eq. (7.25) we see that the non-cusp part, $\Delta\gamma^{sc/sub}$, of the anomalous dimension $\gamma^{sc/sub}$ is a linear combination of the corresponding non-cusp pieces of the global soft and soft-collinear functions. Particularly:

$$\Delta\gamma^{sc/sub}(\mu) = \left(\frac{1}{2}\Delta\gamma^s[\alpha_s(\mu)] + \Delta\gamma^{sc}[\alpha_s(\mu)]\right) , \quad (7.80)$$

and this statement is true to all orders in perturbative expansion.

7.6   Numerical results

7.6.1   Numerical results for e^+e^-

In this section, we provide the results of our calculation for $e^+e^- \to 2$ jets computed up to NNLL accuracy. The implementation necessarily needs a choice for the rapidity scales and we have done it using the ζ-prescription as described in ref. [16] and adapting the code `artemide` to the present case. This consisted of performing the evolution of the transverse momentum dependent components within the `artemide` framework, while for all other scales not involved in the rapidity evolution, i.e., the hard and jet functions we applied the virtuality evolution presented in section 7.3.1.

There are some important modifications to the ζ-prescription framework for our case which affect the numerics. One of this is that now $\zeta_A\zeta_B \sim Q^4 z_{\text{cut}}^4$ compared to the di-hadron decorrelation case where $\zeta_A\zeta_B \sim Q^4$. This means that the effective hard scale to which the distributions are sensitive is lower. Because the TMD factorization is valid when q_T is much lower than the hard scale of the process, one needs that the product Qz_{cut} be sufficiently high. In our plots we have considered the case $q_T \lesssim Qz_{\text{cut}}$. Then the evolution of the jet-TMD given in eq. (7.25) is also slightly different from the standard hadron TMD, although the changes are implemented easily in the `artemide` code.
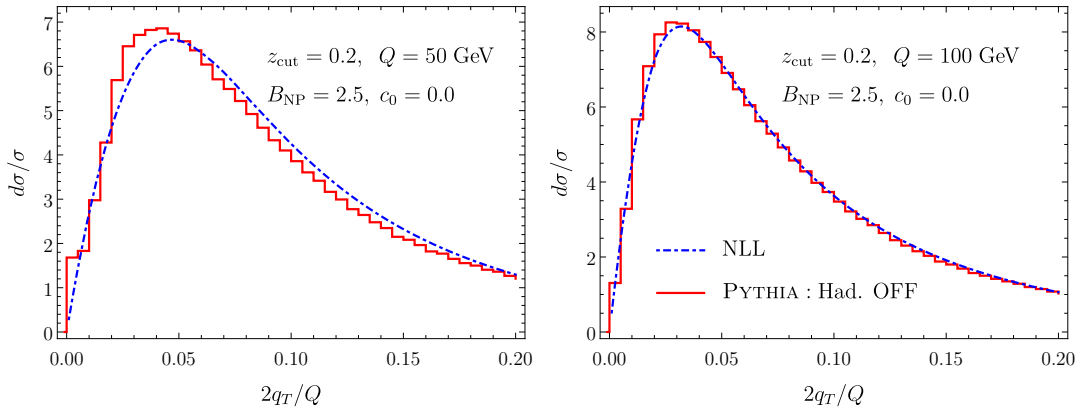

FIGURE 7.6: Comparison of the NLL result against the partonic shower of PYTHIA 8 for $R = 1$ and $e_{\text{cut}} = 0.01$ for two different center of mass energies, LEFT: 50 GeV, RIGHT: 100 GeV.

In fig. 7.6 we compare our analytic result for NLL cross section (normalized) against PYTHIA simulations for $Q = 50$ and 100 GeV. For the purposes of comparison we turn hadronization off in the simulation and we compare against our purely perturbative result. The perturbative calculation depends on the parameter B_{NP} which in practice implements a cutoff in the inverse Laplace transform such that the soft scale, that behaves as $1/b$, does not hit the Landau pole. As long as we choose this parameter such that convergence of the integral is reached before the cutoff, then the perturbative result is not much sensitive to the value of B_{NP}. Although, as we now discuss, the theoretical uncertainty of the cross section for these energies at NLL is quite large, we find very good agreement with the simulations for the canonical choice of scales.

In fig. 7.7 we give the NNLL results including a theoretical uncertainty band. We compare against the NLL cross section and although the error bands seem to be larger than what is typically expected we can clearly see that the result convergences and the theory error decreases by approximately factor of two. To estimate the theoretical uncertainty we first vary all the factorization scales of a factor 2 (0.5) around their canonical value, then we separately take the envelope of the variations involved in rapidity evolution, μ, μ_{sc}, and of the ones involved only in the virtuality evolution of the jet function, μ_{cs}, μ_J. The final error bands we show are the quadrature of the two contributions. The reason for this prescription is that rapidity and virtuality evolutions are in principle uncorrelated. The uncertainty is somewhat larger than what one might expect for a NNLL calculation, and is practically dominated by the variations in the jet function. This is attributed to the small values of the collinear-soft scale, $\mu_{cs} \sim Q\sqrt{e_{\text{cut}}z_{\text{cut}}}$, which approaches the non-perturbative regime even for values of $Q \sim m_Z$. One might attempt to reduce the uncertainty by
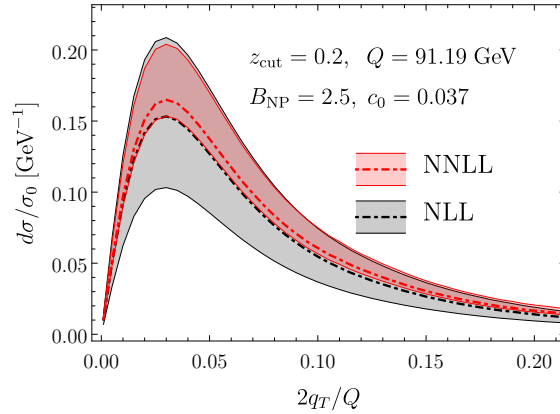
FIGURE 7.7: Transverse momentum de-correlation for $e^+e^- \to$ dijets with center of mass energy at the Z mass.

increasing either e_{cut} or z_{cut}, but caution is needed not to invalidate the corresponding hierarchy. We will see later that when only the mass of one jet is measured (e.g., in DIS or hadron-jet decorrelation) then the error band decreases significantly.

7.6.2   Numerical results for DIS

In this section we use the factorization theorem in eq. (7.18) to obtain numerical results for the TMD spectrum of groomed jets in DIS process. Our analysis is done for two center-of-mass energies, EIC: $\sqrt{s} = 100$ GeV and HERA: 318 GeV. For both energies we integrate over $y = Q^2/(xs)$ and $Q = \sqrt{-q^2}$ in the regions $0.01 < y < 0.95$ and $40 < Q < 50$ GeV. For the TMDPDFs we use the fits obtained from Drell-Yan data [140] with the use of ζ-prescription. In fig. 7.8 we show our results for NLL and NNLL accuracies for the two center of mass choices, including theoretical uncertainties. We estimate the theoretical scale variations as described in sec. 7.6.1. The groomed jet parameters that we choose are the same as in the di-lepton case: $\beta = 0$, $z_{\text{cut}} = 0.2$, and $e_{\text{cut}} = 0.01$. As before we find good convergence between the NLL and NNLL result. The absolute value of theoretical scale variation is improvable with higher logarithmic accuracy (NNLL-prime or perhaps N^3LL), which needs the explicit calculation of several jet hadronic matrix elements at two loops.
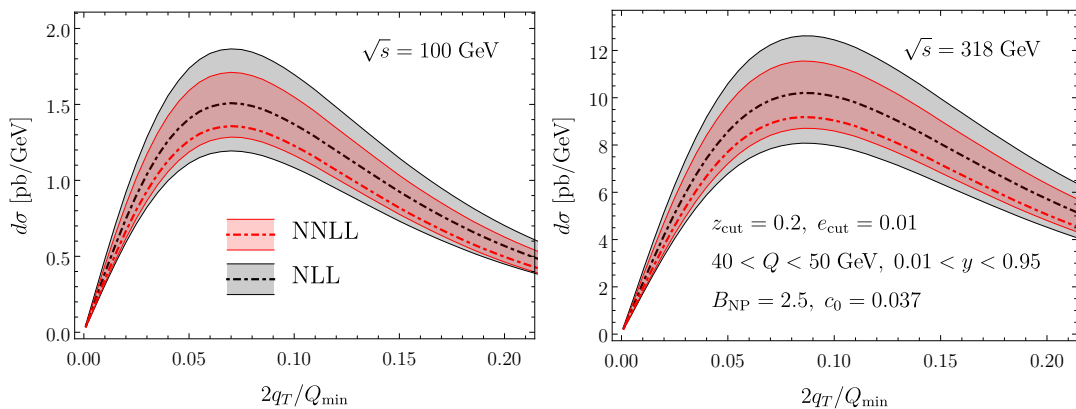

FIGURE 7.8: The NLL and NNLL TMD spectra for groomed jets in DIS for EIC (left: $\sqrt{100}$ GeV) and HERA (right: $\sqrt{s} = 318$ GeV) kinematics. The cross section are integrated in $y = Q^2/(xs)$ and $Q = \sqrt{-q^2}$ (see details in the main text).
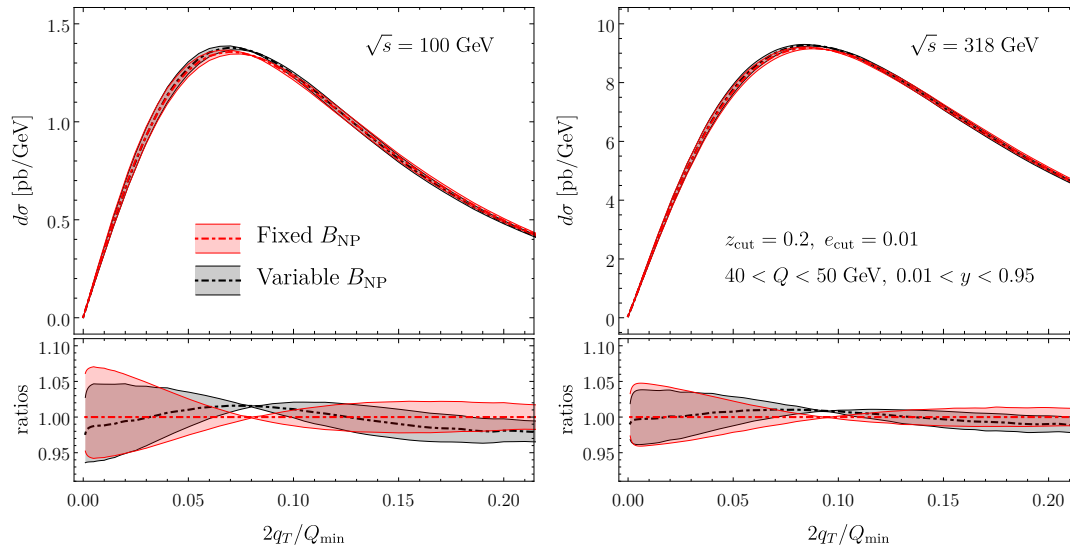
FIGURE 7.9: The NNLL cross-section including modeling of the initial hadronic state effects fitted from Derll-Yan processes using two different scenes: fixed and variable B_{NP}.

We further investigate the size of the uncertainty due to the hadronic initial state and the non-perturbative effects induced by TMD evolution. We do that by varying the model parameters as constrained by the phenomenological analysis in ref. [140] for our NNLL result. We consider both variable and fixed $B_{NP} = 2.5\ \text{GeV}^{-1}$ (for details on the difference of the two schemes see [140]). We find that the effects (for our kinematics) are particularly small, of the order of $\sim 5\%$, which is much smaller than the theoretical uncertainties. This suggests that we need a better control over the theoretical uncertainties in order to further constrain TMD distributions from groomed jets in DIS. As mentioned earlier the uncertainty can be mitigated with higher logarithmic accuracy or by choosing larger values of e_{cut}, still compatible with factorization. This, will require to treat the region III shown in fig. 7.3. For this reason it is interesting to investigate the range of values of e_{cut} for which the energetic wide angle radiation is avoided.

7.7 Hadronization effects

One of the goals of this thesis is to study the non-perturbative effects associated with TMD distributions, in this case the TMDPDF. Usually in any experiment, there are multiple sources of non-perturbative corrections associated with both the initial and final states. To have access to a specific source of corrections, its therefore necessary to separate out the pieces of interest from the uninteresting ones, which in this case constitute the final state hadronization corrections. To access the TMD then, we must already have a good extraction of the rest of the non-perturbative effects. This is the reason why we consider distinct experiments in this chapter. The idea, as we shall demonstrate, is that the final state hadronization corrections are exactly the same in the two experiments. The $e^+e^- \rightarrow 2$ jets case can be used to extract out all the final state hadronization corrections, which can then be used for DIS.

For the e^+e^- observable, the factorization takes the form in eq. (7.7). Then, we can study the non-perturbative corrections for each collinear object $\mathcal{J}_i^\perp$, which by symmetry, are the same for the two objects. If we now look at the factorization

for DIS, eq. (7.20), the key point to note is that $\mathcal{J}_j^\perp(e_{\rm cut}, Q, z_{\rm cut}, \boldsymbol{b}; \mu, \zeta_B)$ is the same object that appears in the the case of e^+e^-, while $F_{i\leftarrow h}$ is just the TMDPDF. Thus it now becomes possible to exclusively access the complete TMDPDF. We now wish to systematically list the sources of the non-perturbative corrections associated with each factorized function that appear in our cross section.

In order to use jets it is important to consider all the non-perturbative effects for the case of our observables and in particular the ones coming from the implementation of (groomed) jets. In fig. 7.1 we have shown that such corrections are expected to be particularly small and we provide here a discussion about their origin from a theory perspective. We have two measurements on the jet: the jet mass, which is ultimately integrated over some interval and acts as a normalization, and the transverse momentum ($p_\perp$) of the radiation that is groomed away. Since we are interested in the shape of the q_T spectrum, we will only consider the non-perturbative effects in cross sections sensitive to it. We are working in the region II of EFT and we are going to discuss how non-perturbative effect arise when we increase the value of q_T (that is, we discuss here the non-perturbative corrections in the small-b limit, where $b \equiv |\boldsymbol{b}|$). Our factorization theorem has four functions in the IR, the collinear, the global soft, the collinear-soft, the soft-collinear functions, see eqs. (7.9-7.10), and all of them can potentially contribute to non-perturbative power corrections. Even though the collinear and collinear-soft functions do not contribute to $\boldsymbol{q}_T$ perturbatively, they can still give a non-perturbative power correction to the $\boldsymbol{q}_T$ spectrum. There are also power corrections of similar magnitude in this region due to the factorization of the *sc* function from the *cs*, but they are perturbative in nature and can be handled by making a smooth transition to region III.

There are two types of non-perturbative corrections that we will consider here. We call *shift* non-perturbative effects the ones which are not altered by the pass and fail procedure of the grooming conditions. An example is the global soft function that is independent of the grooming procedure and it is common to other TMD analysis. We refer to this kind of correction as *shift* non-perturbative effects since, as we will see later, in the simplest case it generates a shift in the TMD spectrum. The second correction instead is related to the grooming procedure with *cs* and *sc* soft functions and the jet shape function. In this case non-perturbative effects are driven by the so called "non-perturbative particles" and it is obviously only possible when perturbative modes are on the boundary of passing and failing soft-drop. We refer to these contributions as *boundary* non-perturbative effects.

7.7.1 *Shift* non-perturbative correction

For the case of shift correction, we assume that the soft-drop condition remains unaltered by any non-perturbative emissions. Now consider the contribution to the shift correction by each function in turn.

The non-perturbative part of the global soft function defined in eq. (7.6) has been studied in the literature in several frameworks [65, 198–202]. Up to $\mathcal{O}(b^4)$ terms it can be written as

$$\langle 0|T[S_n S_{\bar{n}}^\dagger(\boldsymbol{b})]\bar{T}[S_{\bar{n}} S_n^\dagger(0)]|0\rangle = \tilde{S}(b) + b^2\, \bar{C}_i^{(s)}(b)\langle 0|O^i|0\rangle\,, \qquad (7.81)$$

where O^i is the complete set of local operators that have the same quantum numbers as the soft function. Summation over i is implied. Here $\tilde{S}$ is the perturbative calculable part of the soft function and it contains rapidity and UV divergences as well as the rest of other terms in the equation. We can pull this out as a common factor to

write

$$\langle 0|T[S_n S_{\bar{n}}^\dagger(\boldsymbol{b})]\bar{T}[S_{\bar{n}} S_n^\dagger(0)]|0\rangle = \tilde{S}(b)\left(1 + b^2 \, C_i^{(s)}(b)\langle 0|O^i|0\rangle\right). \qquad (7.82)$$

To maintain the UV scale invariance of the cross section, we need that the second term in the brackets be independent of UV divergences. However additional rapidity divergences may be present in the non-perturbative matrix element on the r.h.s. that cancel with the corresponding rapidity divergence arising in the non-perturbative power corrections to the collinear or soft-collinear functions. This is related to the origin of the non-perturbative correction to the rapidity anomalous dimension and it is usually included also in TMD analysis.

We can perform a similar analysis for the soft-collinear (*sc*) function. When an *sc* (perturbative) mode passes soft-drop, then it does not contribute to q_T since it becomes part of the groomed jet. But since it has a large + component, it drives the groomed jet mass outside the region of measurement and hence such events are dropped. Therefore, we only need to consider the case when the *sc* mode fails soft drop. In this case the non-perturbative emission contributes to the q_T measurement if it lies outside the groomed jet. Given the angular scaling of this mode, which is much larger than the collinear-soft (*cs*) and collinear modes that form the groomed jet, the phase space region available is effectively unconstrained (this is also the reason why we ignore any phase space constraints on the soft non-perturbative emissions). Hence the correction in this case will also be a simple shift type and is implemented in the same manner as in the case of the global soft function. As before, we can pull out a common perturbative factor (that includes the perturbative soft drop condition), and write

$$\tilde{S}_{sc}^\perp(b, z_{\text{cut}})|_{\text{hadr.}} = \tilde{S}_{sc}^\perp(b, Q z_{\text{cut}})\left(1 + b^2 C_i^{(sc)}(b, z_{\text{cut}}) \, \langle 0|O^i|0\rangle\right). \qquad (7.83)$$

Notice that now all the z_{cut} dependence of the power correction is included in the perturbative calculable coefficient $C^{(sc)}(b, z_{\text{cut}})$, which multiplies the same non-perturbative power correction present also in the global soft function case. The calculation of $C^{(s)}$, $C^{(sc)}$ is doable perturbatively, although this consideration goes beyond the present work.

We can then combine all shift corrections that have an unconstrained phase space for non-perturbative emissions together so that in b space we have a multiplicative correction to the perturbative cross section of the form

$$SS_{sc}^\perp|_{\text{hadr.}} = (1 + b^2(\Omega_s + \Omega_{sc}))SS_{sc}^\perp|_{\text{pert.}}, \qquad (7.84)$$

where Ω_s is the same as the TMD case and Ω_s is a single parameter to be fitted from $e^+ e^-$ experiments. It is clear that, in the event of non-trivial $C^{\{(s),(sc)\}}$, $\Omega_{s,sc}$ can have a mild (logarithmic) dependence on q_T so that this model will work well over a limited range of q_T which may be sufficient for most cases.

We now consider the shift corrections coming from the collinear-soft and the collinear functions. Since these modes determine the region of the groomed jet, we can consider two possible scenarios which give a non-trivial power correction.

1. Collinear-soft (*cs*) particles pass soft-drop:
   If the *cs* particles pass the soft-drop then any non-perturbative emission scaling as the *cs* mode can contribute to q_T when it lies outside the groomed jet. In this case, we need to calculate the catchment area of the groomed jet that is determined by the angular distance of the *cs* subject that passed soft-drop.

As was pointed out in [188], it is possible at NLL, using a coherent branching formalism, to factorize a purely non-perturbative function from all the calculable perturbative effects (including grooming). A detailed analysis of these corrections will be presented in a future work.
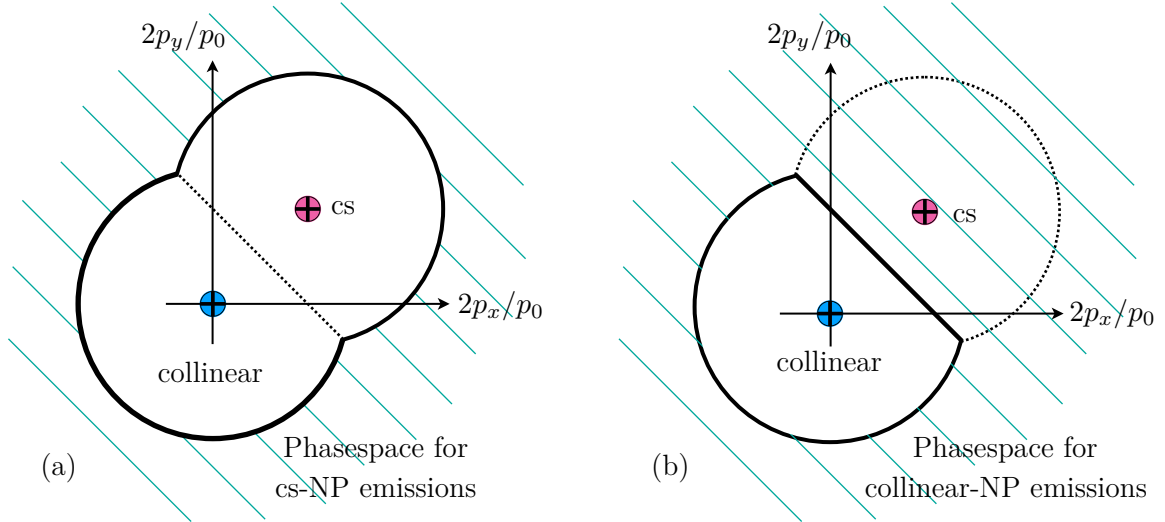

FIGURE 7.10: (a) When the collinear-soft (*cs*) function passes soft drop, the non-perturbative (NP) emissions, with the angular scaling of the *cs* mode , with a virtuality Λ_{QCD} must fall in the phase space shown by the blue shaded area in order to contribute to q_T. (b) When the *cs* function fails soft drop, the NP emission with the angular scaling of the collinear modes must not be clustered with the collinear sub-jet in order to contribute to q_T.

2. Collinear-soft particles fail soft-drop:
   In this case collinear modes are the only ones that pass soft-drop, so that any non-perturbative mode scaling as *cs* has an unconstrained phase space, by the same logic as for the soft and the *sc* functions, so that we get a simple shift correction of the same form as the soft, *sc* and TMD collinear functions.[1] There is another possible interesting correction that will come from the collinear NP emission that lies outside the catchment region that is now determined by the collinear modes alone.

   In this case there are two ways of approaching the problem. In one, we consider separating out the non-perturbative corrections before factorizing the *cs* and collinear modes. The other way is to realize that in the case where *cs* fails soft-drop, the entire groomed jet mass measurement comes from the jet function alone and using this condition we can define a catchment area for the collinear non-perturbative emissions *without explicitly accessing any information from the cs function*, so that the factorization between the collinear and *cs* modes is maintained. In this case, we can do a diagrammatic analysis, similar to [188], for the collinear function, to check if it is possible to factorize the non-perturbative effects from the perturbative. We leave this work for the future.

---

[1]Technically in this case the perturbative value of $p_{\perp cs}$ would give a larger correction. However, this correction can eventually be handled by transitioning to a new EFT in which the *sc* and *cs* functions merge together. For now we will ignore them and only keep track of the other non-perturbative corrections.

7.7.2 Boundary corrections

We now consider boundary corrections that leave the q_T measurement function unchanged but only require an expansion of the soft-drop condition in q^-/Q. The functions that do not explicitly have a soft-drop condition can then be ignored, which leaves us with only the *sc* and *cs* functions. We can follow the same line of reasoning as in [188].
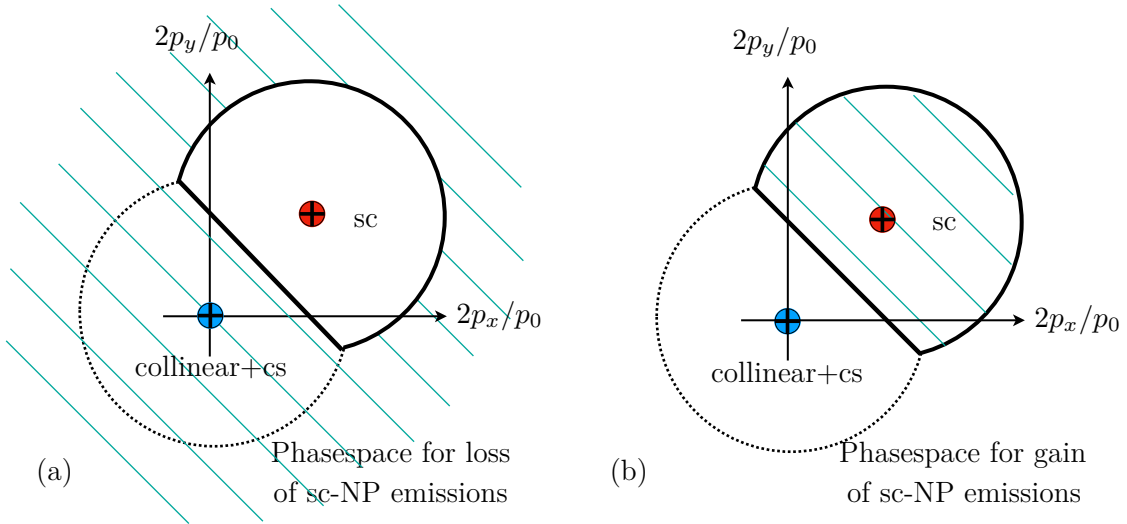

FIGURE 7.11: (a) The case where the sc subjet loses an NP emission
(b) The case when the sc subjet gains an NP emission

1. *sc* emissions

   In this case we demand that either an addition or removal of the non-perturbative emission cause the soft-collinear function to fail soft-drop. Otherwise it will drive up the jet mass outside the measured range. If we consider a non-perturbative emission q^μ along with a perturbative momentum p^μ, then we can expand out the soft-drop condition in the non-perturbative momentum. We can write the complete measurement function as

$$\Theta^{p\pm q} = \Theta\left(\frac{p+q}{E_J} - z_{\text{cut}}\right)\delta^2(\boldsymbol{p}_{\perp sc} - \boldsymbol{p}_\perp \mp \boldsymbol{q}_T)\,, \qquad (7.85)$$

   where p is the momentum of the perturbative *sc* sub-jet while q^μ is the momentum of the non-perturbative emission. The $\pm$ signs indicate whether the perturbative *cs* subjet gains or loses a non-perturbative momentum after hadronization. In the case where the *sc* sub-jet gains a non-perturbative emission, the measurement expanded to leading order looks like

$$\Theta^{p+q} \approx \Theta^p_{sd}\delta^2(\boldsymbol{p}_{\perp sc} - \boldsymbol{p}_\perp) + \frac{q^-}{E_J}\Theta^{\text{b.c.}}(\theta_q, \theta_p, \Delta\phi)\delta^p_{sd}\left[\delta^2(\boldsymbol{p}_{\perp sc} - \boldsymbol{p}_\perp)\right]\,, \quad (7.86)$$

   with

$$\Theta^p_{sd} \equiv \Theta\left(\frac{p}{E_J} - z_{\text{cut}}\right)\,, \qquad\qquad \delta^p_{sd} \equiv \delta\left(\frac{p}{E_J} - z_{\text{cut}}\right)\,. \qquad (7.87)$$

In this case, the non-perturbative emission q^μ gets clustered with the *sc* subject. Note that we have expanded q_i from the $p_\perp$ measurement since we are working at leading order. The phase-space constraint, $\Theta^{\text{b.c.}}$, gives the condition that ensures q^μ gets clustered with the *sc* part.

The second case is when q^μ is emitted off p^μ but it is not clustered with the *sc* jet. The short distance condition now acts on $p - q$, which can then be expanded out to give

$$\Theta^{p-q} \approx \Theta^p_{sd}\delta^2(\boldsymbol{p}_{\perp sc} - \boldsymbol{p}_\perp) - \frac{q^-}{E_J}\bar{\Theta}^{\text{b.c.}}(\theta_q, \theta_p, \Delta\phi)\delta^p_{sd}\left[\delta^2(\boldsymbol{p}_{\perp sc} - \boldsymbol{p}_\perp)\right] , \quad (7.88)$$

$\bar{\Theta}^{\text{b.c.}}$ is the phase space region for q so that it falls outside the sc subjet. We can see that the leading power correction scales as q^-/E_J, which, given the angular scaling of the *sc* mode, scales as $q_T z_{cut}/Q$. Given a typical value of $z_{cut} \sim 0.1$, this factor is then comparable to the q_T^2/Q^2 correction that we get from the shift terms.

2. Soft -Collinear function
   We expect that since perturbatively this function does not contribute to q_T, the boundary correction should have no effect on the q_T measurement.

We now have listed out all the possible NP corrections to the transverse momentum measurement.

Chapter 8

Conclusions

"We are all apprentices in a craft where no one ever becomes a master."

Ernest Hemingway

In this thesis we investigated how the extraction of transverse momentum distributions from experiments can be improved and how these methods can be applied to future experiments as the Electron-Ion Collider (EIC).

Part I of this thesis was devoted to study transverse momentum distributions (TMDs) with different polarizations and their matching over their corresponding integrated PDFs in perturbation theory. These TMDs are crucial objects to study processes with polarized hadrons that will be relevant in future experiments as EIC [203] or LHCSpin [204]. Increasing the perturbative order of the matching coefficients of the polarized TMD distributions at least up to the same order that their unpolarized counterparts is important in order to decrease the theoretical errors and improve the extraction of nonperturbative information from the experiments. A fundamental tool to understand theoretically cross sections with hadronic components are the *factorization theorems* derived using the tools provided by Soft-Collinear Effective Theory (SCET) discussed in chapter 1 that allow to obtain a proper definition of the TMD distributions as we summarized in chapter 2.

Chapter 3 completed the definition of the TMD given in chapter 2 introducing the dependence on the polarization. Also, the renormalization of the TMD operator was discussed in details, reinforcing the idea that it is independent on the polarization of the operator. A complete discussion on the matching of TMD distributions to the twist-2 integrated distributions in the regime of small-b (or equivalently, large-q_T) was provided. To perform the matching we have evaluated the operator product expansion (OPE) of a generic TMD operator near the light-cone.

The evaluation of OPE for a generic TMD operator revealed the condition which should be satisfied in order match the rapidity divergences of a TMD operator and the leading order TMD soft factor. The conditions presented in eqs. (3.21, 3.23) restrict the Dirac and Lorentz structure of the TMD operators. The TMD distributions whose operators meet these conditions, are known as TMD distributions of leading dynamical twist (twist-2). In this way, we demonstrated that the next-to-leading-dynamical-twist contributions to the TMD factorization theorem (i.e., the power suppressed contributions to the TMD cross-section) with different Dirac or Lorentz structures necessarily have a different structure of rapidity divergences.

In chapter 4 the matching coefficients of the twist-2 parton distributions were evaluated and they constitute the first original results of this thesis. The TMD distributions that have non-zero matching are helicity (g_{1L}, g_{1L}^g), transvesity (h_1), pretzelosity ($h_{1T}^\perp$) and linearly polarized gluon ($h_1^{\perp g}$) distributions (we do not take the unpolarized TMD distribution into consideration because it has been considered in many articles. The evaluation was performed using the same regularization as the one used here can be found in [18]). Most part of the coefficient functions at NLO were evaluated separately for quarks and gluons by different groups [77, 83]. We agreed with their evaluations (taking into account that in ref. [83], a different renormalization scheme was used). In addition, we provided new results for transversely polarized distributions and linearly polarized gluons up to NNLO.

First of all, the matching of the helicity distribution up to NLO was discussed. We provided a discussion on the schemes of γ_5 and ϵ_T-definition in dimensional regularization, which had been neglected by previous authors and it is important in order to perform a systematic study of helicity distribution. We have shown that the definition of γ_5 suggested by the popular Larin scheme [91] was not compatible with the condition of the leading dynamical twist, and thus, it is inapplicable in TMD calculations. We suggested an updated version of Larin scheme (Larin$^+$ scheme eq. (4.19)), which supports the condition and has simpler properties than the traditional one. Our calculation has been performed in Larin$^+$ and HVBM [89, 90] schemes. At NLO the difference between schemes arised only in the ϵ-suppressed terms. We discussed about the normalization of the distributions and derive the finite renormalization constant (4.26) for TMD helicity distributions in both schemes. The evaluation of the matching has been performed at finite ϵ. The ϵ-suppressed terms, although do not contribute directly to NLO, contribute to higher perturbative orders (see e.g. discussion in [18]).

We studied the twist-2 matching of transversity and pretzelosity (or quadrupole) TMD distributions. We derived the matching coefficients for these distributions at next-to-next-to-leading order (NNLO) in the strong coupling. We checked that the renormalization of rapidity divergences worked exactly in the same way as for unpolarized distributions, as it was predicted by the transverse momentum dependent factorization theorem. The present calculation had a structure similar to the one of the NNLO matching of unpolarized TMDs made in [18].

In the case of transversity, we considered both the TMDPDF and the TMDFF cases. We found several analogies and identities between the matching coefficients of transversity and unpolarized distributions, that can serve as a cross-check of both results. The matching coefficients for transversity (see eqs. (4.39, 4.40, 4.41) and eqs. (4.58, 4.59, 4.60)) can be readily used in phenomenological applications. A recent review of the phenomenology of transversity in fragmentation can be found in [107]. Our result is the first calculation of the NNLO matching for transversely polarized TMD operator. To our knowledge the NLO matching coefficient for transversity TMDFF (eq. 4.57)) is also given in this thesis for the first time. We stress that this is also the first NNLO evaluation of the matching for a polarized TMD distribution. Therefore, given the result of this work, the transversity TMD distribution is known to the same perturbative order as unpolarized distributions. This fact is important to establish phenomenologically the universality of TMD evolution.

The pretzelosity distribution has ϵ-suppressed matching coefficients up to NNLO. This offers a natural explanation of the smallness of this distribution in phenomenological analyses [108]. We have found that the expected two-loop matching coefficient is actually zero, despite the fact that the matrix element over free quark for

pretzelosity distribution is non-zero. This is an unexpected result, since the analogous quadrupole distribution in the gluon sector (namely linearly polarized TMD gluon distribution) has a non-zero matching already at one-loop level. We have also checked that the LO of the large-N_f expansion (given by diagrams with an arbitrary number of fermion bubble insertions, for details see [66]) also vanishes. Although these facts do not demonstrate completely that the twist-2 part of pretzelosity is zero at all orders in perturbation theory, certainly they are an evidence for this statement. We conjecture that the pretzelosity distribution does not match the twist-2 distribution. Recently, this conjecture has been proved in ref. [114] and its non-zero matching at twist-3 has been demonstrated. We performed the calculation of pretzelosity only for the case of TMDPDF, but, we expect the same result for the TMDFF.

We closed this chapter showing the NNLO matching of the linearly polarized gluon transverse momentum dependent parton distribution function (lpTMDPDF) over the unpolarized PDF. Thanks to this calculation, lpTMDPDF can be considered at the same level of theoretical accuracy as the unpolarized gluon TMDPDF [18, 81]. This distribution typically accompanies unpolarized gluon TMDPDF within a TMD factorized cross-section and an interesting example is the factorization formula for the Higgs-production cross-section, where these distributions enter in a plain sum. For this reason, both distributions should be considered at the same order of perturbative accuracy. In chapter 5 we apply the perturbative result obtained to study the influence of the lpTMDPDF over the Higgs production cross section. The module for the numerical evaluation of lpTMDPDF is added to the `artemide` package that can be downloaded from [117].

The impact of NNLO correction for lpTMDPDF is very significant and practically doubles the value of the function for moderate **b**. This fact should not be considered very surprising given that LO term (a_s^0-term) for lpTMDPDF vanishes. The relevance of this effect in the Higgs cross section has been discussed in sec. 5.1 and it is summarized in figs. 5.2-5.4. Unfortunately, at the moment we have not a reliable model for the non-perturbative part of the gluon TMD distribution, and in this chapter, we have adapted values for distributions extracted in refs. [66, 140]. A more detailed study on the non-perturbative part of the gluon TMDPDF is certainly warranted in the future (for work done in this sense see [205]).

In several papers, it has been suggested that unpolarized and linearly polarized gluon TMDPDFs can be measured in association with heavy-quark production [133–139]. We leave an analysis of these processes for future work because at the moment we miss a full factorization theorem for these cases. Nevertheless, the consistency of data with the factorization hypothesis can always be checked with the result provided in this work.

Part II of this thesis studied different methods to extract information about transverse momentum distributions. Instead of increasing the perturbative accuracy of the matching coefficients for TMD distributions in this part we studied new ways to access the hadronic information through processes involving jets. A clear advantage is that the jet momentum can be calculated in perturbation theory to a large extent, while the fragmentation of hadrons is an intrinsically nonperturbative process.

In chapter 6 we provide an initial formulation of this idea, using a modern definition of jets. There we observed, for the first time, that the cross section for dijet production in e^+e^- collisions and SIDIS with a jet in the final state can have the same factorization as for hadronic TMD measurements, simply replacing a TMD fragmentation function by our TMD jet function. This factorization depends on the jet radius R and recombination scheme, holding only for all values of R if the Winner-Take-All axis is used. In particular, in the regime of small q_T, which is interesting for

extracting the intrinsic transverse momentum of partons in the proton, the cross section for the standard jet axis does not satisfy the usual TMD factorization. To explore the ramifications of these ideas, we presented numerical results for Belle II and LEP (e^+e^- collisions), and HERA and the EIC (SIDIS), building on the existing `artemide` code. We reported the details of the NLO calculations of the TMD jet function, and have also numerically evaluated the NNLO contribution in the large-radius limit with `Event2`. This was motivated by the observation that the NLO result is well described using the large-R jet function, for all experimental cases we consider. Consequently we achieved the same N3LL accuracy as in the corresponding hadronic TMD cases. We verified the perturbative convergence of our numerical predictions, achieving perturbative uncertainties of order 5% in the peak of the distribution at N^3LL. We also found that our cross sections have similar sensitivity to nonperturbative effects as the corresponding hadronic case, without the burden of additional nonperturbative effects from fragmentation. Specifically, we investigated how the cross section changes when varying the nonperturbative parameters within the errors provided in [140], concluding that in principle these experiments can provide important constraints on these parameters. Here we benefit from using the ζ-prescription, which ensures that the nonperturbative parts of the evolution kernel and the rest of the TMD are uncorrelated. The nonperturbative effects to the jet TMD have not been estimated in this chapter. However our factorization theorems ensure that these effects can be included in the definition of the jet functions and are therefore universal, i.e., the same in e^+e^- collisions and SIDIS. In this respect, the hadronization of jets can be treated in the same way as the nonperturbative part of a hadron TMD, and is therefore expected to be subdominant compared to the nonperturbative part of the evolution. Consequently, jet measurements may provide one of the best ways to constrain the nonperturbative part of the evolution kernel.

In chapter 7, we presented the computation of the transverse momentum decorrelation observable for fat jets groomed using the Soft-Drop algorithm. We considered two scattering experiments: $e^+e^- \to$ di-jets and semi-inclusive DIS. In the former, we measured the transverse momentum imbalance between the two groomed jets. We imposed a jet mass constraint on our jets in order to ensure collimated jet configurations. Simulation using PYTHIA showed that grooming greatly reduces the impact of underlying events as well as final state hadronization. We showed that the factorization theorem for this observable involves the universal soft function which also appears in the traditional definition of TMDs. We proposed that this observable can be used as a probe of the non-perturbative rapidity anomalous dimension, which is a universal parameter for TMD distributions. We proved within our EFT that the cumulant jet mass constraints only add to the overall normalization of the perturbative cross section and hence do not impact the shape of the transverse momentum distribution although it does contribute to the uncertainty. We collected or computed all the ingredients necessary to evaluate the cross section to NNLL accuracy and a numerical study for the cases of interest. In the implementation we used the `artemide` code [66, 117, 140] which contains the most recent extraction TMDPDF at higher perturbative orders. As part of the numerical analysis we used the ζ-prescription [16] which allows a complete disentanglement of non-perturbative effects of rapidity evolution from the rest. An uncertainty analysis gave us an error band of approximately $\pm$ 10 %. The main ingredient of this error is the perturbative uncertainty which can be systematically improved. As shown in fig. 7.1 the hadronization corrections at low q_T are significantly smaller than the case of a standard jet axis and it is therefore one of the major advantage of using grooming. These effects are expected to be the same in e^+e^- and SIDIS because of

the factorization of the cross section. In the case of e^+e^- these corrections constitute all of non-perturbative effects and they are associated with the final state shower. In order to do a meaningful extraction of non-perturbative parameters in this case, it is therefore necessary to improve the uncertainty from perturbative physics to be better than 5%. This can be achieved by moving to a higher order in resummation accuracy (N^3LL).

In the SIDIS case we measured the transverse momentum imbalance between the groomed jet and the recoiling lepton. Once again we demanded a jet mass measurement in order to ensure sensitivity to collinear physics only. A large part of the contribution to this comes from the soft and collinear radiation that lies outside the jet and, for low transverse momentum, probes the complete TMDPDF. The cross section was again presented to NNLL accuracy and involves much of the same ingredients as in the case of $e^+e^- \rightarrow$ dijets. A higher order perturbative calculation is expected to reduce significantly errors also in this case.

Concerning the hadronization effects we observed that grooming the jet allows us to have a wide angle jet, which is preferred in low energy experiments, while still being free from non-global logarithms, which are non-factorizable and they are usually present in un-groomed jets. Nevertheless it is possible to measure directly the hadronization effects due to grooming. The idea is to parametrize and extract all of the non-perturbative effects from $e^+e^- \rightarrow$ dijets and use them in SIDIS since they contain all the same matrix elements (in addition to the TMDPDF) as explained in section 7.7. This gives us a robust way to access the TMDPDF while maintaining control over all other non-perturbative effects.

Appendix A

Perturbative ingredients

In this appendix we present the perturbative results for quantities needed along this thesis but which are not calculated for first time in the context of the original work made in this thesis. These are: anomalous dimensions for the TMD/jet operators, hard functions of the considered processes to make phenomenological predictions, soft function and renormalization constants for TMD distributions.

A.1 Anomalous dimensions

We list the anomalous dimensions that enter the double-scale evolution described in eqs. (2.55, 2.56). The phenomenological predictions obtained along this thesis use N^3LL resummation by default, corresponding to the first row in table A.1. An exception is fig. 6.5, where we compare different orders to test the convergence of resummed perturbation theory.

- The QCD β-function, $\beta(\alpha_s) = d\alpha_s/d\ln\mu$, with $\beta = -2\alpha_s \sum_{n=1}^{\infty} \beta^{(n)} \left(\frac{\alpha_s}{4\pi}\right)^n$

$$\beta^{(1)} = \frac{11}{3}C_A - \frac{4}{3}T_r N_f \equiv b_0,$$

$$\beta^{(2)} = \frac{34}{3}C_A^2 - \frac{20}{3}C_A T_r N_f - 4C_F T_r N_f,$$

$$\beta^{(3)} = \frac{2857}{54}C_A^3 + \left(2C_F^2 - \frac{205}{9}C_F C_A - \frac{1415}{27}C_A^2\right) T_r N_f$$

$$+ \left(\frac{44}{9}C_F + \frac{158}{27}C_A\right) T_r^2 N_f^2,$$

$$\beta^{(4)} = \frac{149753}{6} + 3564\zeta_3 - \left(\frac{1078361}{162} + \frac{6508}{27}\zeta_3\right) N_f + \left(\frac{50065}{162} + \frac{6472}{81}\zeta_3\right) N_f^2$$

Order	F.O.	Γ_{cusp}	γ_V	$\mathcal{D}$
N^3LL	a_s^2	a_s^4	a_s^3	a_s^3
NNLL	a_s^1	a_s^3	a_s^2	a_s^2
NLL	a_s^0	a_s^2	a_s^1	a_s^1

TABLE A.1: Various orders in resummed perturbation theory, and the fixed-order (F.O.) and resummation ingredients they involve. The fixed-order ingredients are the perturbative expansion of the hard function, jet function and the coefficients in the matching of the TMD PDFs onto collinear PDFs. We also use the PDFs extracted at this order as well, and use the corresponding running of the coupling.

$$+ \frac{1093}{729} N_f^3 . \tag{A.1}$$

- The cusp anomalous dimension $\Gamma_{cusp}^q = 4C_F\Gamma$, $\quad \Gamma_{cusp}^g = 4C_A\Gamma$, $\quad \Gamma = \sum_{n=1}^{\infty} a_s^n \Gamma^{(n)}$

$$\Gamma^{(1)} = 1, \qquad \Gamma^{(2)} = \left(\frac{67}{9} - \frac{\pi^2}{3}\right) C_A - \frac{20}{9} T_r N_f,$$

$$\Gamma^{(3)} = C_A^2 \left(\frac{245}{6} - \frac{134\pi^2}{27} + \frac{11\pi^4}{45} + \frac{22}{3}\zeta_3\right) + C_A T_r N_f \left(-\frac{418}{27} + \frac{40\pi^2}{27} - \frac{56}{3}\zeta_3\right)$$

$$+ C_F T_r N_f \left(-\frac{55}{3} + 16\zeta_3\right) - \frac{16}{27} T_r^2 N_f^2 . \tag{A.2}$$

- The anomalous dimension $\gamma_V = \sum_{n=1}^{\infty} a_s^n \gamma_V^{(n)}$ for quarks and gluons,

$$\gamma_V^{q(1)} = -6C_F,$$

$$\gamma_V^{q(2)} = C_F^2 \left(-3 + 4\pi^2 - 48\zeta_3\right) + C_F C_A \left(-\frac{961}{27} - \frac{11\pi^2}{3} + 52\zeta_3\right)$$

$$+ C_F T_r N_f \left(\frac{260}{27} + \frac{4\pi^2}{3}\right),$$

$$\gamma_V^{q(3)} = C_F^3 \left(-29 - 6\pi^2 - \frac{16\pi^4}{5} - 136\zeta_3 + \frac{32\pi^2}{3}\zeta_3 + 480\zeta_5\right)$$

$$+ C_F^2 C_A \left(-\frac{151}{2} + \frac{410\pi^2}{9} + \frac{494\pi^4}{135} - \frac{1688}{3}\zeta_3 - \frac{16\pi^2}{3}\zeta_3 - 240\zeta_5\right)$$

$$+ C_F C_A^2 \left(-\frac{139345}{1458} - \frac{7163\pi^2}{243} - \frac{83\pi^4}{45} + \frac{7052}{9}\zeta_3 - \frac{88\pi^2}{9}\zeta_3 - 272\zeta_5\right)$$

$$+ C_F^2 T_r N_f \left(\frac{5906}{27} - \frac{52\pi^2}{9} - \frac{56\pi^4}{27} + \frac{1024}{9}\zeta_3\right)$$

$$+ C_F C_A T_r N_f \left(-\frac{34636}{729} + \frac{5188\pi^2}{243} + \frac{44\pi^4}{45} - \frac{3856}{27}\zeta_3\right) \tag{A.3}$$

$$+ C_F T_r^2 N_f^2 \left(\frac{19336}{729} - \frac{80\pi^2}{27} - \frac{64}{27}\zeta_3\right),$$

$$\gamma_V^{g(1)} = -\frac{22}{3}C_A + \frac{8}{3}T_r N_f,$$

$$\gamma_V^{g(2)} = C_A^2 \left(-\frac{1384}{27} + \frac{11\pi^2}{9} + 4\zeta_3\right) + C_A T_r N_f \left(\frac{512}{27} - \frac{4\pi^2}{9}\right) + 8C_F T_r N_f.$$

$$\gamma_V^{g(3)} = 2C_A^3 \left(\frac{-97186}{729} + \frac{6109}{486}\pi^2 - \frac{319}{270}\pi^4 + \frac{122}{3}\zeta_3 - \frac{20}{9}\pi^2\zeta_3 - 16\zeta_5\right)$$

$$+ 2C_A^2 T_r N_f \left(\frac{30715}{729} - \frac{1198}{243}\pi^2 + \frac{82}{135}\pi^4 + \frac{712}{27}\zeta_3\right)$$

$$+ 2C_A C_F T_r N_f \left(\frac{2434}{27} - \frac{2}{3}\pi^2 - \frac{8}{45}\pi^4 - \frac{304}{9}\zeta_3\right) - 4C_F^2 T_r N_f$$

$$+ 2C_A T_r^2 N_f^2 \left(-\frac{538}{729} + \frac{40}{81}\pi^2 - \frac{224}{27}\zeta_3\right) - \frac{88}{9} C_F T_r^2 N_f^2 \tag{A.4}$$

- It is convenient to write the expression for the function $\mathcal{D}$ as an expansion:

$$\mathcal{D}^f(\mu, \boldsymbol{b}_T) \;=\; C^f \sum_{n=1}^{\infty} a_s^n \sum_{k=0}^{n} \mathbf{L}_\mu^k d^{(n,k)}, \tag{A.5}$$

where $C^f = C_F$ for quarks and $C^f = C_A$ for gluons, and

$$
\begin{aligned}
d^{(1,1)} &= 2\Gamma^{(1)}, \qquad d^{(1,0)} = 0, \\
d^{(2,2)} &= \Gamma^{(1)}\beta^{(1)}, \qquad d^{(2,1)} = 2\Gamma^{(2)}, \\
d^{(2,0)} &= C_A\left(\frac{404}{27} - 14\zeta_3\right) - \frac{112}{27}T_r N_f. \\
d^{(3,3)} &= \frac{2}{3}\Gamma^{(1)}(\beta^{(1)})^2, \qquad d^{(3,2)} = 2\Gamma^{(2)}\beta^{(1)} + \Gamma^{(1)}\beta^{(2)}, \\
d^{(3,1)} &= 2\beta^{(1)}d^{(2,0)} + 2\Gamma^{(3)}, \\
d^{(3,0)} &= \frac{-1}{2}C_A^2\left(-\frac{176}{3}\zeta_3\zeta_2 + \frac{6392\zeta_2}{81} + \frac{12328\zeta_3}{27} + \frac{154\zeta_4}{3} - 192\zeta_5 - \frac{297029}{729}\right) \\
&\quad - C_A T_r N_f\left(-\frac{824\zeta_2}{81} - \frac{904\zeta_3}{27} + \frac{20\zeta_4}{3} + \frac{62626}{729}\right) \\
&\quad - 2T_r^2 N_f^2\left(-\frac{32\zeta_3}{9} - \frac{1856}{729}\right) - C_F T_r N_f\left(\frac{-304\zeta_3}{9} - 16\zeta_4 + \frac{1711}{27}\right).
\end{aligned}
$$

The result for $d^{(3,0)}$ has been recently computed in [63]. The rest of $d^{(3,i)}$ can be found also in [181].

A.2 Hard functions and tree-level cross sections

The hard function for Drell-Yan production/electron-positron annihilation up to two-loop accuracy is [61, 206, 207]

$$
\begin{aligned}
H_{DY/e^+e^-}(s,\mu) &= 1 + 2a_s C_F\left(-\mathbf{l}_s^2 - 3\mathbf{l}_s^2 - 8 + \frac{7\pi^2}{6}\right) + 2a_s^2 C_F\bigg\{ C_F\bigg[\mathbf{l}_s^4 + 6\mathbf{l}_s^3 \\
&\quad + \left(25 - \frac{7\pi^2}{3}\right)\mathbf{l}_s^2 + \left(\frac{93}{2} - 5\pi^2 - 24\zeta_3\right)\mathbf{l}_s + \frac{511}{8} - \frac{83\pi^2}{6} - 30\zeta_3 + \frac{67\pi^4}{60}\bigg] \\
&\quad + C_A\bigg[-\frac{11}{9}\mathbf{l}_s^3 + \left(-\frac{233}{18} + \frac{\pi^2}{3}\right)\mathbf{l}_s^2 + \left(-\frac{2545}{54} + \frac{22\pi^2}{9} + 26\zeta_3\right)\mathbf{l}_s \\
&\quad - \frac{51157}{648} + \frac{1061\pi^2}{108} + \frac{313}{9}\zeta_3 - \frac{4\pi^4}{45}\bigg] \\
&\quad + n_f T_F\bigg[\frac{4}{9}\mathbf{l}_s^3 + \frac{38}{9}\mathbf{l}_s^2 + \left(\frac{418}{27} - \frac{8\pi^2}{9}\right)\mathbf{l}_s + \frac{4085}{162} - \frac{91\pi^2}{27} + \frac{4}{9}\zeta_3\bigg]\bigg\} \\
&\quad + \mathcal{O}(a_s^3), \tag{A.6}
\end{aligned}
$$

where $\mathbf{l}_s = \ln\left(s/\mu^2\right)$ and s stands for the center of mass energy of hadrons (Drell-Yan) or leptons (electron-positron anmihilation).

DIS-like processes are related to Drell-Yan production/electron-positron annihilation at the level of the amplitude by $s \to -Q^2$ (where Q^2 is the virtuality of the transferred photon). For the hard function this leads to

$$H_{\text{DIS}}(Q^2,\mu) \;=\; H_{DY/e^+e^-}(Q^2,\mu) - 2a_s \pi^2 C_F$$

$$+ 2a_s^2 \pi^2 C_F \left[C_F \left(2l_{Q^2}^2 + 6l_{Q^2} + 16 - \frac{4}{3}\pi^2 \right) \right.$$

$$+ C_A \left(-\frac{11}{3}l_{Q^2} - \frac{233}{18} + \frac{\pi^2}{3} \right)$$

$$\left. + N_f T_F \left(\frac{4}{3}l_{Q^2} + \frac{38}{9} \right) \right] + \mathcal{O}(a_s^3). \tag{A.7}$$

The respective tree-level cross sections are given by

$$\sigma_0^{e^+e^-}(s) = \sum_q \frac{4\pi\alpha^2 N_c}{3s} \bar{e}_q^2(s), \tag{A.8}$$

$$\sigma_{0,q}^{\text{DIS}}(Q^2, x) = \frac{2\pi\alpha^2}{Q^4} \left[1 + \left(1 - \frac{Q^2}{xs} \right)^2 \right] \bar{e}_q^2(Q^2), \tag{A.9}$$

where the effective lepton charge $\bar{e}_q^2$ includes the contribution from Z boson production,

$$\bar{e}_q^2(Q^2) = e_q^2 + \frac{(v_q^2 + a_q^2)(v_\ell^2 + a_\ell^2) - 2e_q v_q v_\ell (1 - m_Z^2/Q^2)}{(1 - m_Z^2/Q^2)^2 + m_Z^2 \Gamma_Z^2/Q^4}. \tag{A.10}$$

Here e_q is the electric charge of the quark, v_i and a_i are its vector and axial couplings, m_Z is the mass of the Z and Γ_Z its decay width. Our numerical predictions always include Z boson corrections, though their effect is small for Belle and SIDIS.

A.3 Soft function

The soft function used along this thesis to renormalize rapidity divergences in unsubstracted TMD distributions and jet functions is written as

$$S(\boldsymbol{b}) = \exp\left[a_s C_F \left(S^{[1]} + a_s S^{[2]} + \mathcal{O}(a_s^3) \right) \right]. \tag{A.11}$$

This function is calculated in modified δ-regularization scheme up to NNLO in [52]. The NLO expression given in the exponent of eq. (A.11) is

$$S^{[1]} = -4C_K \boldsymbol{B}^\epsilon \Gamma(-\epsilon) \left(\boldsymbol{L}_{\sqrt{\zeta}} + 2\lambda_\delta - \psi(-\epsilon) - \gamma_E \right), \tag{A.12}$$

where $C_K = C_F(C_A)$ for quark (gluon) case. The NNLO contribution reads

$$S^{[2]} = C_K \left[d^{(2,2)} \left(\frac{3}{\epsilon^3} + \frac{2l_\delta}{\epsilon^2} + \frac{\pi^2}{6\epsilon} + \frac{4}{3}\boldsymbol{L}_\mu^3 - 2\boldsymbol{L}_\mu^2 l_\delta + \frac{2\pi^2}{3}\boldsymbol{L}_\mu + \frac{14}{3}\zeta_3 \right) \right.$$

$$- d^{(2,1)} \left(\frac{1}{2\epsilon^2} + \frac{l_\delta}{\epsilon} - \boldsymbol{L}_\mu^2 + 2\boldsymbol{L}_\mu l_\delta - \frac{\pi^2}{4} \right) - d^{(2,0)} \left(\frac{1}{\epsilon} + 2l_\delta \right)$$

$$+ C_A \left(\frac{\pi^2}{3} + 4\ln 2 \right) \left(\frac{1}{\epsilon^2} + \frac{2\boldsymbol{L}_\mu}{\epsilon} + 2\boldsymbol{L}_\mu^2 + \frac{\pi^2}{6} \right) + C_A (8\ln 2 - 9\zeta_3) \left(\frac{1}{\epsilon} + 2\boldsymbol{L}_\mu \right)$$

$$+ \frac{656}{81}T_R N_f + C_A \left(-\frac{2428}{81} + 16\ln 2 - \frac{7\pi^4}{18} - 28\ln 2\,\zeta_3 + \frac{4}{3}\pi^2\ln^2 2 \right.$$

$$\left. \left. - \frac{4}{3}\ln^4 2 - 32\text{Li}_4\left(\frac{1}{2}\right) \right) + \mathcal{O}(\epsilon) \right], \tag{A.13}$$

where $C_K = C_F(C_A)$ for quark (gluon) soft-factor. Here, the logarithm $\mathbf{l}_\delta = \ln\left(\mu^2/|\delta^+\delta^-|\right)$, while after substitution $\delta^- = \delta^+\zeta/(p^+)^2$ it reads

$$\mathbf{l}_\delta = \ln\left(\frac{\mu^2}{(\delta^+/p^+)^2\zeta}\right) = \mathbf{l}_\zeta - 2\lambda_\delta. \tag{A.14}$$

The constants $d^{(n,k)}$ are given in section A.1.

A.4   Renormalization constants for fields and TMD operators

For the completeness of exposition we also present the renormalization constants for quark and gluon fields up to NNLO [208]

$$Z_2^{[1]} = -\frac{1}{\epsilon}C_F, \qquad\qquad Z_3^{[1]} = \frac{1}{\epsilon}\left(\frac{5}{3}C_A - \frac{4}{3}T_rN_f\right). \tag{A.15}$$

$$
\begin{aligned}
Z_2^{[2]} &= \frac{C_F}{\epsilon^2}\left(\frac{C_F}{2} + C_A\right) + \frac{C_F}{\epsilon}\left(\frac{3}{4}C_F - \frac{17}{4}C_A + T_rN_f\right), \\
Z_3^{[2]} &= \frac{C_A}{\epsilon^2}\left(-\frac{25}{12}C_A + \frac{5}{3}T_rN_f\right) + \frac{1}{\epsilon}\left(\frac{23}{8}C_A^2 - \frac{5}{2}C_AT_rN_f - 2C_FT_rN_f\right).
\end{aligned}
\tag{A.16}
$$

The quark and gluon TMD operator constants are calculated up to NNLO in [18] and read

$$Z_q^{[1]} = -C_F\left(\frac{2}{\epsilon^2} + \frac{4+2\mathbf{l}_\zeta}{\epsilon}\right), \qquad Z_g^{[1]} = -C_A\left(\frac{2}{\epsilon^2} + \frac{2+2\mathbf{l}_\zeta}{\epsilon}\right), \tag{A.17}$$

$$
\begin{aligned}
Z_q^{[2]} &= \frac{2C_F^2}{\epsilon^4} + \frac{C_F}{2\epsilon^3}\left(8C_F(2+\mathbf{l}_\zeta) + 11C_A - 4T_rN_f\right) + \frac{C_F}{\epsilon^2}\bigg[2C_F(4+4\mathbf{l}_\zeta+\mathbf{l}_\zeta^2) + \\
&\quad C_A\left(\frac{25}{9} + \frac{\pi^2}{6} + \frac{11}{3}\mathbf{l}_\zeta\right) - T_rN_f\left(\frac{8}{9} + \frac{4}{3}\mathbf{l}_\zeta\right)\bigg] + \frac{C_F}{\epsilon}\bigg[C_F\left(\pi^2 - 12\zeta_3\right) + \\
&\quad C_A\left(-\frac{355}{27} - \frac{11\pi^2}{12} + 13\zeta_3 + \left(-\frac{67}{9} + \frac{\pi^2}{3}\right)\mathbf{l}_\zeta\right) \\
&\quad + T_rN_f\left(\frac{92}{27} + \frac{\pi^2}{3} + \frac{20}{9}\mathbf{l}_\zeta\right)\bigg],
\end{aligned}
\tag{A.18}
$$

$$
\begin{aligned}
Z_g^{[2]} &= \frac{2C_A^2}{\epsilon^4} + \frac{C_A}{2\epsilon^3}\left(C_A(19+8\mathbf{l}_\zeta) - 4T_rN_f\right) + \frac{C_A}{\epsilon^2}\bigg[C_A\left(\frac{55}{36} + \frac{\pi^2}{6} + \frac{23}{3}\mathbf{l}_\zeta + 2\mathbf{l}_\zeta^2\right) + \\
&\quad T_rN_f\left(\frac{1}{9} - \frac{4}{3}\mathbf{l}_\zeta\right)\bigg] + \frac{C_A}{\epsilon}\bigg[C_A\left(-\frac{2147}{216} + \frac{11\pi^2}{36} + \zeta_3 + \left(-\frac{67}{9} + \frac{\pi^2}{3}\right)\mathbf{l}_\zeta\right) + \\
&\quad T_rN_f\left(\frac{121}{54} - \frac{\pi^2}{9} + \frac{20}{9}\mathbf{l}_\zeta\right)\bigg].
\end{aligned}
\tag{A.19}
$$

Appendix B

Loop integrals for TMD higher order calculations

B.1   1-loop integrals

We present here the integrals needed in the evaluation of the Feynman diagrams that give the one-loop contribution to the different (un)polarized TMDPDF and TMDFF along this thesis. At 1-loop accuracy we have one loop particle to integrate over its momentum. This particle can be a real or virtual one. Once we simplify the integrand of the diagrams we have only one non-trivial integral

$$F_\alpha\,[R] = \int \frac{d^d k}{(2\pi)^d} \frac{\text{Disc}\,D(k)\delta(K^+ - k^+)\,R\,e^{i(kb)}}{[(k+p)^2]^{1+\alpha}}, \tag{B.1}$$

where $K^+ = -\bar{x}p^+$ (for PDFs) or $K^+ = \bar{z}/z\,p^+$ (for FFs) and the value of R can be $R = 1$ (unpolarized or transversity TMD), $R = \{1, \hat{k}^2\}$ (helicity TMD) or $R = \{1, (\mathbf{kb})^2\}$ (pretzelosity or linearly polarized gluon TMD). The integral in eq. (B.1) can be obtained from the basic transverse integral

$$\int \frac{d^{d-2}k_T}{(2\pi)^{d-2}} \frac{e^{i(\mathbf{kb})}}{(k_T^2)^{1+\delta}} = \frac{1}{(4\pi)^{\frac{d-2}{2}}} \frac{\Gamma(-\epsilon-\delta)}{\Gamma(1+\delta)} \left(\frac{b^2}{4}\right)^{\epsilon+\delta} \tag{B.2}$$

because all the non trivial structures in R are transverse. So, we can do derivatives with respect to the impact parameter and then contract the result with $\hat{g}^{\mu\nu}$ (to get the integral with $R = \hat{k}^2$) and $b^\mu b^\nu$ (to get the integral with $R = (kb)_T^2$). The final results of these integrals (for PDFs) are

$$F_0 \equiv F_0[1] = \frac{\mathbf{B}^\epsilon}{(4\pi)^{d/2}}\Gamma(-\epsilon), \tag{B.3}$$

$$F_1[(\mathbf{kb})^2]/\mathbf{B} = \frac{-2\bar{x}}{(4\pi)^{d/2}}(1+2\epsilon)\Gamma(-\epsilon)\frac{\mathbf{B}^\epsilon}{p^+}, \tag{B.4}$$

$$F_1[\hat{k}^2] = \frac{\bar{x}}{(4\pi)^{d/2}}\Gamma(1-\epsilon)\frac{\mathbf{B}^\epsilon}{p^+}\left(1+\frac{\hat{\mathbf{B}}}{\mathbf{B}}\right), \tag{B.5}$$

where $\mathbf{B} = b^2/4 > 0$ and the term $\hat{\mathbf{B}}/\mathbf{B} \ll 1$ is supressed. These integrals are used in intermediate passages on two-loop integrals presented in the next section.

B.2   2-loop integrals

Three different types of diagrams arise in the calculation of the unsubstracted TMD-PDF matrix element for the diferent (un)polarized TMD distributions and they can be addressed on the basis that the exchanged gluons are pure-virtual, virtual-real or real-real. The pure-virtual diagrams, are zero in the dimensional regularization due to the absence of a Lorentz-invariant scale in our scheme of calculation. The virtual-real and real-real diagrams have respectively one and two cut propagators and should be computed directly. The calculation of these two types of diagrams draws from two general master integrals. The first one is the master integral for virtual-real diagrams,

$$F_{abcde}[R] = -(2\pi) \int \frac{d^d k \, d^d l}{(2\pi)^{2d}} \frac{R p^+ \, \delta(\omega p^+ + l^+) \delta(K^+ - k^+) \, e^{i(kb)} \delta(k^2) \theta(\pm k^-)}{[(l+p)^2]^a [(k+p)^2]^b [(k+l+p)^2]^c [(k+l)^2]^d [(l^2)]^e} \, ,$$

(B.6)

where K^+ has the same values that in the 1-loop case and the positive (negative) sign inside the step function stands for the PDF (FF) case. The second type of integrals is the corresponding to real-real diagrams,

$$F_{abcd}[R] = (2\pi)^2 \int \frac{d^{d-1} k \, d^{d-1} l}{(2\pi)^{2d}} \frac{R \, e^{i(kb)} e^{i(lb)} \delta(k^2) \theta(-k^-) \delta(l^2) \theta(-l^-)}{[(l+p)^2]^a [(k+p)^2]^b [(k+l+p)^2]^c [(k+l)^2]^d} \, . \quad \text{(B.7)}$$

In both cases, $R = \{1, (kb)^2, (kb)(lb), (lb)^2\}$ because the two-loop momenta structure is richer than the discussed in section before. The collinear components of loop momenta can be integrated with the help of the introduction of a delta function in each case, introducing the parameter ω (for virtual-real diagrams) as

$$1 = \int_{-\infty}^{\infty} d\omega \, p^+ \delta \left(\omega p^+ + l^+ \right) \quad\quad\quad \text{(B.8)}$$

and the parameter η (for real-real diagrams) as

$$1 = \int_{-\infty}^{\infty} d\eta \, p^+ \delta \left(\bar{\eta} p^+ + l^+ \right) . \quad\quad\quad \text{(B.9)}$$

the residual dependence on these parameters should be integrated out at the end of the calculation of each integral over momenta.

B.2.1   Integrals for unpolarized and transversity TMDPDFs

The integrals which appear in the study of these two distributions have a simple momenta structure in their integrands, due to the simplicity of the projectors related to this particular polarizations, see eqs. (3.4,3.5). So, the only possible value of R for these particular TMDs is $R = 1$. So, we rename $F_{abcde}[1] \equiv F_{abcde}$ and $F_{abcd}[1] \equiv F_{abcd}$. These type of integrals were calculated for first time in [18].

In the following we discuss the possible integrals which appear in the calculation of diagrams for these TMD distributions. For virtual-real like integrals all the cases

with a decoupled virtual loop are zero. So,

$$F_{02001} = F_{02100} = F_{11001} = F_{11100} = F_{12000} \tag{B.10}$$
$$= F_{01110} = F_{02010} = F_{02100} = F_{01011} = 0.$$

Also, integrals with negative index can be rewritten using identity

$$(k + l + p)^2 + l^2 = (p + l)^2 + (p + k)^2 + (k + l)^2.$$

The only non-zero integrals with positive indices are (see)

$$F_{01101}^{FF} = \frac{-i(-1)^{-\epsilon}}{p^+(4\pi)^d} \frac{\Gamma(-2\epsilon)}{\epsilon} \left(\frac{\bar{z}}{z}\right)^{\epsilon} \boldsymbol{B}^{2\epsilon} \frac{z\theta(0 < \omega z < 1)}{(z\omega(1 - z\omega))^{\epsilon}},$$

$$F_{01101}^{PDF} = \frac{i}{p^+(4\pi)^d} \frac{\Gamma(-2\epsilon)}{\epsilon} \bar{x}^{\epsilon} \boldsymbol{B}^{2\epsilon} \frac{\theta(0 < \omega/x < 1)/x}{(\omega/x(1 - \omega/x))^{\epsilon}}, \tag{B.11}$$

$$F_{10101}^{FF} = \frac{-i(-1)^{-\epsilon}}{p^+(4\pi)^d} \Gamma(-2\epsilon) \left(\frac{\bar{z}}{z}\right)^{\epsilon} \boldsymbol{B}^{2\epsilon} \int [dx] \frac{\delta\left(\omega - x_1 - \frac{x_2}{z}\right)}{(x_2 x_3)^{1+\epsilon}},$$

$$F_{10101}^{PDF} = \frac{i}{p^+(4\pi)^d} \Gamma(-2\epsilon) \bar{x}^{\epsilon} \boldsymbol{B}^{2\epsilon} \int [dx] \frac{\delta\left(\omega - x_1 - xx_2\right)}{(x_2 x_3)^{1+\epsilon}}, \tag{B.12}$$

where $[dx] = \delta(1 - x_1 - x_2 - x_3)dx_1 dx_2 dx_3$. We leave the integral over Feynman parameters, since it is convenient to integrate first over ω with the help of δ-function in eq. (B.8). Note that only integrals with sum of indices equal to 3 participate. There are two another integrals that appear in calculation and can be reduced to the previous cases

$$F_{00111}(\omega) = F_{10101}\left(\frac{p^+ + k^+}{p^+} - \omega\right),$$

$$F_{021(-1)1}^{FF} = -\left(z\omega + \bar{z}\left(1 - 2z\omega\right)\right) F_{01101}^{FF},$$

$$F_{021(-1)1}^{PDF} = -\left(\frac{\omega}{x} - \frac{\bar{x}}{x}\left(1 - 2\frac{\omega}{x}\right)\right) F_{01101}^{PDF}. \tag{B.13}$$

For the real-real diagrams, only integrals with sum of indices equal to 2 participate. The list of non-zero integrals is

$$F_{0110} = \frac{-1}{(4\pi)^d} \boldsymbol{B}^{2\epsilon} \frac{\Gamma(-2\epsilon)}{\epsilon}$$
$$\frac{1}{k^+ + p^+} \left(\frac{l^+ p^+ (k^+ + p^+ + l^+)}{k^+ (k^+ + p^+)^2}\right)^{\epsilon} {}_2F_1\left(-\epsilon, -2\epsilon, 1 - \epsilon; \frac{-k^+ (k^+ + p^+ + l^+)}{p^+ l^+}\right),$$

$$F_{1010} = \frac{-1}{(4\pi)^d} \boldsymbol{B}^{2\epsilon} \frac{\Gamma(-2\epsilon)}{\epsilon}$$
$$\frac{1}{l^+ + p^+} \left(\frac{k^+ p^+ (k^+ + p^+ + l^+)}{l^+ (l^+ + p^+)^2}\right)^{\epsilon} {}_2F_1\left(-\epsilon, -2\epsilon, 1 - \epsilon; \frac{-l^+ (k^+ + p^+ + l^+)}{p^+ k^+}\right),$$

$$F_{1100} = \frac{1}{(4\pi)^d} \boldsymbol{B}^{2\epsilon} \frac{\Gamma^2(-\epsilon)}{p^+},$$

$$F_{0020} = \frac{1}{(4\pi)^d} \boldsymbol{B}^{2\epsilon} \frac{\Gamma(-2\epsilon)}{k^+ + l^+ + p^+} \left(\frac{(k^+ + l^+)^2 (k^+ + l^+ + p^+)}{k^+ l^+ p^+}\right)^{\epsilon},$$

$$F_{1001} = \frac{1}{(4\pi)^d} B^{2\epsilon} \frac{\Gamma^2(-\epsilon)}{l^+} \left(\frac{k^+ + l^+}{l^+}\right)^{2\epsilon},$$

$$F_{0101} = \frac{1}{(4\pi)^d} B^{2\epsilon} \frac{\Gamma^2(-\epsilon)}{k^+} \left(\frac{k^+ + l^+}{k^+}\right)^{2\epsilon}, \tag{B.14}$$

To obtain the values of the integrals in eq. (B.14) for the PDF/FF cases, k^+, l^+ should be substituted by their corresponding values given by the corresponding delta functions in each case. The integrals with negative indices can be obtained from the ones presented here, by differentiation with respect to k^+ or l^+.

B.2.2 Integrals for pretzelosity and linearly polarized gluons

In the study of pretzelosity and linearly polarized gluon TMD distributions there are some further difficulties to be taken into account. Due to the more complicated projector used, with a richer momentum structure we have all the possible values of R indicated before. This new feature introduces scalar products of the loop momenta with the impact parameter space vector, $\boldsymbol{b}$ in the numerator of the integrands that complicates the calculations of these integrals.

For virtual-real diagrams this difficulty can be by-passed by calculating separately virtual subdiagrams. This approach allows to contract the projector only with the real loop-momentum, simplifying the calculation of integrals. For real-real integrals no subdiagrams can be calculated, but the results can be obtained in terms of the integrals given for $R = 1$ in eq. (B.14). Thus,

$$F_{0210}[(\boldsymbol{kb})^2]/\boldsymbol{B} = 2\left((1+2\epsilon)(x-\eta) - \frac{\epsilon(1-2\epsilon)}{1+\epsilon}\frac{\bar{\eta}}{x}\right) F_{0110} - \frac{2(1-2\epsilon)}{1+\epsilon}\bar{x}F_{0020},$$

$$F_{0210}[(\boldsymbol{kb})(\boldsymbol{lb})]/\boldsymbol{B} = \frac{2(1-2\epsilon)}{1+\epsilon}\frac{\bar{\eta}}{\bar{\eta}+x}\left(\epsilon\frac{\bar{\eta}}{x}F_{0110} - (1+\epsilon)(\eta-x)F_{0110} + \bar{x}F_{0020}\right)$$
$$+2(\bar{\eta}+x)F_{(-1)210} + 2\eta F_{0110},$$

$$F_{0210}[(\boldsymbol{lb})^2]/\boldsymbol{B} = \frac{x}{(\bar{\eta}+x)^2}\left(\frac{2(1-2\epsilon)}{1+\epsilon}(x(\eta-x) - (1+\epsilon)\bar{\eta})F_{0110}\right.$$
$$\left. +\epsilon\frac{2(1-2\epsilon)}{1+\epsilon}x\bar{x}F_{0020} - 2(1-2\epsilon)\bar{\eta}^2 F_{0110}\right) - 4\bar{\eta}F_{(-1)210}$$
$$-\frac{1}{(\bar{\eta}+x)^2}\left(\frac{2\epsilon(1-2\epsilon)}{1+\epsilon}\frac{\bar{\eta}^3}{x} - 2\eta(1-2\epsilon)\bar{\eta}^2\right) F_{0110}$$
$$-\frac{2(1-2\epsilon)}{1+\epsilon}\frac{\bar{\eta}^2}{(\bar{\eta}+x)^2}\bar{x}F_{0020},$$

$$F_{0120}[(\boldsymbol{kb})^2]/\boldsymbol{B} = \left(4(x-\eta) + \frac{2(1-2\epsilon)}{1+\epsilon}\frac{\bar{x}}{x}(\bar{\eta}+x)\right) F_{0020}$$
$$+\epsilon\frac{2(1-2\epsilon)}{1+\epsilon}\frac{\bar{\eta}}{x^2}(\bar{\eta}+x)F_{0110},$$

$$F_{0120}[(\boldsymbol{kb})(\boldsymbol{lb})]/\boldsymbol{B} = -\frac{2(1-2\epsilon)}{1+\epsilon}\frac{\bar{\eta}}{x}\left(\frac{\epsilon\bar{\eta}}{x}F_{0110} + \bar{x}F_{0020}\right)$$
$$-2F_{0110} + 2(\bar{\eta}+x)F_{(-1)210} + 2\eta F_{0020},$$

$$F_{0120}[(\boldsymbol{lb})^2]/\boldsymbol{B} = \frac{2(1-2\epsilon)}{1+\epsilon}\frac{\bar{\eta}^2}{x(\bar{\eta}+x)}\left(\epsilon\frac{\bar{\eta}}{x}F_{0110} + (1+\epsilon)\frac{x}{\bar{\eta}}F_{0110} + \bar{x}F_{0020}\right)$$
$$-4\bar{\eta}F_{(-1)210},$$

$$
\begin{aligned}
F_{1020}[(kb)^2]/B &= \frac{2(1-2\epsilon)}{1+\epsilon}\frac{(\eta-x)^2}{x\eta}\left(\epsilon\frac{\eta-x}{x}F_{1010}+(1+\epsilon)\frac{x}{\eta-x}F_{1010}+\bar{x}F_{0020}\right) \\
&\quad +4(x-\eta)F_{1(-1)20}, \\
F_{1020}[(kb)(lb)]/B &= -\frac{2(1-2\epsilon)}{1+\epsilon}\frac{\eta-x}{x}\left(\epsilon\frac{\eta-x}{x}F_{1010}+\bar{x}F_{0020}\right) \\
&\quad -2F_{1010}+2(\bar{\eta}+x)F_{0020}+2\eta F_{1(-1)20}, \\
F_{1020}[(lb)^2]/B &= \frac{2(1-2\epsilon)}{1+\epsilon}\frac{\eta}{x}\left(\epsilon\frac{\eta-x}{x}F_{1010}+\bar{x}F_{0020}\right)-4\bar{\eta}F_{0020}, \\
F_{0021}[(kb)^2]/B &= -\frac{2(1-2\epsilon)}{1-\epsilon}\frac{\eta-x}{\bar{x}}\left((\bar{\eta}+x)F_{0020}-(\eta-x)F_{0011}\right) \\
&\quad +4(x-\eta)\left(F_{0011}-F_{0020}-F_{(-1)021}\right), \\
F_{0021}[(kb)(lb)]/B &= \frac{2(1-2\epsilon)}{1-\epsilon}\frac{(\eta-x)\bar{\eta}}{\bar{x}}\left(F_{0020}+F_{0011}\right)+2(1+x-2\eta)F_{(-1)021} \\
&\quad -2\bar{\eta}\left(F_{0011}-F_{0020}\right)-2F_{0020}, \\
F_{0021}[(lb)^2]/B &= -\frac{2(1-2\epsilon)}{1-\epsilon}\frac{\bar{\eta}}{\bar{x}}\left(\eta F_{0020}-\bar{\eta}F_{0011}\right)-4\bar{\eta}F_{(-1)021},
\end{aligned}
\tag{B.15}
$$

Note that in the new integrals for these quantities the sum of the indices *abcd* of the new integrals is 3. Also, the integrals with $R=1$ appear by themselves as parts of the diagrams calculated.

Additionally, we have met three integrals that could not be reduced to a combination of known results: $F_{1110}[(kb)^2]$, $F_{1110}[(kb)(lb)]$, $F_{1110}[(lb)^2]$. For these integrals we have derived the expressions in the Schwinger parameterization, and evaluated them in ϵ-expansion up to the finite term following the strategy described in the book [209]. We make an sketch of the evaluation of these type of integrals from the general integral,

$$
\begin{aligned}
F_{abc0}[R] &= \frac{(-1)^{a+b+c}}{(4\pi)^2}\frac{p^+}{k^+l^+}\left(-\frac{l^+}{p^+}\right)^a\left(-\frac{k^+}{p^+}\right)^b \\
&\quad \int\frac{d^{d-2}k_T d^{d-2}l_T}{(2\pi)^{2d-4}}\frac{Re^{i(kb)+i(lb)}}{[l_T^2]^a[k_T^2]^b(x_1 k_T^2+2(kl)_T+x_2 l_T^2)^c},
\end{aligned}
\tag{B.16}
$$

where

$$
x_1 = -\frac{l^+ + p^+}{k^+}, \qquad x_2 = -\frac{k^+ + p^+}{l^+}.
\tag{B.17}
$$

As the distributions in whose calculation this integral enters are calculated only for the TMDPDF case we focus only in PDF kinematics. So,

$$
x_1 = \frac{\eta}{\eta-x} = 1+\frac{x}{\eta-x} > 1, \qquad x_2 = \frac{\bar{\eta}+x}{\bar{\eta}} = 1+\frac{x}{\bar{\eta}} > 1.
\tag{B.18}
$$

We call the integral in eq. (B.16)

$$
f_{abc}[R] = \int\frac{d^{d-2}k_T d^{d-2}l_T}{(2\pi)^{2d-4}}\frac{Re^{i(kb)+i(lb)}}{[l_T^2]^a[k_T^2]^b(x_1 k_T^2+2(kl)_T+x_2 l_T^2)^c},
\tag{B.19}
$$

which is to be solved in terms of derivatives with respect of the parameters of the following integral

$$
g_{abc} = \int \frac{d^{d-2}k_T d^{d-2}l_T}{(2\pi)^{2d-4}} \frac{Re^{i(\boldsymbol{kb_1})+i(\boldsymbol{lb_2})}}{[l_T^2]^a [k_T^2]^b (x_1 k_T^2 + 2(kl)_T + x_2 l_T^2)^c} \tag{B.20}
$$

$$
= \frac{\pi^{\frac{d-2}{2}}}{\Gamma(a)\Gamma(b)\Gamma(c)} \int_0^\infty d\alpha d\beta d\gamma \frac{\alpha^{a-1}\beta^{b-1}\gamma^{c-1} \exp\left[-\frac{b_1^2 a_1 - 2(b_1 b_2)a_{12} + b_2^2 a_2}{4\Delta_1}\right]}{\Delta_1^{1-\epsilon}},
$$

where

$$
\Delta_1 = a_1 a_2 - a_{12}^2, \qquad a_1 = (\alpha + x_2\gamma), \qquad a_2 = (\beta + x_1\gamma), \qquad a_{12} = \gamma. \tag{B.21}
$$

Next we make the change of variables

$$
\alpha \to L x_2(\alpha_2 - 1), \qquad \beta \to L x_1(\alpha_1 - 1), \qquad \gamma \to L, \tag{B.22}
$$

with

$$
J = \frac{d\alpha d\beta d\gamma}{d\alpha_1 d\alpha_2 dL} = x_1 x_2 L^2, \qquad L > 0, \quad \alpha_{1,2} > 1. \tag{B.23}
$$

Thus, we obtain

$$
g_{abc} = \frac{\pi^{\frac{d-2}{2}}}{\Gamma(a)\Gamma(b)\Gamma(c)} \tag{B.24}
$$

$$
\int_0^\infty dL \int_1^\infty d\alpha_{1,2} \frac{L^{2\epsilon+a+b+c-3} x_2^a x_1^b (\alpha_2-1)^{a-1}(\alpha_1-1)^{b-1} \exp\left[-\frac{b_1^2 x_2\alpha_2 - 2(b_1 b_2) + b_2^2 x_1\alpha_1}{4L\Delta_2}\right]}{\Delta_2^{1-\epsilon}},
$$

where $\Delta_2 = x_1 x_2 \alpha_1 \alpha_2 - 1$.

The integration over L is straightforward $(a + b + c + 2\epsilon < 2)$

$$
g_{abc} = x_2^a x_1^b \pi^{\frac{d-2}{2}} \frac{\Gamma(-2\epsilon - a - b - c + 2)}{\Gamma(a)\Gamma(b)\Gamma(c)} \tag{B.25}
$$

$$
\int_1^\infty d\alpha_{1,2} (\alpha_2-1)^{a-1}(\alpha_1-1)^{b-1} \Delta_2^{1-a-b-c-\epsilon} \left(\frac{b_1^2 x_2\alpha_2 - 2(b_1 b_2) + b_2^2 x_1\alpha_1}{4}\right)^{2\epsilon+a+b+c-2}.
$$

Using the derivative over $\boldsymbol{b}_{1,2}$ we obtain

$$
f_{111}[k_T^\mu k_T^\nu] = \frac{x_1 x_2}{2} \pi^{\frac{d-2}{2}} \mathbf{B}^{2\epsilon} \Gamma(-2\epsilon) \int_1^\infty d\alpha_{1,2} \tag{B.26}
$$

$$
\times \left[\frac{\alpha_2 x_2 (x_1\alpha_1 + x_2\alpha_2 - 2)^{2\epsilon}}{(x_1 x_2 \alpha_1\alpha_2 - 1)^{2+\epsilon}} g_T^{\mu\nu} - 4\epsilon \frac{b^\mu b^\nu}{b^2} \frac{(x_2\alpha_2 - 1)^2(x_1\alpha_1 + x_2\alpha_2 - 2)^{2\epsilon-1}}{(x_1 x_2 \alpha_1\alpha_2 - 1)^{2+\epsilon}} \right]
$$

$$
f_{111}[l_T^\mu l_T^\nu] = \frac{x_1 x_2}{2} \pi^{\frac{d-2}{2}} \mathbf{B}^{2\epsilon} \Gamma(-2\epsilon) \int_1^\infty d\alpha_{1,2} \tag{B.27}
$$

$$
\times \left[\frac{\alpha_1 x_1 (x_1\alpha_1 + x_2\alpha_2 - 2)^{2\epsilon}}{(x_1 x_2 \alpha_1\alpha_2 - 1)^{2+\epsilon}} g_T^{\mu\nu} - 4\epsilon \frac{b^\mu b^\nu}{b^2} \frac{(x_1\alpha_1 - 1)^2(x_1\alpha_1 + x_2\alpha_2 - 2)^{2\epsilon-1}}{(x_1 x_2 \alpha_1\alpha_2 - 1)^{2+\epsilon}} \right]
$$

$$f_{111}[l_T^\mu k_T^\nu] = \frac{x_1 x_2}{2} \pi^{\frac{d-2}{2}} \mathbf{B}^{2\epsilon} \Gamma(-2\epsilon) \int_1^\infty d\alpha_{1,2} \tag{B.28}$$

$$\times \left[-\frac{(x_1\alpha_1 + x_2\alpha_2 - 2)^{2\epsilon}}{(x_1 x_2 \alpha_1 \alpha_2 - 1)^{2+\epsilon}} g_T^{\mu\nu} - 4\epsilon \frac{b^\mu b^\nu}{b^2} \frac{(x_1\alpha_1 - 1)(x_2\alpha_2 - 1)(x_1\alpha_1 + x_2\alpha_2 - 2)^{2\epsilon-1}}{(x_1 x_2 \alpha_1 \alpha_2 - 1)^{2+\epsilon}} \right].$$

We can also write the following relations

$$F_{1110}[k_T^\mu k_T^\nu] = g_T^{\mu\nu} A_{kk} + \frac{b^\mu b^\nu}{b^2} B_{kk}, \tag{B.29}$$

$$F_{1110}[k_T^\mu l_T^\nu] = g_T^{\mu\nu} A_{kl} + \frac{b^\mu b^\nu}{b^2} B_{kl}, \tag{B.30}$$

$$F_{1110}[l_T^\mu l_T^\nu] = g_T^{\mu\nu} A_{ll} + \frac{b^\mu b^\nu}{b^2} B_{ll}. \tag{B.31}$$

Using some algebra we get

$$2(1-\epsilon)A_{kk} + B_{kk} = -(\eta - x)F_{1010}, \tag{B.32}$$

$$2(1-\epsilon)A_{ll} + B_{ll} = -\bar{\eta}F_{0110}, \tag{B.33}$$

$$2(1-\epsilon)A_{kl} + B_{kl} = -\frac{1}{2}F_{1100} + \frac{\eta}{2}F_{0110} + \frac{\bar{\eta}+x}{2}F_{1010}. \tag{B.34}$$

Using these relations we can reduce the number of integrals to evaluate, since

$$F_{1110}[(kb)^2] = b^2(A_{kk} + B_{kk}), \tag{B.35}$$

$$F_{1110}[(lb)^2] = b^2(A_{ll} + B_{ll}), \tag{B.36}$$

$$F_{1110}[(kb)(lb)] = b^2(A_{kl} + B_{kl}). \tag{B.37}$$

Additionally knowing that b is the only dimensional parameter we derive

$$4\epsilon(A_{kk} + 2A_{kl} + A_{ll}) = B_{kk} + 2B_{kl} + B_{ll}. \tag{B.38}$$

Using the definition in eq. (B.16) we obtain

$$\partial_{x_1} F_{abc0}[R] = -cF_{a,b-1,c+1,0}[R], \tag{B.39}$$

$$\partial_{x_2} F_{abc0}[R] = -cF_{a-1,b,c+1,0}[R]. \tag{B.40}$$

And parameterizing

$$F_{abc0}[k_T^\mu k_T^\nu] = g_T^{\mu\nu} A_{kk}^{abc0} + \frac{b^\mu b^\nu}{b^2} B_{kk}^{abc0}, \tag{B.41}$$

$$F_{abc0}[k_T^\mu l_T^\nu] = g_T^{\mu\nu} A_{kl}^{abc0} + \frac{b^\mu b^\nu}{b^2} B_{kl}^{abc0}, \tag{B.42}$$

$$F_{abc0}[l_T^\mu l_T^\nu] = g_T^{\mu\nu} A_{ll}^{abc0} + \frac{b^\mu b^\nu}{b^2} B_{ll}^{abc0}. \tag{B.43}$$

We obtain

$$2(1-\epsilon)A_{kk}^{abc0} + B_{kk}^{abc0} = -(\eta - x)F_{a,b-1,c0}, \tag{B.44}$$

$$2(1-\epsilon)A_{ll}^{abc0} + B_{ll}^{abc0} = -\bar{\eta}F_{a-1,bc0}, \tag{B.45}$$

$$2(1-\epsilon)A_{kl}^{abc0} + B_{kl}^{abc0} = -\frac{1}{2}F_{ab,c-1,0} + \frac{\eta}{2}F_{a-1,bc0} + \frac{\bar{\eta}+x}{2}F_{a,b-1,c0}, \tag{B.46}$$

$$A_{kk}^{abc0} + 2A_{kl}^{abc0} + A_{ll}^{abc0} = \frac{B_{kk}^{abc0} + 2B_{kl}^{abc0} + B_{ll}^{abc0}}{2(2\epsilon + a + b + c - 3)}. \tag{B.47}$$

So, we can get the relation

$$
\begin{aligned}
F_{abc0}[(\boldsymbol{kb})(\boldsymbol{lb})]/\boldsymbol{B} \;=\; & -\frac{1}{2} F_{abc0}[(\boldsymbol{kb})^2]/\boldsymbol{B} - \frac{1}{2} F_{abc0}[(\boldsymbol{lb})^2]/\boldsymbol{B} \\
& + \frac{1+4\epsilon}{1+\epsilon} \Big(-F_{ab,c-1,0} + (1+2x-2\eta)F_{a,b-1,c0} - (1-2\eta)F_{a-1,bc0} \Big),
\end{aligned}
$$

where $a + b + c = 3$.

Another three integrals that could not be reduced to a combination of known integrals but that can be related with $F_{1110}[R]$ through a change of variable are: $F_{0111}[(\boldsymbol{kb})^2]$, $F_{0111}[(\boldsymbol{kb})(\boldsymbol{lb})]$, $F_{0111}[(\boldsymbol{lb})^2]$.

Appendix C

Laplace and Fourier transformations

We define the Fourier transform, $\mathcal{FT}[f](\boldsymbol{b}) = f(\boldsymbol{b})$ of a function, $f(\boldsymbol{q}_T) = \mathcal{FT}^{-1}[f](\boldsymbol{q}_T)$ as follows,

$$f(\boldsymbol{b}) = \int_{-\infty}^{+\infty} d\boldsymbol{q}_T \, f(\boldsymbol{q}_T) \exp(-i\boldsymbol{b} \cdot \boldsymbol{q}_T) \,, \tag{C.1}$$

and the inverse transform

$$f(\boldsymbol{q}_T) = \int_{-\infty}^{+\infty} \frac{d\boldsymbol{b}}{(2\pi)^2} f(\boldsymbol{b}) \exp(i\boldsymbol{b} \cdot \boldsymbol{q}_T) \,. \tag{C.2}$$

In order to get the Fourier transforms of the plus distributions that appear in the factorization theorem we use,

$$\frac{1}{(2\pi)\mu^2} \left(\frac{\mu^2}{q_T^2} \right)^{1+\alpha} = -\frac{1}{2\alpha} \delta^{(2)}(\boldsymbol{q}_T) + \mathcal{L}_0(q_T^2, \mu^2) - \alpha \mathcal{L}_1(q_T^2, \mu^2) + \mathcal{O}(\alpha^2) \,. \tag{C.3}$$

Taking the Fourier transform of the left-hand-side (LHS) we get (see eq. (E.2) of ref. [14])

$$\int_{-\infty}^{+\infty} \frac{d\boldsymbol{q}_T}{(2\pi)} \frac{1}{\mu^2} \left(\frac{\mu^2}{q_T^2} \right)^{1+\alpha} \exp(-i\boldsymbol{b} \cdot \boldsymbol{q}_T) \qquad = -\frac{e^{-2\alpha\gamma_E}}{2\alpha} \frac{\Gamma(1-\alpha)}{\Gamma(1+\alpha)} \left(\frac{\mu}{\mu_E} \right)^{2\alpha}$$

$$= -\frac{1}{2\alpha} + \ln\left(\frac{\mu}{\mu_E} \right) + \alpha \ln^2\left(\frac{\mu}{\mu_E} \right) + \mathcal{O}(\alpha^2) \tag{C.4}$$

where $\mu_E = 2 \exp(-\gamma_E)/b$ and $b \equiv |\boldsymbol{b}|$ and in the second line we expanded in α. Comparing this result with the RHS of eq. (C.3) we get,

$$\mathcal{FT}\left[\delta^{(2)}(\boldsymbol{q}_T) \right](\boldsymbol{b}) \qquad = 1 \,,$$

$$\mathcal{FT}\left[\mathcal{L}_0(q_T^2, \mu^2) \right](\boldsymbol{b}) \quad = \ln\left(\frac{\mu_E}{\mu} \right) \,,$$

$$\mathcal{FT}\left[\mathcal{L}_1(q_T^2, \mu^2) \right](\boldsymbol{b}) \quad = \ln^2\left(\frac{\mu_E}{\mu} \right) \,. \tag{C.5}$$

We define the convolution $f \otimes g$ with

$$\left[f \otimes g \right](\boldsymbol{q}_T) = \int d\boldsymbol{\ell}_\perp \, f(\boldsymbol{q}_T - \boldsymbol{\ell}_\perp) g(\boldsymbol{\ell}_\perp) \,, \tag{C.6}$$

such that

$$\mathcal{F}\left[f \otimes g \right](\boldsymbol{b}) = f(\boldsymbol{b}) \times g(\boldsymbol{b}) \,. \tag{C.7}$$

Similarly for the distribution in the jet-thrust we often work in Laplace space

where the corresponding convolutions translate to products. For these reason we define the Laplace transformation $\mathcal{LT}[f](s) = f(s)$ of jet-trust distribution $f(e) = \mathcal{LT}^{-1}[f](e)$ as follows:

$$f(s) = \int_{-\infty}^{\infty} de \ \exp(-se)f(e) \,, \tag{C.8}$$

and the corresponding inverse transform

$$f(e) = \frac{1}{2\pi i} \int_{\gamma-i\infty}^{\gamma+i\infty} ds \ \exp(se)f(s) \,. \tag{C.9}$$

Similarly with the case of Fourier transform we use the following expansion to identify the Laplace transform of plus distributions that are present in the fixed order expansion of the jet and collinear-soft functions,

$$\frac{1}{\xi}\left(\frac{\xi}{e}\right)^{1+\alpha}\Big|_{e>0} = -\frac{1}{\alpha}\delta(e) + \mathcal{L}_0(e,\xi) - \alpha\mathcal{L}_1(e,\xi) + \mathcal{O}(\alpha^2) \,, \tag{C.10}$$

taking the Laplace transform of the LHS we get

$$\int_0^{\infty} \frac{de}{\xi}\left(\frac{\xi}{e}\right)^{1+\alpha}\exp(-se) = s^{\alpha}\Gamma(-\alpha) = -\frac{1}{\alpha} - \ln(\xi\tilde{s}) - \alpha\left(\frac{1}{2}\ln^2(\xi\tilde{s}) + \frac{\pi^2}{12}\right) + \mathcal{O}(\alpha^2) \,, \tag{C.11}$$

where $\tilde{s} \equiv s\exp(\gamma_E)$ and thus from comparing eq. (C.10) and (C.11) we have

$$\mathcal{LT}\Big[\delta(e)\Big](s) \qquad = 1 \,,$$
$$\mathcal{LT}\Big[\mathcal{L}_0(e,\xi)\Big](s) \qquad = -\ln(\xi\tilde{s}) \,,$$
$$\mathcal{LT}\Big[\mathcal{L}_1(e,\xi)\Big](s) \quad = \tfrac{1}{2}\ln^2(\xi\tilde{s}) + \tfrac{\pi^2}{12} \,. \tag{C.12}$$

Summary

Title: Transverse momentum dependent distributions for the Electron-Ion Collider era

Introduction and outline

The physical theory which deals with the strong interactions between quarks and gluons in known as Quantum Chromodynamics (QCD). This theory, together with the ones that deal with electromagnetic and weak interactions (unified in electroweak theory) are combined into the Standard Model (SM). This theory is built in terms of a Lagrangian of quantized fields describing fundamental degrees of freedom, quarks and leptons, and bosons that act as carriers of the cited interactions.

One of the more fundamental open questions in QCD is to understand how the observed properties of hadrons are generated by the dynamics of their inner constituents. In order to shed some light on this question physicists use different theoretical approaches from different perspectives, like perturbative QCD, effective field theories, lattice QCD, etc. A very interesting research field to test and understand QCD is the exploration of the multi-dimensional structure of hadrons. The main goal of this field is to reconstruct multi-dimensional images of a hadron investigating the distribution of partons, namely quarks and gluons, inside it. In this way, issues such as the role of quarks and gluons in generating the nucleon's spin or partonic angular momentum can be investigated. There is a high interest into hadron structure in the experimental community, with important facilities such JLab, DESY, BNL, CERN, KEK. Also, the LHC can help a lot in this field, especially to understand the role of gluons inside the protons. Recently, the US government has approved the construction of a new accelerator, the Electron-Ion Collider (EIC) at BNL. Part of the predictions given in this thesis are suitable to be tested in this new accelerator.

A very interesting type of observables that can give information about hadron structure are the ones with non-vanishing transverse momentum dependence. This interest was already there in the first years after the establishment of QCD as a fundamental theory of strong interactions [1–5]. These observables are very interesting for hadron colliders and have very relevant impact on, e.g., the study of Higgs boson production and the search for physics Beyond Standard Model. A crucial point to deal with these type of processes is obtaining well defined factorization theorems and resumming large logarithmic contributions to perform phenomenological analyses. A large amount of work has been done to establish factorization theorems with un-integrated transverse momentum for very relevant processes as Drell-Yan production (proton-proton collision leading to a pair of leptons in the final state) or semi-inclusive deep inelastic scattering (electron-proton collisions leading to a hadron in the final state) [6–17]. In general terms, a factorized cross section is written in terms of a hard factor that includes all the high-energy physics and two objects that include information about the distribution of partons inside the hadrons in the process. These elements are known as transverse momentum dependent parton distribution functions (TMDPDFs).

Main results and conclusions

The main body of this thesis is divided in two parts, studying factorization theorems and the hadronic information in two different contexts, but aiming at the same goal: improving the extraction of the three-dimensional information of hadrons.

Part I of this thesis is dedicated to the study of spin dependent TMDPDFs arising from factorization theorems established for processes involving hadrons with a particular polarization. In chapter 3 the definition of the unpolarized TMDPDF of [18] is extended in order to obtain definitions for spin dependent TMDPDFs. At leading dynamical twist we obtain different spin-dependent distributions for quarks and gluons. The results of the perturbative information derived from the large transverse momentum limit of these TMDPDFs (known as matching coefficients) up to second order in perturbation theory are given in chapter 4. In this way we achieve the same level of precision for spin dependent TMDPDFs as for their unpolarized counterparts. This improvement of the perturbative order known for the different spin-dependent TMDs will help to decrease the theoretical errors in phenomenological predictions involving polarized hadrons and will allow a cleaner extraction of nonperturbative physics associated to the transverse momentum dependent distributions. As an application, in chapter 5 we use the new perturbative results obtained for linearly polarized gluon TMD to see their impact in the transverse momentum spectrum of the Higgs boson.

Part II of this thesis is dedicated to establishing factorization theorems including jets in final states of the considered processes. In principle, the use of jets in the final state decreases the nonperturbative contamination compared to using hadrons in a final state, because jet properties can be calculated to a large extent in perturbation theory. Thus, processes with jets in the final state (e.g. jet SIDIS) should offer a cleaner way to access information about the structure of hadrons in the initial state. Of course, some hadronization effects associated with the jets appear (e.g. due to the determination of the position of the axis). Thus, in this part of the thesis we study the establishment of different factorization theorems for some particularly interesting processes using different jet definitions. This allows one to study the advantages and disadvantages of different jet definitions in the extraction of information about hadrons in initial states. In chapter 6 a new definition for TMD jets is given through the establishment of different factorization theorems in different regimes related mainly to the size of the considered jet. This leads to a particular choice of the jet axis that allows the establishment of factorization theorems in any regime and will allow us to obtain numerical predictions that can be tested in future experiments as the EIC. Finally, in chapter 7 a different definition of the jet is used in order to obtain numerical predictions. In this case, we introduce the concept of grooming that removes the soft contamination to the jet. Thus only the collinear core of the jet remains and the hadronization effects should be mostly suppressed. So, this way to proceed represent another way to access to the nonperturbative information of hadrons in a cleaner manner of using processes with hadrons in the final state.

Resumen

Título: Distribuciones dependientes de momento transverso para la era del Electron-Ion Collider

Introducción y esquema

La teoría física que se ocupa de las interacciones fuertes entre quarks y gluones se conoce como la Cromodinámica Cuántica (QCD por sus siglas en inglés). Esta teoría, junto con las que se ocupan de las interacciones electromagnéticas y débiles (unificadas en la teoría electrodébil) se combinan en el Modelo Estándar. El Modelo Estándar se construye en términos de un lagrangiano de campos cuantizados que describen grados fundamentales de libertad, quarks y leptones, y bosones que actúan como portadores de las interacciones citadas.

Una de las preguntas abiertas más fundamentales en QCD se basa en entender cómo las propiedades de los hadrones observadas son generadas por la dinámica de sus componentes internos. Para dar algo de luz a esta pregunta, los físicos usan diferentes enfoques teóricos desde diferentes perspectivas, como QCD perturbativa, teorías de campo efectivas, QCD en el retículo, etc. Un campo de investigación muy interesante que puede ayudar mucho en este sentido, es la exploración de la estructura tridimensional de los hadrones. El objetivo principal de este campo es hacer una imagen tridimensional de un hadrón investigando la distribución de partones, conocidos como quarks y gluones, dentro de él. De esta manera, se pueden investigar cuestiones como el papel de los quarks y los gluones en la generación del espín del nucleón o el momento angular partónico. Por otro lado, existe un gran interés en la estructura de hadrónica por parte de la comunidad experimental con importantes instalaciones como JLab, DESY, BNL, CERN o KEK. Además, el LHC puede ayudar mucho en este tema, especialmente para comprender el papel de los gluones dentro de los protones. Recientemente, el gobierno de los Estados Unidos ha dado luz verde para comenzar la construcción de un nuevo acelerador, el Electron-Ion collider (EIC). Parte de las predicciones dadas en esta tesis están orientadas a ser probadas en este nuevo acelerador.

Un tipo muy interesante de observables que pueden proporcionar información sobre la estructura hadrónica son los que tienen una dependencia no nula del momento transverso. Este interés proviene de poco tiempo después del establecimiento de QCD de una teoría fundamental de las interacciones fuertes [1–5]. Un punto crucial para tratar con este tipo de procesos es obtener teoremas de factorización bien definidos y así resumar las contribuciones de logaritmos grandes para realizar análisis fenomenológicos. Se ha trabajado mucho en este sentido para establecer teoremas de factorización para procesos con momento transverso no nulo para procesos muy relevantes como la producción de Drell-Yan (colisión protón-protón que conduce a un par de leptones en el estado final) o dispersión profundamente inelástica (colisiones electrón-protón que conducen a un hadrón en el estado final) [6–17]. En líneas generales, una sección eficaz factorizada se escribe en términos de un factor *hard* que incluye toda la física de altas energías y dos objetos que incluyen información sobre

la distribución de partones dentro de los hadrones en el proceso. Estos elementos se conocen como funciones de distribución de partones dependientes del momento transverso (TMDPDF por sus siglas en inglés).

Resultados principales y conclusiones

El cuerpo principal de esta tesis se divide en dos partes, estudiando los teoremas de factorización y la información hadrónica en dos contextos diferentes, pero persiguiendo el mismo objetivo: mejorar la extracción de la información tridimensional de los hadrones.

La parte I de esta tesis está dedicada al estudio de TMDPDF dependientes del espín que surgen de los teoremas de factorización establecidos para procesos que involucran hadrones con una polarización particular. En el capítulo 3, la definición de la TMDPDF despolarizada de [18] se amplía para obtener definiciones de TMDPDF dependientes del espín. En el llamado *leading dynamical twist*, obtenemos diferentes distribuciones dependientes del espín para quarks y gluones. Los resultados de la información perturbativa extraída de la coincidencia de estas TMDPDF sobre las PDF integradas (conocidos como coeficientes de matching) hasta el conocido como next-to-next-to-leading order se obtienen en el capítulo 4. De esta forma, alcanzamos el mismo nivel de precisión para las TMDPDF dependientes del espín que para sus contrapartes no polarizadas. Esta mejora del orden perturbativo conocida por las diferentes TMD dependientes del espín ayudará a disminuir los errores teóricos en las predicciones fenomenológicas que involucran hadrones polarizados y permitirá una extracción más limpia de la física no perturbativa asociada a las distribuciones dependientes del momento transverso. En el capítulo 5 utilizamos los nuevos resultados perturbativos obtenidos para la TMD de gluones linealmente polarizados para ver su impacto en el espectro de momento transverso del bosón de Higgs.

La parte II de esta tesis está dedicada a ayudar a mejorar la extracción de las TMD hadrónicas con una estrategia diferente a la utilizada en la primera parte de la tesis, es decir, establecer teoremas de factorización que incluyen jets en estados finales de los procesos considerados. En principio, el uso de jets en el estado final de los procesos disminuye la contaminación no perturbativa que un hadron en un estado final introduce en el problema, porque pueden calcularse completamente en teoría de perturbaciones. Por lo tanto, el canal para obtener información sobre un hadron en un estado inicial (por ejemplo, en un proceso de SIDIS+jet) sería más limpio. Por supuesto, aparecen algunos efectos de hadronización asociados a los jets (por ejemplo, debido a la determinación de la posición del eje). Por lo tanto, a lo largo de esta parte de la tesis, estudiamos el establecimiento de diferentes teoremas de factorización para algunos procesos particularmente interesantes utilizando diferentes definiciones de jet. Ésto permite estudiar las ventajas y desventajas de las diferentes definiciones de jet en la extracción de información sobre hadrones en estados iniciales. En el capítulo 6 se da una nueva definición para las jet TMDs mediante el establecimiento de diferentes teoremas de factorización en diferentes regímenes relacionados principalmente con el tamaño del jet considerado. Ésto nos llevará a una elección particular del eje del jet que permitirá el establecimiento de teoremas de factorización en cualquier régimen y nos permitirá obtener predicciones numéricas que se pueden probar en experimentos como el futuro EIC. Finalmente, en el capítulo 7 se usa una definición diferente del jet para obtener predicciones numéricas. En este caso, presentamos el concepto de *grooming* que elimina la contaminación soft del jet. Por lo tanto, sólo queda el núcleo colineal del jet y los efectos de hadronización

deben suprimirse en su mayoría. Entonces, esta forma de proceder representa otra forma de acceder a la información no perturbativa de los hadrones de una manera más limpia que al utilizar procesos con hadrones en el estado final.

Bibliography

[1] G. Parisi and R. Petronzio, "Small Transverse Momentum Distributions in Hard Processes," *Nucl. Phys. B*, vol. 154, pp. 427–440, 1979.

[2] G. Curci, M. Greco, and Y. Srivastava, "QCD Jets From Coherent States," *Nucl. Phys. B*, vol. 159, pp. 451–468, 1979.

[3] Y. L. Dokshitzer, D. Diakonov, and S. Troian, "Hard Processes in Quantum Chromodynamics," *Phys. Rept.*, vol. 58, pp. 269–395, 1980.

[4] J. C. Collins and D. E. Soper, "Parton Distribution and Decay Functions," *Nucl. Phys.*, vol. B194, pp. 445–492, 1982.

[5] J. C. Collins and D. E. Soper, "Back-To-Back Jets in QCD," *Nucl. Phys. B*, vol. 193, p. 381, 1981. [Erratum: Nucl.Phys.B 213, 545 (1983)].

[6] J. C. Collins, D. E. Soper, and G. F. Sterman, "Factorization of Hard Processes in QCD," *Adv. Ser. Direct. High Energy Phys.*, vol. 5, pp. 1–91, 1989.

[7] A. Bacchetta, M. Diehl, K. Goeke, A. Metz, P. J. Mulders, and M. Schlegel, "Semi-inclusive deep inelastic scattering at small transverse momentum," *JHEP*, vol. 02, p. 093, 2007.

[8] A. Bacchetta, D. Boer, M. Diehl, and P. J. Mulders, "Matches and mismatches in the descriptions of semi-inclusive processes at low and high transverse momentum," *JHEP*, vol. 08, p. 023, 2008.

[9] T. Becher and M. Neubert, "Drell-Yan Production at Small q_T, Transverse Parton Distributions and the Collinear Anomaly," *Eur. Phys. J.*, vol. C71, p. 1665, 2011.

[10] J. Collins, *Foundations of perturbative QCD*. Cambridge University Press, 2013.

[11] M. G. Echevarria, A. Idilbi, and I. Scimemi, "Factorization Theorem For Drell-Yan At Low q_T And Transverse Momentum Distributions On-The-Light-Cone," *JHEP*, vol. 07, p. 002, 2012.

[12] M. G. Echevarria, A. Idilbi, and I. Scimemi, "Soft and Collinear Factorization and Transverse Momentum Dependent Parton Distribution Functions," *Phys. Lett.*, vol. B726, pp. 795–801, 2013.

[13] M. G. Echevarria, A. Idilbi, and I. Scimemi, "Unified treatment of the QCD evolution of all (un-)polarized transverse momentum dependent functions: Collins function as a study case," *Phys. Rev.*, vol. D90, no. 1, p. 014003, 2014.

[14] J.-Y. Chiu, A. Jain, D. Neill, and I. Z. Rothstein, "A Formalism for the Systematic Treatment of Rapidity Logarithms in Quantum Field Theory," *JHEP*, vol. 1205, p. 084, 2012.

[15] A. Vladimirov, "Structure of rapidity divergences in soft factors," *JHEP*, vol. 04, p. 045, 2018.

[16] I. Scimemi and A. Vladimirov, "Systematic analysis of double-scale evolution," *JHEP*, vol. 08, p. 003, 2018.

[17] I. Scimemi and A. Vladimirov, "Non-perturbative structure of semi-inclusive deep-inelastic and Drell-Yan scattering at small transverse momentum," *JHEP*, vol. 06, p. 137, 2020.

[18] M. G. Echevarria, I. Scimemi, and A. Vladimirov, "Unpolarized Transverse Momentum Dependent Parton Distribution and Fragmentation Functions at next-to-next-to-leading order," 2016.

[19] C. W. Bauer, S. Fleming, D. Pirjol, and I. W. Stewart, "An Effective field theory for collinear and soft gluons: Heavy to light decays," *Phys. Rev.*, vol. D63, p. 114020, 2001.

[20] C. W. Bauer, D. Pirjol, and I. W. Stewart, "Soft collinear factorization in effective field theory," *Phys. Rev.*, vol. D65, p. 054022, 2002.

[21] M. Beneke, A. Chapovsky, M. Diehl, and T. Feldmann, "Soft collinear effective theory and heavy to light currents beyond leading power," *Nucl. Phys. B*, vol. 643, pp. 431–476, 2002.

[22] T. Becher, "Les Houches Lectures on Soft-Collinear Effective Theory," in *Les Houches summer school: EFT in Particle Physics and Cosmology*, 3 2018.

[23] A. G. Grozin, "Introduction to effective field theories. 1. Heisenberg-Euler effective theory, decoupling of heavy flavours," in *Helmholtz International School - Workshop on Calculations for Modern and Future Colliders*, 8 2009.

[24] C. Burgess, "Introduction to Effective Field Theory," *Ann. Rev. Nucl. Part. Sci.*, vol. 57, pp. 329–362, 2007.

[25] M. Beneke and V. A. Smirnov, "Asymptotic expansion of Feynman integrals near threshold," *Nucl. Phys.*, vol. B522, pp. 321–344, 1998.

[26] V. A. Smirnov, "Applied asymptotic expansions in momenta and masses," *Springer Tracts Mod. Phys.*, vol. 177, pp. 1–262, 2002.

[27] M. Beneke and T. Feldmann, "Multipole expanded soft collinear effective theory with nonAbelian gauge symmetry," *Phys. Lett. B*, vol. 553, pp. 267–276, 2003.

[28] T. Becher, A. Broggio, and A. Ferroglia, *Introduction to Soft-Collinear Effective Theory, LNP*, vol. 896. Springer, 2015.

[29] A. V. Manohar, T. Mehen, D. Pirjol, and I. W. Stewart, "Reparameterization invariance for collinear operators," *Phys. Lett.*, vol. B539, pp. 59–66, 2002.

[30] A. von Manteuffel, E. Panzer, and R. M. Schabinger, "Cusp and collinear anomalous dimensions in four-loop QCD from form factors," *Phys. Rev. Lett.*, vol. 124, no. 16, p. 162001, 2020.

[31] P. A. Baikov, K. G. Chetyrkin, A. V. Smirnov, V. A. Smirnov, and M. Steinhauser, "Quark and gluon form factors to three loops," *Phys. Rev. Lett.*, vol. 102, p. 212002, 2009.

[32] T. Gehrmann, E. Glover, T. Huber, N. Ikizlerli, and C. Studerus, "The quark and gluon form factors to three loops in QCD through to $\mathcal{O}(\epsilon^2)$," *JHEP*, vol. 11, p. 102, 2010.

[33] M. A. Ebert, I. W. Stewart, and Y. Zhao, "Towards Quasi-Transverse Momentum Dependent PDFs Computable on the Lattice," *JHEP*, vol. 09, p. 037, 2019.

[34] C. Shugert, T. Izubichi, L. Jin, C. Kallidonis, N. Karthik, S. Mukherjee, P. Petreczky, and S. Syritsyn, "Pion quasi parton distribution function on a fine lattice," *PoS*, vol. LATTICE2018, p. 110, 2018.

[35] Z.-Y. Fan, Y.-B. Yang, A. Anthony, H.-W. Lin, and K.-F. Liu, "Gluon Quasi-Parton-Distribution Functions from Lattice QCD," *Phys. Rev. Lett.*, vol. 121, no. 24, p. 242001, 2018.

[36] J. C. Collins, D. E. Soper, and G. F. Sterman, "Transverse Momentum Distribution in Drell-Yan Pair and W and Z Boson Production," *Nucl. Phys.*, vol. B250, pp. 199–224, 1985.

[37] S. Mantry and F. Petriello, "Factorization and Resummation of Higgs Boson Differential Distributions in Soft-Collinear Effective Theory," *Phys. Rev.*, vol. D81, p. 093007, 2010.

[38] S. Mantry and F. Petriello, "Transverse Momentum Distributions in the Non-Perturbative Region," *Phys. Rev.*, vol. D84, p. 014030, 2011.

[39] T. Becher, M. Neubert, and D. Wilhelm, "Electroweak Gauge-Boson Production at Small q_T: Infrared Safety from the Collinear Anomaly," *JHEP*, vol. 02, p. 124, 2012.

[40] A. Idilbi, X.-d. Ji, and F. Yuan, "Transverse momentum distribution through soft-gluon resummation in effective field theory," *Phys. Lett. B*, vol. 625, pp. 253–263, 2005.

[41] X.-d. Ji, J.-P. Ma, and F. Yuan, "QCD factorization for spin-dependent cross sections in DIS and Drell-Yan processes at low transverse momentum," *Phys. Lett.*, vol. B597, pp. 299–308, 2004.

[42] P.-y. Chen, A. Idilbi, and X.-d. Ji, "QCD Factorization for Deep-Inelastic Scattering At Large Bjorken $x(B) \sim 1 - \mathcal{O}(\Lambda_{\mathrm{QCD}}/Q)$," *Nucl. Phys. B*, vol. 763, pp. 183–197, 2007.

[43] A. V. Belitsky, X. Ji, and F. Yuan, "Final state interactions and gauge invariant parton distributions," *Nucl. Phys.*, vol. B656, pp. 165–198, 2003.

[44] X.-d. Ji and F. Yuan, "Parton distributions in light cone gauge: Where are the final state interactions?," *Phys. Lett. B*, vol. 543, pp. 66–72, 2002.

[45] D. Boer, P. J. Mulders, and F. Pijlman, "Universality of T odd effects in single spin and azimuthal asymmetries," *Nucl. Phys.*, vol. B667, pp. 201–241, 2003.

[46] M. Garcia-Echevarria, A. Idilbi, and I. Scimemi, "SCET, Light-Cone Gauge and the T-Wilson Lines," *Phys. Rev.*, vol. D84, p. 011502, 2011.

[47] C. Lee and G. F. Sterman, "Momentum Flow Correlations from Event Shapes: Factorized Soft Gluons and Soft-Collinear Effective Theory," *Phys. Rev. D*, vol. 75, p. 014022, 2007.

[48] T. Becher and G. Bell, "Analytic Regularization in Soft-Collinear Effective Theory," *Phys. Lett. B*, vol. 713, pp. 41–46, 2012.

[49] J.-y. Chiu, A. Jain, D. Neill, and I. Z. Rothstein, "The Rapidity Renormalization Group," *Phys. Rev. Lett.*, vol. 108, p. 151601, 2012.

[50] Y. Li, D. Neill, and H. X. Zhu, "An Exponential Regulator for Rapidity Divergences," *Submitted to: Phys. Rev. D*, 2016.

[51] M. G. Echevarria, I. Scimemi, and A. Vladimirov, "Transverse momentum dependent fragmentation function at next-to-next-to-leading order," *Phys. Rev.*, vol. D93, p. 011502, 2016.

[52] M. G. Echevarria, I. Scimemi, and A. Vladimirov, "Universal transverse momentum dependent soft function at NNLO," *Phys. Rev.*, vol. D93, no. 5, p. 054004, 2016.

[53] J. Gatheral, "Exponentiation of Eikonal Cross-sections in Nonabelian Gauge Theories," *Phys. Lett. B*, vol. 133, pp. 90–94, 1983.

[54] J. Frenkel and J. Taylor

[55] A. Mitov, G. F. Sterman, and I. Sung, "Computation of the Soft Anomalous Dimension Matrix in Coordinate Space," *Phys. Rev. D*, vol. 82, p. 034020, 2010.

[56] A. Mitov, G. Sterman, and I. Sung, "Diagrammatic Exponentiation for Products of Wilson Lines," *Phys. Rev. D*, vol. 82, p. 096010, 2010.

[57] A. Mitov, G. F. Sterman, and I. Sung, "The Massive Soft Anomalous Dimension Matrix at Two Loops," *Phys. Rev. D*, vol. 79, p. 094015, 2009.

[58] E. Gardi, J. M. Smillie, and C. D. White, "The Non-Abelian Exponentiation theorem for multiple Wilson lines," *JHEP*, vol. 06, p. 088, 2013.

[59] E. Gardi, J. M. Smillie, and C. D. White, "On the renormalization of multiparton webs," *JHEP*, vol. 09, p. 114, 2011.

[60] S. Moch, J. A. M. Vermaseren, and A. Vogt, "The Quark form-factor at higher orders," *JHEP*, vol. 08, p. 049, 2005.

[61] T. Gehrmann, E. W. N. Glover, T. Huber, N. Ikizlerli, and C. Studerus, "Calculation of the quark and gluon form factors to three loops in QCD," *JHEP*, vol. 06, p. 094, 2010.

[62] A. A. Vladimirov, "Soft-/rapidity- anomalous dimensions correspondence," 2016.

[63] Y. Li and H. X. Zhu, "Bootstrapping rapidity anomalous dimension for transverse-momentum resummation," *Submitted to: Phys. Rev. Lett.*, 2016.

[64] J. C. Collins and D. E. Soper, "Back-To-Back Jets: Fourier Transform from B to K-Transverse," *Nucl. Phys.*, vol. B197, pp. 446–476, 1982.

[65] I. Scimemi and A. Vladimirov, "Power corrections and renormalons in Transverse Momentum Distributions," 2016.

[66] I. Scimemi and A. Vladimirov, "Analysis of vector boson production within TMD factorization," *Eur. Phys. J.*, vol. C78, no. 2, p. 89, 2018.

[67] S. Moch, J. A. M. Vermaseren, and A. Vogt, "The Three loop splitting functions in QCD: The Nonsinglet case," *Nucl. Phys.*, vol. B688, pp. 101–134, 2004.

[68] A. Vogt, S. Moch, and J. A. M. Vermaseren, "The Three-loop splitting functions in QCD: The Singlet case," *Nucl. Phys.*, vol. B691, pp. 129–181, 2004.

[69] S. Moch, J. A. M. Vermaseren, and A. Vogt, "The Three-Loop Splitting Functions in QCD: The Helicity-Dependent Case," *Nucl. Phys.*, vol. B889, pp. 351–400, 2014.

[70] W. Vogelsang, "Next-to-leading order evolution of transversity distributions and Soffer's inequality," *Phys. Rev.*, vol. D57, pp. 1886–1894, 1998.

[71] S. V. Mikhailov and A. A. Vladimirov, "ERBL and DGLAP kernels for transversity distributions. Two-loop calculations in covariant gauge," *Phys. Lett.*, vol. B671, pp. 111–118, 2009.

[72] R. Angeles-Martinez *et al.*, "Transverse Momentum Dependent (TMD) parton distribution functions: status and prospects," *Acta Phys. Polon.*, vol. B46, no. 12, pp. 2501–2534, 2015.

[73] K. Goeke, A. Metz, and M. Schlegel, "Parameterization of the quark-quark correlator of a spin-1/2 hadron," *Phys. Lett.*, vol. B618, pp. 90–96, 2005.

[74] P. J. Mulders and J. Rodrigues, "Transverse momentum dependence in gluon distribution and fragmentation functions," *Phys. Rev.*, vol. D63, p. 094021, 2001.

[75] S. Meissner, A. Metz, and K. Goeke, "Relations between generalized and transverse momentum dependent parton distributions," *Phys. Rev. D*, vol. 76, p. 034002, 2007.

[76] D. Boer, L. Gamberg, B. Musch, and A. Prokudin, "Bessel-Weighted Asymmetries in Semi Inclusive Deep Inelastic Scattering," *JHEP*, vol. 10, p. 021, 2011.

[77] M. G. Echevarria, T. Kasemets, P. J. Mulders, and C. Pisano, "QCD evolution of (un)polarized gluon TMDPDFs and the Higgs q_T-distribution," *JHEP*, vol. 07, p. 158, 2015.

[78] S. M. Aybat and T. C. Rogers, "TMD Parton Distribution and Fragmentation Functions with QCD Evolution," *Phys. Rev.*, vol. D83, p. 114042, 2011.

[79] I. O. Cherednikov and N. G. Stefanis, "Wilson lines and transverse-momentum dependent parton distribution functions: A Renormalization-group analysis," *Nucl. Phys.*, vol. B802, pp. 146–179, 2008.

[80] I. O. Cherednikov and N. G. Stefanis, "Renormalization, Wilson lines, and transverse-momentum dependent parton distribution functions," *Phys. Rev.*, vol. D77, p. 094001, 2008.

[81] T. Gehrmann, T. Luebbert, and L. L. Yang, "Calculation of the transverse parton distribution functions at next-to-next-to-leading order," *JHEP*, vol. 06, p. 155, 2014.

[82] T. Gehrmann, T. Lubbert, and L. L. Yang, "Transverse parton distribution functions at next-to-next-to-leading order: the quark-to-quark case," *Phys. Rev. Lett.*, vol. 109, p. 242003, 2012.

[83] A. Bacchetta and A. Prokudin, "Evolution of the helicity and transversity Transverse-Momentum-Dependent parton distributions," *Nucl. Phys.*, vol. B875, pp. 536–551, 2013.

[84] D. Gutierrez-Reyes, I. Scimemi, and A. A. Vladimirov, "Twist-2 matching of transverse momentum dependent distributions," *Phys. Lett.*, vol. B769, pp. 84–89, 2017.

[85] D. Gutierrez-Reyes, I. Scimemi, and A. Vladimirov, "Transverse momentum dependent transversely polarized distributions at next-to-next-to-leading-order," *JHEP*, vol. 07, p. 172, 2018.

[86] D. Gutierrez-Reyes, S. Leal-Gomez, I. Scimemi, and A. Vladimirov, "Linearly polarized gluons at next-to-next-to leading order and the Higgs transverse momentum distribution," *JHEP*, vol. 11, p. 121, 2019.

[87] A. Bacchetta, V. Bertone, C. Bissolotti, G. Bozzi, F. Delcarro, F. Piacenza, and M. Radici, "Transverse-momentum-dependent parton distributions up to N^3LL from Drell-Yan data," *JHEP*, vol. 07, p. 117, 2020.

[88] M. G. A. Buffing, M. Diehl, and T. Kasemets, "Transverse momentum in double parton scattering: factorisation, evolution and matching," *JHEP*, vol. 01, p. 044, 2018.

[89] G. 't Hooft and M. J. G. Veltman, "Regularization and Renormalization of Gauge Fields," *Nucl. Phys.*, vol. B44, pp. 189–213, 1972.

[90] P. Breitenlohner and D. Maison, "Dimensional Renormalization and the Action Principle," *Commun. Math. Phys.*, vol. 52, pp. 11–38, 1977.

[91] S. A. Larin, "The Renormalization of the axial anomaly in dimensional regularization," *Phys. Lett.*, vol. B303, pp. 113–118, 1993.

[92] S. A. Larin and J. A. M. Vermaseren, "The alpha-s**3 corrections to the Bjorken sum rule for polarized electroproduction and to the Gross-Llewellyn Smith sum rule," *Phys. Lett.*, vol. B259, pp. 345–352, 1991.

[93] Y. Matiounine, J. Smith, and W. L. van Neerven, "Two loop operator matrix elements calculated up to finite terms for polarized deep inelastic lepton - hadron scattering," *Phys. Rev.*, vol. D58, p. 076002, 1998.

[94] V. Ravindran, J. Smith, and W. L. van Neerven, "NNLO corrections to massive lepton pair production in longitudinally polarized proton proton collisions," *Nucl. Phys.*, vol. B682, pp. 421–456, 2004.

[95] P. M. Nadolsky, D. Stump, and C. Yuan, "Phenomenology of multiple parton radiation in semiinclusive deep inelastic scattering," *Phys. Rev. D*, vol. 64, p. 114011, 2001.

[96] A. Airapetian *et al.*, "Effects of transversity in deep-inelastic scattering by polarized protons," *Phys. Lett.*, vol. B693, pp. 11–16, 2010.

[97] M. Alekseev *et al.*, "Collins and Sivers asymmetries for pions and kaons in muon-deuteron DIS," *Phys. Lett.*, vol. B673, pp. 127–135, 2009.

[98] C. Adolph *et al.*, "Collins and Sivers asymmetries in muonproduction of pions and kaons off transversely polarised protons," *Phys. Lett.*, vol. B744, pp. 250–259, 2015.

[99] L. Adamczyk *et al.*, "Transverse spin-dependent azimuthal correlations of charged pion pairs measured in $p^\uparrow$+p collisions at $\sqrt{s}$ = 500 GeV," *Phys. Lett.*, vol. B780, pp. 332–339, 2018.

[100] M. Anselmino, M. Boglione, U. D'Alesio, A. Kotzinian, F. Murgia, A. Prokudin, and C. Turk, "Transversity and Collins functions from SIDIS and e+ e- data," *Phys. Rev.*, vol. D75, p. 054032, 2007.

[101] M. Anselmino, M. Boglione, U. D'Alesio, A. Kotzinian, F. Murgia, A. Prokudin, and S. Melis, "Update on transversity and Collins functions from SIDIS and e+ e- data," *Nucl. Phys. Proc. Suppl.*, vol. 191, pp. 98–107, 2009.

[102] M. Anselmino, M. Boglione, U. D'Alesio, S. Melis, F. Murgia, and A. Prokudin, "Simultaneous extraction of transversity and Collins functions from new SIDIS and e+e- data," *Phys. Rev.*, vol. D87, p. 094019, 2013.

[103] Z.-B. Kang, A. Prokudin, P. Sun, and F. Yuan, "Nucleon tensor charge from Collins azimuthal asymmetry measurements," *Phys. Rev.*, vol. D91, p. 071501, 2015.

[104] Z.-B. Kang, A. Prokudin, P. Sun, and F. Yuan, "Extraction of Quark Transversity Distribution and Collins Fragmentation Functions with QCD Evolution," *Phys. Rev.*, vol. D93, no. 1, p. 014009, 2016.

[105] H.-W. Lin, W. Melnitchouk, A. Prokudin, N. Sato, and H. Shows, "First Monte Carlo global analysis of nucleon transversity with lattice QCD constraints," *Phys. Rev. Lett.*, vol. 120, no. 15, p. 152502, 2018.

[106] A. Prokudin, Y. Hatta, Y. Kovchegov, and C. Marquet, eds., *Proceedings, Probing Nucleons and Nuclei in High Energy Collisions: Dedicated to the Physics of the Electron Ion Collider: Seattle (WA), United States, October 1 - November 16, 2018*, WSP, 2020.

[107] A. Metz and A. Vossen, "Parton Fragmentation Functions," *Prog. Part. Nucl. Phys.*, vol. 91, pp. 136–202, 2016.

[108] C. Lefky and A. Prokudin, "Extraction of the distribution function $h_{1T}^\perp$ from experimental data," *Phys. Rev.*, vol. D91, no. 3, p. 034010, 2015.

[109] B. Parsamyan, "Measurement of target-polarization dependent azimuthal asymmetries in SIDIS and Drell-Yan processes at COMPASS experiment," *PoS*, vol. QCDEV2017, p. 042, 2018.

[110] I. Scimemi and A. Vladimirov, "Matching of transverse momentum dependent distributions at twist-3," 2018.

[111] R. L. Jaffe and X.-D. Ji, "Chiral odd parton distributions and Drell-Yan processes," *Nucl. Phys.*, vol. B375, pp. 527–560, 1992.

[112] W. Vogelsang and F. Yuan, "Next-to-leading Order Calculation of the Single Transverse Spin Asymmetry in the Drell-Yan Process," *Phys. Rev.*, vol. D79, p. 094010, 2009.

[113] H. Avakian, A. V. Efremov, P. Schweitzer, and F. Yuan, "Transverse momentum dependent distribution function h1T [perpendicular] and the single spin asymmetry $A(UT)sin(3\phi - \phi_S)$," *Phys. Rev.*, vol. D78, p. 114024, 2008.

[114] V. Moos and A. Vladimirov, "Calculation of transverse momentum dependent distributions beyond the leading power," 8 2020.

[115] T. Becher, M. Neubert, and D. Wilhelm, "Higgs-Boson Production at Small Transverse Momentum," *JHEP*, vol. 05, p. 110, 2013.

[116] M.-X. Luo, T.-Z. Yang, H. X. Zhu, and Y. J. Zhu, "Transverse Parton Distribution and Fragmentation Functions at NNLO: the Gluon Case," 2019.

[117] "`arTeMiDe` web-page, https://teorica.fis.ucm.es/artemide/."

[118] J. R. Ellis, M. K. Gaillard, and D. V. Nanopoulos, "A Phenomenological Profile of the Higgs Boson," *Nucl. Phys.*, vol. B106, p. 292, 1976.

[119] M. Spira, A. Djouadi, D. Graudenz, and P. M. Zerwas, "Higgs boson production at the LHC," *Nucl. Phys.*, vol. B453, pp. 17–82, 1995.

[120] A. Djouadi, "The Anatomy of electro-weak symmetry breaking. I: The Higgs boson in the standard model," *Phys. Rept.*, vol. 457, pp. 1–216, 2008.

[121] S. Catani, E. D'Emilio, and L. Trentadue, "The Gluon Form-factor to Higher Orders: Gluon Gluon Annihilation at Small Q^-transverse," *Phys. Lett.*, vol. B211, pp. 335–342, 1988.

[122] S. Catani and M. Grazzini, "QCD transverse-momentum resummation in gluon fusion processes," *Nucl. Phys.*, vol. B845, pp. 297–323, 2011.

[123] D. Boer, W. J. den Dunnen, C. Pisano, M. Schlegel, and W. Vogelsang, "Linearly Polarized Gluons and the Higgs Transverse Momentum Distribution," *Phys. Rev. Lett.*, vol. 108, p. 032002, 2012.

[124] G. Bozzi, S. Catani, D. de Florian, and M. Grazzini, "Transverse-momentum resummation and the spectrum of the Higgs boson at the LHC," *Nucl. Phys.*, vol. B737, pp. 73–120, 2006.

[125] D. de Florian, G. Ferrera, M. Grazzini, and D. Tommasini, "Transverse-momentum resummation: Higgs boson production at the Tevatron and the LHC," *JHEP*, vol. 11, p. 064, 2011.

[126] W. Bizoń, X. Chen, A. Gehrmann-De Ridder, T. Gehrmann, N. Glover, A. Huss, P. F. Monni, E. Re, L. Rottoli, and P. Torrielli, "Fiducial distributions in Higgs and Drell-Yan production at N^{3}LL+NNLO," *JHEP*, vol. 12, p. 132, 2018.

[127] J. Cruz-Martinez, T. Gehrmann, E. W. N. Glover, and A. Huss, "Second-order QCD effects in Higgs boson production through vector boson fusion," *Phys. Lett.*, vol. B781, pp. 672–677, 2018.

[128] D. Boer, S. J. Brodsky, P. J. Mulders, and C. Pisano, "Direct Probes of Linearly Polarized Gluons inside Unpolarized Hadrons," *Phys. Rev. Lett.*, vol. 106, p. 132001, 2011.

[129] A. Metz and J. Zhou, "Distribution of linearly polarized gluons inside a large nucleus," *Phys. Rev.*, vol. D84, p. 051503, 2011.

[130] F. Dominguez, J.-W. Qiu, B.-W. Xiao, and F. Yuan, "On the linearly polarized gluon distributions in the color dipole model," *Phys. Rev.*, vol. D85, p. 045003, 2012.

[131] C. Pisano, D. Boer, S. J. Brodsky, M. G. A. Buffing, and P. J. Mulders, "Linear polarization of gluons and photons in unpolarized collider experiments," *JHEP*, vol. 10, p. 024, 2013.

[132] A. Dumitru, T. Lappi, and V. Skokov, "Distribution of Linearly Polarized Gluons and Elliptic Azimuthal Anisotropy in Deep Inelastic Scattering Dijet Production at High Energy," *Phys. Rev. Lett.*, vol. 115, no. 25, p. 252301, 2015.

[133] A. Mukherjee and S. Rajesh, "Linearly polarized gluons in charmonium and bottomonium production in color octet model," *Phys. Rev.*, vol. D95, no. 3, p. 034039, 2017.

[134] D. Boer, P. J. Mulders, J. Zhou, and Y.-j. Zhou, "Suppression of maximal linear gluon polarization in angular asymmetries," *JHEP*, vol. 10, p. 196, 2017.

[135] A. V. Efremov, N. Ya. Ivanov, and O. V. Teryaev, "How to measure the linear polarization of gluons in unpolarized proton using the heavy-quark pair leptoproduction," *Phys. Lett.*, vol. B777, pp. 435–441, 2018.

[136] A. V. Efremov, N. Y. Ivanov, and O. V. Teryaev, "The ratio $R = \mathrm{d}\sigma_L/\mathrm{d}\sigma_T$ in heavy-quark pair leptoproduction as a probe of linearly polarized gluons in unpolarized proton," *Phys. Lett.*, vol. B780, pp. 303–307, 2018.

[137] R. Kishore and A. Mukherjee, "Accessing linearly polarized gluon distribution in J/ψ production at the electron-ion collider," *Phys. Rev.*, vol. D99, no. 5, p. 054012, 2019.

[138] M. G. Echevarria, "Proper TMD factorization for quarkonia production: $pp \to \eta_c$ as a study case," 2019.

[139] C. Marquet, C. Roiesnel, and P. Taels, "Linearly polarized small-x gluons in forward heavy-quark pair production," *Phys. Rev.*, vol. D97, no. 1, p. 014004, 2018.

[140] V. Bertone, I. Scimemi, and A. Vladimirov, "Extraction of unpolarized quark transverse momentum dependent parton distributions from Drell-Yan/Z-boson production," *JHEP*, vol. 06, p. 028, 2019.

[141] M. A. Shifman, A. I. Vainshtein, M. B. Voloshin, and V. I. Zakharov, "Low-Energy Theorems for Higgs Boson Couplings to Photons," *Sov. J. Nucl. Phys.*, vol. 30, pp. 711–716, 1979. [Yad. Fiz.30,1368(1979)].

[142] M. Kramer, E. Laenen, and M. Spira, "Soft gluon radiation in Higgs boson production at the LHC," *Nucl. Phys.*, vol. B511, pp. 523–549, 1998.

[143] K. G. Chetyrkin, B. A. Kniehl, and M. Steinhauser, "Hadronic Higgs decay to order alpha-s**4," *Phys. Rev. Lett.*, vol. 79, pp. 353–356, 1997.

[144] V. Ahrens, T. Becher, M. Neubert, and L. L. Yang, "Renormalization-Group Improved Prediction for Higgs Production at Hadron Colliders," *Eur. Phys. J.*, vol. C62, pp. 333–353, 2009.

[145] V. Ahrens, T. Becher, M. Neubert, and L. L. Yang, "Origin of the Large Perturbative Corrections to Higgs Production at Hadron Colliders," *Phys. Rev.*, vol. D79, p. 033013, 2009.

[146] R. D. Ball *et al.*, "Parton distributions from high-precision collider data," *Eur. Phys. J.*, vol. C77, no. 10, p. 663, 2017.

[147] T. Sjostrand, S. Mrenna, and P. Z. Skands, "PYTHIA 6.4 Physics and Manual," *JHEP*, vol. 05, p. 026, 2006.

[148] T. Sjostrand, S. Mrenna, and P. Z. Skands, "A Brief Introduction to PYTHIA 8.1," *Comput. Phys. Commun.*, vol. 178, pp. 852–867, 2008.

[149] V. Khachatryan *et al.*, "Measurement of differential cross sections for Higgs boson production in the diphoton decay channel in pp collisions at $\sqrt{s} = 8\,\mathrm{TeV}$," *Eur. Phys. J.*, vol. C76, no. 1, p. 13, 2016.

[150] L. D. McLerran and R. Venugopalan, "Gluon distribution functions for very large nuclei at small transverse momentum," *Phys. Rev.*, vol. D49, pp. 3352–3355, 1994.

[151] D. Gutierrez-Reyes, I. Scimemi, W. J. Waalewijn, and L. Zoppi, "Transverse momentum dependent distributions with jets," *Phys. Rev. Lett.*, vol. 121, no. 16, p. 162001, 2018.

[152] D. Bertolini, T. Chan, and J. Thaler, "Jet Observables Without Jet Algorithms," *JHEP*, vol. 04, p. 013, 2014.

[153] E. C. Aschenauer, I. Borsa, R. Sassot, and C. Van Hulse, "Semi-inclusive Deep-Inelastic Scattering, Parton Distributions and Fragmentation Functions at a Future Electron-Ion Collider," 2019.

[154] R. Bain, Y. Makris, and T. Mehen, "Transverse Momentum Dependent Fragmenting Jet Functions with Applications to Quarkonium Production," 2016.

[155] Z.-B. Kang, J.-W. Qiu, F. Ringer, H. Xing, and H. Zhang, "J/ψ production and polarization within a jet," *Phys. Rev. Lett.*, vol. 119, no. 3, p. 032001, 2017.

[156] Z.-B. Kang, A. Prokudin, F. Ringer, and F. Yuan, "Collins azimuthal asymmetries of hadron production inside jets," *Phys. Lett.*, vol. B774, pp. 635–642, 2017.

[157] Y. Makris, D. Neill, and V. Vaidya, "Probing Transverse-Momentum Dependent Evolution With Groomed Jets," *JHEP*, vol. 07, p. 167, 2018.

[158] Y. Makris and V. Vaidya, "Transverse Momentum Spectra at Threshold for Groomed Heavy Quark Jets," *JHEP*, vol. 10, p. 019, 2018.

[159] A. J. Larkoski, S. Marzani, G. Soyez, and J. Thaler, "Soft Drop," *JHEP*, vol. 05, p. 146, 2014.

[160] D. Neill, I. Scimemi, and W. J. Waalewijn, "Jet axes and universal transverse-momentum-dependent fragmentation," *JHEP*, vol. 04, p. 020, 2017.

[161] D. Neill, A. Papaefstathiou, W. J. Waalewijn, and L. Zoppi, "Phenomenology with a recoil-free jet axis: TMD fragmentation and the jet shape," *JHEP*, vol. 01, p. 067, 2019.

[162] M. G. A. Buffing, Z.-B. Kang, K. Lee, and X. Liu, "A transverse momentum dependent framework for back-to-back photon+jet production," 2018.

[163] X. Liu, F. Ringer, W. Vogelsang, and F. Yuan, "Lepton-jet Correlations in Deep Inelastic Scattering at the Electron-Ion Collider," 2018.

[164] A. Banfi, M. Dasgupta, and Y. Delenda, "Azimuthal decorrelations between QCD jets at all orders," *Phys. Lett.*, vol. B665, pp. 86–91, 2008.

[165] P. Sun, C. P. Yuan, and F. Yuan, "Soft Gluon Resummations in Dijet Azimuthal Angular Correlations in Hadronic Collisions," *Phys. Rev. Lett.*, vol. 113, no. 23, p. 232001, 2014.

[166] P. Sun, C. P. Yuan, and F. Yuan, "Transverse Momentum Resummation for Dijet Correlation in Hadronic Collisions," *Phys. Rev.*, vol. D92, no. 9, p. 094007, 2015.

[167] L. Chen, G.-Y. Qin, S.-Y. Wei, B.-W. Xiao, and H.-Z. Zhang, "Dijet Asymmetry in the Resummation Improved Perturbative QCD Approach," *Phys. Lett.*, vol. B782, pp. 773–778, 2018.

[168] M. Cacciari, G. P. Salam, and G. Soyez, "FastJet User Manual," *Eur. Phys. J.*, vol. C72, p. 1896, 2012.

[169] M. Cacciari, G. P. Salam, and G. Soyez, "The Anti-k_t jet clustering algorithm," *JHEP*, vol. 0804, p. 063, 2008.

[170] Z.-B. Kang, F. Ringer, and I. Vitev, "The semi-inclusive jet function in SCET and small radius resummation for inclusive jet production," 2016.

[171] L. Dai, C. Kim, and A. K. Leibovich, "Fragmentation of a Jet with Small Radius," 2016.

[172] Z.-B. Kang, F. Ringer, and W. J. Waalewijn, "The Energy Distribution of Subjets and the Jet Shape," *JHEP*, vol. 07, p. 064, 2017.

[173] A. V. Manohar and I. W. Stewart, "The Zero-Bin and Mode Factorization in Quantum Field Theory," *Phys. Rev.*, vol. D76, p. 074002, 2007.

[174] M. Dasgupta and G. P. Salam, "Resummation of nonglobal QCD observables," *Phys. Lett.*, vol. B512, pp. 323–330, 2001.

[175] T. Becher, M. Neubert, L. Rothen, and D. Y. Shao, "Effective Field Theory for Jet Processes," *Phys. Rev. Lett.*, vol. 116, no. 19, p. 192001, 2016.

[176] T. Becher, M. Neubert, L. Rothen, and D. Y. Shao, "Factorization and Resummation for Jet Processes," *JHEP*, vol. 11, p. 019, 2016.

[177] A. J. Larkoski, I. Moult, and D. Neill, "Non-Global Logarithms, Factorization, and the Soft Substructure of Jets," *JHEP*, vol. 09, p. 143, 2015.

[178] S. Caron-Huot, "Resummation of non-global logarithms and the BFKL equation," *JHEP*, vol. 03, p. 036, 2018.

[179] J.-y. Chiu, A. Fuhrer, A. H. Hoang, R. Kelley, and A. V. Manohar, "Soft-Collinear Factorization and Zero-Bin Subtractions," *Phys. Rev.*, vol. D79, p. 053007, 2009.

[180] F. Hautmann, I. Scimemi, and A. Vladimirov, "Non-perturbative contributions to vector-boson transverse momentum spectra in hadronic collisions," 2020.

[181] M. G. Echevarria, A. Idilbi, A. Schafer, and I. Scimemi, "Model-Independent Evolution of Transverse Momentum Dependent Distribution Functions (TMDs) at NNLL," *Eur. Phys. J.*, vol. C73, no. 12, p. 2636, 2013.

[182] S. Catani and M. H. Seymour, "A General algorithm for calculating jet cross-sections in NLO QCD," *Nucl. Phys.*, vol. B485, pp. 291–419, 1997. [Erratum: Nucl. Phys.B510,503(1998)].

[183] Y. L. Dokshitzer, G. D. Leder, S. Moretti, and B. R. Webber, "Better jet clustering algorithms," *JHEP*, vol. 08, p. 001, 1997.

[184] M. Wobisch and T. Wengler, "Hadronization corrections to jet cross-sections in deep inelastic scattering," 1998.

[185] S. Catani, Y. L. Dokshitzer, M. Olsson, G. Turnock, and B. R. Webber, "New clustering algorithm for multi-jet cross-sections in e^+e^- annihilation," *Phys. Lett.*, vol. B269, pp. 432–438, 1991.

[186] "`artemide` web-page, https://teorica.fis.ucm.es/artemide/ `artemide` repository, https://github.com/vladimirovalexey/artemide-public."

[187] D. Gutierrez-Reyes, I. Scimemi, W. J. Waalewijn, and L. Zoppi, "Transverse momentum dependent distributions in e^+e^- and semi-inclusive deep-inelastic scattering using jets," *JHEP*, vol. 10, p. 031, 2019.

[188] A. H. Hoang, S. Mantry, A. Pathak, and I. W. Stewart, "Nonperturbative Corrections to Soft Drop Jet Mass," *JHEP*, vol. 12, p. 002, 2019.

[189] S. D. Ellis and D. E. Soper, "Successive combination jet algorithm for hadron collisions," *Phys. Rev.*, vol. D48, pp. 3160–3166, 1993.

[190] S. Catani, Y. L. Dokshitzer, M. Seymour, and B. Webber, "Longitudinally invariant K_t clustering algorithms for hadron hadron collisions," *Nucl. Phys.*, vol. B406, pp. 187–224, 1993.

[191] M. Wobisch, "Measurement and QCD analysis of jet cross-sections in deep inelastic positron proton collisions at $\sqrt{s} = 300\,\text{GeV}$," 2000.

[192] G. Salam, "E_t^∞ Scheme," *Unpublished*.

[193] A. J. Larkoski, D. Neill, and J. Thaler, "Jet Shapes with the Broadening Axis," *JHEP*, vol. 04, p. 017, 2014.

[194] S. Marzani, L. Schunk, and G. Soyez, "A study of jet mass distributions with grooming," *JHEP*, vol. 07, p. 132, 2017.

[195] A. J. Larkoski, S. Marzani, and J. Thaler, "Sudakov Safety in Perturbative QCD," *Phys. Rev.*, vol. D91, no. 11, p. 111501, 2015.

[196] J. R. Gaunt, "Glauber Gluons and Multiple Parton Interactions," *JHEP*, vol. 07, p. 110, 2014.

[197] C. Frye, A. J. Larkoski, M. D. Schwartz, and K. Yan, "Factorization for groomed jet substructure beyond the next-to-leading logarithm," *JHEP*, vol. 07, p. 064, 2016.

[198] M. Beneke and V. M. Braun, "Power corrections and renormalons in Drell-Yan production," *Nucl. Phys.*, vol. B454, pp. 253–290, 1995.

[199] G. P. Korchemsky and G. F. Sterman, "Nonperturbative corrections in resummed cross-sections," *Nucl. Phys.*, vol. B437, pp. 415–432, 1995.

[200] G. P. Korchemsky, G. Oderda, and G. F. Sterman, "Power corrections and nonlocal operators," *AIP Conf. Proc.*, vol. 407, no. 1, p. 988, 1997.

[201] M. Beneke, V. M. Braun, and L. Magnea, "Phenomenology of power corrections in fragmentation processes in e+ e- annihilation," *Nucl. Phys.*, vol. B497, pp. 297–333, 1997.

[202] T. Becher and G. Bell, "Enhanced nonperturbative effects through the collinear anomaly," *Phys. Rev. Lett.*, vol. 112, no. 18, p. 182002, 2014.

[203] A. Accardi *et al.*, "Electron Ion Collider: The Next QCD Frontier: Understanding the glue that binds us all," *Eur. Phys. J. A*, vol. 52, no. 9, p. 268, 2016.

[204] C. Aidala *et al.*, "The LHCSpin Project," 1 2019.

[205] A. Bacchetta, F. G. Celiberto, M. Radici, and P. Taels, "Transverse-momentum-dependent gluon distribution functions in a spectator model," *Eur. Phys. J. C*, vol. 80, no. 8, p. 733, 2020.

[206] G. Kramer and B. Lampe, "Two Jet Cross-Section in e+ e- Annihilation," *Z. Phys.*, vol. C34, p. 497, 1987. [Erratum: Z. Phys.C42,504(1989)].

[207] T. Matsuura, S. C. van der Marck, and W. L. van Neerven, "The Calculation of the Second Order Soft and Virtual Contributions to the Drell-Yan Cross-Section," *Nucl. Phys.*, vol. B319, pp. 570–622, 1989.

[208] E. Egorian and O. V. Tarasov, "Two Loop Renormalization of the QCD in an Arbitrary Gauge," *Teor. Mat. Fiz.*, vol. 41, pp. 26–32, 1979. [Theor. Math. Phys.41,863(1979)].

[209] V. A. Smirnov, "Evaluating Feynman integrals," *Springer Tracts Mod. Phys.*, vol. 211, pp. 1–244, 2004.